SKARN AND ORE FORMATION
AT SERIPHOS, GREECE

as a consequence of granodiorite intrusion

JAN SALEMINK

STELLINGEN

1

Een strakke definitie van het begrip 'skarn' leidt voornamelijk tot
uitzonderingen die de regel niet bevestigen.

2

Het kritische Rayleigh-Darcy getal Ra $\geq$ 1, zoals gebruikt door Parmentier
en Schedl (1981) is 20 - 40 x te klein. Hydrostatische konvektie van
'grondwater' is niet het enige mechanisme ter verklaring van konvexe
temperatuursverdelingen in kontaktaureolen rond epizonale plutonen.

E.M.Parmentier,A.Schedl,(1981)
J.Geol.,89,1-22.

Dit proefschrift.

3

Verlaging van de verhouding $^{18}O/^{16}O$ van een hydrothermale fluid hoeft
niet veroorzaakt te zijn door toevoeging van een laag $\delta^{18}O$ meteorisch
of metamorf water vanuit een extern reservoir.

Dit proefschrift.

4

Het variabele karakter van de vloeibare insluitsels in bepaalde groeizones
in geodische kwartskristallen van Serifos is het gevolg van 'necking-down'.
Het is geen aanwijzing voor een regelmatig koken van de metasomatische
oplossingen tijdens de erts- en skarnvormingen.

C.de Groot,(1975)
Thèse doct.Univ.Nancy,203p.

5

Het voorkomen van niet-kontaktmetamorfe groenschisten op Akra Kiklopa,
SW-Serifos, is geen aanwijzing voor een post-intrusief dekblad.

T.Gourmellas,(1985)
Terra Cognita,5,252.

Voor een goede interpretatie van de veelheid aan gegevens verkregen uit een statistisch-geochemisch exploratie onderzoek is gedetailleerde studie van sterk afwijkende monsters onontbeerlijk omdat daarin gewoonlijk specifieke processen in extreme vorm naar voren komen.

7

Extern gefinancierd onderzoek is niet alleen een bron van inkomsten.

8

De welvaart van een land kan goed worden afgemeten aan de variatie in honde- en kattevoer.

9

Het gebruik van de afkorting atv is een onduidelijke vorm van arbeids-tijdverkorting.

10

Voordeurdeling geeft brandhout.

Utrecht, 28 mei 1985

J.Salemink

Stellingen behorende bij het proefschrift: Skarn and ore formation at Seriphos, Greece.

GEOLOGICA ULTRAIECTINA

SKARN AND ORE FORMATION
AT SERIPHOS, GREECE
as a consequence of granodiorite instrusion

X. VIII. 2 0

SKARN AND ORE FORMATION AT SERIPHOS, GREECE

as a consequence of granodiorite intrusion

SKARN EN ERTS VORMING TE SERIFOS, GRIEKENLAND

ten gevolge van een granodioriet intrusie

(met een samenvatting in het Nederlands)

JAN SALEMINK

GEBOREN OP 25 JULI 1948 TE RHEDEN

PROMOTOR: PROF. DR. R.D. SCHUILING
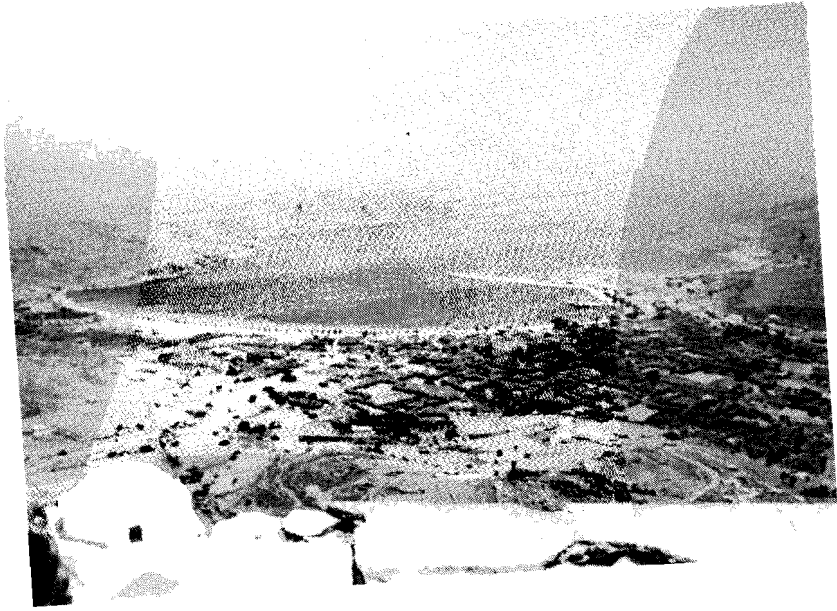
VOORWOORD

Bij het gereed komen van dit proefschrift wil ik in het bijzonder
bedanken:

Mijn promotor, Prof.Dr.R.D.Schuiling, voor het geduld en het
vertrouwen, zijn suggesties tijdens het onderzoek en de review van het
manuscript.

Dr.Arie de Jong, voor het meedenken, de isotopen-analyses en de
plezierige en vruchtbare samenwerking ook bij andere onderzoeks-
projecten.

Paul Anten, voor de hulp en praktische raadgevingen bij de
chemische analyses.

Prof.Dr.A.C.Tobi, voor zijn hulp bij het petrologisch onderzoek.

Dr.Paul van der Maar, voor het toegankelijk maken van de
fasenanalyse, en de kameraadschap zowel in Utrecht als in Griekenland.

Dr.Rob Kreulen, voor het vertrouwd maken met het vloeistof
insluitsel onderzoek.

Dr.Liedeke Vergouwen, voor het beschikbaar stellen van skarn
monsters en analyse gegevens.

Jan de Groot en medewerkers voor het maken van de goede
slijpplaten en dubbel gepolijste doorsneden, vooral die van de vaak
brokkelige en harde skarns.

De mensen van tekenkamer en foto afdeling, vooral J.R.Meye voor
het op het laatste moment tekenen van een toch nog groot aantal
figuren.

Alle medewerkers, (ex-) promovendi en (oud-) studenten van de
afdelingen Geochemie, Petrologie en Kristallografie die door discussies
en/of praktische hulp hebben bijgedragen tot het onderzoek.

Prof.Dr.Jean Verkaeren, rapporteur,(Universite Catholique de
Louvain-la-Neuve), je veux remercier pour son interet.

Dr.Bernard Guy (Ecole des Mines, St-Etienne),je veux remercier
pour les discussion sur les problemes des formation des skarns et des
zonations.

I thank the Director of the Institute of Geology and Mineral
Explortion (Athens) for his permission to carry out the field work.

Een dedeelte van het onderzoek werd mede-gefinancierd en uitgevoerd in het kader van het EEG-project 'Quantification of the skarn and ore formations at Seriphos, Greece', EEC contractno. MPP 42 NL.

SUMMARY

On the island of Seriphos, Greece, the shallow intrusion of a
granodiorite pluton into a series of previously regionally
metamorphosed gneisses, marbles and marble-bearing schists produced a
contact metamorphic aureole and extensive deposits of Ca-Fe-Mg skarns
and Fe-ores. Structural and petrological investigations show that the
contact metamorphic aureole was formed as a result of the (dry) thermal
heating accompanying the emplacement and gradual crystallization of the
magma. At or just after the time of its final solidification the
granodiorite was affected by a major stage of (auto-) brecciation that
caused an intense fracturing of the plutonic body as well as of the
surrounding country rocks. As a consequence of the associated increase
in rock permeabilities intense metasomatic-hydrothermal activities
along the newly formed transport channels caused a leaching of the
granodiorite of its mafic components (Fe, Mg, Mn, etc.) and a
deposition of the same (Fe, Mg, Mn-) components in the skarns and ore
formations in the country rocks.

Thermodynamic analyses of the observed mineral parageneses in the
skarn and ore deposits show that at Seriphos metasomatism continuously
took place under gradually decreasing temperatures and under constant
maintenance of local equilibrium between Fe-saturated, hydrothermal
solutions and the solids locally present along the transport channels.
Fluid inclusion studies indicate that the metasomatic 'juices' were
saline $NaCl-KCl-CaCl_2-MgCl_2-(FeCl_2?)-$ brines with a dominantly magmatic
origin. The fluid inclusion studies also point out that, as
metasomatism progressed and temperatures dropped, fluid pressures
decreased in proportion. Oxygen isotope ratios of quartzes and other
mineral phases from the metasomatic formations indicate that the total
amount of fluid in the hydrothermal fluid flow system must have been
small relative to the total amount of solid phases that equilibrated
with the metasomatic solutions. Apparently a limited amount of
dominantly magma-derived, saline, hydrous solutions percolated along
the cracks and fractures in the permeable solid rock system,
transporting both heat and matter from the cooling, plutonic heat and

fluid source into the adjacent country rocks. Quantitative comparison of the mass exchanges between the granodiorite pluton and the surrounding country rocks confirms that, as a whole, the metasomatic system at Seriphos must have been a largely closed system, and that there were no sources of material outside the granodiorite and its immediate environment.

On the basis of the presented evidence a mathematical model is developed, describing the coupled transfer of heat and mass during the thermal evolution of the intrusive system, both in the magmatic, intrusive stages and in the post-magmatic, hydrothermal cooling stages of the intrusive event. The magmatic stages are modelled by assuming convection in the magma melt and the conductive transfer of heat into the surrounding contact aureole. The post-magmatic, hydrothermal stages of the intrusion are encountered by simulating the advective outflow of metasomatic solutions from the HT-HP plutonic heat and fluid source into its LT-LP environment. Although the simplified model cannot describe in detail the complex interactions of all the processes accompanying the intrusion of a large body of magma into the upper levels of the earth's crust, the model results, in general, are well in agreement with the field observations at Seriphos. The total amount of Fe, for instance, that is modelled to precipitate in the contact metasomatic skarn and ore deposits is in good accordance with the field estimations.

SAMENVATTING

Op het Griekse eiland Serifos leidde de ondiepe intrusie van een
granodioriet plutoon in een serie regionaal gemetamorfoseerde gneissen,
marmers en marmerschisten tot de vorming van een kontakt metamorfe
aureool en tot massieve kontakt metasomatische afzettingen van Ca-Fe-Mg
skarns en Fe-ertsen. Struktureel en petrologisch onderzoek toont aan
dat de kontakt metamorfe aureool ontstond door de (droge) opwarming van
de nevengesteenten tijdens de plaatsing en geleidelijke afkoeling van
het magma. De stolling en ontgassing van het magma ging gepaard met een
intensieve breukvorming, zowel in het gestolde granodioriet gesteente
alsook in de kontaktnabije nevengesteenten. Langs de nieuwgevormde
transportkanalen leidde vervolgens intensieve hydrothermaal-
metasomatische activiteiten tot een uitloging van (vooral) Fe-Mg-Mn
komponenten uit de granodioriet, en een precipitatie van (dezelfde)
Fe-Mg-Mn komponenten in de erts- en skarnafzettingen in de neven-
gesteenten.

Thermodynamische analyse van de mineraalparagenesen in de erts- en
skarnafzettingen te Serifos geeft aan dat de metasomatose plaats vond
onder kontinue dalende temperaturen en voortdurende handhaving van
lokaal chemisch evenwicht tussen Fe-verzadigde, hydrothermale
oplossingen en de (lokaal) langs de transportkanalen aanwezige vaste
fasen. Onderzoek van de vloeibare insluitsels in de skarnmineralen
wijst uit dat de metasomatische 'sappen' gekonsentreerde NaCl-KCl-CaCl$_2$
MgCl$_2$-(FeCl$_2$?)-oplossingen waren van voornamelijk magmatische herkomst
en dat in het verloop van de metasomatische evolutie de vloeistof-
drukken geleidelijk daalden met de temperatuur. De evolutie van de
zuurstof isotopen samenstellingen van de metasomatische nieuwvormingen
geeft aan dat de totale hoeveelheid water in het hydrothermale systeem
betrekkelijk gering moet zijn geweest. Klaarblijkelijk was dus
slechts een beperkte hoeveelheid gekonsentreerde, zoute oplossingen
van voornamelijk magmatische herkomst betrokken bij het metasomatische
massa transport. Kwantitatieve vergelijking van de massa uitwisselingen
tussen de granodioriet en de nevengesteenten bevestigt dat, als geheel,

het metasomatische systeem te Serifos een vrijwel gesloten systeem moet zijn geweest, en dat er geen externe bronnen van materiaal zijn geweest

Op basis van deze waarnemingen is een mathematisch model ontwikkeld dat het gekoppelde transport van warmte en massa beschrijft tussen het plutoon en z'n omgeving, zowel in het magmatische, intrusieve stadium als in het post-magmatische, hydrothermale afkoelingsstadium. Het magmatische model beschrijft de vorming van de kontakt metamorfe aureool door simulatie van de warmte-uitwisselingen tussen een konvekterend magma lichaam en impermeabele nevengesteenten. Het post-magmatische model beschrijft het hydrothermale transport van zowel warmte als opgeloste stoffen vanuit het HT-HP plutoon naar de LT-LP omgeving. Alhoewel het sterk vereenvoudigde model systeem uiteraard geen gedetailleerde beschrijving kan geven van alle processen die geassocieerd zijn met de intrusie van een groot magma lichaam in de hogere aardkorst, zijn de resultaten toch goed in overeenstemming met de waarnemingen te Serifos. De model berekening van de totale hoeveelheid ijzer, bijvoorbeeld, die is de kontakt metasomatische skarns en ertsen komt overeen met de veld waarnemingen.

INDEX

Studies of mineral deposits will be particularly
successful when the investigator is able himself
to unravel the physico-chemical patterns of the
process of mineral formation that he is studying

D.S.Korzhinskii,1953

CHAPTER I: INTRODUCTION

Skarns are metasomatic rocks mainly composed of Ca-Fe-Mg-Si
minerals. They are typically found in Ca-bearing country rocks
surrounding shallow, granitoid intrusions. Associated with them
economically important deposits of Fe, Cu, Zn, Pb, W, Co ore may occur.
Occasionally they may contain significant amounts of Au, Ag, Mo, Sn,
Be, Bi. The skarns, and the accompanying ore deposits, are thought to
have formed during the cooling stages of the intrusions as a result of
thermally driven circulations and percolations of metasomatic fluids
and the associated transport of dissolved chemical components (e.g.
Lindgren, 1933; Smirnov, 1976).

On the island of Seriphos, Cyclades, Greece, a granodiorite pluton
is associated with extensive Ca-Fe-Mg skarns, large Fe-deposits
(magnetite, hematite, limonite), and minor Cu, Pb-Zn and Ba
mineralizations (Marinos, 1951). Within the intrusive body the presence
of numerous hydrothermal veins with bleached zones indicates that the
ore and skarn materials, that were deposited in the country rocks, were
leached from the magmatic rock and transported towards the country
rocks by post-magmatic, metasomatic solutions (Salemink, 1980). The
metasomatic replacements at Seriphos occur in a variety of rock types
and cover a wide range of formation conditions. They provide a good
example to study the complex processes of contact metasomatism and ore
formation that may be associated with the intrusion of a large body of
magma into the upper levels of the earth's crust.

The present study is mainly concerned with the formation
conditions of the skarn and ore deposits at Seriphos and the geological
and physico-chemical controls of the metasomatic differentiation and
concentration processes during the skarn and ore formation. The
geological framework in which the intrusion took place is analyzed by
means of a geological and petrological study, and a reconstruction is
made of the sequence of events associated with the emplacement and
subsequent cooling of the granodiorite pluton (Chapters II, III, IV).
The formation conditions of the skarn and ore deposits are specified
by thermodynamical analysis of the phase assemblages in the
mineralizations and by fluid inclusions studies and stable isotope
investigations (Chapters V, VI). The chemical alterations accompanying
the metasomatic activities are investigated by major and trace element
analyses of unaltered rocks and of their metasomatic replacement
products, and the quantitative scale of the chemical alterations is
indicated by field estimates of the total amounts of skarn and ore
formations (Chapter VII). A theoretical consideration of the formation
processes of metasomatic deposits indicates the influence of such
dominant physico-chemical controls as temperature, fluid pressure,
chemical activity and permeability on the appearance of the skarn and
ore formations (Chapter VIII). How these physico-chemical controls
determine the scale and intensity of the metasomatic activities is
illustrated by a simplified model simulation of the transient heat and
mass exchanges associated with the granodiorite intrusion at Seriphos
(Chapter IX).

The comprehensive study of the chronological evolution and mutual
interrelations of the geological events and physico-chemical mechanisms
associated with the granodiorite intrusion at Seriphos may contribute
to a better understanding of the processes governing contact
metasomatism and ore formation in general. Knowledge of these processes
increases the possibilities of prospecting yet undiscovered, hidden
deposits of economically important metals such as Fe, Cu, Pb, Zn, W and
Sn.

More accurate investigations may shift the boundaries
between the individual series to some extent, but the
fact remains: the Attides are a metamorphic window
within the central chains of Hellas.

L.Kober: Das Alpine Europa, 1931

CHAPTER II: GEOLOGIC SETTING

The island of Seriphos is situated about 100 km SSE of Athens in
the Aegean Sea, Greece. Geologically it belongs to the Attic-Cycladic
Massif. Together with the Menderes Massif in the Eastern Aegean and on
the Turkish mainland, and the Pelagonian and Thessalian Massifs in
Central and Northern Greece, the Attic-Cycladic Massif builds up the
median crystalline 'backbone' of the Alpine orogenic chains of the
Hellenides (fig.1) (Aubouin, 1965; Durr et al.,1978).

The Attic-Cycladic Massif mainly consists of polymetamorphic rocks
(fig.2). On some islands, for instance on Syros, Ios, Milos and
Siphnos, high pressure glaucophane schist facies metamorphic rocks
(blueschists) occur which may show an overprint of a greenschist facies
metamorphic phase (Dixon, 1968; van der Maar, 1980; Kornprobst et
al.,1979; Davis, 1966). On other islands, such as Kea, Kythnos and
Seriphos, greenschist facies metamorphic rocks prevail containing mere
relicts of a previous high pressure metamorphic event (Davis, 1972; de
Smeth, 1975; Salemink, 1980). The islands of Naxos and Paros show
amphibolite facies metamorphism and migmatite formation (Jansen and
Schuiling, 1976; Papanikolaou, 1980). On the islands of Naxos and
Seriphos, for instance, granodiorite intrusions produced contact
metamorphic aureoles and contact metamorphic rocks (Jansen, 1977;
Salemink, 1980).
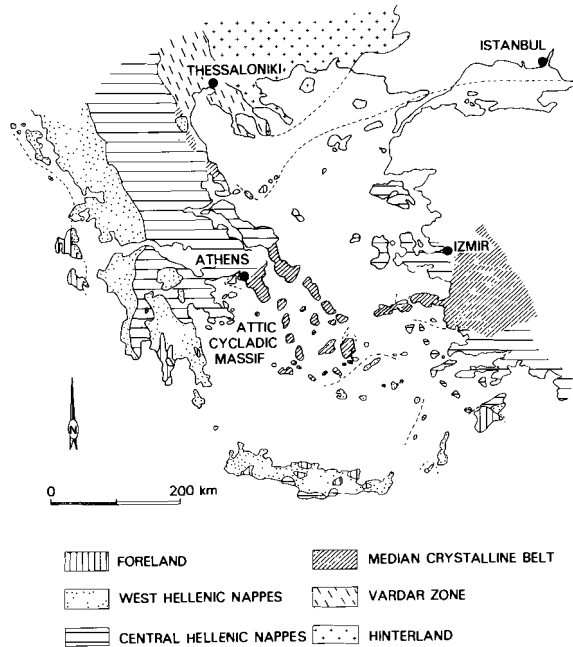
Fig.1: The Hellenides with the Attic-Cycladic Massif.
(after Durr et al.,1978).

In the polymetamorphic rocks of the Attic-Cycladic Massif at least three regionally metamorphic phases can be distinguished (Marinos,1978; van der Maar and Jansen, 1983):

1: a M1 regional metamorphic, high pressure glaucophane schist facies metamorphic event dated at 50 - 40 Ma (Fytikas et al.,1976; Altherr et al.,1979; Andriessen, 1979).

2: a M2 regional metamorphic, medium pressure greenschist facies metamorphic event with thermal domes with amphibolite facies metamorphism and migmatite formation. This event is dated at 30 - 20 Ma (Altherr et al.,1979; Andriessen, 1979).

3: a M3 phase with low pressure contact metamorphism associated with local granitoid plutonism dated at around 10 Ma (Wendt et al.,1977 Durr et al.,1978; Altherr et al.,1982).

Fig.2: Location of Seriphos in the Attic-Cycladic Massif.
Distribution of the metamorphic rocks: 1: B: Pre-Alpine
Basement; 1: M1 glaucophane schist facies to glaucophane
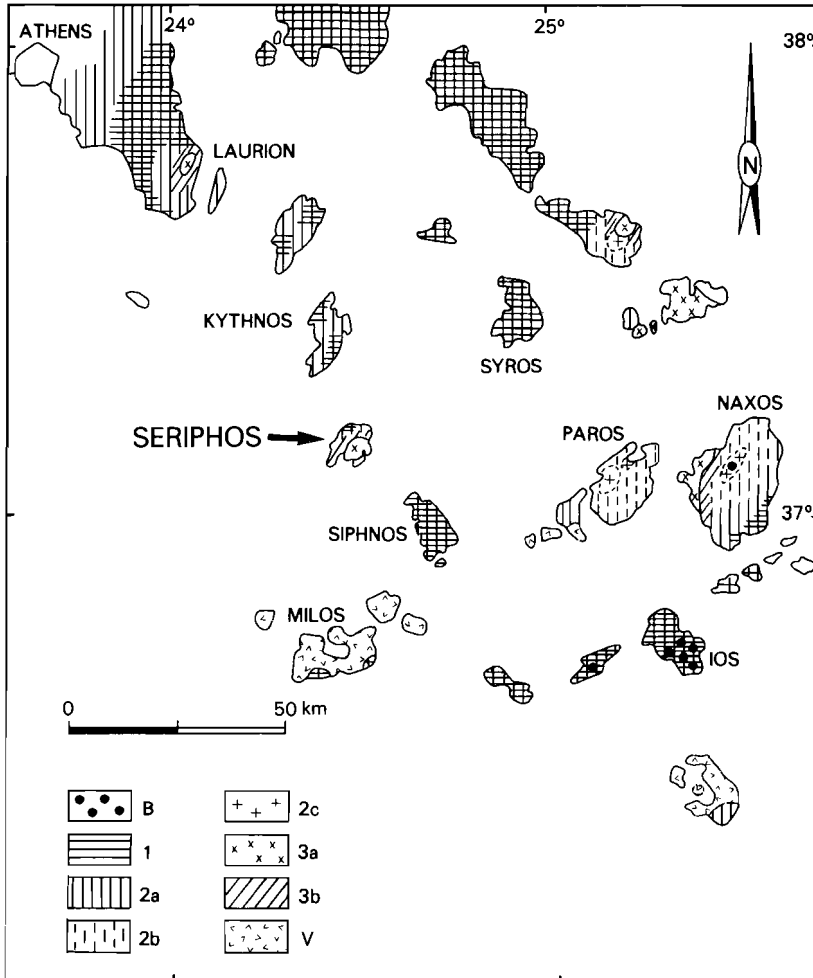greenschist facies metamorphism; 2a: M2 greenschist facies
metamorphism; 2b: M2 amphibolite facies metamorphism;
2c: M2 migmatite; 3a: Late Alpine granodiorite; 3b: M3
contact metamorphism; V: Pliocene to Recent volcanism.
(after van der Maar and Jansen, 1983).

19.

At Seriphos the apex of a granodiorite pluton is exposed which intruded into a sequence of metasedimentary rocks consisting of gneisses, marbles and carbonatic schists (see fig.3). In the metasediments only some rare relicts are preserved of the M1 regional glaucophane schist facies metamorphic event. The medium pressure M2 regional greenschist facies metamorphic event is well preserved in the northern parts of the island. The granodiorite intrusion produced a M3 contact metamorphic aureole and extensive skarn and ore formations in the country rocks and it led to the formation of hydrothermal leaching zones within the plutonic rocks. According to Altherr et al.(1982) the intrusion took place 8 - 9 Ma ago

Nun zu oft ist diess der Gang der Geschichte.
Ueberhaupt ist Seriphos von den alten
Schriftstellern mit stiefmutterlichen
Unbilligkeit behandelt worden.

L.Ross: Insel Reisen, 1840.

CHAPTER III: GEOLOGY

The geology of Seriphos is largely determined by the granodiorite intrusion (Ballindas,1906; Ktenas,1917; Marinos,1951; Salemink,1980). The pluton takes the form of a dome-shaped body occupying the central and southern parts of the island. The metasedimentary country rocks occupy the areas surrounding the pluton (fig.3).

The intrusion of the granodioritic magma caused an overall updoming of the surrounding country rocks. The updoming was accompanied by local scale folding and faulting. The shape of the dome structure indicates that only the apical reaches of the plutonic body are exposed at the present level of erosion (see also fig.4). The flattening of the dome structure from central Seriphos towards the north-west suggests a further expansion of the apex of the pluton in that direction. The contact surface between the intrusive and the country rocks is sharp and well-defined.

The PLUTONIC ROCK at Serihpos is a biotite-hornblende granodiorite. It is present in two facies:
The main mass of the intrusive body consists of non-foliated, fine-grained, equigranulair rocks in which the grain size seldomly exceeds 2 mm. The rock is cut by numerous small fractures that are often curved. Along the fractures hydrothermal leaching produced bleached zones of one to several cm wide from which the dark, mafic constituents of the granodiorite have almost completely disappeared. (Plate 1).

SIMPLIFIED GEOLOGICAL MAP OF SERIFOS GREECE

37° 15'

0   1   2 km

N

W

37° 10'

37° 05'

E

+ +	GRANODIORITE
	BORDERFACIES OF GRANODIORITE
	SCHIST-UNIT
	MARBLE-UNIT
	GNEISS-UNIT
	MASSIVE SKARNZONE
■	SPHALERITE-GALENA
●	HEMATITE-LIMONITE
X	MAGNETITE-PYRITE

ISOGRADS :

—·—·— ACTINOLITE	—— INTRUSIVE CONTACT
– – – DIOPSIDE	– – – – FAULT
– – – – – SCAPOLITE	
·········· GARNET	

1000
500
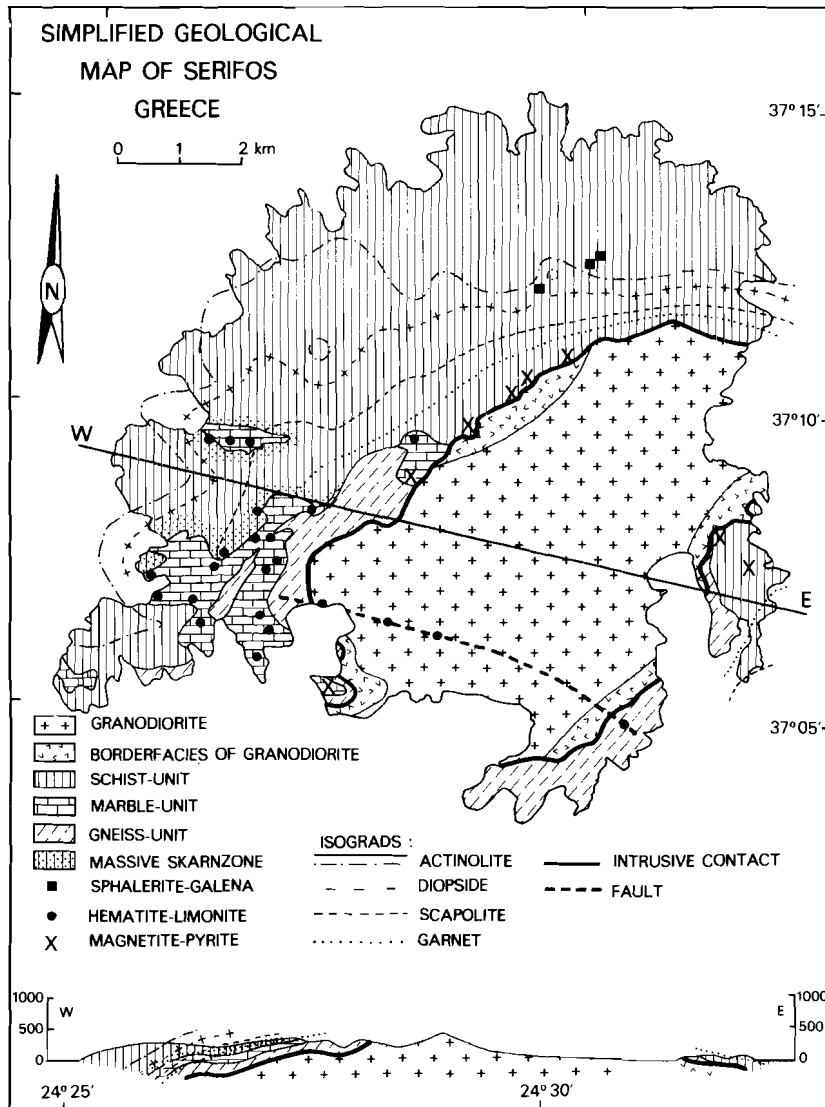0
W

1000
500
0
E

24° 25'   24° 30'

Fig.2: Simplified geological map of Seriphos with a schematic
W–E section.
The magnetite deposits are specifically formed in the
apical parts of the intrusive system, in country rocks
close to the intrusive contact. At larger distances
from the intrusive hematite–limonite deposits are
concentrated in the marble units. (see also fig.4).

22.

GRANODIORITE
GNEISS
MARBLE
HORNFELS
SCHIST
BORDERFACIES
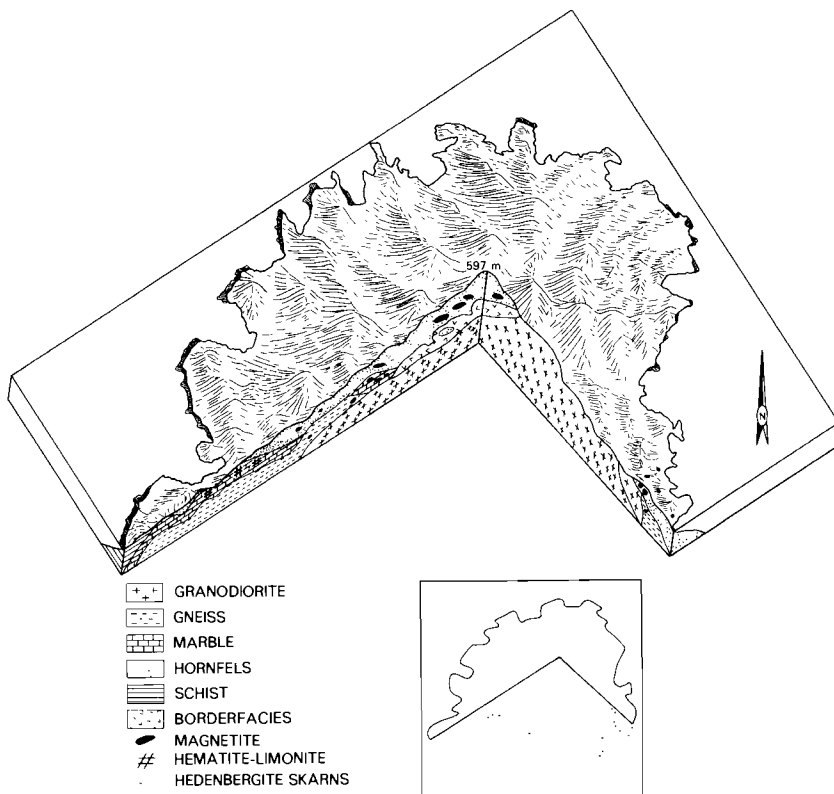MAGNETITE
HEMATITE-LIMONITE
HEDENBERGITE SKARNS

Fig.4: Stereographic diagram of Seriphos, as seen from the south.
(from Marinos, 1951).

In several places close to the intrusive contact, mainly in
areas where the contact surface is flat-lying, the fine-grained main
body granodiorite grades into a borderfacies which is coarser grained
(the average grain size in the borderfacies is about 5 mm) and contains
dioritic enclaves (see fig.3). The enclaves are fine-grained (average
grain size about 1 mm), oval in shape and 2 to 10 cm in diameter. The
contacts between the enclaves and the surrounding granodiorite are
sharp and well-defined and there is no reaction rim. In the field it
was estimated that 1 - 2 % of the total rock volume of the borderfacies
is occupied by the dioritic enclaves. The complex pattern of the small,
curved fractures with the hydrothermal leaching zones, which is typical
for the main mass of the granodiorite, is missing in the coarse-grained
plutonic margins. In the borderfacies fractures are simple and straight

23.

and hydrothermal bleaching is not evident along the fractures. Occasionally the coarse-grained granodiorite rock is replaced by Ca-Fe-Mg endoskarns.

Numerous dikes radiate from the main mass granodiorite into the surrounding rocks of the borderfacies and the metasedimentary series (figs. 5,6). The compositions of the dikes vary from dioritic to granitic but granodioritic compositions prevail. The textures of the dikes are equigranular to porphyritic. Along cracks and fractures the dikes may contain medium and low temperature skarn mineralizations.

In the METASEDIMENTARY COUNTRY ROCKS three stratigraphic units are distinguished: a lower unit of quartz-rich paragneisses; a middle unit composed of lower dolomitic marbles and upper calcitic marbles; and an upper unit of carbonatic schists (fig.3). The three rock units constitute a concordant, stratigraphic sequence.

The lower gneisses are composed of alternating quartzo-feldspathic and biotite-amphibole bands which in general are several mm thick. Locally quartz-rich and quartzitic patches occur that lack the gneissic banding. In other places the gneisses mainly contain mafic minerals and the leucocratic bands are almost lacking. In the upper parts of the gneiss series a few serpentinite bodies are present. In SE-Seriphos marble intercalations up to a few meters thick occur. Near the intrusive contact metasomatic deposits of Ca-Fe-Mg skarns and Fe-ores have been formed. The thickness of the lower gneiss-unit is at least 150 meter.

The marbles of the middle unit conformably overlie the gneisses. In southwestern Seriphos the unit is about 70 m thick. Towards the east the thickness gradually diminishes. In central Seriphos the marble-unit is about 5 m thick. In eastern Seriphos the marbles are completely wedged out. In the lower part of the unit the marbles are grey, dolomitic and thin-bedded with individual beds varying between 1 and 5 cm. The upper part of the marble-unit consists of massive, white calcite marbles with individual beds reaching up to 3 m thick. Both marble series contain quartz lenses often showing boudinage. The dolomitic marbles may also contain appreciable amounts of disseminated
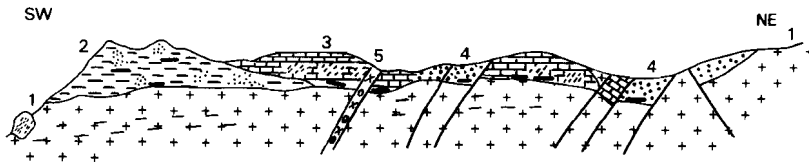
Fig.5: Profile across the intrusive contact in central Seriphos
       (Bounies).
       1: granodiorite; 2: gneiss with garnet skarns; 3: marble
       with diopside skarn; 4: hornfels; 5: granitic porphyrite.
       The magnetite deposits (black) are concentrated near the
       intrusive contact. (from Marinos, 1951).

quartz. In the silica-bearing dolomitic marbles abundant talc is
present which, at least partially, seems to be of hydrothermal origin.
Close to the intrusive contact the siliceous dolomites are partially
replaced by contact metasomatic magnetite deposits and associated
pyroxenite skarns. In both marble series medium and low temperature
hydrothermal activities produced large, irregularly shaped bodies of
brown ankeritic dolomite and hematite-limonite iron ore.

     The upper unit of the country rocks consists of carbonate-rich
schists. In the schist series mica-rich parts of several cm thick
alternate with white colored marble intercalations of similar
dimensions, and with quartz lenses. Locally massive banks of white
calcite marble up to 2 m thick occur. Carbonate-free sections are
present in other parts within the unit. In the calcite schists
metasomatic activities produced abundant Ca-Fe-Mg skarns and Fe-ore
deposits. The thickness of the marble schist-unit is at least 500 m.

     CONTACT METAMORPHISM produced a contact aureole in the country
rocks surrounding the granodiorite pluton (see fig.3).
     At large distances from the intrusive contact the metasedimentary
country rocks contain epidote, chlorite, white mica, albite, quartz and
calcite, which is a typical medium-pressure greenschist facies mineral
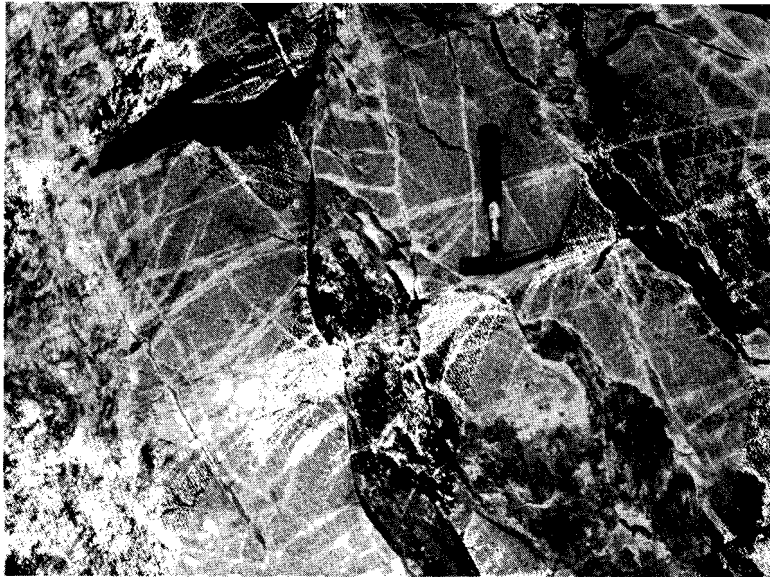
Plate 1: Bleached zones along the small, often curved fractures
in the main body of the granodiorite pluton (loc. 9.2).

Plate 2: Pneumatolytic magnetite deposit in brecciated, epidotized
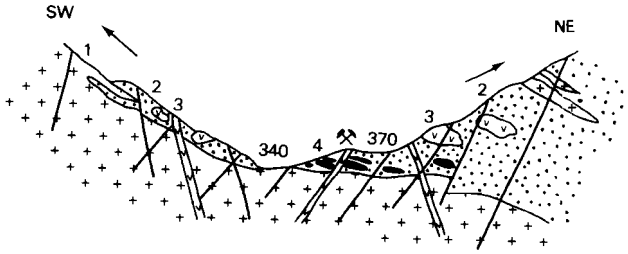hornfelses (loc. 27.7).

26.

Fig.6: Profile across the intrusive contact in central Seriphos
      (Playa).
      1: granodiorite; 2: hornfels (with garnet skarns); 3: aplites
      and porphyrites; 4: magnetite deposits. (from Marinos, 1951).

association. In a few places the relict presence of glaucophane points
to an early, high pressure glaucophane schist facies metamorphic event
prior to the regional greenschist facies metamorphism.

      Towards the intrusive contact the regional metamorphic
greenschists grade into low-pressure greenschist and amphibolite facies
contact metamorphic rocks. In the contact aureole a number of isograds
have been mapped that indicate the increasing intensity of contact
metamorphism in the direction of the intrusive contact.

      The CONTACT METASOMATIC FORMATIONS at Seriphos are predominantly
developed in Si-containing rocks. In pure marbles skarn formations are
rare. Metasomatism mainly affected the country rocks close to the
intrusive contact, but metasomatic deposits also occur along fractures
and other permeable zones at larger distances from the intrusive
contact and along fractures in the granodiorite intrusive (see fig.3).

      High temperature pyroxene-garnet skarns and magnetite-pyrite
deposits occur in irregularly shaped, massive concentrations up to
several thousands m^3 in volume in siliceous country rocks close to the
intrusive contact (see figs. 5,6)(Plate 2). They are mainly developed
in areas where the contact surface between granodiorite and country
rocks is flat-lying or subhorizontal (fig.4).

27.

Up to larger distances from the intrusive contact epidote-actinolite-hematite deposits have formed in dm to cm wide veins cross-cutting the siliceous host rocks as well as the previously formed high temperature skarn and ore deposits. The same minerals are present in the central parts of the bleached zones in the granodiorite pluton. In contrast to the high temperature skarns the medium temperature epidote-actinolite mineralizations also occur as replacement products in aplitic dikes. In southwestern Seriphos a massive zone of hedenbergite-ilvaite skarns has formed in an up to 30 m thick zone situated just on top of the underlying marble series (see fig.3). In northern Seriphos a few small deposits of sphalerite-galena-hematite ore occur.

The low temperature stages of the metasomatic evolution at Seriphos are manifested by mm-thin veins and geodic occurrences of hematite-limonite iron ore with associated mineralizations of barite and fluorite and occasionally malachite or chrysocolla. In the granodiorite an up to 3 m thick body composed of a tight network of low temperature hematite/limonite-barite-fluorite veins occurs along a major fault structure cross-cutting the entire granodiorite pluton from E to W (see fig.3).

In pure marbles the only noteworthy metasomatic alterations are medium temperature formations of brown-colored, ankeritic dolomite and low temperature deposits of hematite/limonite-barite-fluorite. Ca-Fe-Mg skarns are only formed in silica-bearing, dolomitic marbles, or at the contacts of pure marbles with siliceous metasedimentary rocks, granodiorite apophyses or aplitic dikes.

The subterranean inanimate bodies are divided
into two classes, one of which, because it is a
fluid or an exhalation, is called by these names,
and the other class is called the minerals.

Agricola, De Natura Fossilium, 1546.

CHAPTER IV: PETROLOGICAL EVOLUTION

Combination of structural, petrological and mineralogical evidence
leads to a reconstruction of the sequence of physico-chemical events
associated with the granodiorite intrusion at Seriphos. Comparison with
experimental studies and observations on similar, natural occurrences
in other places indicates the P,T-conditions at which the events took
place.

DEPTH OF INTRUSION

The intrusion of the granodiorite was shallow. This is indicated
by the dome-structure of the pluton and by the sharp, well-defined
contacts between the plutonic and the country rocks. A stratigraphic
reconstruction is not possible at Seriphos, but some indication of the
intrusion depth can be obtained by comparing the skarn and ore
formations at Seriphos with similar occurrences in well-known areas.
The study of Popov (1967) concerning the depth of formation and
vertical extent of comparable skarn and ore formations in the western
parts of the Altai Mountains (U.S.S.R.) suggests a formation depth for
the irregular shaped, massive magnetite-pyroxene-garnet skarn bodies at
Seriphos of 3.0 to 3.5 km. The review of Gorzhevskii and Kozerenko
(1967) of the vertical differentiation of ore formation in occurrences
with known formation depths points to a similar depth of formation for
the Seriphos deposits of about 3 - 4 km. A depth of 3 - 4 km for the

Plate 3: Hornblende-biotite granodiorite from Seriphos with cored
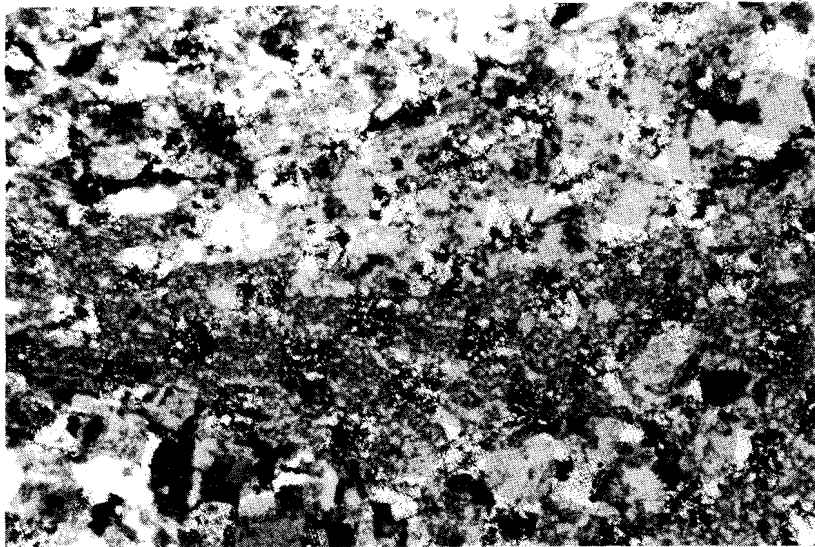and zoned plagioclase (sample no. 9.2A, 25x).

Plate 4: Mylonite in the central parts of a bleached zone in the
granodiorite (see also Plate 1)(sample no. 9.3C,10x).

now exposed apical parts of the intrusion corresponds with a
lithostatic pressure of about 1 to 1.5 kbar and a hydrostatic
equilibrium pressure of around 300 bar at the time of emplacement of
the granodiorite pluton. Fluid inclusions data from Seriphos indicate
hydrostatic equilibrium pressures of some 300 bar (see Chapter VI).

THE INTRUSION

The main mass of the granodiorite pluton at Seriphos is a fine-
grained biotite-hornblende granodiorite with plagioclase, quartz,
K-feldspar, biotite and hornblende as main components and apatite,
sphene, orthite, zircon and magnetite as the major accessory
constituents. The plagioclase grains are subhedral to euhedral in shape
and the crystals are usually zoned with normal and recurrent zoning
both present. Twinning is common (albite as well as Karlsbad). Some of
the plagioclase grains contain a rounded core which is unzoned or only
weakly zoned (Plate 3). The cores frequently contain inclusions of
hornblende, biotite and/or apatite. Partial alteration of the
plagioclase to fine grained white mica is common and usually more
intense in the cores than in the surrounding mantles. The composition
of the plagioclases varies from andesine to oligoclase (An40 to An20)
in the zoned mantles and in the rounded cores it is andesine-oligoclase
(An30). The hornblende in the granodiorite is dark olive-green in color
and its subhedral grains often show simple twinning. Biotite is usually
partially altered to chlorite. K-feldspars (both othoclase and
microcline) and quartz occur interstitially in anhedral grains and they
represent the latest crystallization products of the granodioritic
magma. Chemical compositions and CIPW-norms of three granodiorite
samples are given in table I. In fig.7 the granodiorite compositions
are plotted in a normative Qz-Ab-Or diagram; the samples plot near the
5 - 10 kb eutectic minima for water saturated conditions as given by
Luth (1969).
The temperature of the intruding granodioritic magma must have
been between its liquidus and its solidus temperature. This is

TABLE I

Chemical analyses and CIPW-norms of various igneous rocks from Seriphos.

	1	2	3	4	5	6	7	8	9	10	11	12
	ON 9.3C	ON 9.3D	ON 9.3E	RG 11.1	DV 106B	GG 21.12	GG 8.4	GG 7.5	GG 2.1	GE 9.2D	GE 9.2E	GE 9.3
SiO_2	67.03	65.92	65.14	66.53	53.56	75.59	69.85	71.14	74.98	68.13	67.38	69.14
Al_2O_3	15.51	16.93	16.32	15.25	21.34	17.93	14.85	14.74	13.21	15.87	16.28	15.52
Fe_2O_3	1.84	2.15	2.13	1.84	5.60	2.87	1.30	1.41	0.07	0.34	0.73	0.43
FeO	1.09	1.20	1.13	1.70	1.96	4.58	1.17	1.05	0.09	0.32	0.60	0.23
MnO	0.04	0.05	0.05	0.03	0.12	0.10	0.04	0.03	0.01	0.02	0.03	0.02
MgO	1.64	1.88	1.84	1.84	3.01	3.40	1.16	0.58	0.11	0.64	1.37	0.58
CaO	4.20	4.12	4.01	3.85	7.13	6.42	3.70	2.59	0.29	3.75	3.34	3.42
Na_2O	4.52	4.49	4.30	3.95	4.61	3.41	3.86	3.81	2.91	6.40	5.36	7.42
K_2O	2.10	2.52	2.36	2.86	1.67	1.79	3.12	2.72	5.31	1.96	3.64	1.42
TiO_2	0.57	0.56	0.55	0.64	0.65	1.32	0.57	0.51	0.11	0.39	0.38	0.30
P_2O_5	0.06	0.05	0.04	0.06	0.04	0.08	0.06	0.04	0.01	0.05	0.05	0.04
H_2O^+	0.58	0.98	1.26	0.54	0.60	1.25	0.72	0.68	0.89	2.04	1.20	1.78
H_2O^-	0.10	0.03	0.16	1.01	0.25	0.37	0.31	0.25	0.33	0.16	0.24	0.05
Total	99.28	100.88	99.29	100.10	100.54	101.11	100.71	99.55	98.32	100.07	100.60	100.35
Qz	20.6	17.4	19.0	20.4	1.3	9.3	24.7	30.3	35.4	15.4	13.3	13.6
C	-	-	-	-	-	-	-	1.1	2.5	-	-	-
Or	12.7	15.0	14.2	17.3	9.7	10.7	18.5	16.5	32.7	11.7	21.3	8.3
Ab	41.2	40.2	39.3	36.0	41.3	31.0	34.8	35.0	27.2	57.5	47.7	66.3
An	16.0	18.5	18.5	15.7	32.5	28.7	14.2	12.7	1.5	8.8	9.5	4.8
Wo	1.9	0.5	0.5	1.2	0.9	1.1	1.7	-	-	3.7	2.7	4.5
En	4.5	5.2	5.2	5.2	8.3	9.5	3.3	1.6	0.4	1.7	3.7	1.6
Hy	0.5	0.5	0.5	1.5	-	5.5	0.9	0.8	0.1	0.3	0.5	0.1
Mt	2.0	2.2	2.3	2.0	4.8	3.1	1.4	1.5	-	0.3	0.8	0.4
Hm	-	-	-	-	0.6	.	.	.	0.1	-	-	-
Ru	0.4	0.4	0.4	0.5	0.4	0.9	0.4	0.3	0.1	0.4	0.3	0.2
Cp	0.2	0.1	0.1	0.2	0.2	0.2	0.1	0.2	-	0.2	0.2	0.2
$\rho(gr/cm^3)$	2.67	2.64	2.63	2.66	2.76	2.72	2.62	2.62	2.53	2.60	2.48	2.57

no. 1: unaltered granodiorite from the main intrusive body (sample no. 9.3C) [1])
   2:   "   "   "   " " " " " ("   9.3D)
   3:   "   "   "   " " " " " ("   9.3E)
   4: granodiorite from the borderfacies   ("   11.1)
   5: dioritic enclave from the borderfacies   ("   106B)
   6: eqnigranular hornblende-biotite-granodiorite dyke   ("   21.12)
   7: porphyritic hornblende-granodiorite dyke   ("   8.4)
   8:   "   biotite granophyre   ("   7.5)
   9:   "   rhyolite   ("   2.1)
 10: bleached zone from the main body granodiorite   ("   9.2D)
 11: "   "   " " " " "   " ("   9.2E)
 12:   "   "   " " " " "   " ("   9.3)

1) For sample locations see Appendix

Analyses mainly by ICP; Si by XRF; Fe^{II}/Fe^{III} titriometric

32.

indicated by the presence of the unzoned, rounded oligoclase-andesine cores inside the zoned plagioclase mantles (Piwinskii, 1968; Chapell, 1978). The plot of the normative Qz,Ab,Or-values of samples from unaltered main body granodiorite in the Qz-Ab-Or triangle of fig.7 suggests that it formed by anatexis of deep-seated rocks, possibly at pressures of some 5 to 10 kb. According to the experimental data combined by Wyllie (1977) granodioritic magmas with biotite and hornblende components in solution and residual plagioclase crystals in suspension can be formed by anatexis at moderate water pressures, resulting in magmas with about 2 - 5 wt% H_2O. At total pressures of 5 to 10 kb such magmas would form at temperatures somewhat above 900°C and the melts probably are crystal mushes containing some 20 to 40 % crystals (Wyllie, 1977). According to experimental studies of the melting relations in synthetic and natural granodiorite mixtures the order of crystallization in the Seriphian granodiorite (plagioclase → hornblende → biotite → K-feldspar → quartz) points to a solidification range for the intruded magma at Seriphos from about 900 to about 750°C taking an overall pressure of some 1 kb and a water content of 2 - 5 wt% H_2O in the magma (Piwinskii, 1973; Whitney, 1975; Winkler, 1979).

The main body granodiorite was strongly affected by a stage of (auto-)brecciation at or near the time of its final solidification. Large biotite crystals of 5 mm in size, which are occasionally present in the fine-grained main body granodiorite, are usually tectonically bent or broken and in all its exposures the main body granodiorite is cut by numerous small fractures and fracture zones in an irregular, complex and often curved pattern. Along the fractures post-magmatic, hydrothermal processes produced cm-wide bleached zones (Plate 1). The bleached zones, which are often strongly brecciated, mainly consist of albite and quartz and minor sericite (Plate 2). Locally within the bleached zones small amounts of medium and low temperature 'endoskarns' occur with epidote, actinolite, pyrite, hematite/limonite, quartz and calcite as main minerals and barite and fluorite as occasional formations. In table I the chemical compositions and CIPW-norms are

33.

given of three samples from the bleached granodiorite. The plot of the samples in the Qz-Ab-Or trangle of fig.7 clearly shows the effect of the post-magmatic, hydrothermal alteration (albitization).

The leaching of the granodiorite must have occurred at or near the time of the final solidification of the main mass of the granodiorite pluton, during a stage of degassing and (auto-)brecciation. As a result of the hydrofracturing bulk rock permeabilities must have increased sufficiently to allow the circulation of high-temperature fluids along the newly formed transport channels and the leaching of the granodiorite along the fractures. The leaching probably occurred at temperatures between 750 and 450^{0}C (see below). At lower temperatures the action of the hydrothermal fluids reversed and the leaching of Fe-Mg components was followed by a precipitation of epidote/actinolite-hematite-pyrite-quartz-calcite deposits in the inner parts of the bleached zones. Such deposits may form at temperatures between 450 and 300^{0}C (see below). The medium-temperature actinolite-hematite deposits were followed by still later precipitations of hematite/limonite-barite fluorite in the central parts of the veins (fractures), evidencing a further temperature drop to temperatures below 300^{0}C.

The coarse-grained, enclave containing borderfacies of the granodiorite probably formed as a 'chilled margin' some time before the final solidification of the main mass of the pluton. The mineralogy of the borderfacies is in conformity with the mineralogy of the main mass of the granodiorite with green hornblende, biotite, cored and zoned oligoclase-andesine, orthoclase, microcline and quartz as major components and sphene, apatite, zircon, orthite and magnetite as main accessory constituents. The chemical composition of the borderfacies is the same as the chemical composition of the main body granodiorite (see table I). There is no evidence for substantial chemical changes in the borderfacies due to assimilation of the nearby, calcic country rocks.

The identical mineralogical and chemical composition of the two granodiorite facies indicate that both facies originated from the same magma. The coinciding plot of the two granodiorite types in the Qz-Ab-Or triangle of fig.7 confirms their common origin. In the
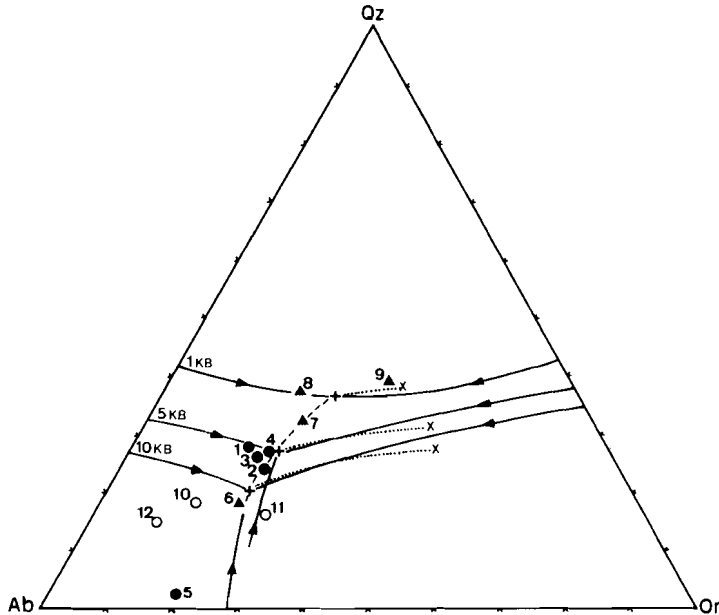
Fig.7: Normative Qz–Ab–Or diagram (wt%) for the granitoid rocks on
Seriphos. Dots represent rocks from the plutonic body; triangles
represent dike samples. Unaltered rocks are indicated by solid
solid symbols; open symbols present altered rocks (see table I).
The solid curves are isobaric cotectic lines in the water
saturated system Qz–Ab–Or for 1, 5 and 10 kbar respectively. The
dashed curve joins the water saturated eutectic and minima
points between 10 and 1 kb. The dotted curves indicate the
the approximate direction of the shift of the eutectic and
minima points from the water saturated system (+) to the water
free system (x) for 1, 5 and 10 kb respectively (Luth, 1969).

borderfacies, however, K-feldspar has a subhedral grain shape similar
to hornblende, biotite and plagioclase (in the main body K-feldspar is
interstitial between those minerals). Biotite crystals, usually 5 mm in
size, are not bent or broken as in the main mass of the pluton. The
fractures in the 'chilled margins' usually are straight and they
continue into the adjacent country rocks. The post-magmatic leaching
features, which are typical for the main body granodiorite, are

35.

generally lacking along the fractures in the borderfacies. In the 'chilled margins' the mafic minerals are partially replaced by alteration products such as actinolite, chlorite and sericite. Locally the borderfacies granodiorite is replaced by pyroxene and garnet skarns and by magnetite deposits.

The fine-grained dioritic enclaves in the borderfacies are composed of the same mineral components as the surrounding granodiorite, but their abundances differ in accordance with the compositional difference between the two rock types (see table I). Subhedral green hornblende, biotite and cored and zoned plagioclase (oligoclase-andesine) are more abundant in the dark-colored enclaves than in the surrounding granodiorite, while interstitial K-feldspar and especially interstitial quartz are less frequent. Sphene is a dominant accessory constituent in the dioritic xenoliths.

The plot of the normative composition of a dioritic enclave in the Qz-Ab-Or diagram of fig.7 clearly shows that the enclaves are not in equilibrium with the surrounding granodiorite. The similarity in mineralogy between the xenoliths and the granodiorite, however, points to a cogenetic relationship between the two rock types and possibly the enclaves represent a refractory residuum from the original melting process (Didier, 1973; Chapell, 1978; Pitcher, 1979). The exclusive occurrence of the oval-shaped dioritic enclaves in the borderfacies of the granodiorite might be due to the more rapid cooling of the chilled margins; in the main mass of the pluton prolonged reaction and desintegration must have resulted in their complete obliteration.

Magmatic dikes penetrate the metasedimentary country rocks as well as the borderfacies granodiorite and the apical reaches of the main mass of the intrusive body. Their compositions are predominantly granodioritic but dioritic and granitic compositions also occur (see Table I). The textures vary from equigranular to porphyritic. The mineralogy of the dikes is essentially the same as the mineralogy of the plutonic rocks with cored and zoned oligoclase-andesine plagioclase, green hornblende, biotite, K-feldspar and quartz as major components and sphene, apatite, zircon and ore minerals as accessory

constituents. Usually green hornblende and biotite are both present, but in some dikes only one of the two mafic minerals occurs. K-feldspar is often myrmekitic.

The dikes probably represent magmatic seggregations from the bulk mass of the granodioritic magma. This is indicated by their mineralogy and also by the plot of a number of representative dike samples in the Qz-Ab-Or diagram of fig.7. The two samples of granodiorite dikes plot near the water-saturated, polybaric granitic minima line near the main body granodiorite rocks but at different 'formation pressures' (slight changes in the chemical composition of the rocks may be due to the assimilation of carbonatic country rocks or from post-magmatic, metasomatic alterations). The samples of a porphyritic biotite granophyre and a porphyritic rhyolite plot respectively near the water-saturated granitic minimum at 1 kb and near the granitic minimum in the dry Qz-Ab-Or system at 1 kb. This suggests that differentiation processes were active during the magmatic evolution of the Seriphian intrusion.

The aplitic and porphyritic dikes may cross-cut previously formed high-temperature pyroxene-garnet skarns, but in their turn the dikes may be replaced by medium-temperature epidote-actinolite mineralizations. Apparently a major stage of aplite intrusion occurred after the emplacement and solidification of the now exposed apical reaches of the granodiorite pluton and after the formation of the high-temperature skarn deposits, but before the formation of the medium-temperature hydrosilicate deposits.

CONTACT METAMORPHISM

The paragneisses of the lower unit of the metasedimentary country rocks are exposed only within the reaches of the contact metamorphic aureole (see fig.3). Their main constituent is quartz, which often shows the polygonal development typical of hornfelses. Plagioclase is a minor rock component; its composition varies from oligoclase in Ca-poor biotite-gneisses to labradorite-bytownite in Ca-rich diopside gneisses

37.

TABLE II

Chemical analyses of representative samples
of Seriphian gneisses, schists and hornfelses.

	13	14	15	16	17	18	19	20	21	22	23	24
	20.14	10.6	20.15	20.17	8.3	26.6	27.42	7.4B	9.6	20.24	140-1	139-1
SiO_2	67.02	47.52	59.24	54.83	36.31	52.74	53.50	41.81	36.66	38.16	54.62	59.73
Al_2O_3	14.06	16.33	14.60	19.55	10.25	15.37	18.38	16.76	16.60	14.76	13.80	9.40
Fe_2O_3	0.17	2.08	2.24	1.44	3.68	1.35	5.80	1.97	6.32	3.75	1.27	1.16
FeO	4.89	7.26	3.59	4.74	0.95	4.67	1.38	10.83	4.60	9.20	8.48	10.32
MnO	0.04	0.11	0.07	0.10	0.07	0.15	0.09	0.16	0.16	0.13	0.10	0.12
MgO	1.67	7.42	3.39	1.86	2.60	3.13	1.98	7.60	6.69	7.08	4.02	4.53
CaO	3.59	10.38	7.69	11.71	22.27	6.69	9.43	12.61	22.91	16.20	4.73	5.13
Na_2O	5.38	4.82	3.55	2.63	3.21	3.56	5.00	3.92	1.45	4.14	0.64	2.74
K_2O	1.56	0.31	3.50	1.78	2.04	2.85	1.43	0.40	0.25	0.67	7.78	3.89
TiO_2	0.60	0.65	0.40	0.84	0.37	0.58	0.58	1.29	1.25	0.72	0.68	0.44
P_2O_5	0.04	0.02	0.04	0.17	0.43	0.07	0.35	0.90	0.12	0.06	0.13	0.06
H_2O^+	0.82	1.81	1.32	0.56	17.28[*]	9.23[*]	1.79	0.84	1.56	2.03	2.64	2.76
H_2O^-	0.43	0.32	0.76	0.43	0.03	0.41	0.69	0.27	0.43	0.12	0.12	0.58
Total	100.27	99.03	99.49	100.64	99.49	100.85	100.20	99.36	99.00	99.02	99.01	100.86
$\rho(gr/cm^3)$	2.64	2.84	2.64	2.71	2.73	2.69	2.81	2.68	3.04	2.90	2.50	2.64

no.13: biotite gneiss   (sample no. 20.14) [1]
  14: hornblende gneiss   (" 10.6)
  15: epidote-hornblende gneiss   (" 20.15)
  16: epidote-diopside-hornblende gneiss   (" 20.17)
  17: quartz-albite-epidote-calcite schist   (" 8.3)
  18: quartz-albite-calcite schist   (" 26.6)
  19: quartz-albite-epidote schist   (" 27.42)
  20: hornblende hornfels   (" 7.4B)
  21: scapolite-hornblende hornfels   (" 9.6)
  22: epidote-scapolite-hornblende hornfels   (" 20.24)
  23: hornblende hornfels relict from the massive skarnzone   (" 140-1)
  24: " " " " " " " (" 139-1)

[1] For sample locations see Appendix
[*] Mostly CO_2

Analyses mainly by ICP; Si by XRF; Fe^{II}/Fe^{III} titriometric

close to the intrusive contact. The dark bands of the gneisses typically consist of biotite with green hornblende and/or diopside. In the stratigraphic lower parts of the gneiss series biotite is the dominant dark mineral while in the more calcareous, higher levels of the series hornblende and diopside are more abundant. K-feldspar and/or muscovite may be present in small amounts. In Ca-rich gneisses rounded grains of epidote appear and occasionally small grains of contact metamorphic, isotropic garnet occur. Calcite is present in local marble

intercalations. Sphene, zircon, apatite and magnetite are accessory constituents. In table II chemical compositions of three representative gneiss samples are given. In fig.8 the gneiss compositions are plotted in an ACF-diagram together with the mineral parageneses for low-pressure amphibolite metamorphism.

In the gneisses quartz and feldspar are present in strongly elongated crystals as well as in typically contact metamorphic aggregates of fine-grained, polygonal crystals. The dark minerals are present in idiomorphic crystals arranged parallel to the lineation of the gneisses as well as in later formed, idiomorphic crystals with random orientations. Apparently the lineation of the gneisses was partly obliterated by later, contact metamorphic recrystallizations. In sections perpendicular to the lineation the texture of the gneisses is typically the texture of a medium pressure greenschist facies rock with quartz, plagioclase and epidote porphyroblasts embedded in a finer grained matrix of quartz-feldspar and biotite-amphibole-clinopyroxene bands or layers. Probably this lepidoblastic character of the gneisses is a relict of the pre-intrusive, overall-Cycladic, M2 greenschist facies metamorphic event.

The ultramafic intercalations in the gneisses predominantly consist of serpentine with magnetite. The rocks are highly tectonized but occasionally some rounded grains of relict olivine are still recognizable. The serpentinite rock is intersected by small, secondary veins with hematite and/or quartz or opal.

The marbles of the middle-unit of the stratigraphic sequence at Seriphos also are only exposed within the reaches of the contact metamorhic aureole (fig.3).

The thin-bedded, lower dolomitic marbles mainly consist of calcite and dolomite. The two carbonate minerals appear in fine-grained, mixed layers, and in separate calcite and dolomite beds. The more competent dolomitic beds often show boudinage. Minor quartz is regularly present in disseminated grains and in nodules. Locally some plagioclase occurs. Close to the intrusive contact the plagioclase is partially replaced by scapolite. Talc is abundantly present in lens-like concentrations and

around quartz nodules. Graphite is a subordinate but regular
constituent of the grey-colored, dolomitic marbles.

The upper calcite marbles predominantly consist of calcite. In the
white-colored, thick-bedded carbonate rock quartz is only a very minor
constituent. It is occasionally present in disseminated grains and in a
few quartz lenses. Due to boudinage the quartz lenses are usually
broken into drawn-out series of well-separated quartz nodules
Wollastonite was only found in calcite marbles in the south of
Seriphos, in a roof pendant composed of gneisses and marbles containing
gneissic intercalations (see below).

The upper unit of the marble-schists is continuously exposed
throughout the northern half of Seriphos, from well beyond the contact
metamorphic aureole up to the intrusive contact (see fig.2). Because of
this continuous exposure, and also because of its suitable chemical
composition, the marble-schists provide a good picture of the
metamorphic changes in the contact aureole.

In the outer reaches of the schist-series, outside the contact
aureole, the schists mainly consist of quartz, albite, white mica
(phengitic muscovite) and chlorite. Epidote/clinozoisite is a very
regular constituent in the regional metamorphic albite-sericite-
chlorite schists. Calcite is present in varying amounts, ranging from
a few disseminated grains in some schists to cm-thick marble
intercalations in others. Occasionally massive marble beds occur up to
1 m thick. Sphene, apatite and magnetite are common accessory minerals.
Hematite, pyrite and anatase are regular accessories. Graphite is
occasionally present. In all schist series small flakes of poorly
crystallized biotite appear within muscovite-chlorite aggregates.
Albite and quartz are typically present as porphyroblasts which are
often broken, distorted and/or rotated. In table II chemical
compositions of three representative samples of the outer greenschists
are given. In fig.8 the three schist samples are plotted in an
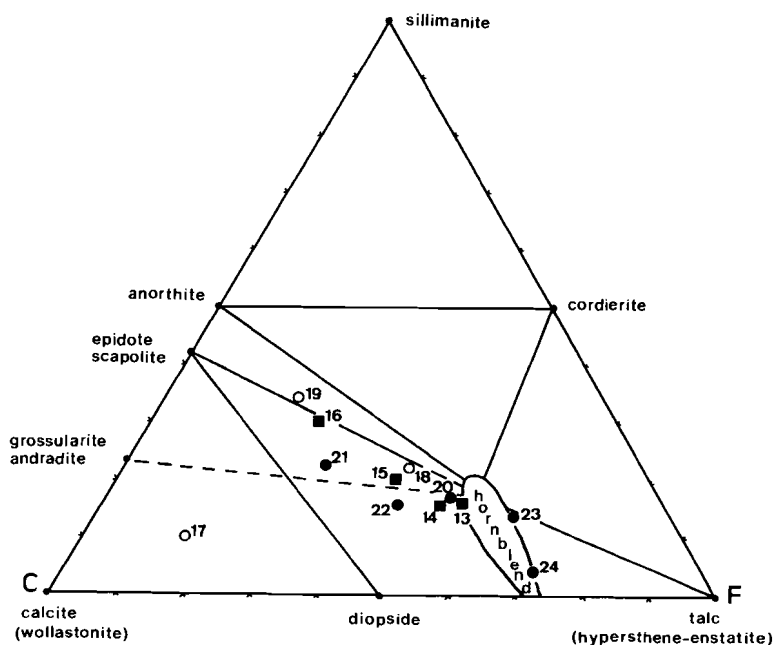ACF-diagram.

Fig.8: ACF-diagram for the metasedimentary rocks on Seriphos. Squares
represent gneiss samples; circles represent rocks from the
schist-unit. Open symbols indicate samples from regional
metamorphic greenschists; solid symbols indicate contact
metamorphic assemblages (see table II for individual analyses).
The ACF-diagram also gives the mineral associations for
low-pressure amphibolite facies metamorphism.

The equilibrium mineral assemblage albite + quartz + muscovite +
chlorite + clinozoisite + calcite (+ biotite), and the lepidoblastic
texture of the schists with the tectonically deformed and/or rotated
porphyroblasts of albite and quartz point to a low-grade, Barrovian
type of regional greenschist facies metamorphism, formed at
temperatures around $400\,^{0}C$ and pressures of about 3 - 4 kbar (Epstein
and Taylor, 1967; Myashiro, 1973; Winkler, 1979). The medium pressure
greenschist facies metamorphism at Seriphos probably coincides with the
overall-Cycladic, M2 medium pressure greenschist facies metamorphic
event postulated by van der Maar and Jansen (1983).

41.

In the regional metamorphic greenschists of northern Seriphos occasionally partially dissolved, relict blue amphibole crystals occur with a violet-colored crystal core. Within some albite porphyroblasts tiny, violet-colored amphibole inclusions were identified as glaucophane (Plate 5). The relict preservation of the glaucophanitic amphibole points to a high-pressure blueschist facies metamorphic event prior to the formation of the greenschists. This HP metamorphic event probably corresponds to the overall-Cycladic, M1 glaucophane schist metamorphic event postulated by van der Maar and Jansen (1983).

In the contact aureole four contact metamorphic zones are distinguished (see fig.3):

1: an outer zone of epidote-actinolite schists. The beginning of this zone is indicated by the first formation of blue-green actinolite from chlorite + calcite + quartz. The actinolite-isograd, marking the first appearance of actinolite in the field, is located at a distance of about 700 m perpendicular to the intrusive contact. Schurmann (1967) experimentally performed the actinolite-forming reaction in an Al-bearing system at temperatures between 440 and 410^{0}C at P_{H_2O} = 1000 bar and P_{CO_2} = 50 bar (P_{fluid} = P_{total}).

2: a zone of diopside-hornblende hornfelses. This zone begins with the first formation of light-green diopside from actinolite + calcite + quartz. The diopside-isograd is situated at a distance of about 500 m perpendicular to the intrusive contact. Metz (1970) experimentally simulated the diopside-forming reaction in an Al,Fe-free system. At P_{tot} = P_{fluid} = P_{CO_2} + P_{H_2O} = 1 kbar diopside formed at temperatures between 450 and 525^{0}C, depending on the X_{CO_2} of the coexisting fluid.

About 30 m nearer towards the intrusive contact green hornblende is first formed at the expense of still remaining actinolite and also by (partial) replacement of epidote and plagioclase. Towards the intrusive contact the amount of hornblende gradually increases and the composition of the coexisting plagioclase gradually changes from albite at the beginning of this zone to andesine at the inner side. Biotite gradually increases in abundance. Muscovite and epidote remain present. Sphene, apatite and opaques still are the main accessory constituents.
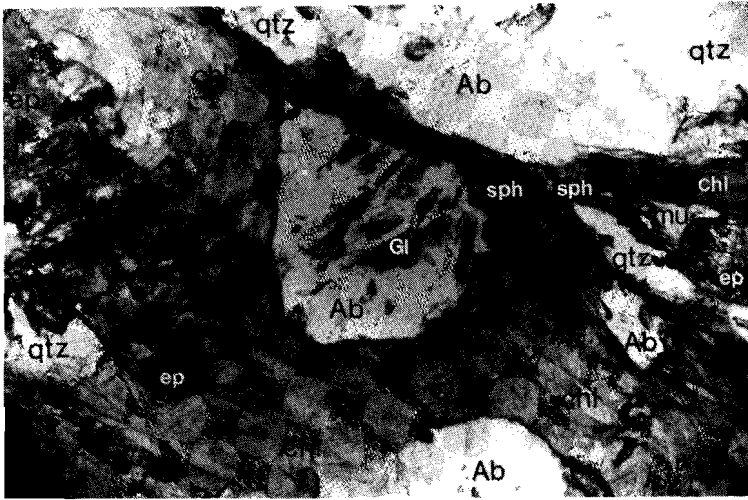
42.

Plate 5:Relict glaucophane inclusions in an albite porphyroblast in
the albite-sericite-chlorite schist (sample no. 26.57, 100x).
Ab= albite; Gl= glaucophane; chl= chlorite; mu= muscovite;
qtz= quartz; ep= epidote; sph= sphene.

Liou et al.(1974) experimentally investigated the transition between
greenschist and amphibolite facies in natural rocks with mineralogical
compositions comparable to the rocks of the schist-unit at Seriphos.
Liou's results indicate that at H_2O-pressures of about 1 kb the
formation of hornblende begins at temperatures around $520 - 530^0C$.
According to the experiments the gradual change from albite to
intermediate plagioclase takes place between $480 - 550^0C$ and chlorite,
left over in assemblages in which calcite was used up by the actinolite
formation, is consumed between 450 to 530^0C.

3: a zone of scapolite-diopside-hornblende hornfelses, beginning
with the first formation of scapolite from plagioclase + calcite. This
zone extends between 250 and 150 m perpendicular to the intrusive
contact. Shaw (1960a, 1960b) indicated that scapolite can be formed
over a wide range of P,T-conditions. Orville (1975) experimentally
established the important role of fluid- and NaCl-activity on the

43.

stability relations of scapolite. It seems likely, therefore, that the scapolite-'isograd' on Seriphos not just represents a temperature boundary, but that it also indicates the onset of a zone of increased fluid- (and NaCl-)activity.

4: a zone of scapolite-garnet-hornblende hornfelses, comprising the inner 150 m of the contact aureole. This zone contains contact metamorphic grandite garnet intermediate in composition between andradite and grossularite. The pink-colored, isotropic garnet occurs in scapolite-bearing rocks, where it (partially) replaces diopside. This suggests that the garnet originated from a reaction between diopside and scapolite (and a fluid phase). Hornblende, plagioclase (locally with up to 80% An), quartz, epidote, muscovite, and biotite remain present in this inner zone of the contact aureole, and apatite, zircon and opaques remain as accessory constituents. The experimental studies of Kotelnikov (1978) on the upper stability limit of scapolite in hydrothermal, NaCl-bearing systems indicate that in Fe,Mg-free situations with $CaCO_3$ present in excess the coexistence of grossularite + calcite is stable over anorthite and scapolite (+ calcite) at temperatures between 600 and 640°C at $P_f = P_{tot}$ = 1 kb and H_2O-rich conditions ($X_{CO_2} < 0.15$); under higher partial CO_2-pressures scapolite (+ calcite) remains stable up to temperatures over 700°C ($X_{CO_2} > 0.3$). According to the experiments and thermodynamic calculations of Taylor and Liou (1978) additions of Fe to the system decreases the lower stability temperatures of grossularite-andradite mixtures by up to 75°C

The amphibolite facies metamorphic assemblages, with hornblende, garnet, diopside, scapolite, plagioclase, epidote, muscovite, biotite and quartz remain stable associations up to the intrusive contact. The coexistence of muscovite + quartz instead of andalusite + K-feldspar suggests that the maximum temperature near the contact did not exceed values much higher than 580°C (Althaus et al.,1970). The coexistence of grandite + quartz instead of their HT-reaction products wollastonite + plagioclase also points to maximum temperatures of about 600°C (Newton, 1966; Taylor and Liou, 1978). The preservation of epidote in the contact-nearby metamorphic assemblages indicates similar maximum temperatures and H_2O-rich conditions (Winkler, 1979).

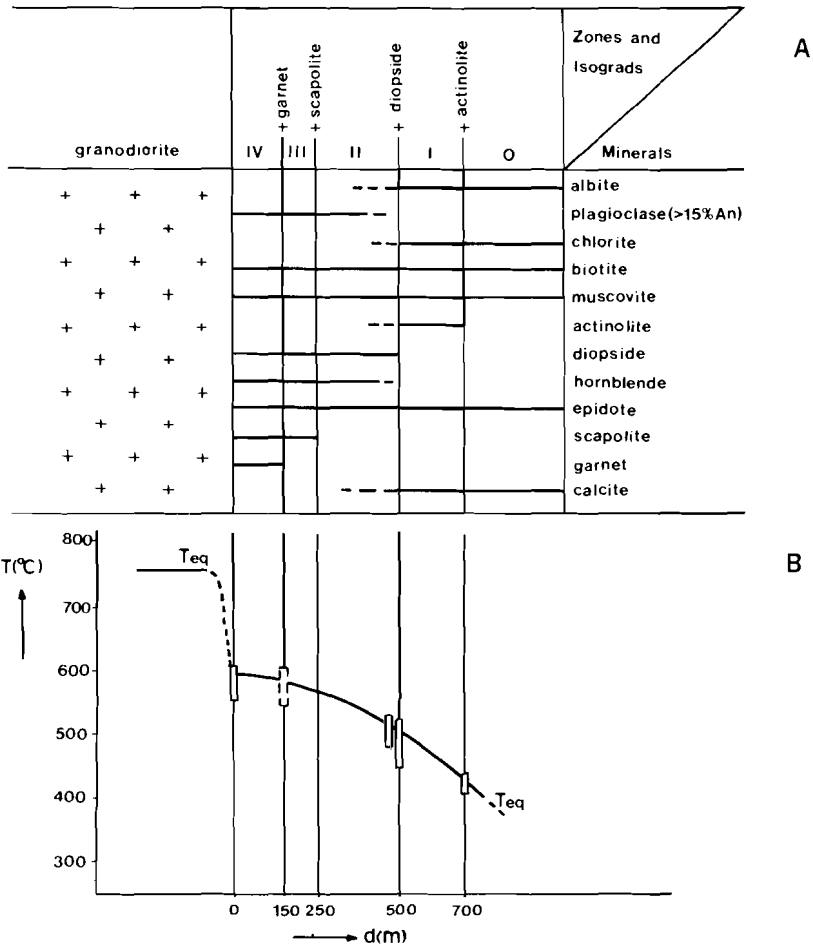Range of occurrence diagram (Fig.9):

Columns: granodiorite | IV | III | II | I | O | Zones and Isograds / Minerals

Isograd labels: +garnet, +scapolite, +diopside, +actinolite

Minerals list:
albite
plagioclase(>15%An)
chlorite
biotite
muscovite
actinolite
diopside
hornblende
epidote
scapolite
garnet
calcite

T(°C) axis values: 800, 700, 600, 500, 400, 300

Teq

d(m) axis values: 0, 150, 250, 500, 700

A

B

Fig.9: Range of occurrence of distinctive metamorphic minerals in
rocks of the schist-unit at Seriphos (fig.9A) and the
corresponding equilibrium temperatures (fig.9B) plotted
against the distance d (in meters) perpendicular to the
intrusive contact. Zone O: albite-sericite-chlorite schists;
I: epidote-actinolite schists; II: diopside-hornblende
hornfelses; III: scapolite-diopside-hornblende hornfelses;
IV: scapolite-garnet-hornblende hornfelses.

Fig.9A summarizes the contact metamorphic mineral formations in the schist-unit as a function of the distance perpendicular to the intrusive contact. Fig.9B shows the corresponding equilibrium temperatures. The reconstructed temperature-distance plot essentially indicates a 'convex' or 'S-shaped' curve for the maximum equilibrium temperatures reached during contact metamorphism. Similar S-shaped T-d-relations have been reported from other contact metamorphic aureoles around comparable granodiorite intrusives (see the review given by Reverdatto et al.,1970).

In table II chemical compositions are given of five representative samples of amphibolite facies rocks from the schist-unit. In fig.8 the samples are plotted in the ACF-diagram for low-pressure amphibolite facies metamorphism (Myashiro, 1973; Winkler, 1979). The contact metamorphic rocks plot in the same stability fields as the regionally metamorphosed greenschist facies rocks from the schist-unit in in northern Seriphos. This indicates that most contact metamorphic reactions were largely isochemical dehydration-decarbonation reactions, induced by 'dry heating' of the country rocks due to a dominantly conductive transfer of heat from the intruding granodiorite into the surrounding metasedimentary rocks. Only near the intrusive contact, in the inner 250 m of the contact aureole, the formation of contact metamorpic scapolite and garnet evidences an increased activity of (NaCl-rich) fluids during contact metamorphism.

Within the contact aureole the texture of the rocks gradually changes from a crystalloblastic texture in the outer parts (schists) to a massive, fine-grained, non-schistose 'hornfelsic' texture near the intrusive contact (hornfelses). Close to the contact quartz often shows the polygonal development typical of hornfelses.

CONTACT METASOMATISM

Contact metasomatism strongly affected the rocks of the schist-unit as well as the other rock units.

46.

In a few locations in contact metamorphic gneisses and hornfelses close to the intrusive contact, especially where there is no borderfacies developed in the adjacent granodiorite pluton, the siliceous country rocks are bleached like the rocks of the neighbouring main body granodiorite (Plate 6,see fig.10). Along fractures and other transport channels the dark components of the contact metamorphic rocks have been removed and the rock is transformed into a leucocratic rock mainly composed of quartz, sodic plagioclase and diopside and/or actinolite. In the outer parts of the bleached zones diopside commonly persists as a stable mineral phase. Towards the central parts of the bleached zones the pyroxene is usually replaced by actinolite. The central parts of the bleached zones are cross-cut by mm-thick epidote veins.

The preservation of diopside in the outer parts of the bleached zones, where hornblende and biotite have disappeared, suggests temperatures for the main stages of bleaching in the contact-nearby contact metamorphic rocks of some $550 - 500^{0}C$ (see above). The formation of actinolite as a replacement product of diopside in the central parts of the bleached zones, and the presence of epidote veins transecting the previously formed leucocratic rocks, indicates that leaching ended at temperatures of around $450^{0}C$ (see above and below).

In most contact-nearby schist and gneiss unit rocks, and also in a few locations in adjacent borderfacies granodiorite high-temperature metasomatism produced massive pyroxene-garnet skarns and magnetite ore bodies of several thousands to ten-thousands of m^{3} in volume consisting of Fe-rich epidote, hedenbergitic clinopyroxene, andraditic garnet and magnetite. The minerals occur in coarse-grained, often nearly monomineralic concentrations along the cracks and fractures that acted as transport channels for the metasomatic solutions (Plate 7). They are also present in polymineralic aggregates in which the minerals are more or less zonally arranged along the transport channels. Smaller mineralizations of phlogopite and pyrite are usually associated with the massive skarn formations. Quartz is occasionally present in small amounts. The high-temperature deposits occur in irregularly shaped
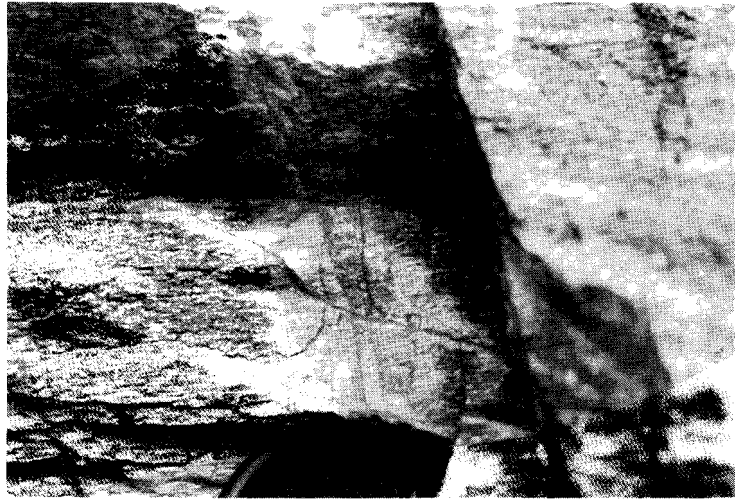
Plate 6: Bleached zone in a hornblende gneiss close to the intrusive
contact with (later) epidote formations in the central parts
of the metasomatic vein (loc. 124).

Plate 7: Pneumatolytic magnetite (mt) breccia and pyroxene-garnet
skarns (sk) in a fracture zone surrounded by epidotized
hornfelses (ep) (loc.27.7)(see also Plate 2).

48.

bodies in the siliceous wall rocks up to a distance of about 200 m perpendicular to the intrusive contact, the largest concentrations being formed close to the contact where the contact surface between granodiorite and wall rocks is flat-lying (figs.3,4). Close to the intrusive contact the deposits are often intensely brecciated as a result of syngenetic fracturing (pneumatolytic deposits)(Plate 2). The syngenetic fractures continue into the adjacent granodiorite.

In general, the first visible metasomatic changes in the siliceous country rocks evidencing high-temperature contact metasomatism are dispersed replacements and massive substitutions of the previously contact metamorphosed country rocks by Fe-rich epidote. The epidote preferentially replaces 'contact metamorphic' scapolite or scapolite/plagioclase aggregates.

Along fractures and fracture zones the epidotized hornfelses are replaced by massive concentrations of coarse-grained hedenbergitic clinopyroxene ($Hd_{15-40}Di_{85-60}$) and magnetite. The two minerals are often arranged in alternating monomineralic bands. In a few instances the epidotized hornfelses are intensely fractured and the hornfels fragments are cemented by pyroxene-magnetite formations.

Together with the pyroxene, or as a subsequent replacement product low-Al, isotropic garnet occurs ($Ad_{100-90}Gr_{0-10}$)(Vergouwen, 1976). The andradite occurs together with the clinopyroxene in alternating monomineralic bands, and within pyroxene-magnetite formations in 'metasomatic zones' along the central transport channels. Minor amounts of phlogopite and pyrite commonly occur in dispersed, monomineralic concentrations. Quartz is occasionally present in disseminated grains.

Experimental investigations of the stabilities of epidote, hedenbergite, andradite and phlogopite (annite) in hydrothermal systems indicate formation temperatures for the massive, pneumatolytic pyroxene-garnet deposits in the calcareous, silica-rich gneiss- and schist-unit rocks from 650 - 600°C to 550 - 500°C at $P_{tot}= P_{H_2O}=$ 1 kb (Kurshakova, 1971; Liou, 1973; Gustafson, 1974; Beane, 1974; Rose and Burt, 1979). $^{18}O/^{16}O$-ratios from coexisting pairs of magnetite + quartz and magnetite + pyroxene from HT pyroxene-garnet-magnetite skarn deposits give comparable formation temperatures from 560 to 500°C (see table III).
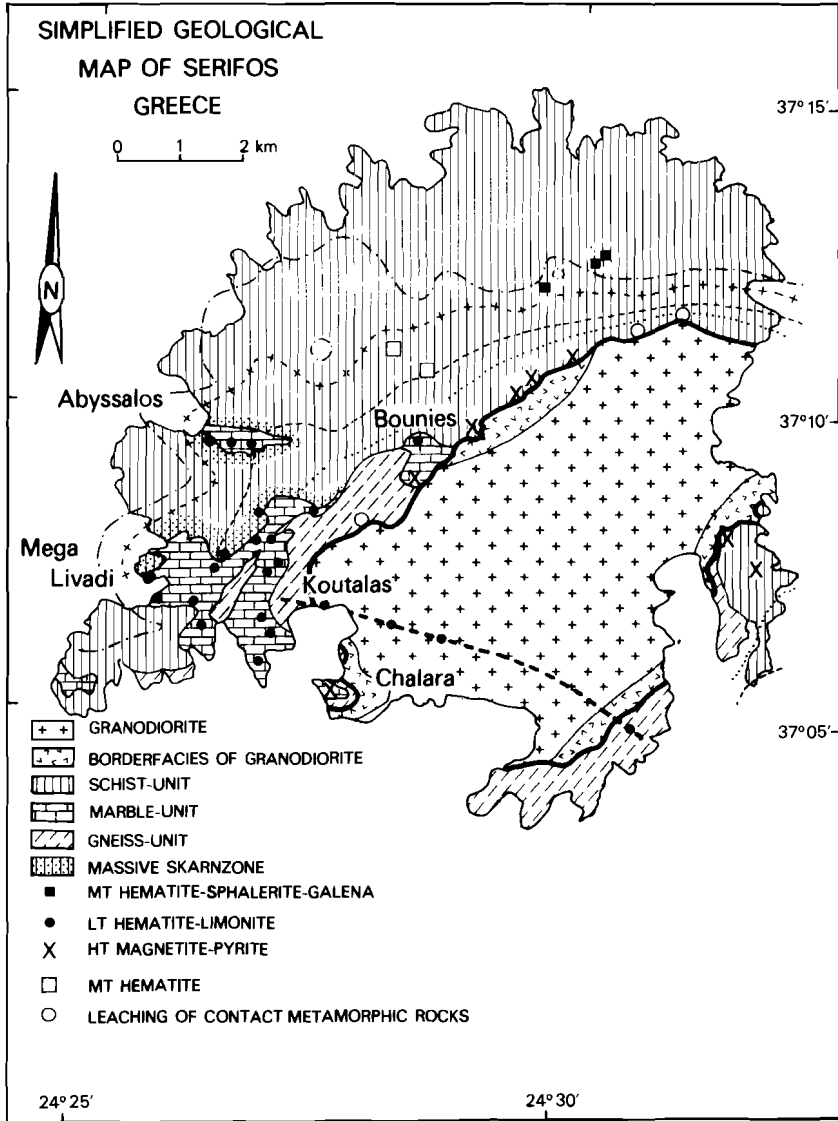
SIMPLIFIED GEOLOGICAL
MAP OF SERIFOS
GREECE

0   1   2 km

N

Abyssalos

Bounies

37° 15'

37° 10'

Mega
Livadi

Koutalas

Chalara

37° 05'

	GRANODIORITE
+ +	
	BORDERFACIES OF GRANODIORITE
	SCHIST-UNIT
	MARBLE-UNIT
	GNEISS-UNIT
	MASSIVE SKARNZONE
■	MT HEMATITE-SPHALERITE-GALENA
●	LT HEMATITE-LIMONITE
X	HT MAGNETITE-PYRITE
□	MT HEMATITE
○	LEACHING OF CONTACT METAMORPHIC ROCKS

24° 25'

24° 30'

Fig.10:Geological map of Seriphos with indication of locations with
major metasomatic features (see text).

50.

The high-temperature, massive pyroxene-andradite skarns grade into dm-cm wide garnet-actinolite veins containing aluminous andradite garnet, ferrous actinolite, phlogopite, magnetite or calcite, quartz and pyrite. The minerals usually occur in various combinations in polymineralic veins cross-cutting the previously formed pneumatolytic deposits, the contact metamorphic rocks up to distances of 200 - 300 m perpendicular to the intrusive contact, and also, in a few locations, the rocks of the borderfacies granodiorite.

Along vein structures within massive magnetite-pyroxene-andradite skarns the HT silicates are replaced by optically anomalous, grossularite-bearing andradite $(Ad_{70-60}Gr_{30-40})$(Vergouwen, 1976). The grossularitic andradite is formed in idiomorphic crystals surrounding isotropic andradite crystal cores, and in brecciated, pneumatolytic deposits cementing angular fragments of previously formed magnetite-pyroxene skarns. The aluminous garnet is often strongly zoned with alternating isotropic and anisotropic zones typically arranged parallel to the crystal faces of the idiomorphic garnet (Plate 8). According to Verkaeren (1972) such alternating zoning in aluminous skarn andradites is caused by alternating variations in the Fe/Al-ratio of the garnets. The variations probably result from oscillatory changes in the physico-chemical conditions during the garnet growth.

The anisotropic garnet is commonly associated with green-colored actinolite. The amphibole is low in Al and intermediate in composition between Mg-tremolite and Fe-actinolite (Mg/Fe= 3/2)(Vergouwen, 1976). The actinolite replaces hedenbergitic clinopyroxene along vein structures cross-cutting massive magnetite-pyroxene deposits. The actinolite also occurs together with grossularitic andradite, and with magnetite and/or quartz, phlogopite and pyrite in dm-wide veins cross-cutting the massive pyroxene-andradite deposits, and the contact metamorphic assemblages. Occasionally some calcite is present in magnetite-free garnet-actinolite vein assemblages.

Experimental data on the stability fields of hedenbergite and actinolite indicate formation temperatures for the garnet-actinolite deposits between 550 - 500°C and 450 - 400°C (Ernst, 1966; Schürmann and Hellner, 1966).

TABLE III

Formation temperatures of skarn assemblages
from $^{18}O/^{16}O$ of coexisting mineral pairs.

sample no. [1]	assemblage	$\delta^{18}O_{qtz}$	$\delta^{18}O_{mt}$	$\delta^{18}O_{cpx}$	$\delta^{18}O_{cc}$	T(°C)
27.7A	cpx + mt + qtz	14.7	6.0			560
126B	cpx + ad + mt		4.8	11.2		520
27.17	cpx + ad + mt		4.8	11.6		500
26.49	mt/hm + qtz	11.6	−1.5			410
26.48	mt/hm + qtz	12.3	−1.2			400
26.87	ac + ep + mt/hm + qtz	13.3	0.0			405
137	ac + mt/hm + qtz + cc	14.7	0.5			390
ML-2.2	ac + mt + qtz	16.6	−4.6			265
ML- 1	ac + mt + qtz	16.5	−4.9			260
ML-2.4	qtz + cc	22.0			18.8	125

[1] For sample locations see Appendix

The garnet-actinolite assemblages are cross-cut and replaced by
cm-wide epidote-actinolite veins. Frequently Fe-rich epidote (Fe/Al =
1/2) is the only mineral constituent in the veins. In other veins the
epidote occurs together with actinolite, quartz, magnetite and/or
hematite and pyrite. K-feldspar (adularia) may be present instead of
phlogopite. In epidote-actinolite veins without magnetite/hematite some
calcite may occur.

The medium-temperature epidote-actinolite veins cross-cut the
previously formed metasomatic deposits and the contact metamorphic
rocks up to a distance of about 400 – 500 m perpendicular to the
intrusive contact. They also occur along permeable zones in the
borderfacies granodiorite and in the central parts of the bleached
zones that are developed in contact-nearby gneisses and schist-unit
rocks. $^{18}O/^{16}O$-ratios from coexisting pairs of quartz + magnetite (+
(+ hematite) from medium-temperature vein deposits in the calcareous,
silica-rich schist-unit rocks give formation temperatures around 400°C
(table III).

The medium-temperature, cm-wide epidote-actinolite veins grade into medium to low temperature cm-mm wide calcite-quartz veins and veinlets mainly containing hematite, calcite, quartz, adularia and pyrite. Epidote is occasionally present in the veinlets. Green to blue colored actinolite frequently occurs as fibrous inclusions within quartz or calcite crystals. In a few places with tight networks of MT-LT veins sphalerite-galena-pyrite-hematite deposits have formed (see figs 3,10).

The cm-mm wide calcite-quartz-hematite veins occur in the siliceous country rocks up to 700 - 800 perpendicular to the intrusive contact and in the borderfacies of the granodiorite. The deposits probably formed at temperatures between 350 and 250^{0}C (see above and below).

The final stages of the metasomatic evolution in the calcareous, silica-rich rocks at Seriphos are indicated by low-temperature, hydrothermal precipitations of hematite/limonite, talc, chlorite, adularia and calcite in geodes and small, mm-wide veinlets cross-cutting the previously formed high and medium temperature metasomatic mineralizations, and the country rocks up to a distance of more than 1000 m perpendicular to the intrusive contact. In places with dense, interwoven networks of the late stage hydrothermal veinlets small amounts of malachite and/or chrysocolla may occur.

The low-temperature precipitations also occur along permeable zones in the borderfacies granodiorite, and in the central parts of the bleached zones in the main body of the intrusive. In a major fault structure cross-cutting the entire granodiorite pluton from E to W a tight network of small fractures with bleached zones is largely replaced by hematite/limonite with barite and minor fluorite (see fig.2).

Fluid inclusions homogenization temperatures indicate formation temperatures for the late stage hydrothermal vein deposits from about 250^{0}C to less than 150^{0}C (de Groot, 1975; Varekamp, 1976; see also chapter VI).
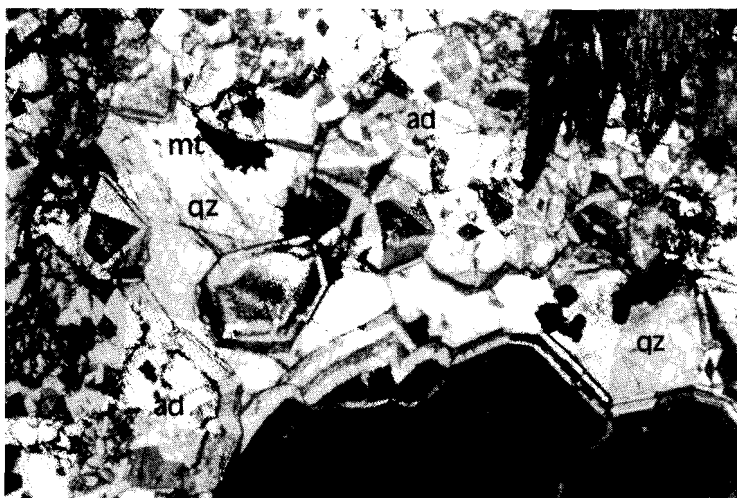
Plate 8: Anisotropic skarn andradite (ad) with alternating zonings.
The garnet replaces hedenbergite (hd) and is followed by
quartz (qz) and magnetite (mt) (+ actinolite) (Bounies).
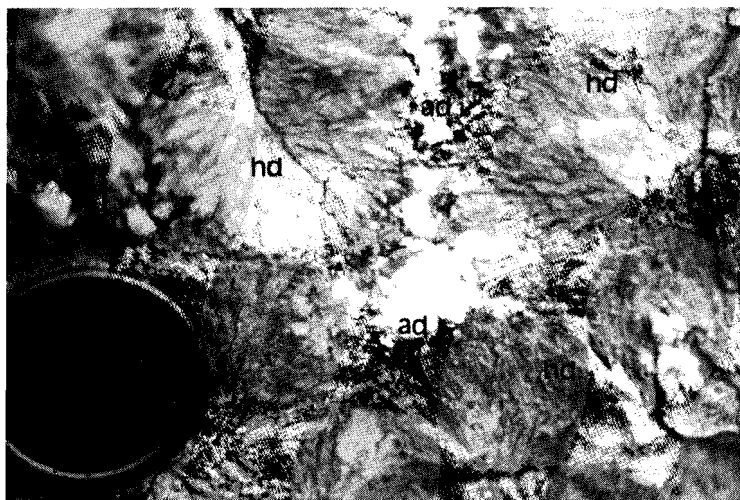
Plate 9: Replacement of massive, monomineralic hedenbergite aggregates
(hd) by andradite (ad) (+ quartz + magnetite) (Bounies).

54.

In the schist-unit rocks in southwestern Seriphos a massive pyroxene skarn zone is formed in which the hornfelses are almost completely replaced by hedenbergitic clinopyroxene. The pyroxenite zone occurs in a distinct stratigraphic horizon situated directly on top of the underlying marble series. In the southwest the skarn zone is about 30 m thick; towards the east the thickness gradually decreases, and in central Seriphos the pyroxenite zone wedges out together with the underlying marbles (see figs. 3,10,11).

The massive pyroxenite skarn zone predominantly consists of Fe-rich clinopyroxene ($Hd_{65-75}Di_{35-25}$)(Vergouwen, 1976). The hedenbergite is usually developed in coarse-grained, concentrically arranged crystal aggregates in which the individual crystals may reach over 20 cm in size. The pyroxene is frequently uralitic, viz. pseudomorphically replaced by microcrystalline actinolite. Within the uralitic pyroxene masses disseminated grains of magnetite, pyrite and chalcopyrite occur and locally some phlogopite is present interstitially between the hedenbergite crystals.

Within the massive hedenbergite zone only a few relicts are preserved of the original hornfelses. The relicts are preserved in the centres of the concentrically arranged hedenbergite aggregates and usually they are largely replaced by metasomatic epidote. Apart from epidote the amphibolite facies hornfels relicts predominantly consist of green hornblende (see also the plot of two low-epidote relict samples in the ACF-diagram of fig.8). In contrast to the hornfelses in the stratigraphically higher levels of the schist-unit the hornblende hornfelses from the hedenbergite skarn zone may contain up to several vol% of graphite.

Near their outer ends the concentrically arranged pyroxene aggregates change into different assemblages in different areas (fig.10):

a: In central Seriphos, near Bounies, where the massive pyroxenite zone is thin and exposed relatively close to the intrusive contact, the uralitic pyroxene aggregates are replaced by vein-type garnet deposits. (Plates 8,9). The strongly zoned aluminous andradite is commonly associated with actinolite, magnetite and/or quartz. The replacement
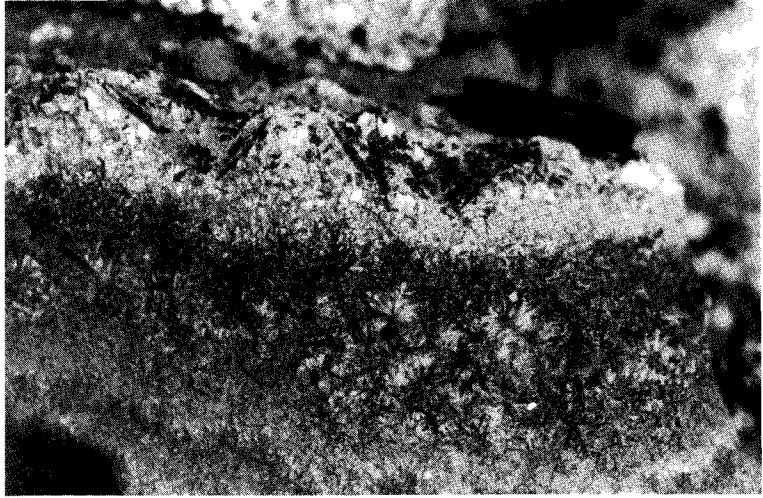
Plate 10: Pyroxenite skarn from southwestern Seriphos with (black)
ilvaite and actinolite (quartz-calcite) replacement (loc.56).
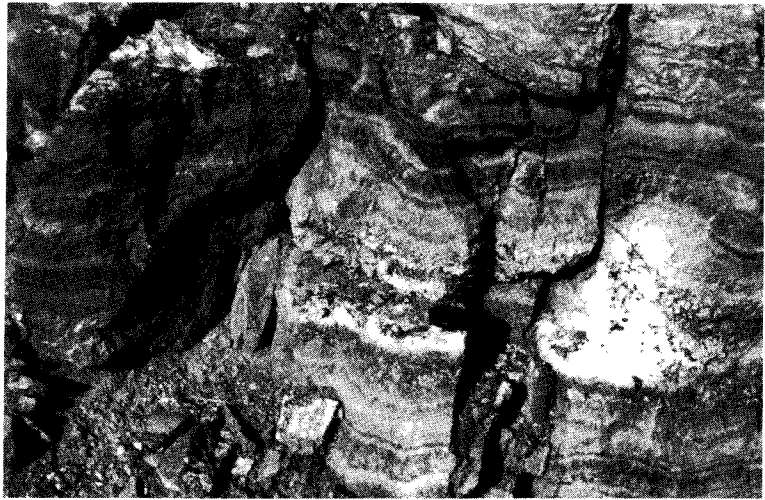
Plate 11: Concentrically arranged, alternating hedenbergite/ilvaite
bands surrounding a geodic cavity with late stage quartz-
calcite-actinolite/talc formations.

products have formed in the central veins separating the hedenbergite spheroids, and in vein structures cross-cutting the earlier formed hedenbergite masses. Both the pyroxenite rocks and the garnet-actinolite veins are cross-cut by thin epidote-actinolite veins, and in their turn the epidote veins are replaced and cross-cut by late stage veinlets with hematite, calcite and quartz in which the quartz frequently contains fibrous inclusions of blue-green colored actinolite.

b: To the west, between the locations of Bounies and Abyssalos and at a larger distance from the intrusive contact, the garnet is lacking and the hedenbergite agregates are directly replaced on their outer ends by epidote-actinolite assemblages.

c: In western Seriphos, in Abyssalos, at a still larger distance from the intrusive contact, neither garnet nor epidote is present and the hedenbergite is directly replaced by actinolite-quartz-magnetite and/or hematite with or without green colored (actinolite inclusions containing) calcite, or with talc. The actinolite assemblages occur in veins separating the hedenbergite aggregates, and in geodic cavities. In the central parts of the veins and geodes the actinolite assemblages are replaced by talc-calcite-quartz-hematite.

d: In the south-west, near Mega Livadhi, where the pyroxenite zone has its maximum thickness of about 30 m, the pyroxene is replaced by the black-colored, opaque Ca-Fe-silicate ilvaite (also called lievrite: $CaFe_2^{2+}Fe^{3+}Si_2O_8(OH)$). The ilvaite occurs together with the hedenbergite in alternating monomineralic 'zones' within the pyroxene aggregates, or together with actinolite, quartz and occasional magnetite in the transport channels separating the spheroidal hedenbergite-ilvaite aggregates (Plates 10,11). In the central parts of the transport channels, and in geodic cavities developed at transport channel junctions, the ilvaite is missing and the actinolite coexists with magnetite and/or hematite-quartz-calcite and pyrite and adularia. $\delta^{18}O$-values from quartz + magnetite coexisting with actinolite give formation temperatures of about 260^0C. The actinolite-bearing associations in their turn are succeeded by low-temperature formations of talc, chlorite, hematite/limonite, quartz, calcite and occasionally fluorite and barite.
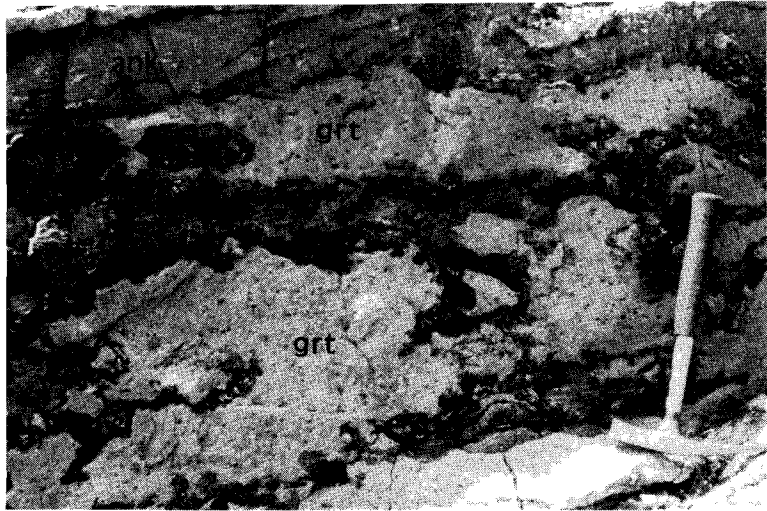
57.

Plate 12: Formation of garnet (dark) at the contact between siliceous granodiorite apophyses (grt) and marbles at Chalara. The marble is ankeritized (ank) (loc.24.5).
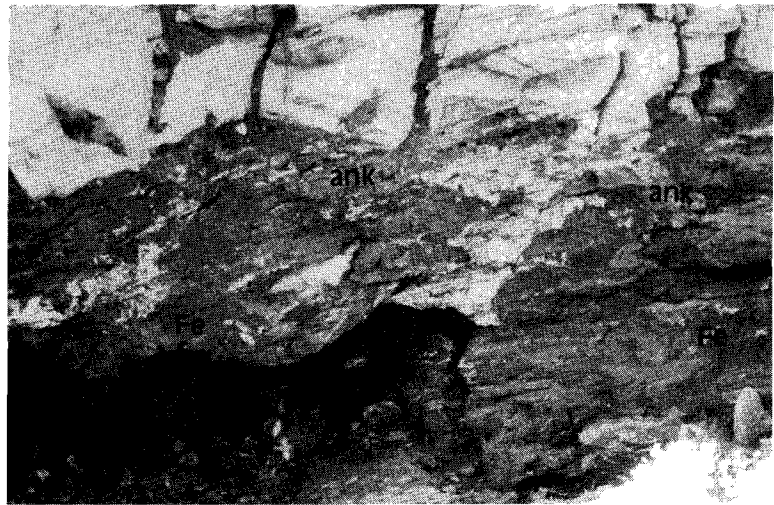

Plate 13: Irregularly shaped, metasomatic formations of ankeritic dolomite (ank) and hematite/limonite (Fe) in the calcite marbles of SW-Seriphos (Koutalas).

e: In the extreme south-west of Seriphos, SW of Mega Livadhi and at a larger distance from the intrusive contact, the hedenbergite may be replaced by ferrotremolite instead of ilvaite. When present, the Fe-amphibole is formed on the outer edges of the concentrically arranged pyroxene aggregates, together with quartz and magnetite. In the central parts of the transport channels the ferrotremolite is replaced by quartz, calcite and magnetite and/or hematite with pyrite at temperatures of about $125°C$ (see table III).

In central Seriphos (Bounies) dolomitic marbles are exposed in direct contact with the granodiorite intrusive (see figs 3,10). In the low-Si, graphite-bearing calcite-dolomite rocks close to the intrusive contact massive, often intensely brecciated magnetite deposits have formed. The pneumatolytic iron formations are associated with light-green colored skarns composed of clinopyroxene and serpentine. The metasomatic replacement minerals typically occur in nearly monomineralic concentrations in alternating bands arranged more or less parallel to the original bedding of the carbonate host rock. The light-geen colored clinopyroxene is Mg-rich ($Hd_{25}Di_{75}$)(Marinos, 1951). Within some serpentine concentrations the relict presence of Mg-rich olivine suggests that the original HT skarn assemblage in the contact-nearby dolomitic marbles probably was magnetite-diopside-forsterite. The skarn formations are accompanied by minor mineralizations of phlogopite, pyrite and the white-colored, fibrous Mg-borate ascharite (also called szaibellyite or camsellite, $Mg_2B_2O_5 \cdot H_2O$). The hydrous Mg-borate probably is a low-temperature, hydrothermal alteration product of the anhydrous Fe-Mg borate mineral ludwigite ($2FeBO_3 \cdot 2(Mg,Fe)O$) (see Barsukov and Kurilchikva, 1957).

Up to large distances from the intrusive contact talc is present in the dolomitic marbles. The Mg-silicate is mainly formed at the contacts between quartz nodules and dolomitic layers. In several places the talc is associated with hydrothermal formations of brown-colored, ankeritic dolomite and hematite/limonite iron ore.

The calcite marbles are only exposed close to the intrusive contact in Chalara, in the south of Seriphos, in a roof pendant

composed of gneisses with intercalated beds of thin-bedded dolomitic
marbles and massive, thick bedded calcite marbles (see figs.10). The
marbles contain gneissic intercalations. The roof pendant is cross-cut
by granodiorite apophyses and aplitic dykes.

In general, the first metasomatic formations at Chalara are
massive replacements of the marble series by pneumatolytic magnetite
with associated formations of hedenbergitic clinopyroxene
($Hd_{20-40}Di_{80-60}$), phlogopite, isotropic garnet ($Ad_{90-80}Gr_{10-20}$) and/or
quartz. The magnetite formations mainly develop at the contacts of the
marbles with major granodiorite apophyses. The skarns mainly formed as
replacements of Al-Si containing gneissic intercalations in the
marbles.

In calcite marbles at a distance from the magnetite deposits the
first metasomatic formations, in general, are coarse-grained, nearly
monomineralic bands and zones of isotropic andradite garnet. The garnet
is usually formed at the contacts between the marbles and intercalated
gneiss pockets or granodiorite apophyses (Plate 12). In a few places
some wollastonite is present at the boundary between marble and
garnetite; occasionally the garnet is associated with and partially
replaced by scapolite.

The HT skarns are partially replaced and cross-cut by veins with
epidote and actinolite with pyrite, hematite, adularia, calcite and
quartz.

In the massive beds of pure, white calcite marble in the roof
pendant at Chalara metasomatism produced irregularly shaped
concentrations of brown-colored, ankeritic dolomite and black-colored
hematite/limonite iron ore.

In the other parts of Seriphos the calcite marbles are only
exposed at a distance from the intrusive contact. In these marbles the
first metasomatic formations are irregularly shaped concentrations of
ankeritic dolomite and disseminated grains of pyrite (Plate 13). The
brown-colored, Fe-rich and Mn-bearing dolomite ($Mg_{100-70}Fe_{0-30}Mn_{0-5}$)
coexists with calcite or with magnesite. In their central parts,
towards the transport channels, the ankeritic bodies grade into

60.

A

Minerals / Mode of occurrence	1 massive bodies (m)	2 veins (dm)	3 veins and veinlets (cm)	4 geode's and veinlets (m/mm)
epidote I	▬ ▬			
hedenbergite	▬ ▬ ▬ ▬			
andradite	▬ ▬ ▬			
epidote II		▬▬▬▬▬▬ ▬ ▬		
ilvaite		▬ ▬▬ ▬		
talc			▬ ▬▬▬ ▬	
actinolite		▬▬▬▬▬▬▬▬		
phlogopite	▬ ▬	▬		
adularia			▬▬▬▬▬▬▬▬ ▬	
quartz	▬ ▬ ▬ ▬▬▬▬▬▬▬▬▬▬▬▬▬▬▬▬ ▪			
calcite		▬ ▬▬▬▬▬▬▬▬▬▬▬▬▬▬ ▪		
magnetite	▬ ▬ ▬ ▬			
hematite		▬ ▬▬▬▬▬▬▬▬ ▬		
limonite			▬ ▬▬▬▬▬	
pyrite	▬ ▬▬▬▬▬▬▬▬▬▬▬▬▬▬▬ ▬ ▬			
sphalerite			▬ ▬▬▬ ▬ ▬	
galena			▬ ▬▬▬ ▬ ▬	
chalcopyrite		▬ ▬▬▬▬▬▬▬▬		
malachite/chrysocolla			▬ ▬▬▬▬▬ ▬ ▬	

HT   ⟶ T   LT

B

granodiorite

1
2
3
4

0   200   500   700   900

d(m)

Fig.11: Schematic representation of (A): the order of formation of
distinctive contact metasomatic minerals in the schist-unit
on Seriphos and their mode of occurrence (temperature
decreasing from left to right), and (B): the approximate
range of formation of the main types of occurrences as a
function of the distance d (in meters) perpendicular to the
intrusive contact.

61.

black-colored mixtured of hematite/limonite and Fe-bearing calcite.
In late formed geodes within the iron deposits idiomorphic
crystallizations of specularite (hematite), goethite, calcite and
siderite occur with varying amounts of barite and fluorite and
occasional precipitations of malachite or chrysocolla.

Fig.11A summarizes the sequence of metasomatic formations at
Seriphos and their mode of occurrence as a function of temperature
(decreasing to the right) and/or time (increasing to the right). In
fig.11B the spatial distribution of the main types of metasomatic
formations is represented as a function of the distance perpendicular
to the intrusive contact. The plot of fig.11B emphasizes that later
formed, lower temperature deposits occur up to larger distances from
the intrusive contact.

SEQUENCE OF EVENTS

Comparison of the figures 9 and 11 stresses the differences in
place and mode of formation between the contact metamorphic rocks and
the contact metasomatic formations. The contact metamorphic rocks were
first formed by largely isochemical reactions from pre-existing
regional metamorphic assemblages, and the various contact metamorphic
facies occur in discrete zones at well-defined distances from the
intrusive contact. The contact metasomatic deposits were later formed
by metasomatic exchange reactions between pre-existing contact
metamorphic mineral assemblages and an invading hydrothermal fluid, and
the various skarn and ore associations occur in overlapping zones at
distances from the intrusive contact that gradually spread out with
decreasing temperature.
The spatially well-defined occurrence of the contact metamorphic
zones suggests that their formation was mainly due to a 'dry' heating
of the initially regional metamorphic rocks as a result of a
dominantly conductive heat transfer from the intruding magma into the
surrounding country rocks. The temperatures indicated by the reaction
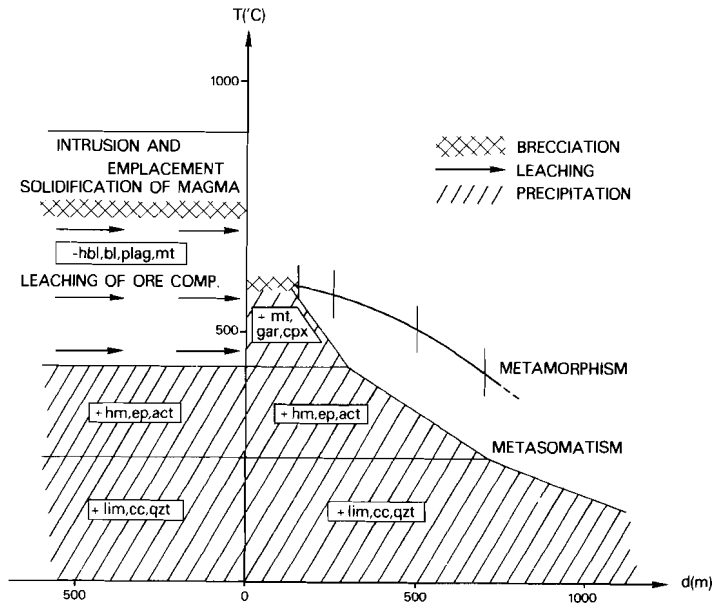
Fig.12:Schematic review of the main events associated with
      the granodiorite intrusion at Seriphos as deduced
      from the petrological and mmineralogical evidence.

isograds probably represent maximum temperatures; possibly they were
reached more or less simultaneously during the final stages of the
contact metamorphic heating.

   The uniform mineralogy and chemistry of the plutonic rocks
indicate that the granodiorite intrusion comprised essentially one
major phase of magma injection. The chilled margins of the singular
intrusion obviously were formed before the final solidification of the
main mass of the granodiorite. This suggests that the bulk of the
intruded magma persisted as a (partial) melt for some time during the
early stages of the intrusive event.

   At or just after its final solidification the granodiorite
intrusive was affected by an intense phase of (auto-)brecciation,
probably as a result of degassing of the solidifying, water-saturated
magma. In the (probably still semi-solid) main mass of the granodiorite

the (auto-)brecciation caused the formation of numerous randomly
orientated and often curved fracture zones. In the adjacent,
apparently more rigid chilled margins and country rocks fracturing
was straight and the fractures generally radiate outward from the
intrusive.

        Bulk rock permeabilities increased as a consequence of the
hydrofracturing and hydrothermal fluid circulations along the newly
formed transport channels resulted in extensive metasomatic mass
exchanges in the (semi-)solid granodiorite as well as in the
surrounding contact metamorphic rocks. In the granodiorite the
metasomatic actions caused a leaching of Fe-Mg-Mn components during
the early, high-temperature stages of the post-magmatic evolution, and
a precipitation of Fe-Mg-Mn components during the later,
low-temperature stages of the hydrothermal activities. In the country
rocks the metasomatic processes added considerable amounts of Fe-Mg-Mn
components to the contact metamorphic rocks during all stages of the
post-magmatic, hydrothermal cooling of the intrusion. The metasomatic
mineral assemblages differ with temperature and in different types of
country rock or geochemical environment as a consequence of locally
controlled, temperature dependent chemical equilibria between the
locally present solid phases and the invading metasomatic solutions.

        In fig.12 a schematic review is given of the major events
associated with the granodiorite intrusion at Seriphos, and the
corresponding temperature evolution as deduced from the petrological
and mineralogical evidence.

I will now speak of the compounds which are
composed of the simple minerals cemented
together by nature.

Agricola, De Natura Fossilium,1546.

CHAPTER V: FORMATION CONDITIONS OF THE SKARNS

Thermodynamic analysis of the sequence of phase assemblages in a
skarn deposit defines the path of metasomatism during the skarn
formation. Comparison of the skarn sequences in different host rock
systems specifies the difference in geochemical environment and the
influence of local buffering on the skarn formation.

THERMODYNAMIC APPROXIMATIONS

The Gibbs free energy of a phase or system is defined as

$$G = H - TS = \sum_i \mu_i n_i \qquad (5-1)$$

where μ_i = chemical potential of a component i; n = number of moles of
component i in the phase of interest; the summation extends over all
components. H = enthalpy; T = absolute temperature; S = entropy (Wood
and Frazer, 1977).

For a chemical reaction the change $(\Delta G)_{P,T}$ in Gibbs free energy at
any P and T is given by:

$$
(\Delta G)_{P,T} = \Sigma G_{P,T}^{products} - \Sigma G_{P,T}^{reactants} =
$$

$$
= (\Delta H)_{P_0 T_0} + \int_{T_0}^{T} \Delta c_p dT - T(\Delta S)_{P_0 T_0} - T \int_{T_0}^{T} \frac{\Delta c_p}{T} dT + \int_{P_0}^{P} \Delta V dP
$$

$$(5-2)$$

For the standard conditions $P_0 = 1$ bar and $T_0 = 298\,^0K$ and with the assumption that $\Delta c_p = 0$, equation (5-2) simplifies to:

$$(\Delta G)_{P,T} = \Delta H^0 - T\Delta S^0 + \int_{P_0}^{P} V\,dP \tag{5-3}$$

Further simplification leads to different approximations for different reaction types:

a: solid-solid reactions

For solid-solid reactions the changes in molar volume of the solid phases as a result of pressure changes can be neglected and the only significant changes are the volume changes ΔV_s due to chemical reaction:

$$\Delta \int_{1}^{P} V_s\,dP = \Delta V_s \int_{1}^{P} dP = \Delta V_s(P-1)$$

$$(\Delta G)_{P,T} = \Delta H^0 - T\Delta S^0 + (P-1)\Delta V_s \tag{5-4}$$

b: solid-fluid reactions

The molar volume V_f of a fluid strongly depends on pressure:

Perfect Gas:
$$PV_i = RT$$

$$\int_{1}^{P} V_i\,dP = \int_{1}^{P} \frac{RT}{P}\,dP = RT \int_{1}^{P} \frac{1}{P}\,dP = RT \ln P$$

$$(\Delta G)_{P,T} = \Delta H^0 - T\,\Delta S^0 + (P-1)\Delta V_s + RT \ln P \tag{5-5}$$

Non-perfect Gas:

The molar volume V_n of a non-perfect gas differs from the molar volume V_i of a perfect gas under the same conditions:

$$\int_{1}^{P} V_n\,dP = \int_{1}^{P} V_i\,dP + \int_{1}^{P} (V_n - V_i)\,dP = RT \ln P + RT \cdot \ln \Gamma_n^P = RT \ln f_n^P$$

$$f_n^P = P \cdot \Gamma_n^P$$

f_n^P = fugacity of the non-perfect gas at the given conditions of P and T
Γ_n^P = fugacity coefficient.

66.

For a chemical reaction between a number of solid phases and a non-perfect gas, e.g. dehydration and decarbonation reactions:

$$(\Delta G)_{P,T} = \Delta H^0 - T.\Delta S^0 + (P-1)\Delta V_s + RT \ln f_n^P \qquad (5-6)$$

c: reactions with fluid mixtures

For ideally mixing fluids:

$$f_A = P.X_A.\Gamma_A^P$$

X_A = mol.fraction of gas species A in the fluid mixture.

For chemical reactions between solid phases and a composite fluid:

$$(\Delta G)_{P,T} = \Delta H^0 - T\Delta S^0 + (P-1)\Delta V_s + aRT \ln X_A f_A^{*,P} - bRT \ln X_B f_B^{*,P} \qquad (5-7)$$

where a = stoichiometric coefficient of a gas species A produced by a chemical reaction, and b = stoichiometric coefficient of a gas species B consumed by the reaction. $f_A^{*,P}$ = fugacity of the pure gas phase A at the given pressure P, and $f_B^{*,P}$ = fugacity of pure B at the pressure P.

Neglecting the volume changes in the solid phases ($\Delta V_s = 0$) and rewriting the volume terms for the gaseous species results in:

$$(\Delta G)_{P,T} = \Delta H^0 - T\Delta S^0 + RT \ln \frac{(X_A \Gamma_A)^a}{(X_B \Gamma_B)^b} \qquad (5-8)$$

Since $G = \Sigma n_i \mu_i$:

$$(\Delta G)_{P,T} = \Delta G_s^0 + a\mu_a - b\mu_b$$

For chemical equilibrium:

$$(\Delta G)_{P,T} = 0 \; ; \quad a\mu_A - b\mu_B = -\Delta G_s^0 = \text{constant} \qquad (5-9)$$

In a $\mu_A - \mu_B$ diagram, therefore, the equilibrium of a solid-fluid reaction is given by a straight line; the slope of the equilibrium line in the μ_A / μ_B -space is given by the ratio a/b of the stoichiometric coefficients of the gaseous species A and B in the reaction equation of the considered equilibrium (Korzhinskii, 1959; Burt, 1972).

PHASE DIAGRAMS

Idealized chemical compositions can be used to establish the topological relations between the main mineral phases in the skarn assemblage at Seriphos. With thermodynamic data given in the literature and approximate data obtained from experimental results the topologies can be expanded to simplified phase diagrams.

a: The system $Fe-O_2-H_2O$.

Consider the system
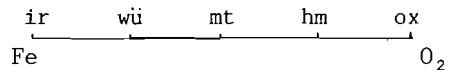
with the phases: ir : iron (metal) : Fe

wu : wüstite   : FeO

mt : magnetite   : Fe_3O_4

hm : hematite   : Fe_2O_3

ox : oxygen   : O_2

For this ((c=2)+3)-system the topological relations are given by
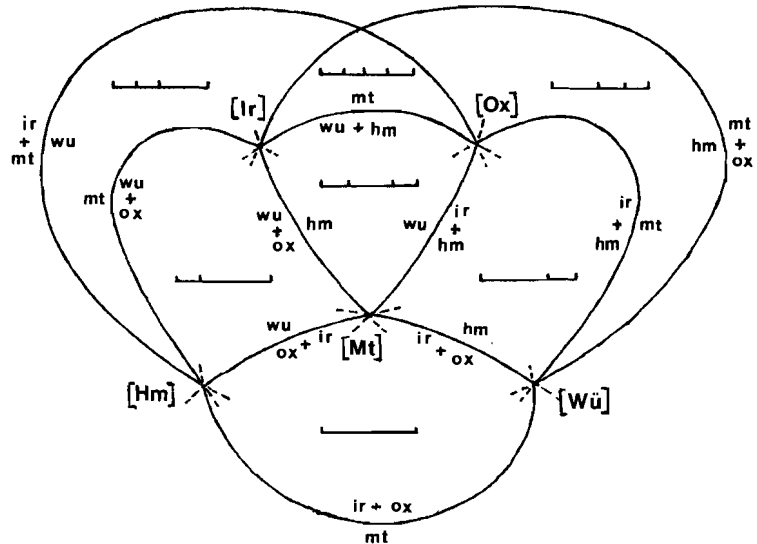
(see Zen, 1966, 1967; van der Maar, 1978)

In situations with O_2 always present as an excess phase the chemographic representation of the system simplifies to:

ir   wü   mt   hm $\boxed{+O_2}$
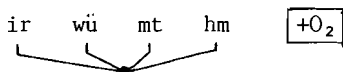
and for this ((c=1)+3)-system the topological relations are given by:
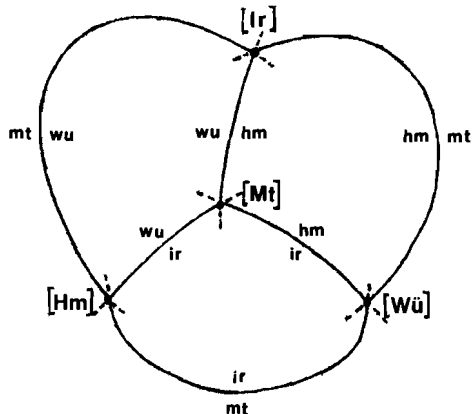
with the reaction equilibria:

			μ_{H_2O}/μ_{O_2}
|Mt,Ir|	$1/2\ O_2\ +\ 2\ FeO$	$=\ \ Fe_2O_3$	0
|Mt,Wu|	$3/2\ O_2\ +\ 2\ Fe$	$=\ \ Fe_2O_3$	0
|Mt,Hm|	$1/2\ O_2\ +\ \ \ Fe$	$=\ \ FeO$	0
|Hm,Ir|	$1/2\ O_2\ +\ 3\ FeO$	$=\ \ Fe_3O_4$	0
|Hm,Wu|	$2\ O_2\ +\ 3\ Fe$	$=\ \ Fe_3O_4$	0
|Wu,Ir|	$1/2\ O_2\ +\ 2\ Fe_3O_4$	$=\ 3\ Fe_2O_3$	0

Extension of the above Fe-O_2-system with the additional component H_2O involves addition of the phases water (H_2O) and goethite (gt: FeOOH). With H_2O always present as an excess phase the only additional reactions to be considered are the hydration reactions:

			μ_{H_2O}/μ_{O_2}
|Wu,Mt,Hm|	$3/2\ O_2 +\ \ H_2O\ +\ 2\ Fe$	$=\ 2\ FeOOH$	+ 0.67
|Ir,Mt,Hm|	$1/2\ O_2 +\ \ H_2O\ +\ 2\ FeO$	$=\ 2\ FeOOH$	+ 2.00
|Ir,Wu,Hm|	$1/2\ O_2 + 3\ H_2O\ +\ 2\ Fe_3O_4$	$=\ 6\ FeOOH$	+ 6.00
|Ir,Wu,Mt|	$H_2O\ +\ \ \ Fe_2O_3$	$=\ 2\ FeOOH$	+ ∞
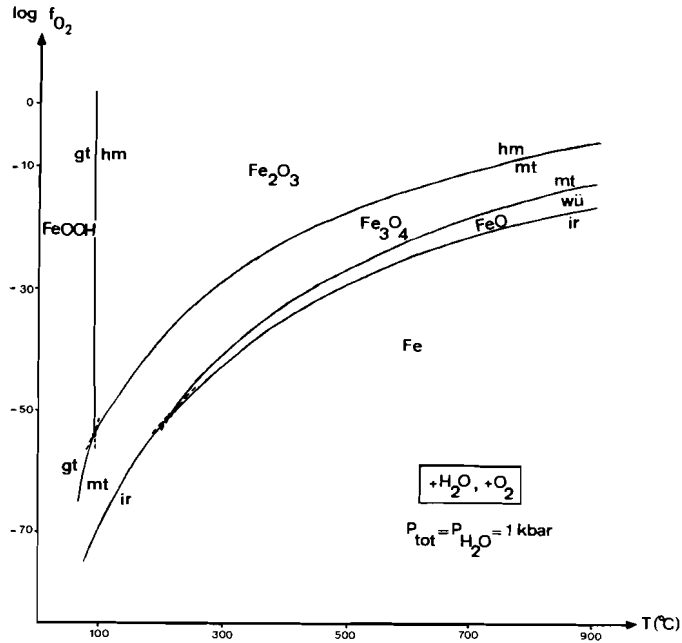
Fig.13: log f_{O_2}- T diagram for the system Fe-O_2-H_2O at $P_{H_2O} = P_{tot} = 1$ kb

Dehydration reactions reduce the μ_{H_2O} in the solid phases. Dehydration usually takes place as the temperature increases. Oxidation reactions increase the μ_{O_2} in the solid phases. In a $-\mu_{H_2O}/\mu_{O_2}$-diagram, therefore, the mutual relations of the various stability fields in a given system are the same as in a log f_{O_2}- T -diagram (Burt, 1971). For the Fe-O_2-H_2O-system the $-\mu_{H_2O}/\mu_{O_2}$-diagram is:
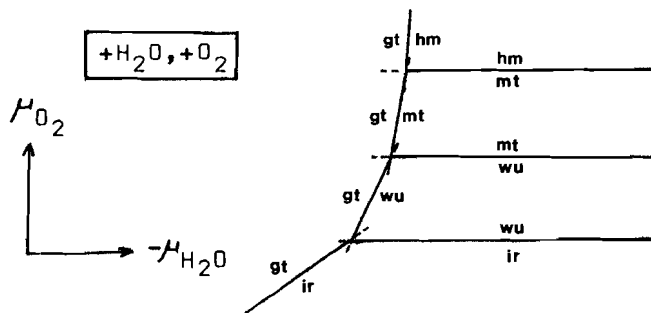
The H_2O-free, solid-O_2-reactions hm = mt, mt = wü and wü = ir can be calculated as singular functions of T and f_{O_2} by means of eq.(5-6) and the thermodynamic data given by Robie et al. (1978). The goethite-forming hydration equilibria, involving the two gaseous species O_2 and H_2O, can be defined as singular functions of T and f_{O_2} for any fluid pressure $P = P_{H_2O}$ using eq.(5-8) and the fugacity data for H_2O tabulated by Helgeson and Kirkham (1974). Fig.13 gives the T-log f_{O_2}-diagram for the system Fe-O_2-H_2O calculated for $P_{tot} = P_{H_2O} = 1$ kbar.

b: The system Ca-Fe-Si-O_2-H_2O

Consider the system
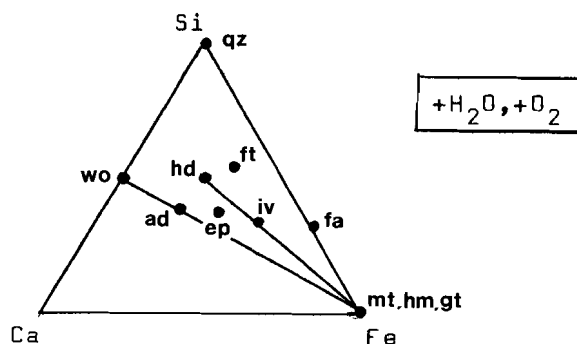
qz	: quartz	: SiO_2
gt	: goethite	: $FeOOH$
hm	: hematite	: Fe_2O_3
mt	: magnetite	: Fe_3O_4
fa	: fayalite	: Fe_2SiO_4
wo	: wollastonite	: $CaSiO_3$
ad	: andradite	: $Ca_3Fe_2Si_3O_{12}$
hd	: hedenbergite	: $CaFeSi_2O_6$
ep	: Fe-epidote	: $Ca_2Fe_3Si_3O_{12}(OH)$
iv	: ilvaite	: $CaFe_3Si_2O_8(OH)$
ft	: ferrotremolite	: $Ca_2Fe_5Si_8O_{22}(OH)_2$

The chemography of the H_2O-free subsystem wo–qz–ad–hd–fa–mt is given
by:
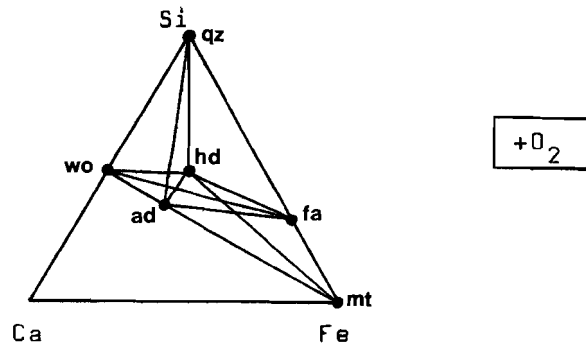
Abolishment of the degenerations wo–ad–mt and qz–fa–mt in this
((c=3)+3)–system leads to the core polygon:

type Te–RPIV
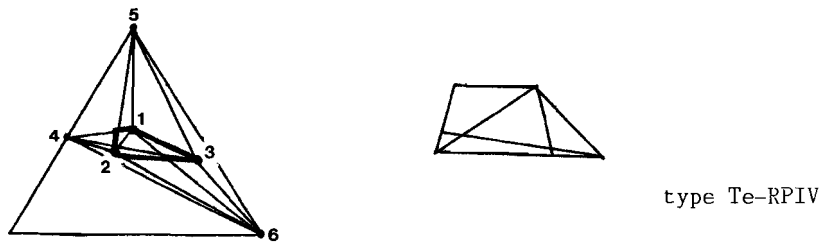
and to the representation polyhedron
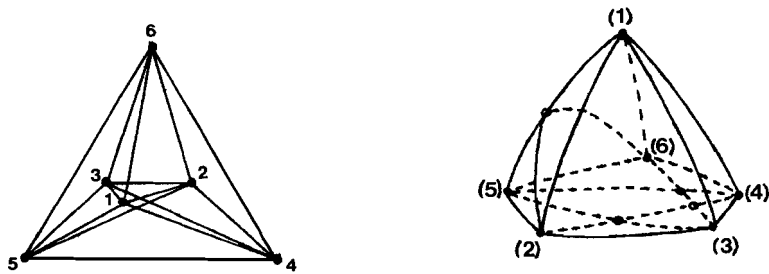
The topology of the degenerated ((c=3)+3)-system becomes
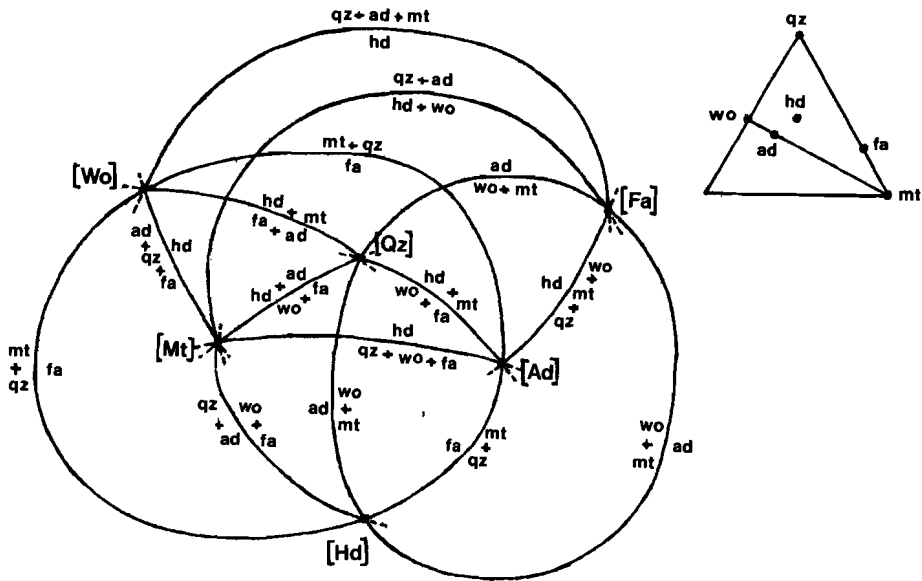
(see Zen and Rooseboom, 1972; van der Maar, 1978).

In Si-saturated systems with quartz present as excess phase in all assemblages the chemographic representation of the ((c=3)+3)-system simplifies to

wo   ad hd   fa,mt   + Qz

with the topology
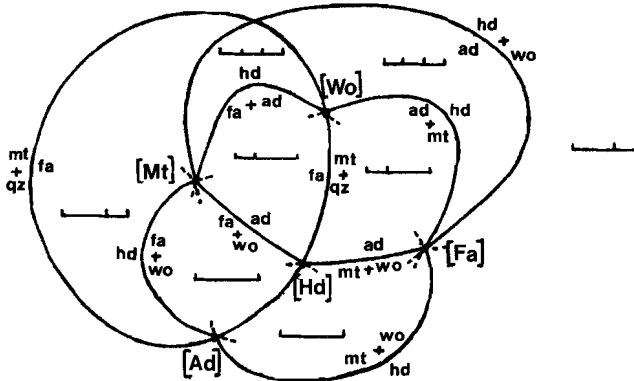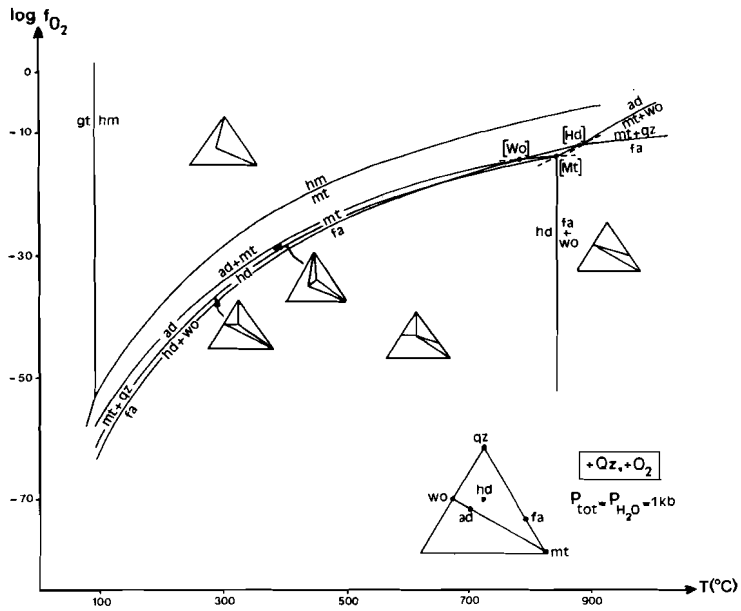
Fig.14: log f_{O_2} - T diagram for the Si-saturated system Ca-Fe-Si-O$_2$.

and the reactions:

|Wo,Hd,Ad|		$O_2 + 3\ fa = 2\ mt + 3\ qz$
|Wo,Fa|		$2\ O_2 + 9\ hd = 3\ ad + mt + 9\ qz$
|Hd,Fa|	$O_2 + 2\ mt + 9\ wo = 3\ ad$
|Ad,Fa|		$O_2 + 3\ hd = 3\ wo + mt + 3\ qz$
|Wo,Mt|		$O_2 + 6\ hd = 2\ ad + fa + 5\ qz$
|Hd,Mt|	$O_2 + fa + 3\ wo = ad + qz$
|Ad,Mt|	$2\ qz + fa + 2\ wo = 2\ hd$
|Mt,Fa|		$O_2 + wo + 2\ hd = ad + 2\ qz$
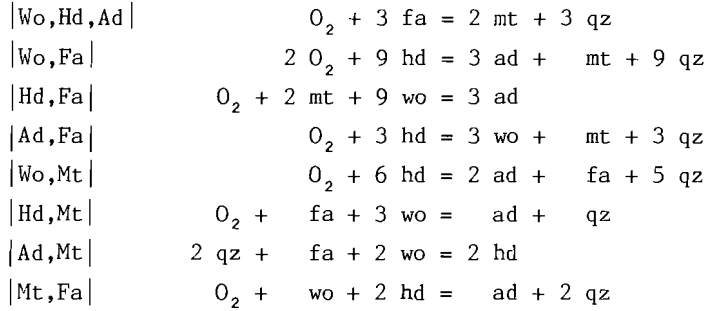
The thermodynamic data for magnetite, fayalite, wollastonite, quartz and O$_2$ are given by Robie et al. (1978). Appropriate data for andradite and hedenbergite are obtained from the experimentally determined reaction equilibria |Hd,Fa|: ad = mt + wo (Kurshakova, 1971; Gustafson, 1974) and |Mt,Fa|: qz + ad = hd + wo (Gustafson, 1974; Liou, 1974). With eq.(5-8) and the thermodynamic data given in table IV the

reaction equilibria are determined as singular functions of f_{O_2} and T. The topology fixes the arrangement of the stable parts of the reaction equilibria. In fig.14 the calculated $\log f_{O_2}$- T diagram is given for the Si-saturated subsystem Ca-Fe-Si-O_2. The diagram also includes the stability fields of hematite and goethite.

Consider the H_2O-bearing, Si-saturated subsystem

```
   ad    hd    ft    iv    mt        +Qz, +H₂O,+O₂
   |_____|_____|_____|_____|
   Ca                      Fe
```
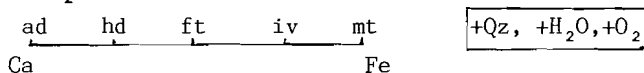
The topological relations in this ((c=2)+3)-subsystem are given by
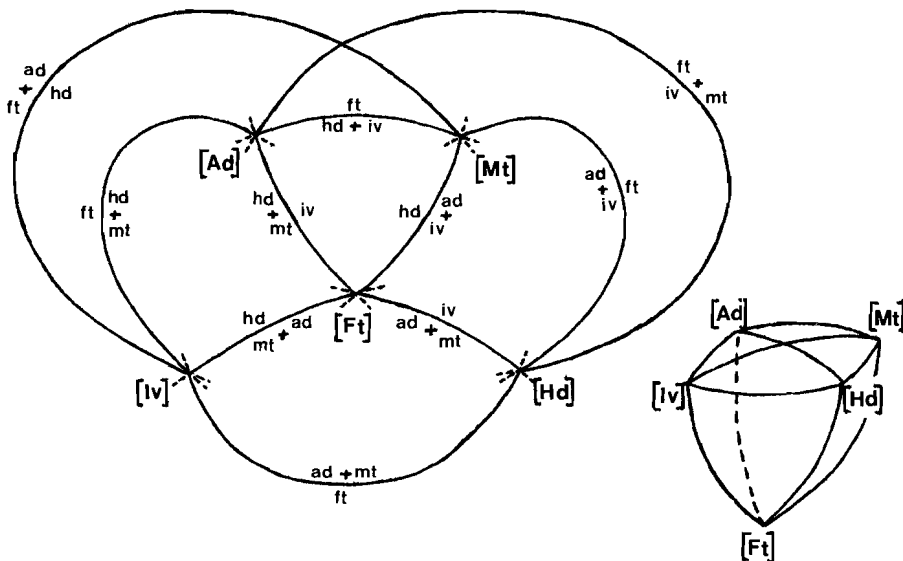
In Fe-Si-saturated systems with both quartz and magnetite present as excess phases the reactions are:

		$-\mu_{H_2O}/\mu_{O_2}$
$\lvert$Ft,Iv$\rvert$	$2O_2 + 9hd = 3ad + mt + 9qz$	0
$\lvert$Ft,Ad$\rvert$	$1/2O_2 + 6iv = 6hd + 4mt + 3H_2O$	−6.00
$\lvert$Ft,Hd$\rvert$	$11/2O_2 + 18iv = 6ad + 14mt + 18qz + 9H_2O$	−1.64
$\lvert$Iv,Hd$\rvert$	$17/2O_2 + 9ft = 6ad + 11mt + 54qz + 9H_2O$	−1.06
$\lvert$Iv,Ad$\rvert$	$1/2O_2 + ft = 2hd + mt + 4qz + H_2O$	−2.00
$\lvert$Ad,Hd$\rvert$	$12qz + 6iv = 3ft + mt + O_2$	0

75.
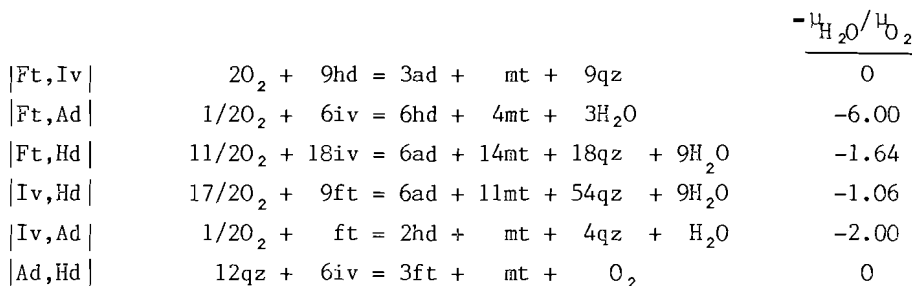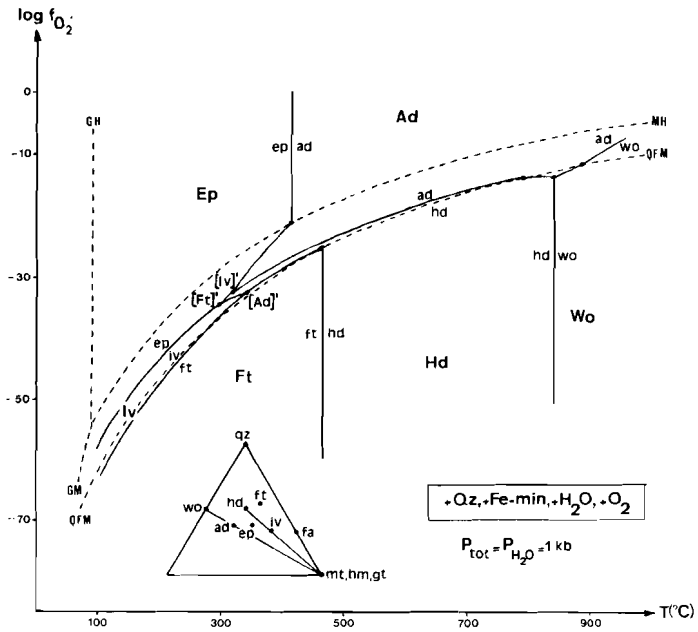
Fig.16: The Fe–Si–saturated system Ca–Fe–Si–H_2O–O_2.

In Fe-undersaturated, Si-saturated systems the following reactions occur:

$$-\mu_{H_2O}/\mu_{O_2}$$

|Ft,Mt|	$5/2 O_2 + H_2O + 14hd = 4ad + 2iv + 12qz$	$+0.40$
|Ad,Mt|	$3/2 O_2 + 4ft = 2hd + 6iv + 16qz + H_2O$	-0.67
|Hd,Mt|	$13/4 O_2 + 7ft = ad + 11iv + 31qz + 3/2 H_2O$	-0.46
|Iv,Mt|	$3/2 O_2 + H_2O + 11hd = ft + 3ad + 5qz$	$+0.67$
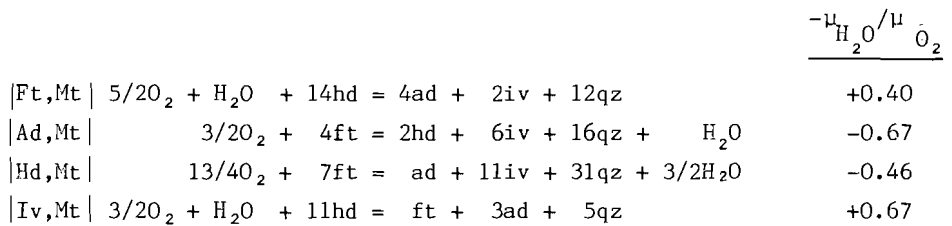
The $-\mu_{H_2O}/\mu_{O_2}$ -diagram for the mt–iv–ft–hd–ad+Qz+H_2O+O_2-subsystem is:

76.
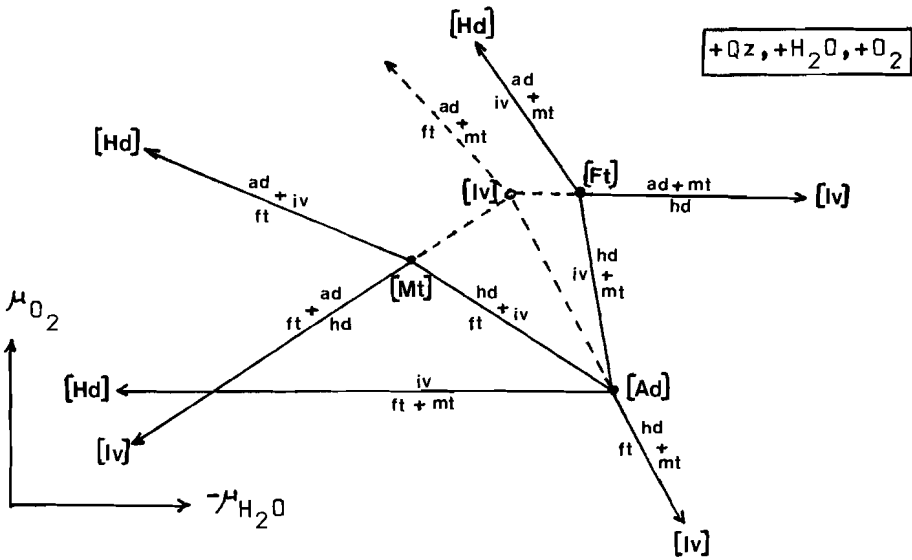
Similarly Fe-epidote can be introduced into the system. For the Fe-Si-saturated subsystem iv-ft-ep-hd-ad+Mt+Qz+H 0+0 the $-\mu_{H_2O}$ / μ_{O_2}- diagram is:

77.
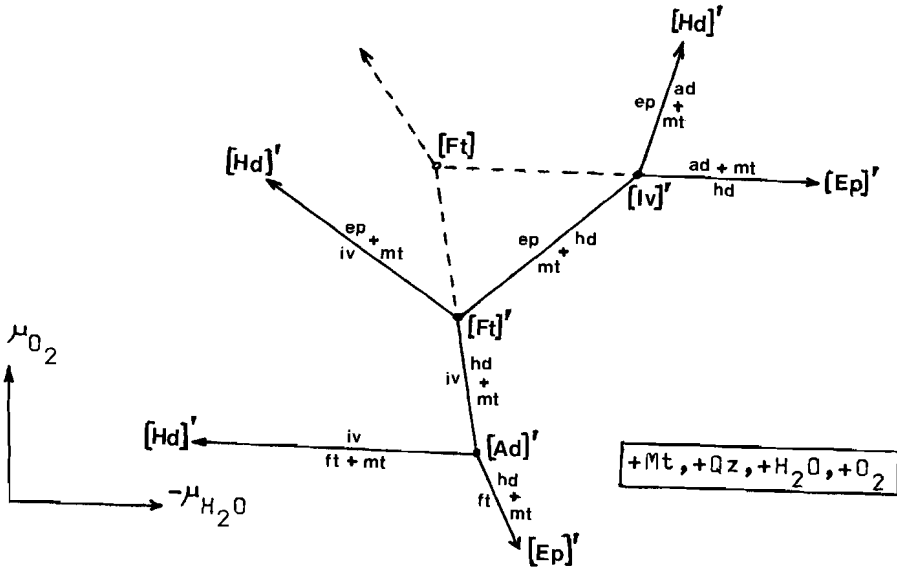
with the additional reactions:

$$-\mu_{H_2O}/\mu_{O_2}$$

$|Iv,Ep|$ $5/4O_2 + 9/2H_2O + 9qz + 5mt + 6ad = 9ep$ $+3.60$

$|Iv,Ft|$ $7/4O_2 + 3/2H_2O + mt + 6hd = 3ep + 3qz$ $+0.86$

$|Hd,Ft|$ $1/2H_2O + qz + mt + ep = 2iv + 3/4O_2$ -0.67

For ferrotremolite and ilvaite approximate thermodynamic data are obtained by comparing the experimental results for the reactions ft = fa + hd + qz (Ernst, 1966) and iv = hd + mt (Gustafson, 1974) with the topological relations given above. Thus, for both ferrotremolite and ilvaite a 'best fit' of thermodynamic data is found satisfying the experimental results as well as the topological requirements. For Fe-epidote approximate thermodynamic data are obtained by extrapolating the thermodynamic data for zoisite-pistacite-solid solutions given by Holdaway (1972). The data are given in table IV.

In fig.15 a log f_{O_2} - T -diagram is presented for the Fe-Si saturated system iv-ft-ep-hd-ad-wo +(Fa,Mt,Hm,Gt)+Qz+H_2O+O_2 calculated for $P_{tot}= P_{H_2O}$= 1 kbar using the thermodynamic data given in table IV and tabulated data for f_{H_2O}.

c: The system Ca-Fe-Mg-Si-H_2O-O_2

Olivines, clinopyroxenes and tremolites are solid solutions with respect to Fe and Mg. Talc is a pure Mg-phase:

olivine   : $(Fe,Mg)_2SiO_4$

clinopyroxene : $Ca(Fe,Mg)Si_2O_6$

tremolite   : $Ca_2(Fe,Mg)_5Si_8O_{22}(OH)_2$

talc   : $Mg_3Si_4O_{10}(OH)_2$

Addition of Mg to the Fe-Si-saturated system Ca-Fe-Si-O_2-H_2O leads to additional talc forming reactions and to a shift of the stability fields of the Fe-Mg-solid solution series towards the Mg-endmembers forsterite (fo), diopside (di) and tremolite (tr).
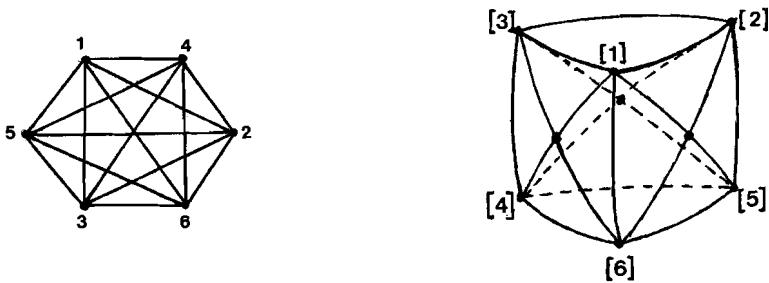
Consider the ((c=3)+3)-system
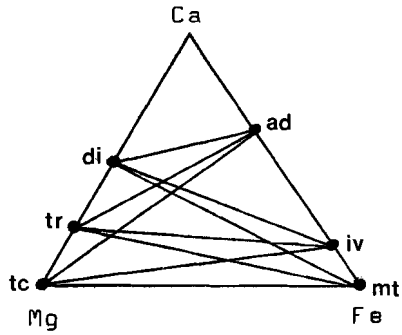
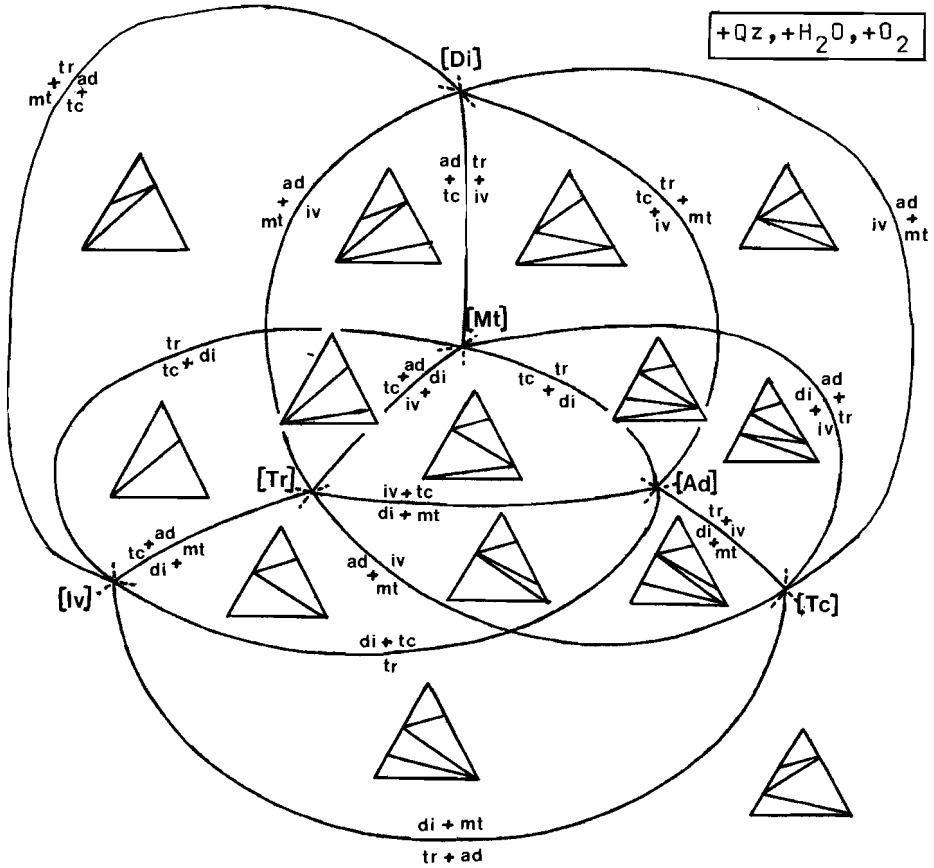Abolishment of the degenerations leads to the core polygon:
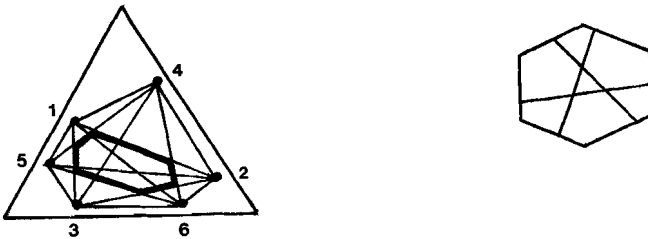

and to the representation polyhedron:

The topology of the degenerated ((c=3)+3)-system becomes:

$+Qz,+H_2O,+O_2$

In Fe-Si-saturated assemblages the reactions are:

		$-\mu_{H_2O}/\mu_{O_2}$
$\lvert$Di,Tc,Tr$\rvert$	$11/2O_2+ 18iv = 6ad + 14mt + 18qz + 9H_2O$	-1.64
$\lvert$Ad,Iv,Mt$\rvert$	$tr = 2di + tc$	$-$
$\lvert$Di,Ad$\rvert$	$3/2O_2+ 6iv + 5tc = 3tr + 6mt + 8qz + 5H_2O$	-3.33
$\lvert$Di,Iv$\rvert$	$2ad + 5tc = 3tr +4/3mt + 2qz + 2H_2O +1/3O_2$	$+6.00$
$\lvert$Tc,Ad$\rvert$	$3/4O_2+ 3iv + tr = 5di + 3mt + 4qz +5/2H_2O$	-3.33
$\lvert$Tc,Iv$\rvert$	$ad + tr = 5di +2/3mt + qz + H_2O +1/6O_2$	$+6.00$
$\lvert$Tr,Ad$\rvert$	$3/4O_2+ 3iv + tc = 3di + 3mt + 4qz +5/2H_2O$	-3.33
$\lvert$Tr,Iv$\rvert$	$ad + tc = 3di +2/3mt + qz + H_2O +1/6O_2$	$+6.00$

The thermodynamic data of diopside, tremolite and talc are given by Robie et al.(1978) and in table IV. According to these data tremolite is always stable with respect to diopside + talc, and the stable projection in the $-\mu_{H_2O}/\mu_{O_2}$-diagram, therefore, is given by:
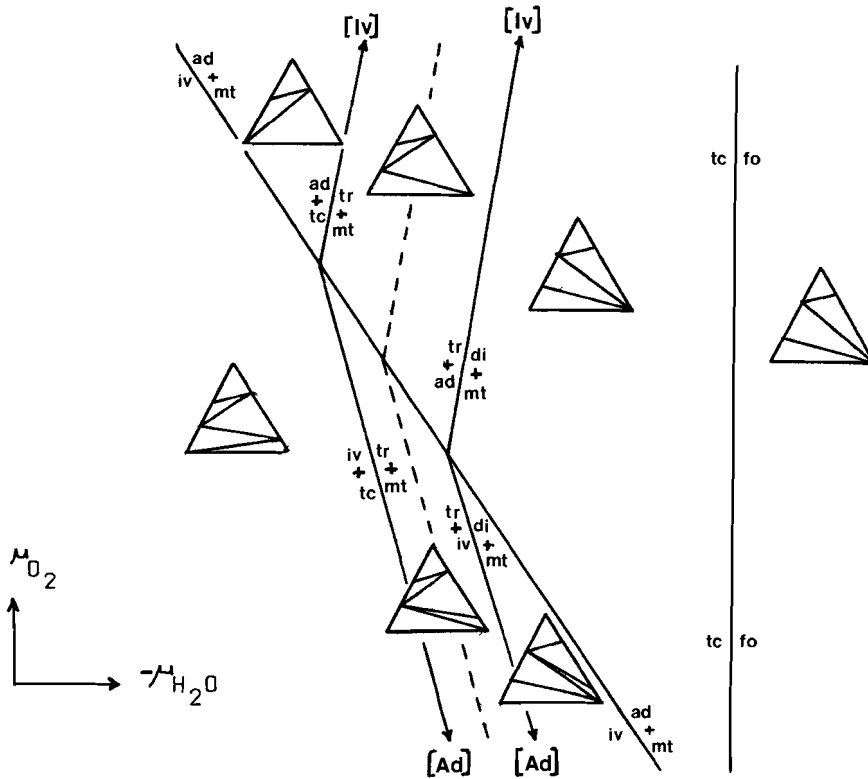
Talc is stable with respect to forsterite + quartz at temperatures $T \leq 922\ ^{0}C$ at $P_{tot} = P_{H_2O} = 1$ kbar.

In fig.16 the $\log f_O - T$ -diagram is presented for the Fe-Si-saturated system Ca-Fe-Mg-Si-H$_2$O-O$_2$ at $P_{tot} = P_{H_2O} = 1$ kbar, calculated with the thermodynamic data given in table IV and the tabulated data for f_O (compare fig.18). The diagram comprises the stability relations of the pure Fe- and pure Mg-endmembers of the olivine-, pyroxene-, and amphibole-solid solution series as well as the stability boundaries of the intermediate compositions $Fe_{50}Mg_{50}$: olivine (ol), salite (sa), actinolite (ac) (dashed curves). The $Fe_{50}Mg_{50}$-curves are calculated assuming ideal mixing of Fe and Mg in the solid solutions.
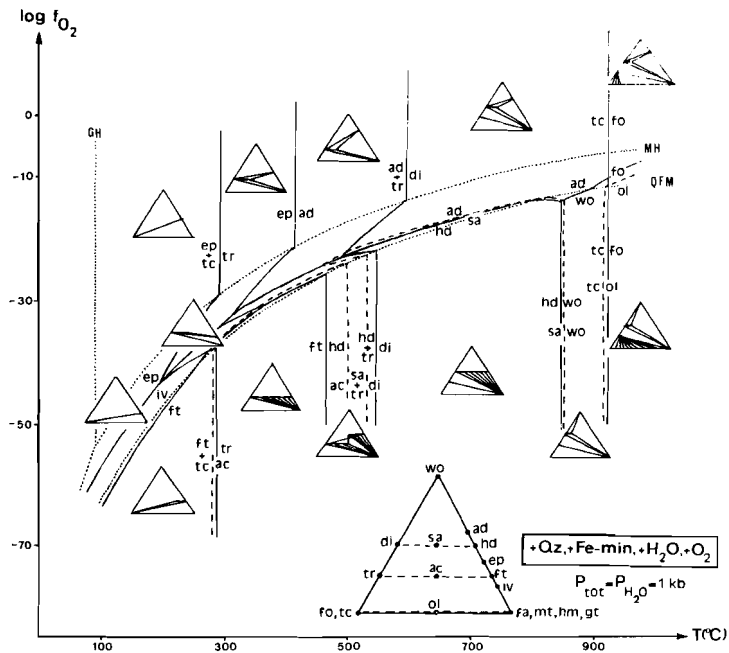
Fig.16: The Fe-Si saturated system Ca-Fe-Mg-Si-H_2O-O_2.

In Fe-Si-saturated systems quartz will always be present with an Fe-mineral (fayalite, magnetite, hematite, goethite) and one or two Ca-Fe-Mg-Si-minerals. Due to the solid solution behavior of Fe and Mg in olivines, pyroxenes and amphiboles the reaction equilibria change as the P,T,f_{O_2} -conditions change and zoned crystals can be formed.
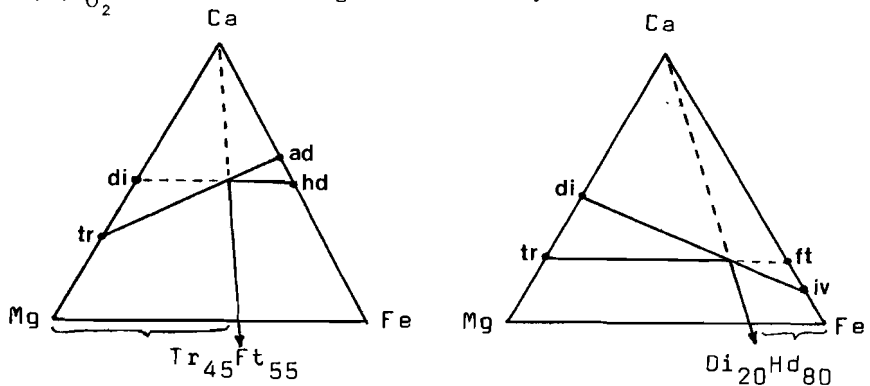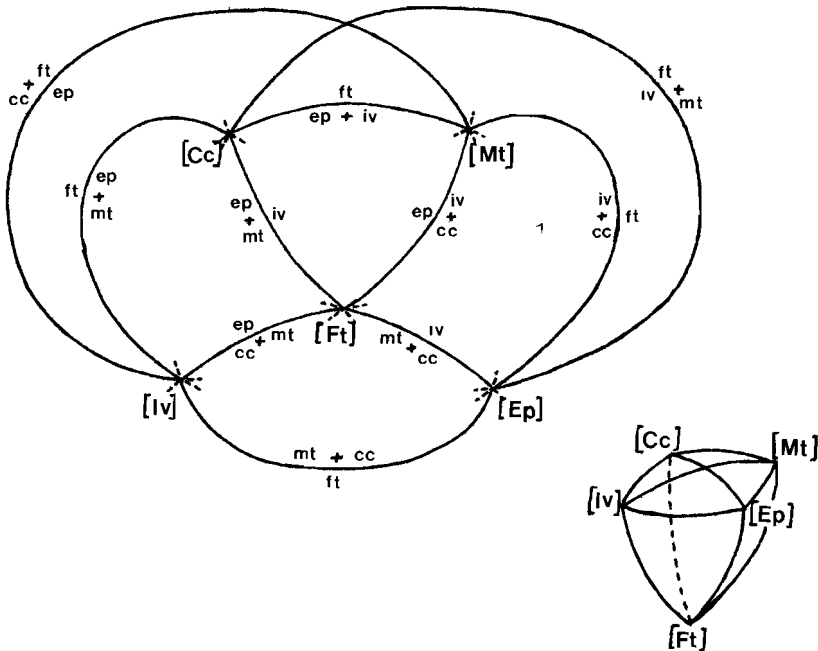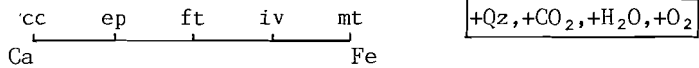
In Fe-rich assemblages ferrotremolite cannot coexist with garnet due to the interference of the stability field of hedenbergitic pyroxene (see figs.15 and 16). In Mg-rich systems garnet and Mg-tremolite form stable associations (fig.19). Graphical analysis of the system in a Ca-Fe-Mg-triangle shows that only Mg-rich amphiboles with compositions up to $Tr_{45}Ft_{55}$ can coexist with andradite.

In Mg-rich assemblages diopside-rich clinopyroxene cannot coexist with ilvaite, while in Fe-rich systems hedenbergite (+ magnetite) breaks down to ilvaite (+ talc)(see figs.18 and 19). According to the graphical analysis in the Ca-Fe-Mg triangle the maximum Mg-content in pyroxenes coexisting with ilvaite is about $Di_{20}Hd_{80}$.
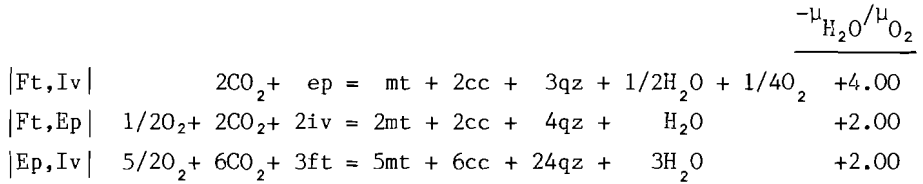
d: The system $Ca-Fe-Mg-Si-CO_2-H_2O-O_2$

In CO_2-containing systems the additional presence of calcite (cc: $CaCO_3$) and CO_2 has to be considered.

Consider the subsystem

83.

In Fe-Si-saturated assemblages the additional reactions are:

$$-\mu_{H_2O}/\mu_{O_2}$$

$|Ft,Iv|$ $2CO_2 + ep = mt + 2cc + 3qz + 1/2H_2O + 1/4O_2$ +4.00

$|Ft,Ep|$ $1/2O_2 + 2CO_2 + 2iv = 2mt + 2cc + 4qz + H_2O$ +2.00

$|Ep,Iv|$ $5/2O_2 + 6CO_2 + 3ft = 5mt + 6cc + 24qz + 3H_2O$ +2.00

In hedenbergite-bearing Fe-Si-saturated assemblages the additional reaction occurs:

$$1/2O_2 + 3CO_2 + 3hd = mt + 3cc + 6qz \qquad -\infty$$
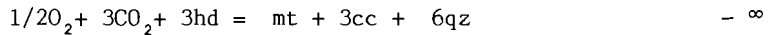
The breakdown of andradite is given by:

$$9CO_2 + 3ad = 2mt + 9cc + 9qz + 1/2O_2 \qquad -\infty$$
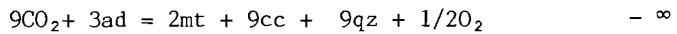
In Mg-bearing Fe-Si saturated systems tremolite decomposes according to:

$$2H_2O + 6CO_2 + 3tr = 5tc + 6cc + 4qz \qquad -3.00$$

and diopside according to:

$$H_2O + 3CO_2 + 5di = tr + 3cc + 2qz \qquad -3.00$$
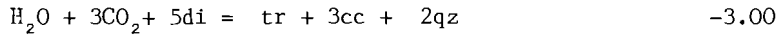
Decarbonation reactions decrease the μ_{CO_2} in the solid phases. Dehydration reactions diminish their μ_{H_2O}. Usually decarbonation and dehydration both take place at increasing temperature. Presentation of the decarbonation and dehydration reactions in a $-\mu_{CO_2}/-\mu_{H_2O}$-diagram indicates the relative sensibilities of the equilibria as functions of temperature and fluid composition. For the system cc-ad-hd-ep-ft-iv+Mt+Qz a possible $-\mu_{CO_2}/-\mu_{H_2O}$-diagram is:
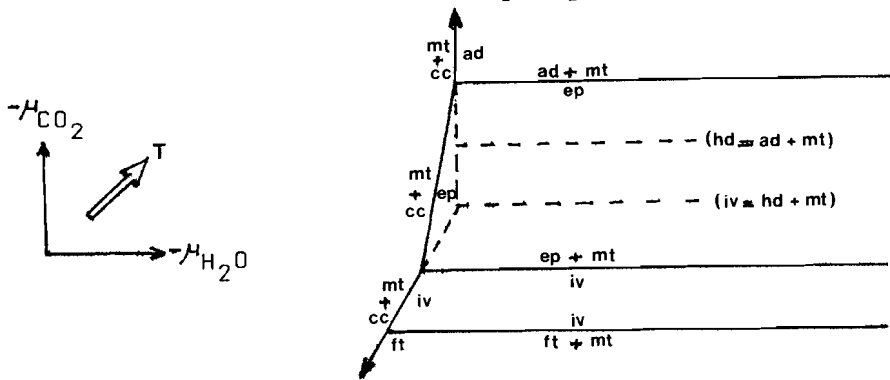
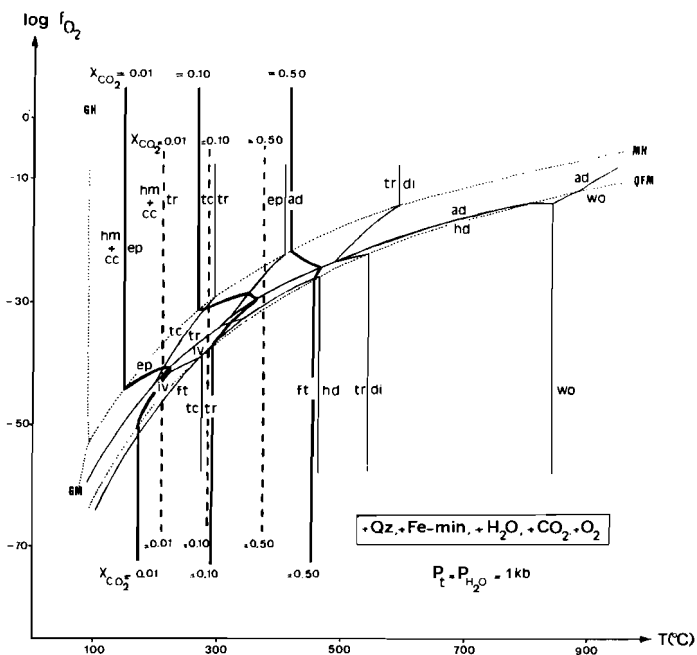Fig.17: The Fe-Si saturated system Ca-Fe-Mg-Si-CO_2-H_2O-O_2.

In the above $-\mu_{H_2O}/-\mu_{O_2}$ -diagram only the slopes of the equilibrium curves are fixed, not their positions relative to each other. Depending on the conditions of P,T,f_{O_2} epidote may be stable over hedenbergite or vice versa, or ferrotremolite may be stable over ilvaite. The absolute positions of the reaction curves have to be fixed by thermodynamic calculations.

In fig.17 the lof f_{O_2} - T -diagram is given for the Fe-Si saturated system Ca-Fe-Si-CO -H_2O-O_2 at P_{tot}= P_{H_2O}+ P_{CO_2} = 1 kbar and the fluid compositions X_{CO_2} = 1 - X_{H_2O}= 0.00, 0.01, 0.10 and 0.50 (compare fig.15). The diagram is calculated using eq.(5-8), the thermodynamic data given in table IV and tabulated data for f_{H_2O} (Helgeson and Kirkham, 1974) and CO_2 (Mel'nik, 1974). The data for calcite are from Robie et al.(1974). As the CO_2-content of the fluid increases the stability fields of the calcite-bearing assemblages are enlarged.

85.

According to fig.17 Fe-rich epidote can only be formed if $X_{CO_2} < 0.50$; ilvaite only occurs if $X_{CO_2} > 0.10$. The occurrence of ilvaite in the massive pyroxenite zone of SW-Seriphos and its breakdown into magnetite + calcite instead of into Fe-epidote suggests that in the siliceous rock systems X_{CO_2} was about 0.01 to 0.05 during the skarn formation. The coexistence of ilvaite with actinolite (tremolite) similarly suggests H_2O-rich fluids with $X_{H_2O} = 0.95 - 0.99$.
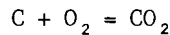
e: The system Ca-Fe-Mg-Si-C-O-H

At low f_{O_2}-values methane (CH_4) can be formed in the fluid phase by the reaction:

$$2H_2O + CO_2 \rightleftharpoons CH_4 + O_2$$
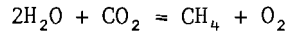
For given conditions of T and P_{fluid} and a fixed fluid composition in terms of X_{H_2O}, X_{CO_2} and X_{CH_4} a corresponding value for f_{O_2} is found. In the log f_{O_2}- T -diagram of fig.21 the equilibrium curve for the above reaction is given for a fluid composition $X_{CO_2} + X_{CH_4} = 0.01$; $X_{H_2O} = 0.98$, calculated under the assumption of ideal mixing of the fluid phases (eq.5-8) and using the thermodynamic data given in table IV, the tabulated fugacity data for H_2O and CO_2, and assuming CH_4 to be perfect gas (Robie et al.,1978; Helgeson and Kirkham, 1974; Mel'nik, 1974).

In the solid phases graphite (C) may appear as a result of the reaction:

$$C + O_2 = CO_2$$

The oxidation equilibrium of graphite roughly coincides with the X_{CO_2}-X_{CH_4}-equilibrium (see fig.18)

Fig.18 also gives the stability fields of the solid phases in the Fe-Si saturated system Ca-Fe-Mg-Si-C-O-H coexisting with the fluid composition $X_{CO_2} + X_{CH_4} = 0.02$; $X_{H_2O} = 0.98$. The stability fields of ilvaite and ferrotremolite and most of the hedenbergite and fayalite fields fall within the domain of the H_2O-CH_4-fluids.

86.
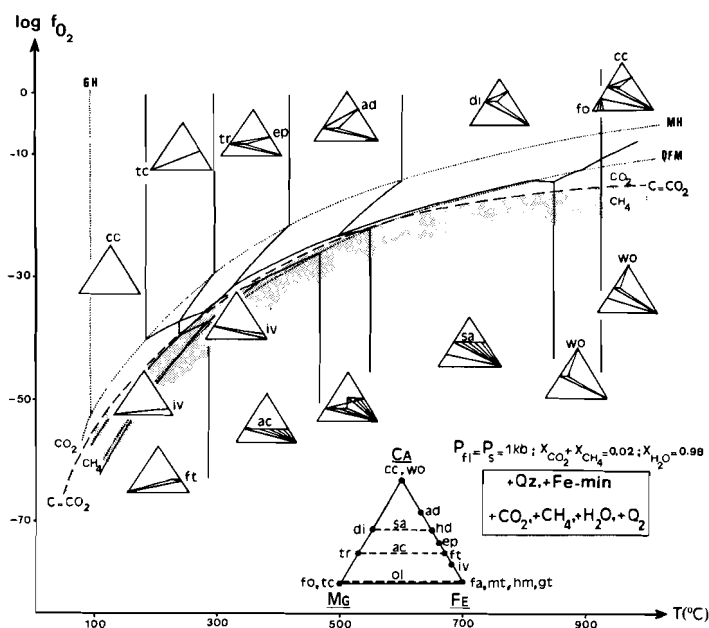
Fig.18: The Fe-Si saturated system Ca-Fe-Mg-Si-C-O-H

SKARN FORMATION AT SERIPHOS

The calculated phase relations in the Fe-Si saturated system Ca-Fe-Mg-Si-C-O-H agree well with the phase relations observed in the skarns at Seriphos.

In the gneisses and the higher stratigraphic levels of the schist-unit skarn formation must have taken place under oxidizing conditions roughly according to the path indicated by the arrow A in fig.19. In conformity with the temperature determinations by $\delta^{18}O$-measurements in coexisting magnetite + quartz and pyroxene + magnetite the arrow A crosses the hd/ad-boundary at temperatures around 550^0C, and the boundary cpx = ad + ac at temperatures of 500^0C or less. The mt = hm transition is crossed at temperatures around 400^0C (table III).

87.

According to the calculated phase diagram the multi-stadial
mineralization sequence in the Fe-Si saturated system along path A is:

$$\left| \quad cc + tc \quad \right| \quad ep + tc \quad \left| \begin{array}{c} ep + tr_{ss} \\ mt/hm \end{array} \right| ad + tr_{ss} \left| ad + di_{ss} \right| sa_{ss}$$

fissure   wall

rocks

$\longleftarrow$

T,t $\boxed{+Qz,+Mt/Hm}$
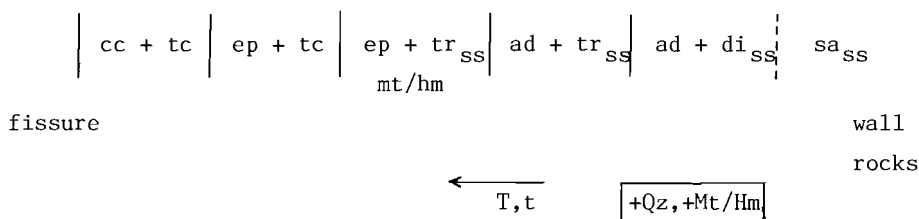
This sequence agrees well with the observed sequence in the skarns in
the gneisses and stratigraphic higher levels of the schist-unit, where
massive, pneumatolytic deposits uniformly composed of clinopyroxene
($Hd_{40-15}Di_{60-85}$) + magnetite $\pm$ quartz $\pm$ andradite grade into and are
cross-cut by vein-type deposits of andradite $\pm$ actinolite
($Tr_{60-70}Ft_{30-40}$) + quartz $\pm$ magnetite. The ad + tr_{ss} + qz + mt
assemblages, in their turn, are cross-cut by epidote-actinolite veins
containing ep $\pm$ tr_{ss} + qz + mt/hm. The final stages are represented by
veinlets with qz $\pm$ cc + hm $\pm$ tr_{ss}/tc.

The high-temperature, pneumatolytic skarn deposits have sharp and
well-defined contacts with the surrounding wall rocks. Around the
pneumatolytic formations the scapolite-bearing contact metamorphic
hornfelses are usually epidotized. The epidotization probably results
from the infiltration of the Fe-rich metasomatic solutions from the
pyroxene-magnetite deposits into the aluminous wall rocks.

In the low-temperature stages of the metasomatic evolution in the
gneisses and schists the common association is tr + qz + hm $\pm$ cc
instead of the association ep + tc + hm + qz indicated by the
thermodynamic analyses. This could point to a fluid composition
$X_{CO_2}= 0.15$, $X_{H_2O}= 0.85$ instead of the composition $X_{CO_2}= 1 - X_{H_2O}= 0.02$
assumed in the calculations (see fig.17). Microprobe analyses, on the
other hand, indicate that the Fe-rich epidotes contain considerable
amounts of alumina (Fe/Al = 1/2)(Vergouwen, 1976), and this will also
affect the stability relations calculated for pure Fe-epidote.
According to the experiments of Holdaway (1972) addition of alumina to
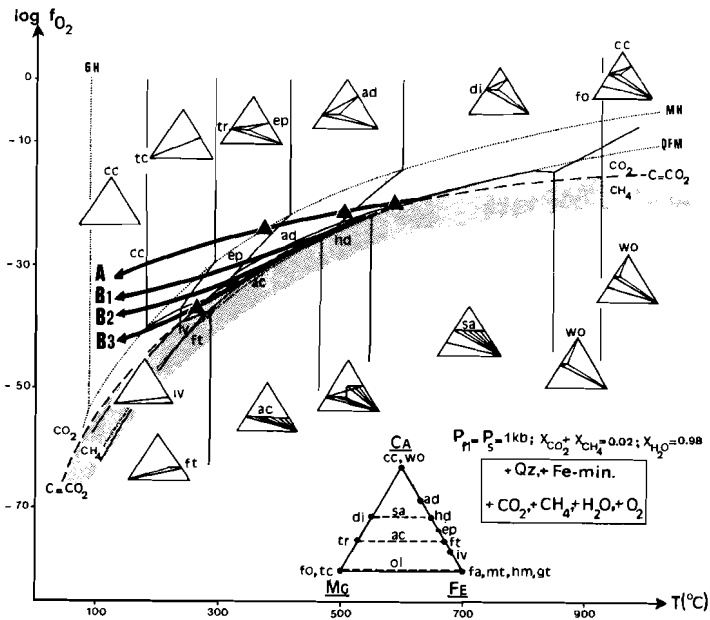
Fig.19: Metasomatic differentiations at Seriphos as evidenced by
the mineralogical evolutions in the various country rock
subsystems in the schist-unit (arrows A, B_1, B_2, B_3)(see text).
Black triangles indicate formation temperatures as measured
by $^{18}O/^{16}O$ of coexisting mineral pairs.

the system causes a shift of the stability field of epidote towards
higher temperatures.

In central-southwestern Seriphos the massive pyroxene skarn zone,
developed in the graphitous, hornblende-rich hornfelses situated
directly on top of the underlying marble series, must have formed at
lower f_{O_2}-values than the skarns in the higher stratigraphic levels of
the schist-unit. The oxygen fugacities must, at least partly, have been
buffered by the graphite buffer $C = CO_2$ (arrows B_1-B_3 in fig.19).
According to the calculated phase diagrams the uralitic pyroxenite
rock, composed of hedenbergitic clinopyroxene ($Hd_{65-75}Di_{35-25}$) +

actinolite (ac_{ss}–tr_{ss}) $\pm$ magnetite $\pm$ quartz may remain a stable skarn
formation in the Fe–Si saturated Ca–Fe–Mg–Si system from the early
stages of metasomatism down to temperatures as low as 300^0C, as long as
the f_{O_2} remains buffered by the graphite. The different mineral
assemblages that have formed at the outer ends of the concentrically
arranged pyroxene aggregates in different areas must have resulted from
differences in the effectivity of the graphite buffering, or to
differences in the amount of graphite originally present in the
metasedimentary host rocks. The different mineralogical developments
point to a gradual increase in the amount of graphite from central
Seriphos towards the south–west.

In central Seriphos, near Bounies, the massive pyroxenite skarn
zone is replaced by ad $\pm$ tr_{ss}+ mt + qz, followed by ep $\pm$ tr_{ss} $\pm$ mt/hm $\pm$
qz and, in the late stages, by $tr_{ss}\pm$ cc + hm + qz. Apparently skarn
formation in central Seriphos was only slightly buffered by graphite,
and only during the early stages of the metasomatic evolution
(arrow B1).

Towards the west, in the direction of Abyssalos, the garnet is
lacking from the medium–temperature formations and the uralitic
pyroxenite rock is replaced along the central transport channels by
ep $\pm$ $tr_{ss}\pm$ mt/hm $\pm$ qz, followed by $tr_{ss}\pm$ cc + hm + qz. In Abyssalos
neither garnet nor epidote is present and the hedenbergitic
clinopyroxene is directly replaced by tr_{ss}+ cc + mt/hm + qz. Towards
the west the thickness of the massive pyroxenite zone increases and,
apparently, graphite–buffering persisted down to lower temperatures
(arrow B2).

In southwestern Seriphos, near Mega Livadhi, the clinopyroxene
from the hedenbergite–actinolite rock is replaced by ilvaite, resulting
in the assemblage iv + $tr_{ss}\pm$ mt $\pm$ qz. The final stages are represented
by the sequence tr_{ss}+ cc $\pm$ mt/hm + qz $\rightarrow$ tc + cc + ˙hm + qz. According
to the thermodynamic analyses the ilvaite–bearing skarns must have
formed under reducing conditions down to temperatures of 300^0C or less
(arrow B3). δ^{18}O–values in quartz + magnetite coexisting with hematite
and actinolite on the outer ends of the ilvaite assemblages give
formation temperatures of some 260^0C (table III). The appearance of

TABLE IV

Thermodynamic data used in the calculations of

the phase equilibria (see text for references).

Mineral phase		H^o J/mol	S^o J/mol.^{o}K	V_s J/bar.mol
qz: quartz	SiO_2	− 912,010	41.46	2.271
gt: goethite	$FeOOH$	− 560,410	60.46	2.087
hm: hematite	Fe_2O_3	− 826,690	87.53	3.034
mt: magnetite	Fe_3O_4	− 1,120,400	150.97	4.458
fa: fayalite	Fe_2SiO_4	− 1,481,480	148.54	4.642
fo: forsterite	Mg_2SiO_4	− 2,173,480	95.32	4.387
tc: talc	$Mg_3Si_4O_{10}(OH)_2$	− 592,440	261.21	13.643
wo: wollastonite	$CaSiO_3$	− 1,637,565	82.12	3.997
cc: calcite	$CaCO_3$	− 1,209,200	92.81	3.700
ad: andradite	$Ca_3Fe_2Si_3O_{12}$	− 5,810,560	288.27	13.232
ep: epidote	$Ca_2Fe_3Si_3O_{12}(OH)$	− 5,656,500	290.49	14.707
iv: ilvaite	$CaFe_3Si_2O_8(OH)$	− 3,725,530	269.00	10.157
hd: hedenbergite	$CaFeSi_2O_6$	− 2,867,890	146.65	6.809
di: diopside	$CaMgSi_2O_6$	− 3,215,360	143.30	6.573
ft: ferrotremolite	$Ca_2Fe_5Si_8O_{22}(OH)_2$	−10,531,720	691.06	28.157
tr: tremolite	$Ca_2Mg_5Si_8O_{22}(OH)_2$	−12,372,792	549.69	27.320
C : graphite	C	0	5.74	0.532
methane	CH_4	− 74,920	186.54	
carbondioxide	CO_2	− 394,070	214.07	
water	H_2O	− 242,170	188.97	
oxygen	O_2	0	205.31	

hematite in the final stages of the metasomatic sequence evidences an increase in f_{O_2} towards the end of the mineralizing activities, probable because all accessible graphite was completely consumed by the continuous reaction with the invading hydrothermal solutions. In SW-Seriphos the initial presence of abundant graphite is testified by its preservation in epidotized hornfels relicts surrounded by a protective rim of massive pyroxenite.

In a few places in the extreme south-west of Seriphos the hedenbergite is replaced by ferrotremolite instead of ilvaite. The ferrotremolite, in its turn, is replaced by cc + mt/hm + qz. The absence of ilvaite from these assemblages is in conflict with the phase diagram of fig.18 calculated for $P_{tot} = P_{fl} = 1$ kbar. At decreasing fluid

pressures (H_2O-fugacities), however, the stability field of ferrotremolite expands at the expense of ilvaite and, probably, the absence of ilvaite from the ferrotremolite-bearing assemblages in SW-Seriphos, at a large distance from the intrusive contact, is due to a decrease in the fluid pressures, and to lower temperatures. $\delta^{18}O$-determinations on coexisting quartz + calcite on the outer end of a ferrotremolite mineralization indicate a formation temperature of $125^{\circ}C$ (table III).

The f_{O_2}-buffering by graphite during the hedenbergite, ilvaite, and ferrotremolite formation in the massive pyroxene skarn zone of SW-Seriphos indicates that local buffering of the hydrothermal solutions by solid-fluid equilibria was a dominant control of the mineralogical evolution (maintenance of local equilibrium). Fluid flow and mass transport, on the other hand, also must have played an important role during the metasomatic actions as is indicated by the increase in f_{O_2} during the final stages of metasomatism when all accessible graphite must have been consumed and local buffering of the f_{O_2} by the invading solutions became ineffective, and by the continuous maintenance of Fe-saturation during the precipitation of the skarn assemblages.

CONCLUSION

The thermodynamic analysis of the skarn assemblages from Seriphos testifies that the skarn assemblages in the Si-saturated gneissic and schistous country rocks are Fe-Si saturated skarns that formed over a wide temperature range as a result of the continuous interaction of Fe-rich, hydrous solutions with the Si-saturated wall rocks. The chronological order in the skarn assemblages evidences that skarn formation proceeded at gradually decreasing temperatures.

....and the rising fumes pass into the veins
and stringers and are united through the
effect of the planets and made into ore.

Bergbuchlin, 1520

CHAPTER VI: THE FLUID PHASE

Study of the fluid inclusions in a mineralization defines the
fluid phase in terms of fluid density, nature of the fluid phase, and
salt content of the hydrous solution. Investigation of the oxygen
isotope composition of the fluid phase points out the influence of
local (isotopic) conditions on the isotopic composition of the fluid.
Together the isotopic and fluid inclusions give an indication of the
source of the metasomatic solutions.

METHOD OF INVESTIGATION

Fluid inclusions in the solid phases of a mineralization contain
tiny samples of the hydrothermal fluids that coexisted with the solid
minerals at the time of their formation. Temperature measurements of
the phase transitions in individual inclusions in the transparent
minerals from a hydrothermal equilibrium assemblage by means of a
microscope equipped with a freezing and heating stage permit
determination of the density and bulk chemical composition of the
hydrothermal fluid. With temperature indications given by the
thermodynamic analysis of the skarn assemblages, or temperature
determinations by $^{18}O/^{16}O$-ratios from coexisting mineral pairs, the
fluid inclusions data further specify the formation conditions of an
equilibrium assemblage in terms of temperature (T), fluid pressure (P_f)
fluid composition (X_f), and salt content of the hydrous solution.

The isotopic composition of the fluid phase from which the solid phases of a mineral assemblage precipitated can be determined from the $^{18}O/^{16}O$-ratios of the mineral phases, provided the isotopic equilibrium fractionation is known at the (measured or estimated) equilibrium temperature. The $^{18}O/^{16}O$-composition of the fluid phase indicates whether the metasomatic solution was in local (isotopic) equilibrium with the host rocks adjacent to the transport channel, or that the metasomatic solution was an externally derived fluid that imposed its isotopic composition on the solid phases in the metasomatic mineralization. The isotopic results, combined with the fluid inclusions data, may point out the source of the metasomatic solutions.

ANALYTICAL PROCEDURES

Melting point and phase homogenization data were obtained for fluid inclusions in quartz, barite and fluorite using an optical microscope equipped with a Chaixmeca freezing and heating stage (Poty, 1976). $^{18}O/^{16}O$-compositions of whole rock silicate samples and skarn minerals were obtained by treating the powdered samples with HCl to remove possibly attached carbonate, extracting the oxygen with BrF_5, converting it to CO_2, and measuring the isotopic composition by mass spectrometry (Clayton and Mayeda, 1963). Barite samples were powdered, mixed with excess graphite powder, and converted to CO_2 in an induction oven at 1200^0C; small amounts of CO were oxidized to CO_2 using an electric discharge (Clayton and Epstein, 1958). The isotopic compositions were measured in a VG-Micromass 602 mass spectrometer.

$^{18}O/^{16}O$-results are reported in the δ-notation, defined as

$$\delta(\%.) = \left\{ ^{18}O/^{16}O(sample)/^{18}O/^{16}O(standard) - 1 \right\} \times 1000 \qquad (6-1)$$

and converted to SMOW (Graig, 1961). Analysis of NBS-28 quartz standard yielded 9.3 ± 0.2 %..

THE METASOMATIC SOLUTIONS

The unaltered granodiorite

In quartz grains from unaltered samples of the main body granodiorite primary fluid inclusions (1 – 200 μ) contain a dark colored vapor bell and 2 or 3 solid phases. The volume of the vapor bubble is 1/15 to 1/10 times the total volume of the fluid inclusion (V_b/V_t= 0.07 – 0.10); the dark color of the vapor phase indicates low vapor pressures in the bubble. The major solid phase in the fluid inclusions is NaCl, which appears in colorless, cubic crystals with volumes 1 – 2 times the volume of the vapor bubble (V_s/V_b= 1.5–2.0). (Plate 14). Small, elongated crystals of a colorless solid (gypsum?) are usually present and often the primary fluid inclusions also contain a tiny grain of a third, colorless solid phase.

Upon heating the vapor bubble disappears at homogenization temperatures of T_h= 240 – 260 ^{0}C. At temperatures between 350 and 400 ^{0}C the NaCl–phase is completely dissolved. The NaCl dissolution temperatures, T_s= 350 – 400 ^{0}C, points to total salt contents in the hydrous solution equivalent to 40 – 45 wt% NaCl (see fig.20). The other solid phases in the primary fluid inclusions remain present up to temperatures over 450 ^{0}C.

Upon cooling to temperatures as low as –165 ^{0}C the vapor bubble only changes its shape due to the formation of the ice in the hydrous solution; no phase transitions were observed in the vapor that could betray the presence of a significant amount of CO_2 or CH_4 in the vapor. The first melting of ice occurs at the eutectic temperature T_e= –58 ^{0}C. This temperature corresponds to the eutectic temperatures in the system $NaCl-CaCl_2-MgCl_2$ (see fig.21). All ice is molten at the melt temperature T_m= –35 ^{0}C. At higher temperatures all ice has disappeared, but an additional, colorless, cubic solid appears besides the NaCl–cube. This second cubic solid, KCl, is dissolved at –4 ^{0}C, pointing to a KCl–content in the hydrous solution of 20–25 eq.wt.% KCl (fig.23).

Secondary inclusions in the unaltered granodiorite usually only contain a dark colored vapor bubble (V_b/V_t= 0.2, but also variable) with homogenization temperatures between 320 and 360 ^{0}C. The melt
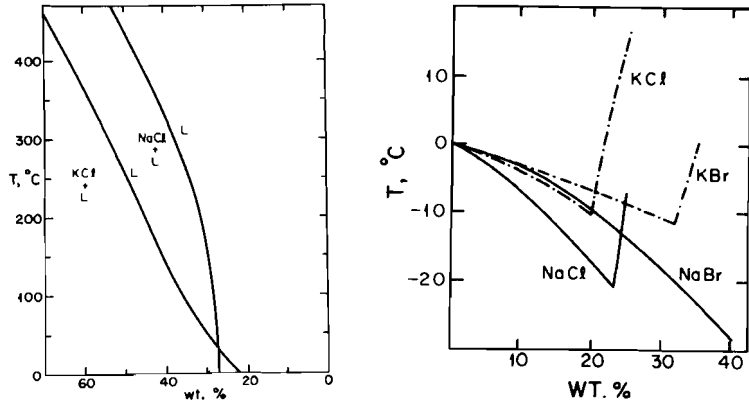
Fig.20: Solubility of NaCl and KCl at elevated temperatures (fig.20a)
and freezing point depression of water for NaCl, NaBr, KCl
and KBr (fig.20b)(from Crawford, 1981).

temperatures of the ice, $T_m = -20^{\circ}C$, point to total salt contents in
these secondary inclusions of about 20-25 eq.wt.% NaCl.

$^{18}O/^{16}O$-isotope ratios of whole rock samples from the unaltered
granodiorite vary between $\delta^{18}O_{SMOW} = 9.2 - 9.6$ %. (table VI). These
isotopic compositions are in the typical range of magmatic rocks
(Taylor, 1968).

The isotopic composition of a whole rock sample is composed of the
isotopic contributions of the constituent mineral phases:

$$\delta^{18}O_{WR} = \frac{n_1 N_1 \delta^{18}O_{M1} + n_2 N_2 \delta^{18}O_{M2} + \ldots\ldots + n_i N_i \delta^{18}O_M}{n_1 N_1 + n_2 N_2 + \ldots\ldots + n_i N_i} \qquad (6-2)$$

where n_i = mol% of mineral i, and N_i = amount of O per mol i. The
isotopic composition of the coexisting water phase is given by:

$$\delta^{18}O_{H_2O} = \delta^{18}O_{WR} - \frac{\Sigma n_i N_i \Delta^{18}O_{M-H_2O}}{\Sigma n_i N_i} \qquad (6-3)$$

where $\Delta^{18}O_{M-H_2O} = \delta^{18}O_M - \delta^{18}O_{H_2O}$ = fractionation of the mineral M with
water. For a simplified composition 25 wt% quartz, 25 wt% K-feldspar,
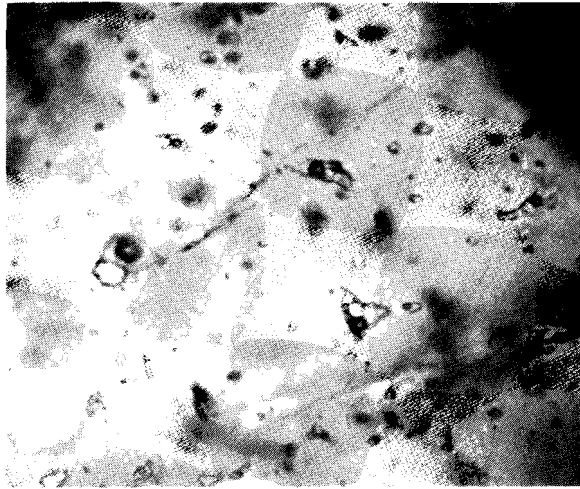
Plate 14: Primary fluid inclusions with NaCl-cubes in quartz in
the Seriphian granodiorite (sample loc.9.4).

and 50 wt% plagioclase (anorthite) and the equilibrium curves $\Delta^{18}O_{qz-H_2O}$
$\Delta^{18}O_{Kf-H_2O}$, $\Delta^{18}O_{An-H_2O}$ summarized by Friedman and O'Neil (1977), and
with a formation temperature T = 750°C for the unaltered granodiorite,
a value $\delta^{18}O_{H_2O}$= 9.9 - 7.5 %. is found for the isotopic composition of
the H_2O-phase that equilibrated with the crystallizing magmatic rock.

Quartz grains, separated from two samples of the unaltered
granodiorite gave isotopic compositions of respectively $\delta^{18}O_{qz}$= 10.4
and 9.7 %.(table VI). At T_f= 750°C the quartz grains must have been in
equilibrium with a H_2O-phase with $\delta^{18}O_{H_2O}$= 9.7 and 9.0 %..This
composition agrees well with the isottopic composition of the H_2O-phase
found to have equilibrated with the whole rock at 750°C.

The bleached granodiorite

Primary fluid inclusions (1 - 200 μ) in quartz grains from the
bleached zones in the main body granodiorite contain a dark colored
vapor bubble (V_b/V_t= 0.10), a NaCl-cube (V_s/V_b= 1-1$\frac{1}{2}$), and sometimes a
tiny grain of an opaque mineral phase (magnetite?). Homogenization
temperatures are T_h= 240-270°C. Eutectic temperatures are uniformly
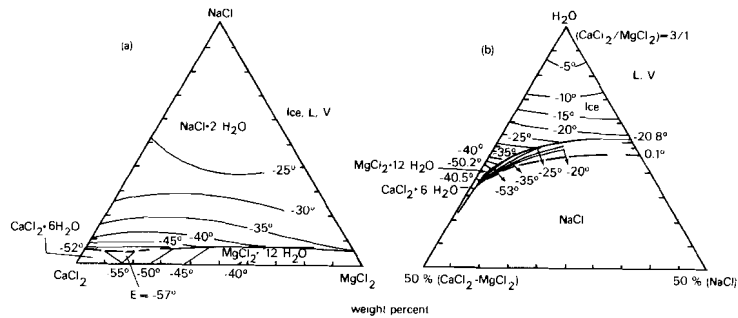
Fig.21:The system NaCl–CaCl$_2$–MgCl$_2$–H$_2$O. Fig.21a: Hydrate–ice phase
relations projected from H$_2$O. Fig.21b: Section through the
system at a CaCl$_2$/MgCl$_2$-ratio of 3 : 1. Liquidus fields are
labelled and separated by heavy lines (from Crawford, 1981).

T$_e$= -58^{0}C. The melt temperatures of the ice, T$_m$, vary between -43 to
-35^{0}C, and the dissolution temperatures of the NaCl-cubes, T$_s$, are
330 - 350^{0}C, conformable to total salt contents of 35 - 40 eq.wt.%
NaCl. KCl could not be identified as a separate solid phase (KCl $\leq$
20 eq.wt.%).

The primary fluid inclusions in the quartzes from the leached
granodiorite are very similar to the primary fluid inclusions in the
quartz grains from the unaltered main body granodiorite. The
homogenization temperatures are about the same, as are the eutectic and
melt temperatures. The somewhat lower NaCl-dissolution temperatures
(T$_s$= 330–350^{0}C instead of 350–400^{0}C) and the absence of KCl as a
separate solid phase, however, point to somewhat lower total salt
contents (40–35 eq.wt.% NaCl instead of 45–40 eq.wt.% NaCl).

The secondary fluid inclusions in the bleached granodiorite are
similar to the secondary fluid inclusions in the unaltered granodiorite
with homogenization temperatures of T$_h$= 300–350^{0}C, no solid phases
present at room temperature, and total salt contents around 20 eq.wt.%
NaCl as indicated by the melt temperatures of T$_m$= -20 to -15^{0}C.
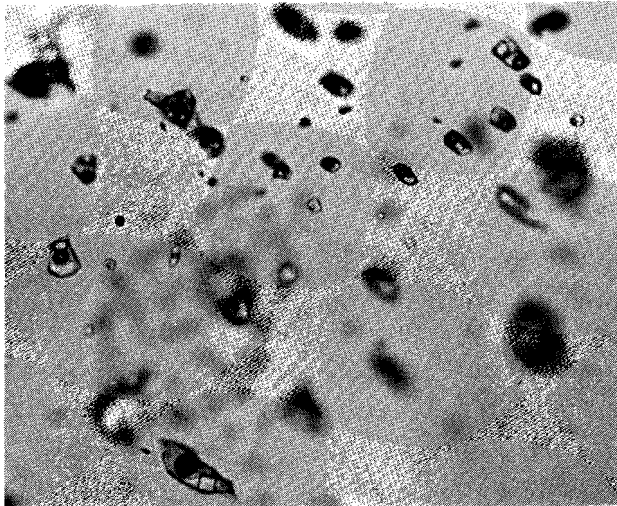
Plate 15: NaCl-supersaturated, primary fluid inclusions in
         quartz from a HT garnet-quartz skarn (sample 120B).

    In a whole rock sample of the bleached granodiorite the isotopic
composition $\delta^{18}O_{WR}$= 10.0 %, and in quartz grains from the same rock
sample $\delta^{18}O_{qz}$= 11.4 %. (table VI). For a simplified rock composition
25 wt% quartz + 75 wt% albite, and an equilibrium formation temperature
T_f= 600-500^{0}C both the whole rock and quartz $\delta^{18}O$-data give comparable
results for the isotopic composition of the coexisting water phase:
$\delta^{18}O_{H_2O}$= 9.0 - 7.8 %. (for respectively 600 and 500^{0}C). Oxygen isotope
ratios in other whole rock samples from the bleached granodiorite are
between 10.6 and 9.6 %.; at T_f= 550^{0}C the corresponding isotopic
equilibrium composition of the coexisting water phase is $\delta^{18}O_{H_2O}$= 9.0 -
7.8 %..

diopside-andradite skarns
    Idiomorphic quartz crystals coexisting with andraditic garnet in
vein-like strucctures cross-cutting previously formed pyroxenite skarns
contain small primary fluid inclusions, 1 - 100µ in size, with a dark
colored vapor bell (V_b/V_t= 0.1-0.2), a NaCl-cube (V_s/V_b= 1-1/3) and one
or two other solid phases that are insoluble up to temperatures over

$450^{\circ}C$. One of the additional solid phases is opaque (magnetite?). The homogenization temperatures T_h of the inclusions vary between 280 and $360^{\circ}C$ with most measurements around $340^{\circ}C$. The eutectic temperatures T_e are about $-45^{\circ}C$ and the ice is entirely molten at $T_m = -40$ to $-35^{\circ}C$, indicating that the hydrous solutions contain considerable amounts of $NaCl$, $KCl(?)$, $CaCl_2$, $MgCl_2$ (and $FeCl_2$?). The NaCl-cubes dissolve at temperatures between 350 and $150^{\circ}C$, pointing to total salt contents of $35 - 30$ eq.wt.% NaCl (Plate 15).

Secondary fluid inclusions in the idiomorphic quartz crystals from the andradite skarns are bi-phase with $V_b/V_t = 0.2$, $T_h = 300^{\circ}C$ and $T_e = -33$ to $-28^{\circ}C$. The melting temperatures T_m of the secondary fluid inclusions are between -0.5 and $-0.1^{\circ}C$. During the final stages of the melting proces, from -2.0 to $-0.1^{\circ}C$, a solid hydrate phase rapidly dissolves and the vapor bubble rapidly doubles in volume. The solid hydrate $Na_2CO_3 \cdot 10H_2O$ has an eutectic temperature of $-2.1^{\circ}C$ and an upper stability temperature of $+32^{\circ}C$ (Schafer and Lax, 1962). The melting temperature $T_m = -0.5$ to $-0.1^{\circ}C$ points to the presence of about 10 wt% carbonate-hydrate in the secondary fluid inclusions, conformable to a CO_2-content of $X_{CO_2} = 0.01-0.02$ in the hydrous fluid.

In the HT-pneumatolytic diopside-andradite skarns with and without quartz the isotopic data on coexisting magnetite + quartz and magnetite + pyroxene indicate equilibrium formation temperatures of 560 to $500^{\circ}C$ using the equilibrium curves $\Delta^{18}O_{mt-qz}$ and $\Delta^{18}O_{mt-di}$ given by Matthews et al.(1983a) (see also table III). The corresponding isotopic composition of the coexisting H_2O-phase must have been $\delta^{18}O_{H_2O} = 12.7$ to 12.2 %.. At similar temperatures of $550-500^{\circ}C$ the $^{18}O/^{16}O$-compositions of magnetites from other di + ad + mt skarns indicate similar water compositions $\delta^{18}O_{H_2O} = 13.0-11.9$ %. (table VI).

In garnet + quartz veins cross-cutting the previously formed pneumatolytic deposits the isotopic compositions of the quartzes are $\delta^{18}O_{qz} = 12.8-12.9$ %.; for $T_f = 450^{\circ}C$ the corresponding fluid compositions are $\delta^{18}O_{H_2O} = 9.2-9.3$ %. (table VI).
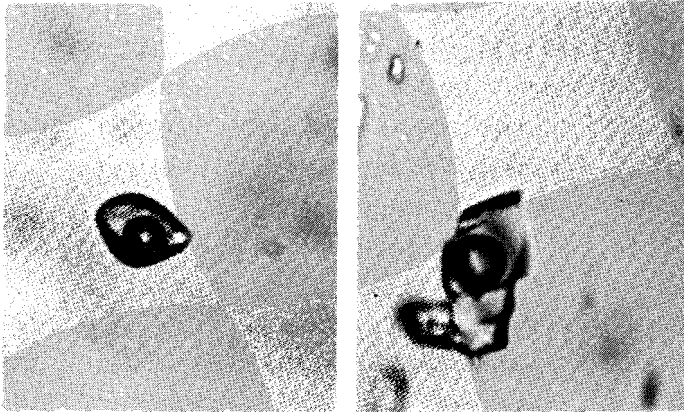
Plate 16: Two primary fluid inclusions from MT epidote-actinolite
skarns. The left inclusion from an epidote-actinolite-
quartz assemblage (no.20.11) contains a tiny NaCl-cube;
the right inclusion from an actinolite-quartz-calcite
parageneses (no.134) is halite-free.

epidote-actinolite skarns

In the MT-stages of the metasomatic evolution in the gneiss-unit
and the upper parts of the schist-unit epidote-actinolite-quartz veins
cross-cutting the older garnetite skarns, are followed by actinolite-
quartz-calcite parageneses (Plates 16).

Quartz grains coexisting with epidote contain primary fluid
inclusions usually consisting of a hydrous solution and a dark-colored
vapor bubble (V_b/V_t= 0.10-0.20). In some inclusions a tiny NaCl-cube is
also present and occasionally another solid phase occurs that is
transparent and insoluble. Upon cooling down to -160^0 C no phase
transitions were observed in the vapor phase. The eutectic temperature
of the hydrous solution is T_e= -37^0 C, and this is close to the eutectic
temperature in the system $NaCl-MgCl_2-H_2O$ (fig.21). The melting
temperature of the ice is T_m= -22^0 C, indicating a total salt content of
23 - 25 eq.wt% NaCl. The occasional presence of small NaCl-cubes with
dissolution temperatures around room temperature point to maximal total
salt contents of about 27 eq.wt% NaCl. The homogenization temperatures
T_h of the primary inclusions in the quartzes coexisting with epidote
are 350-340^0 C.

101.

In quartz and calcite grains coexisting with actinolite all
primary inclusions are bi-phase (V_b/V_t= 0.10-0.20). Upon cooling to
-160°C no phase transitions occurred in the dark colored, low pressure
vapor bubbles. The eutectic temperatures T_e are uniformly -36/-35°C,
and the freezing points T_m are uniformly -15 to - 14°C, indicating
$NaCl-(KCl)-MgCl_2-(FeCl_2?)$-rich, hydrous fluids with total salt contents
of 18-20 eq.wt% NaCl. The homogenization temperatures T_h in primary
inclusions in quartzes as well as calcites coexisting with actinolite
and hematite all fall within the narrow range of 290 to 310°C.

In vein-type epidote-actinolite-qquartz-magnetite/hematite
deposits $\delta^{18}O$-values of coexisting magnetite + quartz indicate
equilibrium formation temperatures of some 400°C (table VI). The
isotopic compositions of the quartzes, $\delta^{18}O_{qz}$= 14.7-11.4 %., point to
compositions $\delta^{18}O_{H_2O}$= 9.6-7.2 %. for the coexisting water phase.
In epidote veins the isotopic compositions of coexisting quartzes
are $\delta^{18}O_{qz}$= 12.6-11.4 %.; for an estimated formation temperature T_f=
400°C the isotopic compositions of the coexisting hydrous solutions
are $\delta^{18}O_{H_2O}$= 8.0-6.8 %. In two quartz + magnetite + hematite veins the
$\delta^{18}O$-compositions of coexisting qquartz and magnetite indicate
formation temperatures of 410-400°C, and equilibrium compositions
$\delta^{18}O_{H_2O}$= 7.2-7.7 %..
In actinolite-calcite-quartz-magnetite/hematite assemblages from
the lower parts of the schist-unit, just above the massive pyroxenite
skarn zone of SW-Seriphos, $\delta^{18}O$-values of coexisting quartz + magnetite
give formation temperatures of T_f= 405-390°C. The quartz compositions
$\delta^{18}O_{qz}$= 14.7-13.3 %. correspond to compositions $\delta^{18}O_{H_2O}$= 9.6-8.8 %. for
the coexisting water phase.

ilvaite-actinolite skarns
In the graphitous, massive pyroxenite skarn zone of SW-Seriphos
ilvaite, actinolite, quartz and/or magnetite occur together in
vein-like structures and geodic cavities throughout the massive
pyroxenite rock.
Primary fluid inclusions in quartzes coexisting with ilvaite

contain a hydrous fluid and a dark colored vapor bubble at room
temperature. Some inclusions also contain a tiny NaCl-cube and in a few
inclusions an insoluble, transparent solid appears. In the vapor bubble
no phase transitions were observed upon cooling down to temperatures of
$-165\,^{0}$C. Eutectic temperatures are T_e= -58 to -51 ^{0}C. Melt temperatures
T_m vary from $-38\,^{0}$C in halite-containing inclusions to $-20\,^{0}$C in the
bi-phase inclusions. The homogenization temperatures T_h vary between
310 and 260 ^{0}C.

The freezing data from the primary fluid inclusions in the
ilvaite-quartz associations indicate that the H_2O-fluids are
$NaCl-(KCl)-MgCl_2-(FeCl_2(?))$-brines with total salt contents around 25
eq.wt% NaCl. Both the salt contents and the homogenization temperatures
are comparable with the salt contents and the homogenization
temperatures in the primary fluid inclusions in the epidote-actinolite-
deposits.

Secondary fluid inclusions in the quartzes have homogenization
temperatures around 180 ^{0}C. The melt temperatures are about 0 ^{0}C due to
the formation of the carbonate-hydrate $Na_2CO_3.10H_2O$ (X_{CO_2} = 0.01-0.02).

In quartzes coexisting with ilvaite the isotopic compositions are
$\delta^{18}O_{qz}$= 12.5 - 13.2 %. The thermodynamic analyses indicate formation
temperatures for the ilvaite-containing assemblages around T_f= 350-300^{0}
At such temperatures the isotopic equilibrium composition of the aquous
solution is $\delta^{18}O_{H_2O}$= 6.8-6.0 %. In two samples containing actinolite +
quartz + magnetite in the central transport channels within ilvaite
occurrences the $\delta^{18}O$-values of coexisting magnetite + quartz give
formation temperatures of 265 - 260^{0}C. The $\delta^{18}O$-values of the quartzes,
$\delta^{18}O_{qz}$= 16.6-16.5 %., indicate isotopic compositions for the coexisting
water phase of $\delta^{18}O_{H_2O}$= 7.5-7.8 %. (table VI).

In geodic cavities, developed at transport channel junctions
within the massive pyroxenite rock, up to 10 cm large, idiomorphic
quartz crystals occur which may show a strong zoning in their fluid
inclusions.

For instance (sample 55/3):

pyroxenite	V_b/V_t	V_s/V_b	T_s	T_e	T_m	T_h	$\delta^{18}O_{qz}$	n^*
I	1/5	3/4–1/2	240–180	−51	−38	260–300	13.2	8
II	1/5	1/5– 0	200	−55	−36	270–290	13.0	5
III	1/5–1/10	–	−22	−48	?	var	11.7	(2)
IV	1/10	–	–	−57	−28	290	12.0	4
V	1/10	–	–	−58	−10	265–285	14.1	4

n^* = number of measured primary fluid inclusions

In the above quartz crystal, with its root in the uralitic hedenbergite skarn and its outer rim covered by a thin layer of late stage calcite + hematite/limonite, the eutectic temperatures in the primary fluid inclusions all are about equal (T_e= −58°C) and near the eutectic temperature in the system $NaCl-(KCl)-CaCl_2-MgCl_2-(FeCl_2?)$. The total salt contents, however, strongly decrease from about 35 eq.wt% NaCl near the root of the crystal (and a NaCl-cube present in the fluid inclusions with T_s= 240–180°C) to about 15 eq.wt% NaCl near the top of the quartz crystal (T_m= −10°C). The homogenization temperatures are about constant (T_h= 290°C), as are the isotopic compositions ($\delta^{18}O_{qz}$= 12–14 %.).

The observed zoning in the quartz crystal, that is the (more or les) continuous decrease in total salt content at (about) constant T_e, T_h and $\delta^{18}O_{qz}$ coincides with the observed changes in the quartzes from the sequence of multi-stadial, Si-saturated assemblages formed in the HT-garnet to MT/LT-actinolite skkarns. The zoning suggests that the quartz crystal grew (more or less) continuously during the metasomatic evolution from (more or less) constantly Si-saturated solutions under (more or less) continuously decreasing temperatures (and fluid pressures).

Other quartz crystals from geodic cavities in the massive pyroxene skarn zone of SW-Seriphos show a similar though usually less pronounced zoning in their fluid inclusions (see also de Groot, 1975).

sphalerite-galena ores

Near the outer actinolite isograd of the contact metamorphic aureol a few deposits of sphalerite-galene-pyrite-hematite + quartz + calcite occur (see fig.3).

Quartz crystals from one of the sulfidic deposits have primary fluid inclusions containing only a hydrous solution and a dark colored vapor phase (V_b/V_t= 0.20). The vapor phase does not respond to cooling to -150°C. The minimum eutectic temperature measured in the fluid inclusions is T_e= -58°C, but most of the ice melts over the range T_e' = -27°C to T = -18°C; this freezing behavior suggests that the solutions are NaCl-dominated, $CaCl_2$-$MgCl_2$-(KCl-FeCl$_2$?)-containing H_2O-fluids with a total salt content of some 22 eq.wt% NaCl. The homogenization temperatures of the fluid inclusions are between 350 and 280°C.

Quartz grains from the sphalerite-galena deposit have isotopic compositions $\delta^{18}O_{qz}$= 11.6-13.8 %..The homogenization temperatures of the fluid inclusions suggest (minimum) formation temperatures of 400-350°C. At such temperatures the corresponding water compostions are $\delta^{18}O_{H_2O}$= 7.0-8.0 %..

late stage sulfidic deposits

Close to the intrusive contact a pyrite-hematite-quartz-calcite occurrence contains idiomorphic quartz crystals with primary fluid inclusions with a dark colored vapor bubble (V_b/V_t= 0.2) and a hydrous solution with an eutectic temperature lower than -43°C. The melting temperatures T_m are between -15 and -10°C, conformable to a total salt content of about 15 eq.wt% NaCl. The homogenization temperatures of the primary fluid inclusions are uniformly T_h= 235-230°C.

In a few inclusions melting temperatures are 0 to +0.5°C due to the formation of $Na_2CO_3.10H_2O$ during the melting proces. The

homogenization temperatures in these relatively CO_2-rich, secondary inclusions are 190 to 200^{0}C.

The isotopic composition of quartz from the late stage LT pyrite-hematite deposits is $\delta^{18}O_{qz}$= 14.8 %.. For an assumed formation temperature of 250^{0}C this corresponds to an isotopic composition $\delta^{18}O_{H_2O}$= 5.2 %. for the coexisting H_2O-phase.

In a late stage pyrite + calcite + quartz deposit in SW-Seriphos $\delta^{18}O$-values of coexisting quartz and calcite are $\delta^{18}O_{qz}$= 22.0 %. and $\delta^{18}O_{cc}$= 18.8 %. (table V). According to the equilibrium curve $\Delta^{18}O_{qz-cc}$ given by Matthews (1983b) the data indicate a formation temperature T_f= 125^{0}C for this very late stage, sulfidic deposit, and a composition $\delta^{18}O_{H_2O}$= 3.5 %. for the water phase during the waning stages of the metasomatic-hydrothermal activities at Seriphos.

fluorite-barite deposits

Idiomorphic crystals of fluorite and barite occur together with hematite-limonite iron ore in the marble-units in SW-Seriphos and in a large fracture zone within the granodiorite intrusive (fig.3).

The primary fluid inclusions in the fluorite and barite contain two or three phases (Plate 17). Around the dark colored vapor bubble a small rim of liquid CO_2 may be present that crystallizes to a solid phase at -57^{0}C. The size of the solid CO_2 grains suggests that the molar fractions of CO_2 in the fluid inclusions is less than X_{CO_2}= $1 - X_{H_2O}$= 0.05. The eutectic temperatures of the hydrous solutions are about T_e= -37^{0}C, or about equal to the eutectic temperature in the system $NaCl-MgCl_2-H_2O$ (fig.21). The melt temperatures T_m vary with the homogenization temperature from T_m= -20^{0}C, T_h= 265^{0}C to T_m= -5^{0}C, T_h= 100^{0}C.

The coupled changes in T_m and T_h indicate a gradual and (more or less) continuous decrease in salt content from 20 eq.wt% NaCl to less than 15 eq.wt% NaCl, and a gradual decrease in formation temperature from some 300^{0}C to less than 200^{0}C.

TABLE V

Summary of the main features of the primary fluid
inclusions in metasomatic formations at Seriphos.

Rock type (sample no.)[1]:	$T_f(^OC)$[2]	;eq.wt%NaCl;	$T_h(^OC)$	:inclusions
unaltered granodiorite (9.4;9.4^II;9.4B)				
	: 750 – 700 :	45 – 40 :	240 – 260 :	
bleached granodiorite (9.4;9.4^III;9.4C)				
	: 700 – 500 :	40 – 35 :	240 – 270 :	
andradite skarn (120B;127)				
ad + mt + qz	: 550 – 400 :	35 – 30 :	300 – 340 :	
epidote-actinolite skarns (20.11;134)				
ep + qz	: 400 – 350 :	30 – 25 :	340 – 350 :	
ac + qz + cc	: 350 – 300 :	25 – 20 :	310 – 290 :	
hedenbergite-ilvaite skarn (55;56;55^III)				
iv + qz	: 350 – 300 :	30 – 20 :	330 – 280 :	
sphalerite-pyrite deposit (26.22)				
sph + py + hm + qz + cc	: 400 – 300 :	22	: 350 – 280 :	
pyrite-hematite deposit (27.7)				
py + hm + qz + cc	: 300 – 250 :	15	: 235	
fluorite-barite deposit (23.11;1A;4M;7C)				
fl + hm/lim	: 300 – 150 :	25 – 10 :	270 – 160 :	
ba + hm/lim/gt	: 250 – 100 :	15 – 5 :	210 – 100 :	

[1] For sample locations see Appendix

[2] Formation temperatures $T_f(^OC)$ are estimated from petrological,
mineralogical and thermodynamic evidence.

107.
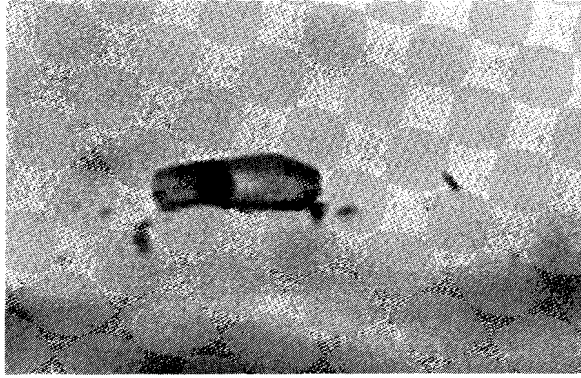
Plate 17: Primary bi-phase inclusion in LT-barite (sample 13.11).

$^{18}O/^{16}O$-analyses of barites give isotopic compositions of $\delta^{18}O_{ba}=$
8.8–10.5 %.. According to the equilibrium curve $\Delta^{18}O_{ba-H_2O}$ given by
Clayton and Epstein (1958) the corresponding compositions of the
coexisting water phases at $T_f= 200^0C$ are $\delta^{18}O_{H_2O}= 4.0$–2.3 %..

CHRONOLOGICAL EVOLUTION OF THE FLUID PHASE

temperature and fluid pressure

Table V gives a summary of the main features of the primary fluid
inclusions in the granodiorite rocks and skarn and ore deposits at
Seriphos. In fig.22 frequency distributions are given of the individual
measurements of the homogenization temperatures T_h in both the primary
and secondary fluid inclusions. In the magmatic rocks as well as in the
skarns and sphalerite deposits homogenization temperatures of the
primary fluid inclusions are very similar. In spite of the large
differences in formation temperature almost all homogenization
temperatures fall within the range 250–350°C.

Fig.23 gives the phase diagram of H_2O with isochores indicating
lines of constant density; each H_2O-isochore represents the range of
possible P_{H_2O}- T conditions at which a hydrous fluid inclusion with a
constant volume and a given fluid density and homogenization
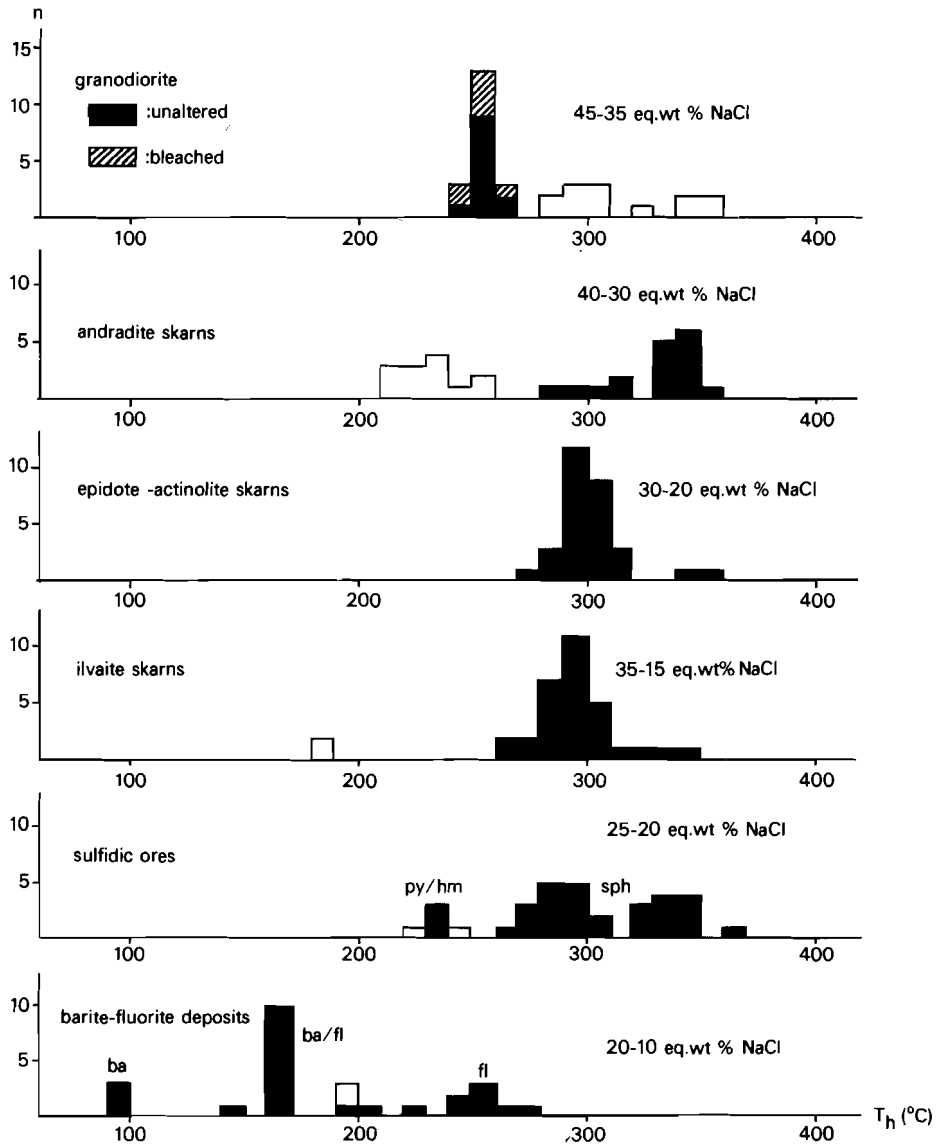
Fig.22: Frequency distributions of homogenisation temperature
measurements of primary and secondary fluid inclusions
in the metasomatic formations at Seriphos. Solid
histograms represent primary fluid inclusions; open
distributions represent secondary inclusions.
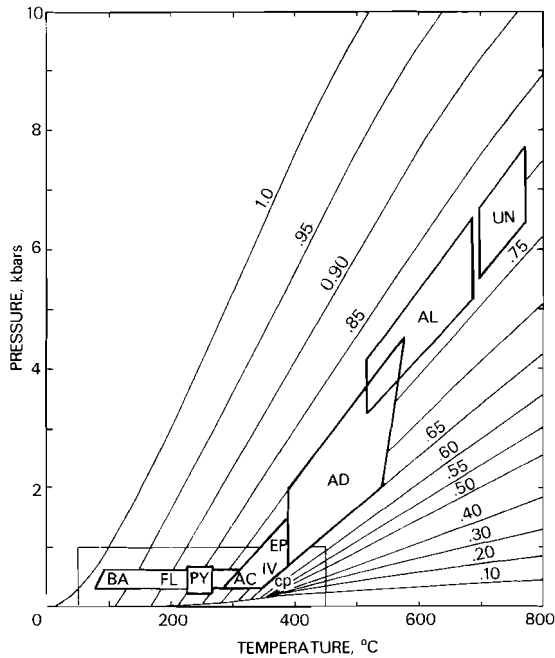
Fig.23: Plot of the formation conditions of primary fluid inclusions in plutonic rocks and metasomatic-hydrothermal deposits from Seriphos in the phase diagram of pure H_2O (see text).
UN= unaltered granodiorite; AL= bleached granodiorite; AD= andradite skarn; EP,AC= epidote-actinolite skarn; IV= ilvaite skarn; SPH= sphalerite-pyrite ore deposit; PY= pyrite-hematite deposit; FL= fluorite; BA= Barite.

temperature could have been entrapped. Fig.23 also gives the plot of the formation and homogenization temperatures of the primary fluid inclusions in the various metasomatic rock types at Seriphos. In the pure H_2O-diagram the high and medium temperature formations all plot along (about) the same isochore. The low-temperature, hydrothermal pyrite-hematite and barite-fluorite deposits, on the other hand, plot at H_2O-densities that strongly increase with T.

110.
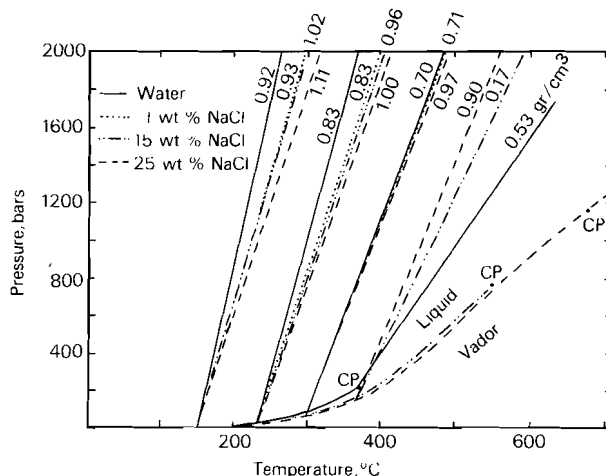
Fig.24: Comparison of isochores for H_2O and aqueous solutions
of various salinities (after Potter and Brown, 1977).

According to the plot of the formation conditions of the fluid
inclusions from the unaltered granodiorite in the P_f- T diagram of pure
H_2O of fig.23 fluid pressures should have been some 6-5 kbar at the
time of the final solidification of the granodioritic magma. The
primary fluid inclusions in the unaltered granodiorite, however,
contain concentrated $NaCl-KCl-CaCl_2-MgCl_2-(FeCl_2?)$-brines instead of
pure H_2O, and the presence of the salts will affect the fluid densities
and the positions of the H_2O-isochores in the P_f- T diagram.

Fig.24 gives the positions of the isochores in the system $H_2O-NaCl$
for salt contents up to 25 wt% NaCl and fluid pressures up to 2 kb
(Potter and Brown, 1977). The diagram indicates that the presence of
dissolved NaCl in the hydrous solutions mainly affects the positions of
the isochores (the absolute values of the fluid densities), but that it
does not significantly alters the slopes of the isochores in comparison
to pure H_2O. Preliminary experimental investigations on the system
$H_2O-MgCl_2$ indicate that the presence of a significant amount of
dissolved $MgCl_2$ in the aquous solutions slightly increases the slopes
of the isochores with respect to pure H_2O (although the absolute values
of the densities change notably due to the presence of $MgCl_2$)(M.Moers,
pers.comm.).
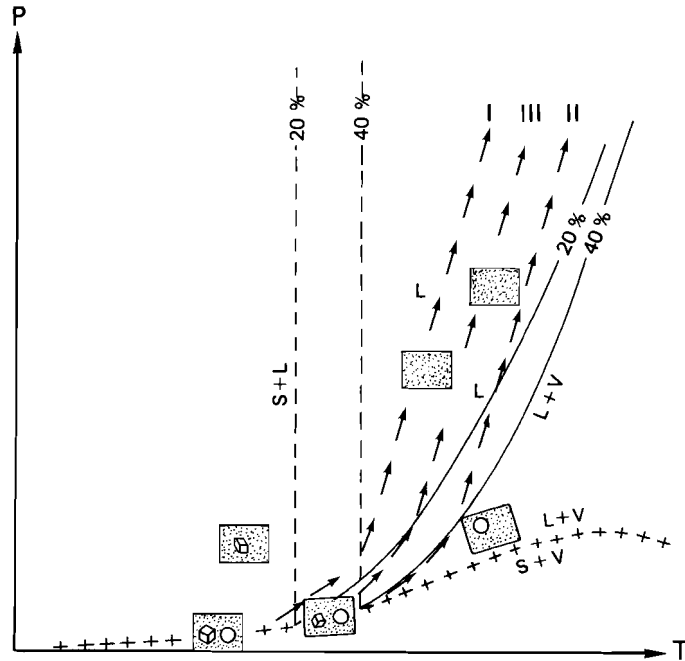
Fig.25: Schematic diagram of the high temperature equilibria in
NaCl-saturated, dense brines (after Weisbrod et al.,1976).
The arrow paths indicate the evolutions of the primary
fluid inclusions at Seriphos: I: granodiorite;
II: HT skarns; III: MT skarns (see text).

Fig.25 gives a somewhat schematic diagram of the high temperature
phase equilibria in NaCl-saturated brines (after Weisbrod et al.,
1976). The presence of solid NaCl in a saturated H_2O-solution
significantly alters the positions of the isochores in the P – T
diagram; as long as a solid NaCl-phase coexists with the hydrous
solution the slope of a given isochore is considerably less than the
slope of the isochore in the halite-free system.
    At room temperature the primary fluid inclusions in the unaltered
granodiorite contain a solid NaCl-cube, a vapor bubble, and a liquid
water phase (and 1 – 2 'insoluble' solids). Upon heating the halite-L-V

inclusions follow the halite+L+V critical curve. Above the
homogenization temperature, T_h= 250 ^{0}C, the halite+L-inclusions follow
the appropriate (flat-lying) isochore situated between the NaCl +L+V-
and L+V-critical curves (path I in fig.28). At the NaCl-dissolution
temperature (T_s= 400 ^{0}C) the 2-phase halite+L-inclusions change into
1-phase L-inclusions and, upon further heating, the fluid inclusions
follow the (steeply sloped) isochore for a concentrated brine solution.
Due to the presence of solid NaCl fluid pressures at the temperature of
formation of the inclusions, T_f= 750 ^{0}C, will be significantly less than
indicated by the pure H_2O-diagram (P_f= 4 kb instead of P_{H_2O}= 6-5 kb).

At the time of the final solidification of the granodioritic magma
at Seriphos fluid pressures probably were about 4 kb (see also fig.29).
These fluid pressures are considerably higher than the lithostatic
equilibrium pressure of 1.5 to 1 kb assumed in chapter IV on the basis
of geological arguments (see also chapter IX).

During the main phase of leaching of the granodiorite, which must
have occurred shortly after the solidification and (auto-)brecciation/
hydrofracturing of the magmatic rock, fluid pressures still must have
been high, probably 3-2 kb.(fig.28). The primary fluid inclusions in
the bleached granodiorite have the same homogenization temperatures as
the primary fluid inclusions in the unaltered rock, and their salt
contents are only slightly less. The formation temperatures, however,
must have been less than the formation temperatures in the unaltered
plutonic rock.

The garnet-quartz skarns, formed after the deposition of the
pneumatolytic pyroxene-andradite skarns along fractures and
vein-structures cross-cutting the older pyroxene-magnetite deposits,
must have formed at fluid pressures of some 2-1 kb (path II in fig.25).
The formation temperatures of the primary fluid inclusions in the
garnet-quartz skarns are comparable to the formation temperatures of
the primary fluid inclusions in the bleached granodiorite (T_f= 550-
450 ^{0}C), but their total salt contents are somewhat less (T_s= 350-150 ^{0}C
instead of 350-300 ^{0}C), and the homogenization temperatures are higher
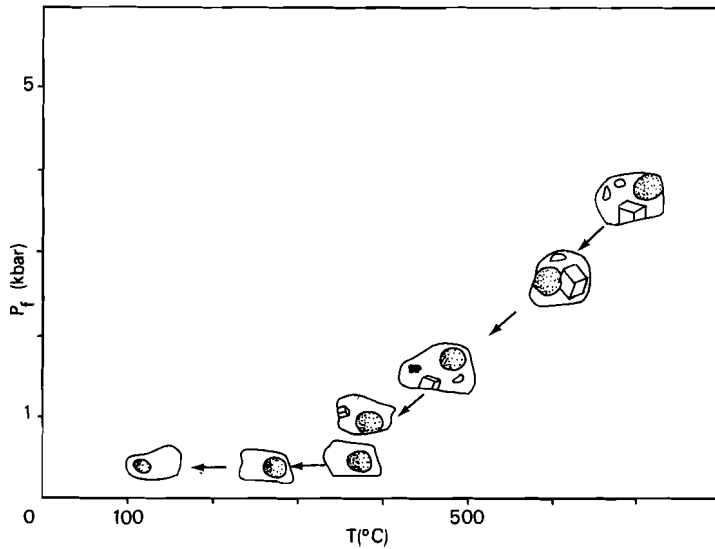
Fig.26: P_f-T evolution of the metasomatic solutions at Seriphos.

(T_h= 280-360°C instead of 240-270°C). The higher homogenization
temperatures in the HT-skarns indicate a decrease in fluid density
during the skarn formation.

The medium-temperature epidote, ilvaite and sphalerite deposits
probably formed at fluid pressures of 1.5 - 0.5 kb. The formation
temperatures as well as the total salt contents of the primary fluid
inclusions in the MT-deposits are significantly less than in the garnet
skarns (T_f= 450-350°C,$T \leq$ 25°C instead of T_f= 550-450°C,T_s= 350-150°C).
The slight decrease in the homogenization temperatures in the
MT-deposits relative to the garnet skarns (T_h= 300°C instead of
T_h= 350°C) probably mainly results from a decrease in salt content at
(about) constant fluid density (path III in fig.25).

In the LT-deposits homogenization temperatures of primary fluid
inclusions strongly decrease with their formation temperature,and fluid
densities correspondingly increase. During the final stages of the

hydrothermal activities fluid pressures must have been about constant, and probably P_f was about equal to the hydrostatic equilibrium pressure, assumed to be some 300-400 bar in chapter IV.

Fig.26 summarizes the P_f- T conditions of formation of the various metasomatic rock types at Seriphos.

During the HT and MT stages of the post-magmatic, metasomatic evolution fluid pressures diminished as temperatures decreased while fluid densities remained (about) constant, as in a closed volume system. Only between the HT-fluids in the magmatic rocks and the skarn fluids a (moderate) drop in fluid density appears (from about $\rho_{H_2O}= 0.8$ to 0.7-0.6 gr/cm^3). The (about) constant fluid densities suggest that the metasomatic fluid flow system, as a whole, was a largely closed fluid flow system in which a limited amount of metasomatic solutions was enclosed in a, more or less, constant fluid volume. Within the largely closed system considerable differences in fluid pressure must have existed between the 'hot' plutonic rocks and the 'cold' country rocks.

Towards the LT-stages of metasomatism fluid pressures dropped to values close to the hydrostatic equilibrium pressure. Lateral fluid pressure gradients largely vanished and in the late, LT-stages of the metasomatic evolution the hydrothermal convection system could have become open to the introduction of fluids from the external environment.

salt content

Fluid inclusions in quartzes from the unaltered granodiorite contain aqueous $NaCl-KCl-CaCl_2-MgCl_2-(FeCl_2?)$-brines with total salt contents of 40 - 45 eq.wt% NaCl (table V). In the HT and MT stages of the post-magmatic, metasomatic evolution the total salt contents gradualy decreased (to some 20 eq.wt% NaCl), but the fluids remained aqueous $NaCl-(KCl)-CaCl_2-MgCl_2(FeCl_2?)$-brines. Only during the LT-stages of the metasomatic evolution the presence of (a small amount) CO_2 in the $NaCl-(CaCl_2)-MgCl_2$-solutions suggests a change in the nature of the metasomatic fluids.
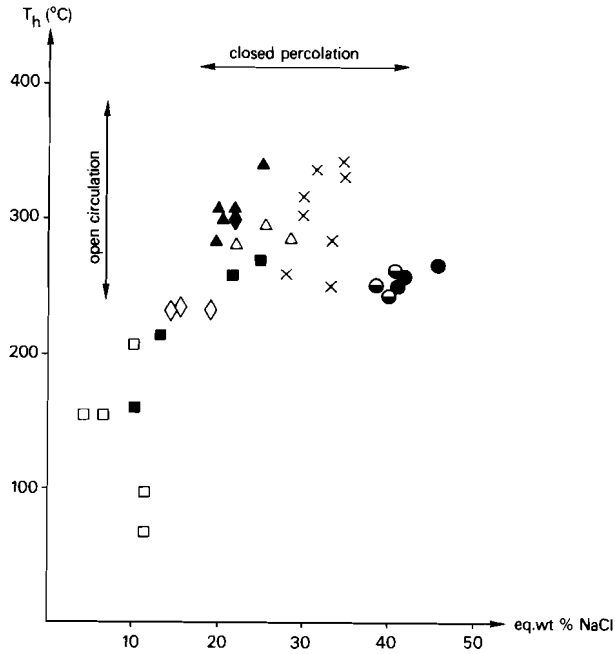
Fig.27: Plot of the total salt content (eq.wt% NaCl) vs. homogenization
temperature T_h(^{0}C) in primary fluid inclusions from individual
crystal samples from metasomatic formations at Seriphos.
●: unaltered granodiorite; ◓: bleached granodiorite;
✕: andradite skarn; ▲: epidote–actinolite skarn; △: ilvaite
skarn; ◆: sphalerite-pyrite deposit; ◊: pyrite–hematite
deposit; ■: fluorite; □: barite.

In fig.27 the average total salt content of all primary fluid
inclusions measured in a single crystal sample is plotted against the
average of the homogenization temperatures measured in the crystal. The
HT and MT metasomatic formations all plot at comparable homogenization
temperatures (fluid densities) and at gradually decreasing total salt
contents. The LT-hydrothermal deposits, on the other hand, all plot at
comparable total salt contents but at rapidly diminishing
homogenization temperatures.

Fig.27 confirms that the formation of the bleached zones in the

TABLE VI

$\delta^{18}O$-values of mineral phases in metasomatic deposits at Seriphos, and $\delta^{18}O_{H_2O}$ of the coexisting aqueous solution at the indicated formation temperature T_f.

sample no. [1]	assemblage	WR	Qz	Mt	Cpx	Cc	Ba	H_2O	$T_{meas.}$	$T_{est.}$	$Qz_{theor.}$ [2]
unaltered granodiorite											
9.3E		9.5						9.8		750	9.6
9.3C		9.2						9.5		750	9.3
9.3D		9.3						9.6		750	9.4
101-1		9.3	9.7					9.1		750	9.7
101-3		9.6	10.4					9.7		750	10.4
bleached granodiorite											
9.3		9.6						8.0		550	10.0
9.2E		10.0						8.4		550	10.4
9.2D		10.6						9.0		550	11.0
101-2a		10.0	11.4					8.4		550	10.4
101-2b		10.4						8.8		550	10.8
gneiss											
124-b1	: unaltered	12.1									
124-b2	: bleached	9.0									
HT-skarns											
27.7A	: cpx + ad + mt + qz		14.7	6.0				12.7	560		14.7
126-c	: cpx + ad + mt			6.1				13.0		550	14.6
126-b	: cpx + ad + mt			4.8	11.2			12.0	520		14.4
24.5	: cpx + ad + mt			4.5				11.9		500	14.5
27.17	: cpx + ad + mt			4.8	11.6			12.2	500		14.8
120-b	: ad + mt + qz		12.9					9.3		450	12.9
127	: ad + mt + qz		12.8					9.2		450	12.8
MT-skarns											
20.11	: ep + qz		11.4					6.8		400	11.4
27.30	: ep + qz		12.6					8.0		400	12.6
26.49	: qz + mt + hm		11.6	-1.5				7.2	410		11.6
26.48	: qz + mt + hm		12.3	-1.2				7.7	400		12.3
26.87	: ep + ac + qz		13.3	0.0				8.8	405		13.3
137	: ac + qz + cc		14.7	0.5				9.6	390		14.7
26.22	: sph + hm + qz		11.6					7.0		400	11.6
8.2	: galena + qz		13.8					8.0		350	13.8
55	: iv + qz		12.6					6.8		350	12.6
55-I11	: iv + qz		12.5					6.0		325	12.5
56	: iv + qz		13.2					6.7		325	13.2
26.35	: qz + mt		14.4	-2.7				7.8	325		14.4
ML-2.2	: ac + qz + mt		16.6	-4.6				7.8	265		16.6
ML-1	: ac + qz + mt		16.5	-4.9				7.5	260		16.5
LT-deposits											
27.7B	: py + hm + qz + cc		14.8					5.2		250	14.8
13.11	: ba + hm/lim						9.5	3.0		200	15.0
23.1	: bs + hm/lim						10.5	4.0		200	16.0
23.11	: ba + hm/lim						8.8	2.3		200	14.3
BA-1	: ba + hm/lim						9.9	3.4		200	15.4
BA-2	: ba + hm/lim						8.9	2.4		200	14.4
ML-2.4	: qz + cc		22.0			18.8		3.5	125		22.0

[1] For sample locations see Appendix

[2] $Qz_{theor} = \delta^{18}O_{qz}$ in equilibrium with H_2O at the measured or estimated formation temperature $T_{meas.}$ or $T_{est.}$

117.

granodiorite and the formation of the HT and MT skarn and ore deposits took place in a constant density, largely closed fluid flow system. Continuous re-equilibration of the primary magmatic $NaCl-(KCl)-CaCl_2-MgCl_2-(FeCl_2?)$-brines with the solid rocks at gradually decreasing temperatures, and diminishing mineral solubilities, could have resulted in a gradual decrease in the salt content of the hydrous solutions.

In the LT-stages the rapid decrease in homogenization temperature at (about) constant total salt content suggests that the hydrothermal solutions in the LT-hydrostatic, largely open circulation system were constant-composition solutions with uniform compositions. The presence of (some) CO_2 in the LT-fluids evidences the incorporation of 'non-magmatic', externally derived materials into the hydrothermal convection system.

$^{18}O/^{16}O$

In table VI the $^{18}O/^{16}O$-ratios are given as measured in the solid phases of samples from the metasomatic-hydrothermal deposits at Seriphos. Table VI also gives the calculated $\delta^{18}O_{H_2O}$ of the aqueous solutions coexisting with the mineral phases at the indicated formation temperature T .

In fig.28a the $\delta^{18}O_{H_2O}$-values are plotted against T_f. As metasomatism progressed and temperatures diminished, $^{18}O/^{16}O$ of the metasomatic solutions gradually decreased. There are no abrupt changes in the $\delta^{18}O_{H_2O}$- T trends pointing to a sudden, substantial influx of isotopically 'alien' fluids derived from some external reservoir.

The dotted curves in fig.28a give the $\delta^{18}O_{H_2O}$-trends as determined by the quartz-H_2O-equilibrium; as temperatures change an aqueous fluid continuously in (local) equilibrium with an excess amount of quartz with a fixed composition $\delta^{18}O_{qz}$ continuously changes its isotopic composition according to the path pointed out by the dotted $\delta^{18}O_{qz}$ - T curves. In the quartz-rich granodioritic and gneiss- and schist-unit rocks from Seriphos the $\delta^{19}O_{H_2O}$-compositions of the metasomatic solutions follow to a large extent the $\delta^{18}O_{H_2O}$- T trends indicated by the SiO_2-H_2O equilibrium. It suggests that, to a large extent, local equilibrium was maintained between the percolating metasomatic
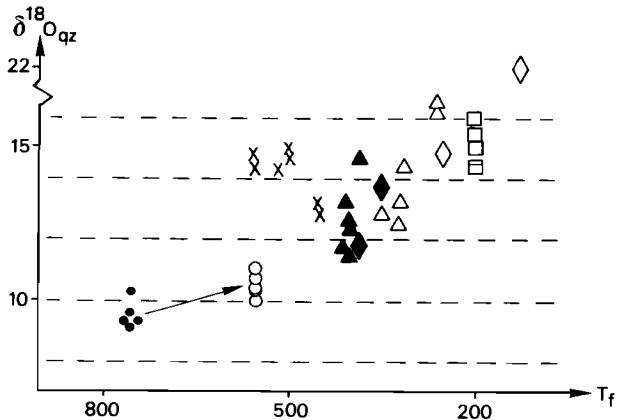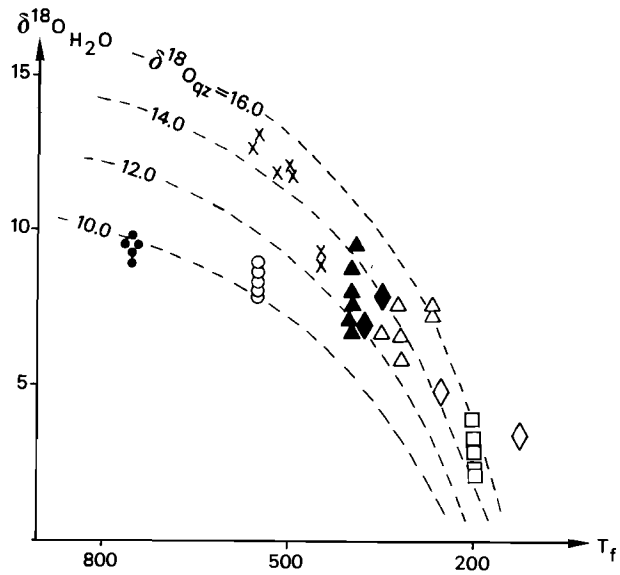
Fig.28: Plot of the formation temperature T_f of metasomatic formations
from Seriphos against $\delta^{18}O_{H_2O}$(SMOW) of the aqueous solutions
coexisting with the mineral formations at that temperature
(fig.28a), and of the formation temperature against $\delta^{18}O_{qz}$ of
the quartz at that temperature (fig.28b) (see also table VI).

●: unaltered granodiorite; o: bleached granodiorite;

X: andradite skarn; ▲: epidote-actinolite skarn;

△: ilvaite-actinolite skarn; ◆: sphalerite vein;

◇: pyrite-hematite deposit; □: barite.

solutions and the quartz-rich rocks adjacent to the transport channels.
(de Jong and Salemink, 1984).

In fig.28b the isotopic composition $\delta^{18}O_{qz}$ of the quartzes from
the Seriphos skarns, as measured or as reconstructed from the $\delta^{18}O_{H_2O}$-
compositions, are plotted against the formation temperature T_f. On
average the $\delta^{18}O_{qz}$-values of the mineralizations in the metasedimentary
country rocks are 2-4 %. higher than $\delta^{18}O_{qz}$ in the magmatic rocks.
This, again, suggests that, to a large extent, local isotopic
equilibrium was maintained between the metasomatic solutions and the
host rocks adjacent to the transport channels. The large scattering of
$\delta^{18}O_{qz}$ in the country rock deposits relative to the more uniform
results from the magmatic rocks probably results from local variations
in the original isotopic (and mineralogical) composition of the wall
rocks.

CONCLUSION

The isotopic results confirm the fluid inclusions evidence that,
during the HT and MT stages of the post-magmatic evolution, the
metasomatic system at Seriphos was a largely closed system in which a
limited amount of magma-derived, aqueous solutions percolated along the
cracks and fractures as well as in the adjacent country rocks, at every
instance maintaining local equilibrium with the solid phases adjacent
to the transport channels while temperatures and fluid pressures
gradually decreased. Only towards the final stages of the hydrothermal
activities, when lateral fluid pressure gradients had vanished, CO_2-
containing, 'externally derived' materials were incorporated into the
hydrothermal convection system.

πεντε απ' εμου και πεντ' απο σου Θησαυρον ορυγε

(you must dig out five of my treasures and five of yours).

1st century A.D. inscripition from Seriphos

CHAPTER VII: MASS EXCHANGES

Chemical alterations during metasomatism can be traced through major and trace elements of unaltered rocks and of their metasomatic replacement products. Comparison of the alterations in different geochemical environments illustrates the influence of local conditions on the metasomatic mass exchanges.

Quantitative comparison of the mass exchanges between the granodiorite and the country rocks, based on quantitative estimates of the amounts of metasomatic formations in the field, provides a measure of the intensity of the metasomatic activities at Seriphos. $^{18}O/^{16}O$- analyses of unaltered rocks and of their metasomatic alteration products give an indication of the total amount of fluids involved in the mass exchanges.

ANALYTICAL PROCEDURES

Major and trace elements in powdered rock samples were determined by X-Ray Fluorescence (Philips PW1400) and by Inductively Coupled Plasma emission spectrometry (ARL 34000). XRF was used on $LiBO_3$-glass beads for major elements in total rock analyses, and on pressed powder tablets for the trace elements W, Sn, Nb, Ta, Zr, Rb, U, Cs in all rock and mineral samples. ICP was used for the major elements Al, Fe, Mn, Mg, Ca, Na, K and the trace elements Be, Ba, Sr, Y, Ce, V, Cu, Zn, S, Li in all analyses after the dissolution of the rock samples at $120^\circ C$ in a mixture of HF, $HClO_4$ and HNO_3 in teflon pressure vessels. The rock samples were crushed and ground in Ni-Cr steel equipment.

XRF and ICP were calibrated against granite standards. Analyses of IGSS granite standards were in agreement with literature data. Major elements determined by XRF as well as ICP were conformable (relative error $\leq$ 10 %).

TABLE VII

Major and trace element compositions (in ppm)
of unaltered and adjacent, metasomatically
altered rocks from Seriphos.

	$\overline{9.3}$	$\overline{9.2}$	124-b1	124-b2	20.24	2.3	9.6	4.1B	139-1	139-2	27.15	27.17	13.9-1	13.9-2
Si	309,000	319,000	231,400	230,200	183,000	174,800	176,000	315,000	280,000	292,000				
Al	86,500	84,800	77,500	71,000	78,000	17,600	88,000	103,100	50,000	5,500	3,600	12,700	1,700	1,975
Fe	26,800	6,500	73,100	44,900	92,500	205,000	81,500	140,000	88,400	157,000	4,700	>105,000	1,000	43,250
Mn	375	175	875	575	1,000	2,000	1,200	900	950	2,600	700	500	300	3,800
Mg	10,800	5,200	52,500	44,600	42,500	10,900	40,100	10,900	27,000	16,500	115,000	149,000	2,500	4,300
Ca	29,500	25,200	67,000	142,000	115,000	199,900	162,700	171,500	36,500	10,400	>250,000	7,600	>250,000	>250,000
Na	33,100	64,400	35,700	31,200	31,000	400	10,700	700	20,400	1,100	125	200	125	275
K	19,400	19,600	4,700	1,250	5,600	2,000	2,100	100	32,200	1,000	100	<35	550	650
Ti*	3,250	2,400	3,250	2,500	3,200	1,500	5,300	3,550	2,050	20	125	1,000	65	65
P*	575	525	270	285	825	925	1,800	400	725	200	625	150	1,050	975
Zr*	200	190	25	25	55	45	200	240	65	<4	5	45	15	<4
V	60	40	245	275	260	660	150	110	125	25	30	45	<2	17
W*	<5	<6	<6	<6	<6	10	<6	<6	<6	<6	<6	<6	<6	<6
Nb*	12	10	<4	<4	<4	<4	<4	<4	<4	<4	<4	<4	<4	<4
Ta*	11	9	<4	8	<4	8	4	10	<4	7	6	8	9	16
Be	3	3	1	1	1	4	3	5	2	7	<1	5	1	1
Ba	775	400	90	40	60	25	100	10	2,100	15	10	5	20	750
Sr	330	160	175	315	320	10	285	900	95	10	110	10	425	40
Y	20	18	12	17	18	295	16	27	17	5	12	4	4	7
Ce	45	48	8	28	22	135	21	70	250	<6	22	<6	<6	25
Cu	6	5	55	80	40	25	20	10	60	20	40	20	35	1,925
Zn	500	40	175	90	175	125	250	120	40	120	10	55	125	600
S	130	30	250	600	575	875	1,525	1,350	175	375	1,250	10	1,350	4,100
Li	15	10	14	19	25	5	20	7	7	4	3	2	1	3
Rb*	100	60	45	10	35	10	20	5	100	20	3	1	8	7
ρ(g/cc)	2.65	2.55	2.82	2.89	2.90	3.30	3.04	2.96	2.64	3.22	2.76	3.04	2.65	2.67

$\overline{9.3}$: unaltered granodiorite   - $\overline{9.2}$: bleached granodiorite
124-b1 : hornblende gneiss   - 124-b2 : bleached gneiss
20.24 : ep-scap-hbl-hornfels   -   2.3 : garnet-pyroxene skarn
9.6 : scap-hbl-hornfels   -   4.1B : ep-ac-qz skarn
139-1 : hornblende hornfels   - 139-2 : hd-iv skarn
27.15 : dolomitic marble   - 27.17 : pyroxenite skarn
13.9-1: calcite marble   - 13.9-2: ankerite-limonite vein

For sample location see Appendix

*) Trace analyses by XRF relative to granite standard

In the Seriphian granodiorite post-magmatic, high temperature metasomatism caused a leaching of the magmatic rock along the numerous cracks and fractures that cross-cut the entire main mass of the exposed apical parts of the granodiorite pluton. According to the chemical analyses of unaltered and bleached granodiorite given in table I the metasomatic leaching mainly resulted in a removal of Fe, Mg, Mn, and to a lesser extent of Ti and Ca, and in an addition of Na, while Si, Al, K and P remained present in more or less constant amounts. Petrologically the metasomatic changes are reflected in the breakdown of hornblende, biotite and plagioclase and the transformation of the plutonic rock into an albite-quartz-sericite assemblage.

In table VII the average contents of major and trace elements are given (in ppm) of the three samples (9.3C, 9.3D, 9.3) of the unaltered granodiorite ($\overline{9.3}$) and of the three samples (9.2D, 9.2E, 9.3) of the bleached granodiorite ($\overline{9.2}$) (see also table I). The results show that, besides Fe, Mg, Mn also (relative) considerable amounts of Zn and S, and of Ba, Sr, Li, Rb and V were removed during the metasomatic leaching. To a lesser extent Nb, Ta (W) were removed, while Zr, Be, Y, Ce and Cu remained present in nearly constant amounts.

In fig.29 the chemical changes in the granodiorite are graphically represented in a 1-dimensional diagram where the relative amount of leaching, X_n, of a given component n is expressed by the negative logarithm of the ratio of the concentration c_n^{UN} of the components n in the unaltered granodiorite (in ppm) and the concentrations c_n^{AL} of n in the bleached magmatic rock:

$$X_n = - \log(c_n^{UN}/c_n^{AL}) \tag{8-1}$$

Components with negative X_n-values are removed from the unaltered rock; positive values of X_n indicate an addition of n to the rock as a result of the metasomatic activities.

In a few places in country rocks close to the intrusive contact high temperature metasomatism also caused a leaching of the contact

metamorphic country rocks (see fig.4). In table VII chemical changes
are given of a hornblende-diopside gneiss with biotite, scapolite and
quartz (124b-1), and of an adjacent bleached gneiss mainly composed of
actinolite, albite and quartz, and with epidote veins (124b-2). The
anayses show a decrease in the major elements Fe, Mg, Mn, Ti, and of K,
Rb, Zn, and the results show an increase in Ca, Sr, Y, Ce, Ta, Cu, S,
while Si, Al, P, Zr, V, Be and also Na, Li are about constant. The
increase in Ca (and Sr, Y, Ce) relative to Al and Si reflects the
abundant precipitation of epidote in the bleached contact metamorphic
rocks (in the granodiorite leaching was accompanied by a (net)
precipitation of Na-feldspar).

Table VII also gives an example of the chemical changes
accompanying HT skarn formation in the siliceous rocks of the schist-
unit. The metasomatic transformation of an epidote-scapolite-hornblende
hornfels (20.24) into a pyroxene-garnet skarn (2.3) involves an almost
complete removal of Na from the hornfels rock, a strong decrease in K,
Mg, Al and Ti, and an addition of Ca, Fe, Mn. The HT skarn formation
also comprised a removal of Ba, Sr, Cu, Zn and Li, Rb, and an addition
of the 'hygromagmatophile' elements V, W, (Nb?), Ta, Be, and of Y, Ce
and S. Si, P, Zr remained largely immobile. The chemical changes
reflect the mineralogical breakdown of hornblende and scapolite, and
the formation of Fe-bearing clinopyroxene and andraditic garnet (and
magnetite and pyrite).

The chemical transformation of a scapolite-hornblende hornfels
(9.6) into an epidote-actinolite-quartz skarn (4.1B) involves a nearly
complete removal of Na as well as K, Ba, Li, Rb and a strong decrease
in Mg, Ti, P, V as well as Cu, Zn (table VII). There is a strong
increase in Si, Fe, Sr, Y, Ce. In contrast to the HT skarn formation Ca
and Al were largely immobile during the epidote formation, while Si was
added (in the garnet-pyroxene skarns Si remained while Ca and Al
decreased and Fe was added).

In the massive pyroxenite skarn zone of SW-Seriphos the
metasomatic alteration of the graphitous hornblendite hornfelses into a
hedenbergite-ilvaite skarn (139-1 → 139-2) was accompanied by a strong
addition of Ca, Fe, Mn, a decrease in Mg, P and an almost complete
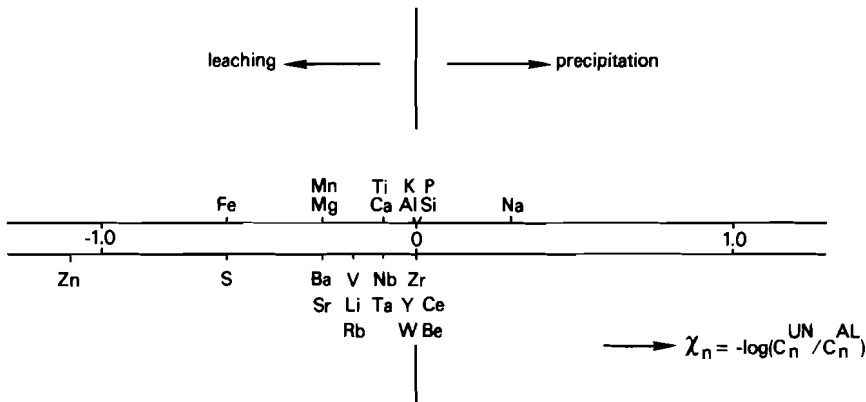
Fig.19: Relative amounts of leaching or precipitation of major
and trace elements as a result of the metasomatic
alteration (bleaching) of the granodiorite at Seriphos.
(see text and also table VII).

removal of K, Na, Al and Ti (table VII). The hedenbergite-ilvaite
formaton also involved a considerable extraction of the trace elements
Zr, V, Ba, Sr, Y, Ce, Li, Rb and Cu, and an addition of Be, Ta, Zn, S.

In the graphitous dolomitic marbles the formation of a
diopside—magnetite skarn mainly involved the removal of Ca and P, and
the addition of Al, Fe and Ti (27.15 → 27.17 in table VII). The HT
skarn formation in the dolomitic marbles was accompanied by a
(relative) considerable addition of Zr, V,(W?, Nb?), Ta, Be and Zn,
whil Ba, Sr, Y, Ce, Cu, S (and Li, Rb) were extracted from the
metasedimentary dolomitic carbonate rocks.

The formation of hematite/limonite deposits in massive calcite
marbles mainly resulted in an addition of Fe, Mg, Mn to the calcitic
rock, while Ca must have decreased (13.9-1 → 13.9-2 in table VII). The
low temperature Fe-Mn-Mg metasomatism was accompanied by a strong
addition of Ba, Cu, Zn, S.

125.
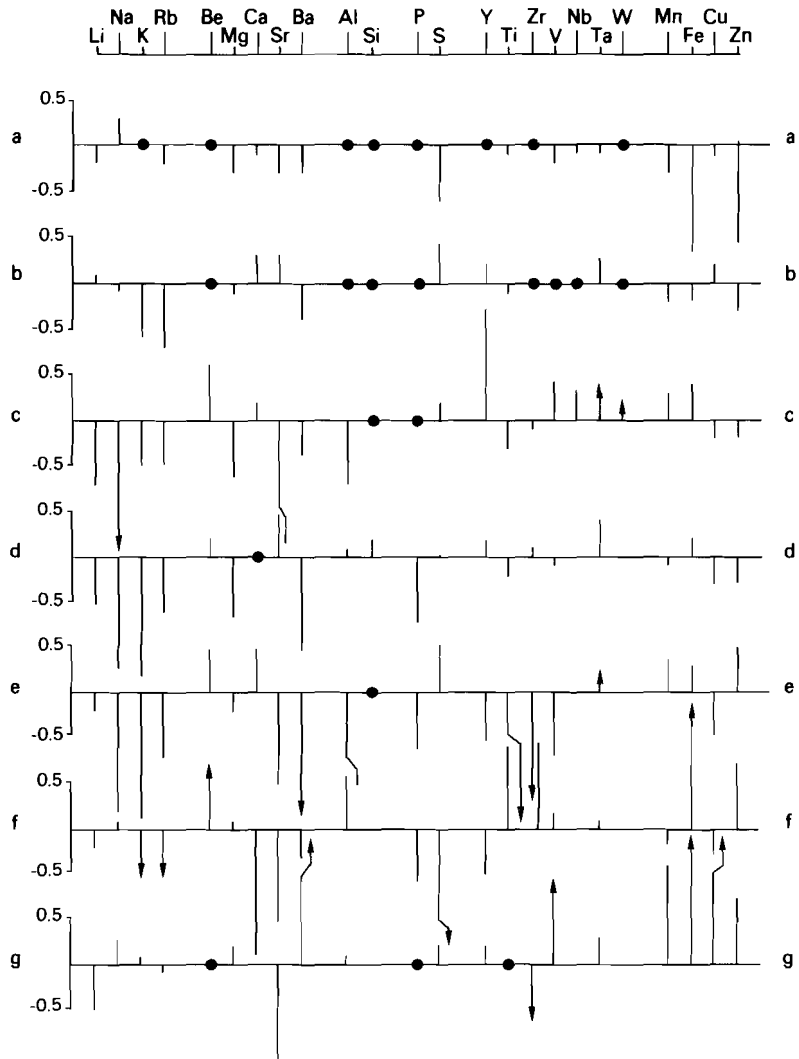
Fig.30: Relative intensities of the metasomatic exchanges of major and
trace elements in different rock types (see also table VII).
a: leaching of the granodiorite; b: leaching of a hornblende
gneiss; c: formation of a garnet-pyroxene skarn; d: formation
of an epidote-actinolite skarn; e: hedenbergite-ilvaite skarn
formation; f: pyroxene skarn development on dolomitic marble;
g: ankerite-hm/lim formation on calcite marbles.

In fig.30 a graphical review is given of the metasomatic mass exchages in the investigated examples.

The results indicate that W is typically concentrated in the HT-skarns, as is V, while Ba dissolves at high temperatures and is typically precipitated in low temperature deposits (as barite). K (and Li, Rb) is generally leached (and deposited at low temperatures at large distances from the intrusive contact as adularia), while Na is generally leached from the country rocks and deposited in the bleached zones within the granodiorite (as albite).Fe and Mn, on the other hand, are leached from the granodiorite and deposited in all types of country rocks during all stages of the metasomatic evolution. The behavior of Al seems to depend strongly on the local conditions. Si is largely immobile, although it migrates in some situations.

The results show that, apart from temperature differences, differences in the (local) geochemical environment also played an important role in the metasomatic mass redistributions. It confirms the mineralogical evidence that maintenance of local equilibrium was a dominant control of metasomatism.

In table VIII trace element analyses are given of a number of mineral separations of skarn deposits.

The results show that the chalcophile elements Cu, Zn, S behave largely independent from the skarn silicates. Of the lithophile elements Ba, Li and Rb˜are specifically concentrated in phlogopite, together with K, while Ce and Y specifically accumulate in garnet and epidote; Sr only increases in epidote. Be is most abundant in ilvaite, but it is also present in (relative) significant amounts in the other Ca-Fe-silicates (where its concentration seems to decrease with decreasing temperature).

W occurs only associated with garnet. The geographical distribution of the high W garnets, exclusively in schists situated just on top of the massive pyroxenite skarn zone, suggests that W specifically occurs with garnets formed at moderate f_{O_2}-values. Probably W is present in the garnet as inclusions of scheelite ($CaWO_4$).

The trace element analyses confirm the results of the bulk rock analyses that local mineralogical controls are the main factor controlling the metasomatic behavior of the trace elements.

TABLE VIII

Some chemical characteristics of a number of mineral separates from the skarn deposits at Seriphos

pyroxenes: $Ca(Fe,Mg)Si_2O_6$

	Fe/Fe + Mg	Mn	Ti*	Zr*	V	W*	Nb*	Ta*	Be	Ba	Sr	Y	Ce	Cn	Zn	S	Li	Rb*
no. 23.35	0.53	2300	<1	<4	20	<6	<4	6	13	40	15	3	<6	475	110	1650	10	9
zone	0.48	1750	<1	<4	30	<6	<4	4	7	20	6	1	<6	15	60	1400	7	2
27.11	0.27	1450	<1	<4	10	<6	<4	5	4	6	11	1	<6	10	60	1550	13	3
12.3	0.49	1700	<1	<4	20	<6	<4	5	10	9	9	2	<6	10	165	1250	9	2
24.5	0.29	1475	<1	<4	130	<6	<4	10	10	12	30	8	8	20	125	1550	15	8
26.99	0.78	1925	<1	<4	15	<6	<4	12	11	30	9	6	16	1100	40	1400	12	8

garnets: $Ca_3(Al,Fe)_2Si_3O_{12}$

	Al/Al + Fe	Mn	Ti*	Zr*	V	W*	Nb*	Ta*	Be	Ba	Sr	Y	Ce	Cn	Zn	S	Li	Rb*
no. 24.5	0.15	2700	210	75	85	6	16	6	7	1675	50	21	35	20	155	2100	<1	9
27.30	0.09	850	<1	<4	15	160	<4	4	8	5	1	13	35	15	125	1950	<1	5
5.4	0.09	900	<1	<4	10	235	5	8	8	10	1	5	<1	15	35	1950	<1	1
20.12	0.06	1400	100	9	15	17	5	10	8	20	4	11	30	15	110	1800	2	1
26.86	0.05	700	145	8	35	125	<4	8	8	20	2	6	<1	15	45	1950	1	1

epidotes: $Ca_2(Al,Fe)_3Si_3O_{12}(OH)$

	Al/Al + Fe	Mn	Ti*	Zr*	V	W*	Nb*	Ta*	Be	Ba	Sr	Y	Ce	Cn	Zn	S	Li	Rb*
no. 20.11	0.64	770	1605	130	105	<6	<4	7	5	75	575	85	65	235	100	1400	2	14
3.3	0.63	665	1365	130	75	<6	7	10	4	45	950	25	70	20	50	1400	1	5
27.7E	0.65	550	660	125	50	<6	<4	9	5	10	1100	10	17	10	60	1450	2	4

phlogopites: $K(Fe,Mg)_3AlSi_3O_{10}(OH)_2$

	Fe/Fe + Mg	Mn	Ti*	Zr*	V	W*	Nb*	Ta*	Be	Ba	Sr	Y	Ce	Cn	Zn	S	Li	Rb*
no. 27.7B	0.24	700	3430	20	35	<6	6	11	3	1000	10	<1	<1	5	170	200	55	635
27.7C	0.05	400	245	<1	10	<6	15	<4	1	950	10	<1	<1	5	75	150	50	750

actinolite: $Ca_2(Fe,Mg)_5Si_8O_{22}(OH)_2$

	Fe/Fe + Mg	Mn	Ti*	Zr*	V	W*	Nb*	Ta*	Be	Ba	Sr	Y	Ce	Cn	Zn	S	Li	Rb*
27.7A	0.18	1700	1	<1	95	<6	<4	<4	4	10	20	<1	<1	25	160	750	12	<1

ilvaite: $CaFe_2^{++}Fe^{+++}Si_2O_7(OH)$

		Mn	Ti*	Zr*	V	W*	Nb*	Ta*	Be	Ba	Sr	Y	Ce	Cn	Zn	S	Li	Rb*
55		2550	40	<1	20	8	<4	8	16	15	5	10	45	15	90	950	<1	<1

For sample locations see Appendix

*) Trace analyses by XRF relative to granite standard

The analytical results confirm the mineralogical evidence that metasomatism at Seriphos was strongly Fe-dominated. Fe was leached from the granodiorite, and also in a few places from siliceous country rocks close to the intrusive contact, and it was deposited in skarn and ore deposits in the country rocks surrounding the pluton. The extraction of Fe from the magmatic rocks mainly resulted from the HT breakdown of hornblende and biotite. The deposition of Fe resulted in skarn and ore formations with mineral assemblages determined by the local conditions of P, T, f_{O_2}, μ_i. In the siliceous rocks Fe-dominated metasomatism resulted in Fe-Si skarn assemblages (Ca-Fe-Mg-Si skarns); in low-Si, Ca-saturated marbles metasomatic formations were largely Ca-Fe-(CO_2)-saturated.

In fig.31(a,b,c,d) field estimates are given of the volumetric amounts of the main skarn and ore formations in the siliceous country rocks surrounding the granodiorite pluton at Seriphos. Metasomatism was most intense close to the intrusive contact in areas where the contact surface between plutonic and country rocks is flat-lying, viz. in central and southeastern Seriphos.

The field estimates indicate that at the exposed surface of the contact metamorphic hornfelses, developed in the at least 500 m thick series of the schist-unit, the hornfelses on average contain about 4.5 vol% epidotite skarn, some 2.5 vol% garnetite, 0.5 vol% pyroxenite, and about 3 vol% magnetite + hematite (mt : hm = 1 : 1). The about 30 m thick massive skarn zone of southwestern Seriphos consists for at least 80 vol% of hedenbergitic clinopyroxene, for some 5 vol% of ilvaite-actinlite skarn, and for about 3 vol% of magnetite + hematite. The up to 30 m thick calcite marbles are almost entirely replaced by ankeritic dolomite (ca 80 vol%) and for some 10 vol% by hematite-limonite iron ore. The up to 40 m thick series of the dolomitic marbles contains, besides some 20 vol% talc, about 5 vol% ankeritic dolomite, about 1 vol% pyroxenite, and some 2 vol% iron ore (magnetite, hematite, limonite). Within the reaches of the contact metamorphic and contact metasomatic aureole the at least 150 m thick,
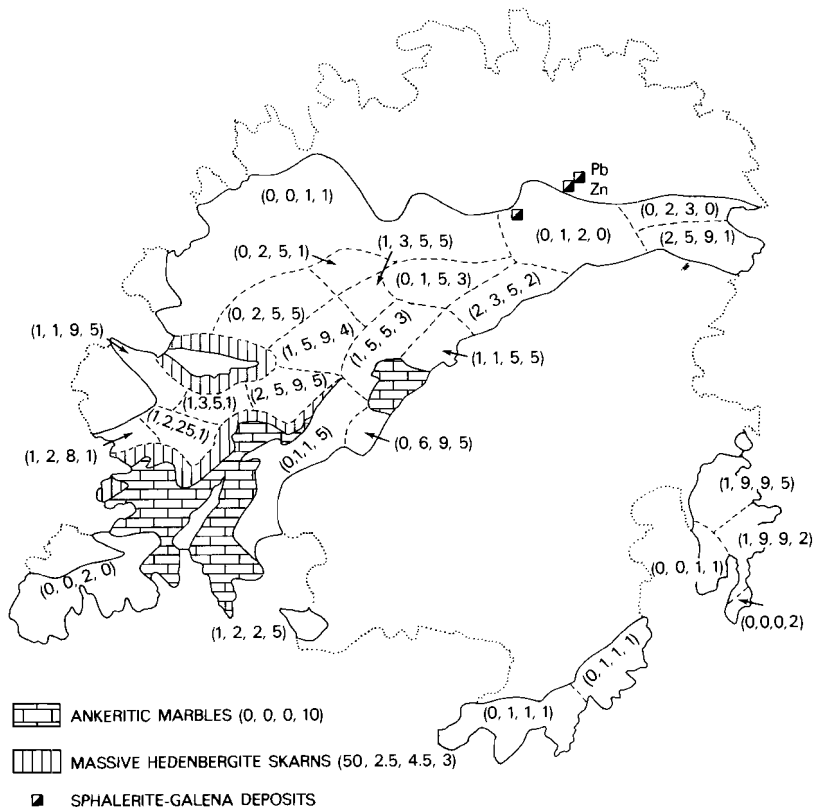
Fig.31:Field estimates of the amounts of major skarn and ore
        formations in the siliceous country rocks surrounding
        the granodiorite pluton at Seriphos. Number combinations
        (a,b,c,d) denote estimated amounts (in vol%) of
        a: pyroxenite; b: garnetite; c: epidotite; d: Fe-ore (mt,hm)

lower gneiss-unit contains on average some 1 vol% pyroxenite, 1 vol%
garnetite, 1 vol% epidote, and 1 vol% of mainly magnetitic iron ore.

    In fig.32 a schematic column is drawn representing a highly
simplified section of the contact metasomatic aureole. The column is
500 m wide (the width of the contact metasomatic aureole), 1 m thick
(arbitrary), and 500 + 30 + 30 + 40 + 150 = 750 m high (total height of
the exposed stratigraphical sequence surrounding the apex of the
granodiorite pluton). According to the field estimates and the
calculated average amounts of metasomatic formations given above for

                                                            130.
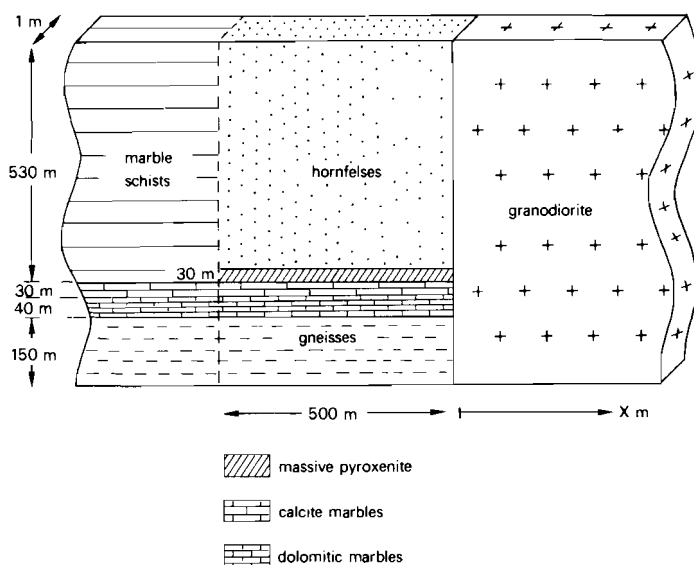
Fig.32: Simplified model column representing the apical parts
of the granodiorite at Seriphos and the surrounding
contact aureole (see text).

each of the stratigraphic units, the simplified column of 500 x 1 x 750
m representing the contact metasomatic aureole, contains 9700 m^3
pyroxene ($CaFe_{0.5}Mg_{0.5}Si_2O_6$), 7000 m^3 garnet ($Ca_3FeSi_3O_{12}$), 12000 m^3
epidote ($Ca_2Al_2FeSi_3O_{12}(OH)$), 19000 m^3 ankeritic dolomite
$CaMg_{0.5}Fe_{0.5}(CO_3)_2$), 4925 m^3 magnetite (Fe_3O_4), and 5675 m^3 hematite
(Fe_2O_3), corresponding with a total amount of 52,785 tons of Fe
(metal).

The unaltered rocks of the schist and gneiss units on average
contain 2.77 gr.Fe_2O_3 + 5.91 gr.FeO or 6.54 gr Fe per 100 gr rock (this
average is the average Fe-content of all gneiss- and schist samples
given in table II). For an average country rock density of 2.7 t/m^3,
this amount corresponds with 0.177 tons Fe/m^3. In the model column of
fig.32 the 29,250 m^3 of siliceous country rocks that are replaced by
the metasomatic formations originally contained 5,180 tons of Fe. In
the marble series the original Fe-content is negligible. The net amount

131.

of Fe added to the country rocks as a result of metasomatism, therefore, is 52,875 - 5,180 = 47,695 tons of Fe.

Field measurements on a number of well-exposed profiles in the Seriphian pluton indicate that 20 - 25 vol% of the exposed apical parts of the magmatic body is bleached (Salemink, 1977). According to the chemical analysis given in table VIII on average 2,026 gr Fe was extracted from the unaltered granodiorite to produce 100 gr of bleached granodiorite. Per 100 gr 'bulk pluton', therefore, an amount of 0.225 x 2.026 = 0.46 gr Fe was removed due to the leaching. For an average rock density of 2.6 t/m^3 this amount corresponds with 0.012 tons of Fe per m granodiorite.

In the model column of 750 m high and 1 m thick of fig.33 a 5300 m wide column of granodiorite suffices to produce the 47,685 tons of Fe that were estimated to have been introduced into the contact metasomatic aureole. This modelled width of 5300 m for the granodiorite column agrees well with the actual dimensions of the granodiorite pluton at Seriphos; the pluton has a diameter of 7 to 10 km.

Similar mass balance calculations for Mg and Mn (including estimates of the amounts of metasomatically formed phlogopite, actinolite, and talc) indicate that a 5500 m wide granodiorite column is sufficient to produce the 13,,452 tons of Mg that were estimated to have been introduced into the country rocks, and a 4900 m wide granodiorite column suffices to produce the 'net' amount of 440 tons of Mn that were estimated to have been added to the country rocks (Salemink, 1977).

The simple mass balance calculations for Fe (and Mg, Mn) show that all Fe-(Mg-,Mn-) materials that were introduced into the metasomatic formations in the country rocks could have been derived entirely from the pluton by HT-metasomatic leaching of the granodiorite.

An indication of the total amounts of fluids involved in the metasomatic mass redistributions in and around the Seriphian pluton can be obtained from the $^{18}O/^{16}O$-exchanges between the percolating solutions and the solids in the granodiorite.

In a closed hydrothermal system the total amount of water participating in the $^{18}O/^{16}O$-exchanges is given by the material balance

$$W\delta^{18}O^i_{H_2O} + R\delta^{18}O^i_{rock} = W\delta^{18}O^f_{H_2O} + R\delta^{18}O^f_{rock}$$

$$W/R = \frac{\delta^{18}O^f_{rock} - \delta^{18}O^i_{rock}}{\delta^{18}O^i_{H_2O} - \delta^{18}O^f_{H_2O}} \qquad (8-2)$$

where i= initial value; f= final value after exchange, W= atom per cent of oxygen in the water phase, and R= at% of rock oxygen (Taylor, 1976).

In the Seriphian magmatics an increase in average whole rock $^{18}O/^{16}O$ occurs from $\delta^{18}O^i_{rock}$= 9.4 %. in the unaltered plutonics to $\delta^{18}O^f_{rock}$= 10.1 %. in the bleached granodiorite, while the composition of the coexisting water phase decreases from $\delta^{18}O^i_{H_2O}$= 9.7 %. to $\delta^{18}O^f_{H_2O}$= 8.5 %. (table VI). Substitution in eq.(8-2) gives:

$$W/R = \frac{10.1 - 9.4}{9.7 - 8.5} = 0.58$$

If, isotopically, the granodiorite was an entirely closed system 58 % of the oxygen atoms initially must have been present in the water phase with $\delta^{18}O_{H_2O}$= 9.7 %. in order to produce the observed $\delta^{18}O$-increase in the bleached granodiorite, and the corresponding $\delta^{18}O$-decrease in the coexisting water phase. Since the granodiorite contains some 45 wt% O, whereas H_2O is 89 wt% O, W/R= 0.58 equals to 29 wt% H_2O. Since only 20-25 vol% ($\approx$wt%) of the granodiorite consists of altered rock, the total amount of water with respect to the total amount of granodiorite is 0.225 x 29 = 6.5 wt% H_2O. If the granodiorite was an entirely closed system, and there was no isotopic exchange with the carbonate-containing, isotopically 'heavy' country rocks, a total amount of 6.5 wt% H_2O with an initial, typically magmatic composition $\delta^{18}O_{H_2O}$= 9.7 %. would have been enough to increase the isotopic composition of 20 - 25 % of the volume of the Seriphian granodiorite from $\delta^{18}O^i_{rock}$= 9.4 %. to $\delta^{18}O^f_{rock}$= 10.1 %. upon bleaching. If there was
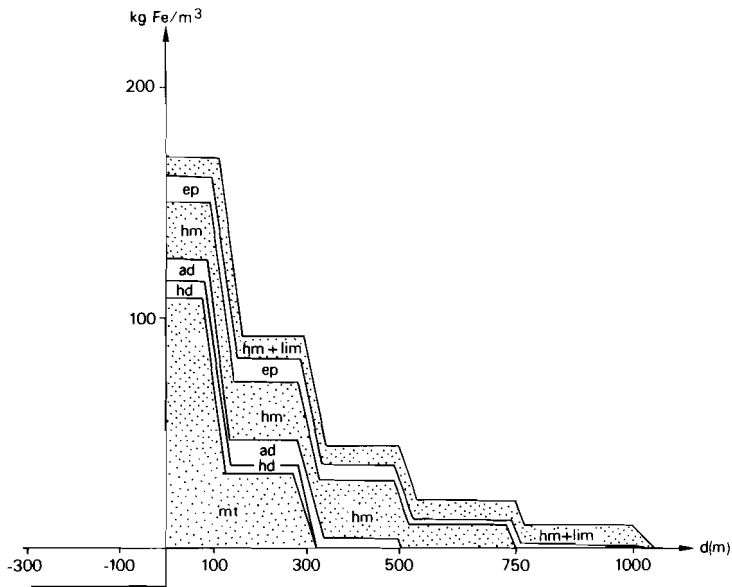
Fig.33: Spatial variation in the estimated amounts of Fe added to
the siliceous hornfelses (in kg Fe per m^3 country rock) as a
function of the distance d(m) perpendicular to the intrusive
contact. mt= magnetite; hd= pyroxenite; ad= garnetite; hm=
hematite; ep= epidote; lim= limonitic iron ore.

an isotopical exchange with the 'heavy' country rocks, the total amount
of H_2O would be less than 6.5 wt% H_2O. A total amount of 6.5 wt% or
less of 'magmatic' H_2O agrees well with the 2 – 5 wt% H_2O that a nearly
water-saturated granodioritic magma releases upon crystallization (see
also chapter IV).

If the granodiorite was a largely closed system a total amount of
6.5 wt% H_2O, or less, must have leached 0.46 wt% Fe from the 'bulk'
granodiorite, and transported it into the surrounding country rocks.
The water phase must have contained 7 wt% Fe, or 16 wt% $FeCl_2$, or more.
Similarly the water phase must have carried at least 34 wt% $MgCl_2$ and
1 wt% $MnCl_2$. Although somewhat too high, Fe-Mg-Mn concentrations in
that order of magnitude do not seem unrealistic for $NaCl-KCl-CaCl_2-MgCl_2$
$-(FeCl_2)$-brines with total salt contents of some 40 eq.wt% NaCl.

With only a limited amount of re-cycling of less than 6.5 wt% H_2O

134.

of magma-derived, metasomatic solutions in a largely closed fluid flow
system the Fe-(Mg-Mn) components could have been leached from the
granodorite and transported into the country rocks.

QUANTITATIVE EVOLUTION OF THE METASOMATIC SYSTEM

The field estimates clearly indicate the existence of a spatial
variation in the amounts of skarn and ore deposits (fig.31(a,b,c,d)).
Close to the intrusive contact skarn formation is very intense.
At large distances from the contact skarn formation is subordinate.
The field estimates also indicate the existence of spatial
variations in the types of mineralization, not only between different
types of host rock, but also within the same rock type unit or
geochemical environment. In the siliceous country rocks, for instance,
the HT-magnetite-pyroxene-garnet deposits are concentrated in the inner
300 m of the contact metasomatic aureole, while the MT-LT
epidote-hematite and limonite formations occur up to distances of more
than 750 m perpendicular to the intrusive contact.
Table IX gives a review of the estimated average amounts (in
vol%) of the major ore and skarn formations in the siliceous hornfelses
as a function of the distance perpendicular to the intrusive contact.

TABLE IX

Field estimates of the average amounts (in vol%) of the
major skarn and ore formations in the siliceous country
rocks at Seriphos in relation to the distance d(m)
perpendicular to the intrusive contact (see fig.31).

d(m)	magnetite	pyroxenite	garnetite	epidotite	hematite
0 - 100	3	2	2	3	1
100 - 300	1	1	3	3	1
300 - 500	-	-	1	2	1
500 - 750	-	-	-	$\frac{1}{2}$	$\frac{1}{2}$
750 - 1000	-	-	-	-	$\frac{1}{4}$

In fig.33 the spatial variations of the metasomatic redistribution of Fe in the siliceous hornfelses, and the adjacent granodiorite, is plotted against the distance perpendicular to the intrusive contact. For each of the major types of skarn and ore formations the net amount of Fe is plotted (in kg per m^3 host rock) that must have been added to or subtracted from the rocks in order to produce the estimated amounts of metasomatic replacements.

The results of fig.33 emphasize that HT-metasomatism was very intense adjacent to the intrusive contact (magnetite-pyroxene-garnet deposits), and that subsequent lower temperature assemblages were formed in decreasing amounts and up to increasing distances from the intrusive contact (epidote-hematite → hematite-limonite). These variations in the quantitative amounts of the metasomatic Fe-redistributions must be a reflection of the spatial and temporal changes in temperature and fluid activity accompanying the gradual cooling (and widening) of the metasomatic system at Seriphos.

CONCLUSION

Chemical analysis of unaltered rocks and of their metasomatic replacement products show that the behavior of major and trace elements was dominantly controlled by the local equilibrium conditions of the minralogical development of the metasomatic formations

In the exposed, apical parts of the pluton 20 - 25 vol% of the magmatic rock consists of bleached granodiorite. Simple mass balance calculations indicate that metasomatic bleaching of 20 - 25 vol% of the entire volume of the granodiorite pluton suffices to produce all the Fe-(Mg-Mn)-materials that were added to the country rocks and deposited in the contact metasomatic skarn and ore formations. Limited recycling of a total amount of less than 6.5 wt% H_2O is sufficient to produce the metasomatic mass exchanges in the granodiorite upon bleaching.

The spatial distribution of the skarn and ore formations at Seriphos points to a gradual decrease in the intensity of the metasomatic mass exchanges with decreasing temperature and increasing distance from the intrusive contact.

Of things formed in the earth some have
their origin from water, others from earth.

Theophrastos, On Stones, 2-nd Century B.C.

CHAPTER VIII: SKARN FORMATION AND FLUID FLOW

Fluid flow is a dominant control of metasomatism. The type of
fluid flow regime (no fluid flow, laminar or steady fluid flow,
turbulent eddying of the fluids) strongly determines the morphology of
metasomatic deposits and the type of 'metasomatic zoning' in the
deposits.

METASOMATISM AND METASOMATIC ZONES

Skarns are metasomatic replacement rocks mainly composed of Ca-Fe-
Mg-Si minerals. The minerals are typically developed in nearly
monomineralic or bimineralic concentrations which may be more or less
zonally arranged parallel to an intrusive contact or parallel to a
central vein or transport channel. In contrast to metamorphic
assemblages the number of mineral phases in a skarn assemblage is
usually small relative to the number of chemical components in the
paragenesis, and in contrast to metamorphic zones significant
discontinuities in bulk composition usually exist between different
metasomatic zones (Zharikov, 1970; Smirnov, 1976; Einaudi et al., 1981;
Einaudi and Burt, 1982). Skarn formation is typically accompanied by
major changes in the amounts of the nonvolatile components (e.g. Ca,
Fe, Mg, Si) in the rocks.
    Skarn systems are open systems. Unlike metamorphic assemblages the
formation of skarns is not only controlled by the conditions of
temperature and (fluid) pressure, but also by the chemical potentials

of the nonvolatile components in the system. According to Gibb's phase
rule:

$$f = c - p + 2 \qquad\qquad (8-1)$$

where   f = number of degrees of freedom

c = number of chemical components

p = number of coexisting phases

the number of coexisting mineral phases in a solid rock is fixed by the
number of nonvolatile components in the rock +2 minus the degrees of
freedom or the number of system parameters that can be varied
independently without changing the mineralogical composition of the
rock.

In a closed, metamorphic rock system with a fixed chemical
compositon the chemical potentials of all nonvolatile components are
fixed and the maximum number of coexisting mineral phases is $p = c + 2$
(only at very specific values of P and T; f = 0). At arbitrary values
of P and T the number of coexisting mineral phases is given by
Goldschmidt's mineralogical phase rule:

$$p = c \qquad\qquad (8-2)$$

(f = 2: P and T can be varied independently within the limits of the
stability field of the assemblage without changing its mineralogical
composition).

In an open, metasomatic system the chemical composition of the
rock may change in response to chemical interactions between the solid
phases and an invading metasomatic solution. The chemical potentials of
at least a number of components will no longer be fixed by the solid
phases in the system, but will be imposed on the system by the
externally controlled metasomatic solution. If there are c_i 'inert'
components in the system, of which the chemical potentials (μ_i) are
buffered by the solid phases, and there are c_m 'perfectly mobile'
components, of which the chemical potentials (μ_m) are externally
controlled, Gibb's phase rule can be written as:

$$f = c_i - p + c_m + 2 \qquad\qquad (8-3)$$

where c_i = number of locally buffered, inert components

c_m = number of perfectly mobile components

(Korzhinskii, 1959, 1965; Thompson, 1970). The number of coexisting

mineral phases in a metasomatic mineralization is given by
Korzhinskii's phase rule:

$$p = c_i \qquad\qquad (8\text{-}4)$$

($f = c_m + 2$: P, T and μ_m can be varied independently within the
stability field of the mineral assemblage without changing its
mineralogical composition). Skarns, in general, contain a fairly
limited number of mineral phases for the number of components present
in the assemblage.

Skarns are often zoned. Monomineralic or bi-, tri-mineralic
concentrations of skarn minerals are more or less zonally arranged
parallel to a central vein or transport channel. The 'metasomatic
zones' can be produced in three different ways, depending on the
prevailing type of fluid flow regime during the metasomatic mass
exchanges:

a: diffusion metasomatism, in which material is transferred by
diffusion through a stationary pore solution (no fluid flow condition)
(Korzhinskii, 1952, 1970; Thompson, 1959; Brady, 1975; Fonteilles,
1978).

b: percolation metasomatism, in which the components are
transferred by a laminary stream of aqueous solutions infiltrating the
pores of a permeable host rock (laminar fluid flow)(Korzhinskii, 1952,
1970; Hofmann, 1972; Fonteilles, 1978; Guy, 1980).

c: pervasion metasomatism, in which mass is exchanged between a
permeable host rock and a turbulently eddying, pneumatolytic
metasomatic solution intruding the cracks and fissues in the solid
medium (turbulent fluid flow)(see Lindgren, 1933; Norton and Cathles,
1972)(this study).

In addition, externally imposed changes in the physico-chemical
conditions of the metasomatic system may lead to changes in the
composition of the invading metasomatic solution, or to changes in its
temperature and/or (fluid) pressure, and these changes may produce a
multi-stadial zoning in the skarn deposits (Pilipenko, 1945; see
Smirnov, 1976).

a: diffusion metasomatism

Consider a solution flowing through a fissure in a porous wall rock saturated with a stationary pore solution. In the fissure the solution is constantly renewed so that its composition remains constant and all its dissolved components can be regarded as externally controlled, perfectly mobile components ($p = c_i = 0$; $c_m = c_{tot}$). In the wall rocks the activities (chemical potentials) of the components dissolved in the stationary pore solution are buffered through dissolution equilibria by mineral phases, and in the wall rocks these components can be regarded as inert components ($p = c_i = c_{tot}$; $c_m = 0$). Due to chemical contrasts between the fissure solution and the wall rock pore solution, diffusion of components will occur from the solution with the highest activity to the solution with the lowest activity.

In the stationary pore solution the activities of the inert components will be constant as long as they are buffered by appropriate mineral phases. There will be no diffusion of inert components. Diffusion can only take place if the components are no longer locally buffered and have become perfectly mobile components, that is at a dissolution boundary between the saturated pore solution and the undersaturated fissure solution. If the rate of the dissolution reactions is rapid relative to the diffusional removal of the components, that is if local equilibrium is maintained, sharp and well-defined dissolution boundaries will develop that migrate away from the fissure into the adjacent wall rocks.

Different components will have different diffusion rates, depending on their specific diffusivities and their specific activity contrasts across the dissolution boundary. Each component, therefore, will dissolve at a different rate, and for each component the corresponding dissolution boundary will migrate at a different rate of advance. A sequence of 'diffusion metasomatic zones' develops in which one mineral is completely replaced at each dissolution front:

diffusion metasomatism without chemical reaction

a_D^L ——————

a_B^L ——————

a_A^L ——————

a_C^L ——————

a_B^s

a_A^s

a_C^s

a_D^s

original fissure

zonation   L | A + L | A + B + L | A + B + C (L')

original wall rock
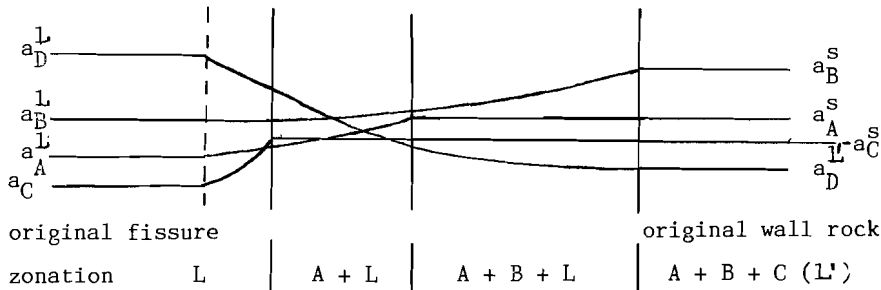
The fissure solution may also contain components that can react with the wall rocks to form new minerals. Formation of new minerals can only take place if their solubility products are exceeded, viz. at specific fluid compositions. At fixed conditions of temperature and (fluid) pressure, a specific fluid composition satisfying a specific solubility product will only be realized at one specific location within the metasomatic diffusion column, at a well-defined reaction boundary or metasomatic replacement front. If local equilibrium is maintained, that is if the reaction rates are rapid relative to the diffusion rates, each replacement front will migrate at its own rate of advance, determined by the diffusion rates of the components participating in the mineral-forming reaction. Due to the occurrence of chemical reactions a sequence of 'diffusion metasomatic replacement fronts' may develop in the wall rocks adjacent to the fissure.

In 'ideal' diffusion metasomatism, dissolution or precipitation of mineral phases only occurs at well-defined replacement fronts. Within the diffusion metasomatic zones the mineralogical composition of the metasomatic rock will be constant. Only in (gradually precipitating) solid solution minerals gradual changes in composition may occur because of the existence of diffusivity gradients in the pore solutions coexisting in local equilibrium with the solid solutions.

For instance, a fissure solution containing iron and magnesia may react with wall rocks composed of calcite and quartz to form Ca-Fe-Mg-Si skarns. Under the given conditions of T and P (and f_{H_2O}, f_{CO_2}, f_{O_2}) the skarns may consist of andradite, hedenbergite-diopside,

141.

and actinolite (tremolite). Fe and Mg will diffuse from the
undersaturated fissure solution into the pore solution in the wall
rocks, and Si and Ca will diffuse from the Ca–Si saturated, stationary
pore solution into the fissure solution. Since diffusion only takes
place from high to low activity there will be a gradual decrease in the
activities of Fe and Mg from the fissure into the wall rocks, and a
gradual increase in the activities of Ca and Si. A diffusive
metasomatic zoning will develop reflecting the differences in the
behavior of Fe, Mg, Si and Ca.

If, for instance, the diffusion rate of silica is small relative
to the diffusivity of the calcite components a diffusion metasomatic
zonation will develop adjacent to the fissure in which quartz remains
while calcite is removed. If, moreover, silica is present in excess so
that quartz is present as an additional mineral phase in all skarn
formations, the mineral zonation in the skarn sequence will depend only
on the activities of the 'perfectly mobile components' Fe, Mg and Ca.
Since the activity of Ca gradually increases towards the unaltered
calcite–quartz wall rock, while a_{Fe} and a_{Mg} gradually decrease in that
direction, only a limited number of zone sequences can develop in the
diffusion metasomatic column.

For instance, with a Fe-rich, Mg-poor fissure solution the
following zonation may develop:

zonation	L		Qz	Hd + Qz	Ad + Qz	Cc + Qz
	fissure					wall rock

The clinopyroxene will be hedenbergitic. Because of the different activity gradients of Fe and Mg within the diffusion metasomatic column (Fe is more consumed than Mg), the pyroxene will be zoned with Fe decreasing and Mg increasing towards the wall rocks (see f.e. Fletcher and Hofmann, 1974; Uchida, 1981; see also fig.34).

In diffusion metasomatic mineral zonation is directly related to the diffusional behavior of the components in the coexisting, stationary pore solution; the activities (chemmical potentials) of the components increase systematically in the direction of their source. Solid solution minerals may show a gradual and continuous compositional variation.
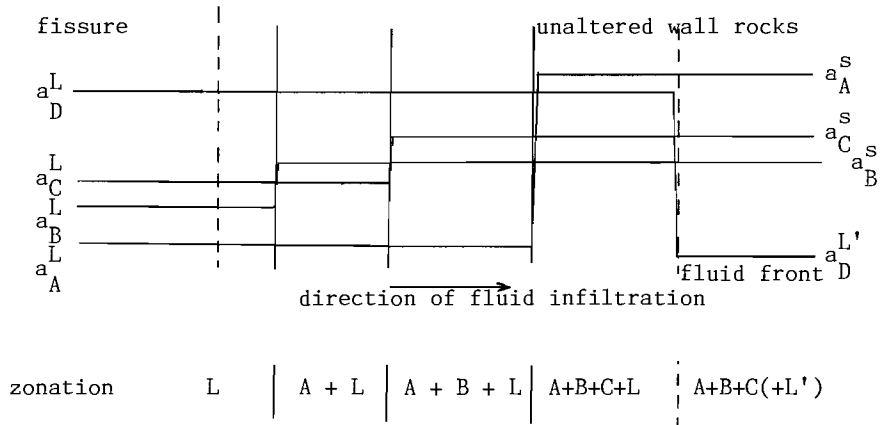
b: percolation metasomatism

Consider a solution flowing through a fissure and infiltrating the pores of the adjacent wall rocks in an uni-directional, laminar way. The pore solution initially present in the wall rocks will be progressively replaced by the infiltrating fissure solution, and in response to chemical contrasts metasomatic mass exchanges will be induced between the invading solution and the wall rock minerals.

As a fluid packet of the laminary flowing, undersaturated fissure solution infiltrates the wall rocks, and replaces a fluid packet of the saturated pore solution, mineral phases will dissolve in order to restore chemical equilibrium. For each mineral phase the amount that dissolves into the fluid packet will be different, depending on the activity contrast between the undersaturated fissure solution packet and equilibrium saturation, and the dissolution rates of the minerals.

If local equilibrium is maintained, that is if reaction rates are rapid relative to the velocity of the fluid infiltration, sharp and well-defined dissolution boundaries will be formed. As fluid percolation continues, and the chromatographic process progresses, the dissolution boundaries will migrate along with the fissure solution into the wall rocks, each boundary at its own rate of advance but more slowly than the infiltrating solution. A sequence of 'percolation metasomatic zones' will develop in the wall rocks adjacent to the fissure:

143.

percolation metasomatism without chemical reaction

fissure   unaltered wall rocks

a_D^L ───────────── a_A^s

                                                                           a_C^s
a_C^L ─────────── a_B^s
a_B^L ──────────
a_A^L

direction of fluid infiltration   'fluid front $a_D^{L'}$

zonation   L │ A + L │ A + B + L │ A+B+C+L ┊ A+B+C(+L')

As in diffusion metasomatism, one inert component becomes
perfectly mobile at each dissolution front, and one wall rock mineral
completely dissolves. In contrast to diffusion metasomatism the
activities of the perfectly mobile components remain constant along the
'ideal' percolation metasomatic column, and equal to their activities
in the fissure solution.

The infiltrating fissure solutions may also contain components
that can react with the wall rocks to form new minerals. If local
equilibrium is maintained, and the mineral-forming reaction is rapid,
precipitation will take place immediately at the contact between the
saturated pore solution and the undersaturated, fissure-derived
solution, at a sharp and well-defined reaction boundary or metasomatic
replacement front.
     As fluid infiltration continues, and a stream of fissure solution
packets passes by, simultaneous dissolution of old and precipitation of
new minerals will continue at a given location until one of the wall
rock minerals participating in the mineral-forming reaction is
completely dissolved. With time the reaction boundaries migrate into
the wall rocks at a rate of advance determined by the velocity of the
fluid percolation and the equilibrium distributions of the replacing
species between solid and fluid. Each reaction boundary migrates at its
own rate of advance.

144.

At constant temperature and (quasi-) constant fluid pressure (a
certain pressure gradient is needed as a driving force for the fluid
percolation), and with a fixed composition of the infiltrating fissure
solution, changes in the equilibrium relations only occur at the
replacement fronts. Within each percolation metasomatic zone both the
chemical composition of the solids and the composition of the
coexisting solution remain constant. Only due to the formation of solid
solution minerals changes in fluid composition may occur within the
percolation metasomatic zone because of mass balance requirements
(Hofmann, 1972). Depending on the shape of the isotherm and the
velocity of the laminary fluid flow, solid solution minerals may have
constant compositions, or there may be a gradual or sudden change in
the composition of the solid solution minerals (Fletcher and Hofmann,
1974; see also Guy, 1984).

For instance, a fissure solution containing iron and magnesia may
infiltrate wall rocks composed of calcite and quartz, and react with
the wall rocks to form andradite, hedenbergite-diopside, and actinolite
(tremolite) skarns. If calcite dissolves more rapidly than quartz, and
the amount of quartz in the wall rocks is such that it is present as an
excess phase in all skarn formations, a sequence of quartz-saturated
skarn assemblages is formed similar to the zonation in a diffusion
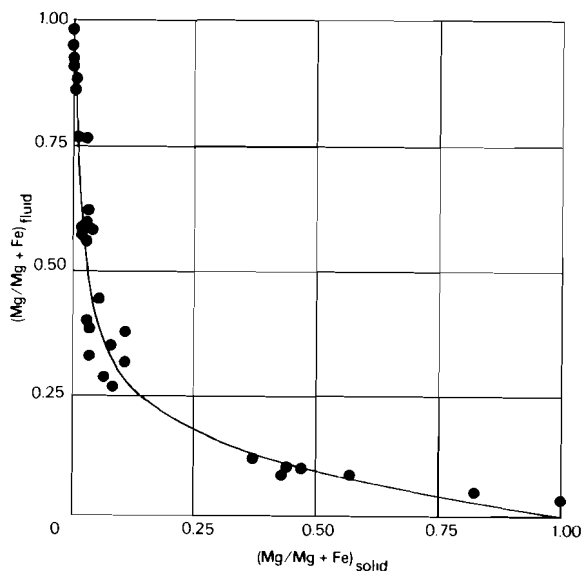metasomatic column. With an Fe-rich, Mg-poor fissure solution:
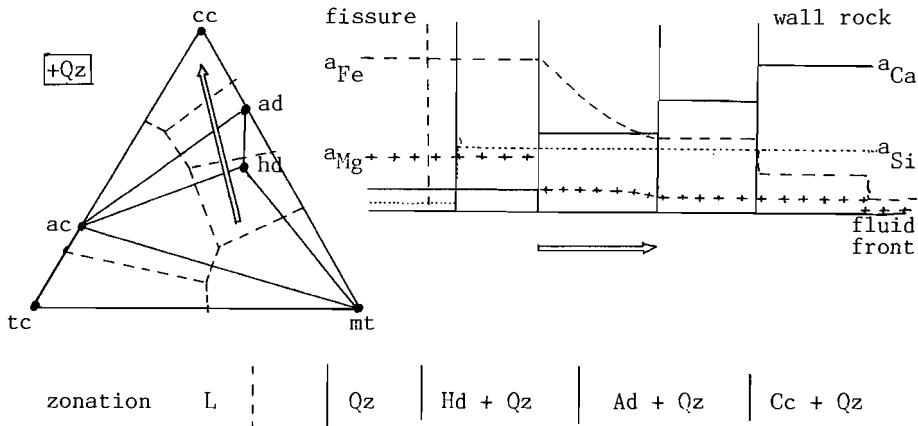
Fig.34: Ion exchange isotherm in the system $CaFeSi_2O_6$ –$CaMgSi_2O_6$ –
$MgCl_2$ –H_2O at 600^0C and 1 kbar (from Uchida, 1981).

The hedenbergite will be an Fe–rich clinopyroxene with a chemical
zoning determined by the Fe/Mg–ratio and the flow velocity of the
percolating fissure solution, and the shape of the pyroxene isotherm
at the given conditions of P and T (see Uchida, 1981; see fig.34).

Since, in a given percolation metasomatic column, the rate of
advance of a replacement front is only determined by the solubilities
of the participating minerals, 'inner zones' may overtake 'outer
zones'. For instance, the andradite zone may be overtaken by the
hedenbergite zone because andradite reacts faster to hedenbergite than
calcite to andradite. The percolation metasomatic column simplifies to:

L | Qz | Hd + Qz | CC + Qz

146.
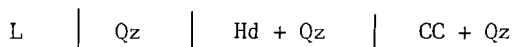
The assemblages separated by the hedenbergite-calcite front are not
in equilibrium with one another (in diffusion metasomatism sharp
concentration discontinuities in the fluid phase are impossible and all
phases coexisting at a diffusion front must be part of an equilibrium
assemblage).

In percolation metasomatism, as in diffusion metasomatism, the
activities of the perfectly mobile components increase systematically
in the direction of their highest activity, but in contrast to
diffusion metasomatism the activity increase in percolation
metasomatism is discontinuous and step-wise at each replacement front.
In contrast to diffusion metasomatism solid solution minerals may have
constant compositions, and zones may be missing from a percolation
metasomatic column; an percolation metasomatic front may form the
contact between mineral assemblages that are incompatible at
equilibrium.

c: pervasion metasomatism

    Consider a solution flowing through a central transport channel
and invading the cracks and fractures in the adjacent wall rocks.
Induced by a sufficiently large fluid pressure gradient the fissure
solution may turbulently eddy into the cracks and fractures in the wall
rocks, and replace and incorporate the initially present wall rock pore
solution. If the fluid pervasion is turbulent enough, and eddying is
intense, the invading undersaturated fissure solution everywhere within
the pneumatolytic fluid flow system will be renewed instantaneously,
and all activity gradients or differences will be leveled immediately.
If local equilibrium is maintained, and reaction rates are rapid, all
wall rock minerals will dissolve (more or less) at the same rate. A
sharp and well-defined dissolution front will form at the ccontactt
between the well-mixed, undersaturated fissure solution and the
unaltered wall rocks with its stationary, saturated pore solution:

pervasion metasomatism without chemical reaction

zonation   L   │ A+B+C(+L')
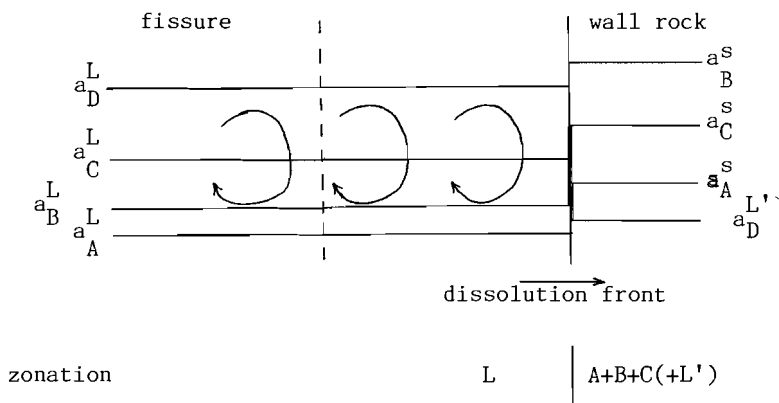
With time the dissolution front will migrate into the wall rocks
at a rate of advance mainly determined by the vigor of the
pneumatolytic fluid turbulence.

The pervading fissure solution may also react with the wall rocks
to form new minerals that can coexist in equilibrium with the
pneumatolytic fissure solution. If local equilibrium is maintained, and
reaction rates are rapid, simultaneous dissolution of old and
precipitation of new minerals will occur only at the boundary between
the well-mixed, constant-composition fissure solution, and the
constant-composition pore soluttion in the unaltered wall rocks. If the
effects off infiltration and diffusion are neglected, the reaction
boundary will be a sharp and well-defined,'pervasion metasomatic
replacement front' that will migrate into the wall rocks.
     At (semi-)constant conditions of temperature and (fluid) pressure,
and a constant composition of the invading metasomatic solution, fluid
compositions as well as solid compositions will remain constant and
uniform everywhere within the turbulent fluid flow system. In 'pure'
pervasion metasomatism, therefore, only one, singular metasomatic
'zone' will develop with a constant mineralogical and chemical
composition and, in the ideal case, it will entirely consist of newly
formed mineral phases composed of components derived from the adjacent
wall rocks as well as from the intruding fissure solution. Solid

solution minerals will have constant compositions in the pervasion metasomatic, pneumatolytic deposits.

For instance, under given conditions of T and P (and f_{H_2O}, f_{CO_2}, f_{O_2}) the turbulent invasion of an Fe-Mg containing, pneumatolytic fissure solution into wall rocks composed of calcite and quartz may lead to the formation of Ca-Fe-Mg-Si skarns consisting of andradite, hedenbergite-diopside, and/or actinolite (tremolite). As the Ca-Si saturated pore solution in the wall rocks is replaced bby the pervading Ca-Si undersaturated fissure solution, calcite and quartz will dissolve at (about) the same dissolution rate. If, due to the simultaneous dissolution of calcite and quartz into the Fe-Mg containing fissure solution, for instance, the solubility product of pyroxene is exceeded, the hedenbergite-diopside precipitates at the dissolution boundary and, as metasomatism proceeds, a singular, monomineralic pyroxene zone is formed in the wall rocks adjacent to the central transport channel:

fissure   wall rock

a_{Fe} a_{Ca}

                  a_{Si}
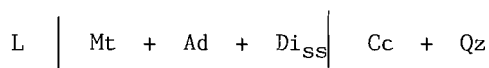
a_{Mg}

zonation   L   Cpx   Cc + Qz
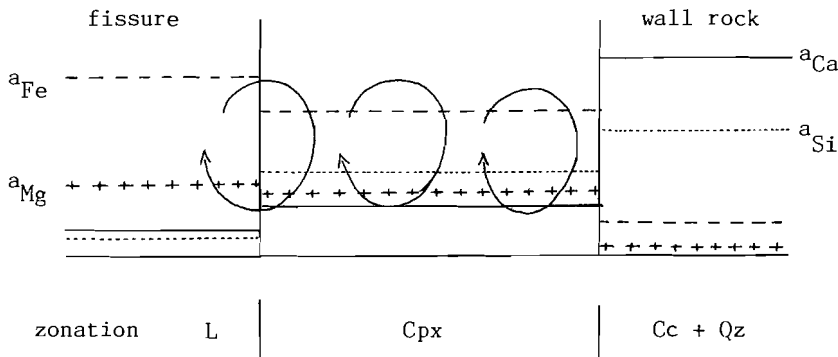
Similarly a singular, bimineralic pyroxene-garnet deposit may develop if the solubility products of both skarn minerals are exceeded.

In the pervasion metasomatic columns the clinopyroxene will be uniform in composition. The Fe/Mg-ratio of the constant-composition hedenbergite-diopside solid solutions will be determined by the Fe/Mg-ratio of the pervading solution and the shape of the isotherm at the given conditions. According to the experimental results of Uchida (1981) the pyroxene, in general, will be Mg-richer than the composition of a coexisting, Cl-bearing Fe-Mg solution (see fig.34).

149.

Because of the interaction of the pervading solution with the wall rocks the composition of the well-mixed metasomatic fluid may also change with respect to components that only indirectly affect the nature of the mineralization ($X_{H_2O}-X_{CO_2}$, f_{O_2}, pH, etc.). For instance, the dissolution of calcite may increase the $CO_3^=$-content of the eddying metasomatic solution, and its f_{CO_2} and pH, and this may cause magnetite to precipitate directly from an initially Fe-undersaturated fissure solution. With time a singular pervasion metasomatic zone may develop entirely composed of pyroxene + magnetite:

$$L \quad \Big| \qquad Mt \; + \; Di_{ss} \qquad \Big| \qquad Cc \; + \; Qz$$
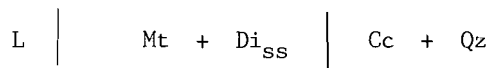
or of pyroxene + andradite + magnetite:

$$L \quad \Big| \quad Mt \; + \; Ad \; + \; Di_{ss} \Big| \quad Cc \; + \; Qz$$

Magnetite precipitation may continue throughout the metasomatic column as long as calcite dissolves and $CO_3^=$ is introduced into the pervading solution (in contrast to 'perfect' percolation metasomatism where the laminary fluid flow is a one-way flow of Fe-undersaturated solutions from the central transport channel into the wall rocks causing earlier formed magnetite to (re-)dissolve as the fluid infiltration progresses. The magnetite persists as a stable mineral phase in the pervasion metasomatic column because of the introduction of an additional equilibrium relation in the system Ca-Fe-Mg-Si-C-O-H.

In pure pervasion metasomatism only one singular metasomatic zone is formed in the wall rocks adjacent to the central transport channel. The zone entirely consists of newly formed mineral phases composed of components supplied by the pervading fissure solution as well as from the dissolved wall rocks (throughout the pervasion metasomatic column mineral formation is partly buffered by the mineral phases in the adjacent, unaltered wall rocks). In a pervasion metasomatic, pneumatolytic deposit the mineralogical and chemical composition will be constant, and solid solution minerals will have constant

compositions. In general, the mineral assemblages on both sides of a pervasion metasomatic replacement front will not be in equilibrium with one another.

d: transition types.

In natural situations, usually, gradual transitions will exist between the processes of pervasion, percolation and diffusion metasomatism as the corresponding types of fluid flow regime (turbulent, laminar, no fluid flow) grade into one another.

For instance, under large fluid pressure gradients, and with sufficiently large bulk rock permeabilties, turbulent fluid flow along the cracks and fractures in the unaltered wall rocks may result in the formation of a massive, pneumatolytic deposit uniformly composed of newly formed skarn and ore minerals. Similarly, the invasion of a metasomatic solution into calcite host rocks may cause the carbonate to dissolve and the permeability to increase sufficiently to induce turbulent fluid flow and the formation of massive, uniform, pervasion metasomatic skarn and ore deposits.

In the wall rocks surrounding a pervasion metasomatic deposit the turbulent fluid flow regime may grade into a fluid flow regime dominated by laminar infiltration because of a decrease in the permeability of the wall rocks. In the wall rocks surrounding a uniform, pneumatolytic deposit a sequence of infiltration metasomatic zones may develop.

On a small scale intergranular diffusion may produce diffusion metasomatic alterations near grain boundaries or at the contacts of relict fragments of unaltered wall rocks within a skarn or ore deposit.
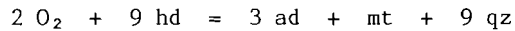

e: multi-stadial metasomatism.

In natural situations, in general, the conditions of P_f, T, μ_i, μ_m will change with time. As metasomatism progresses, fluid pressures and temperatures tend to decrease, and the chemical potentials (activities) of dissolved components may change due to changes in the dissolution

equilibria of the buffering mineral phases within or outside the metasomatic deposit (that is locally buffered, inert components as well as externally controlled, perfectly mobile components). The time-dependent P_f, T, μ_i, μ_m-changes will affect the metasomatic mass exchanges and it may lead to the development of a multi-stadial type of metasomatic zonation.

For instance, in the early stages of a metasomatic event the pneumatolytic, turbulent invasion of a nearly Fe-saturated solution into calcite + quartz host rocks may produce a pervasion metasomatic deposit uniformly composed of hedenbergite + magnetite. As the metasomatic process progresses, temperatures drop and fluid pressure gradients diminish, the vigor of the fluid turbulence will decrease and the pervasion metasomatic aureole around the central transport channel may narrow. If, in addition, the P,T-decrease is such that hedenbergite becomes unstable and decomposes to andradite + magnetite + quartz according to the reaction:

$$2\ O_2\ +\ 9\ hd\ =\ 3\ ad\ +\ mt\ +\ 9\ qz$$

the following multi-stadial metasomatic zoning may develop:
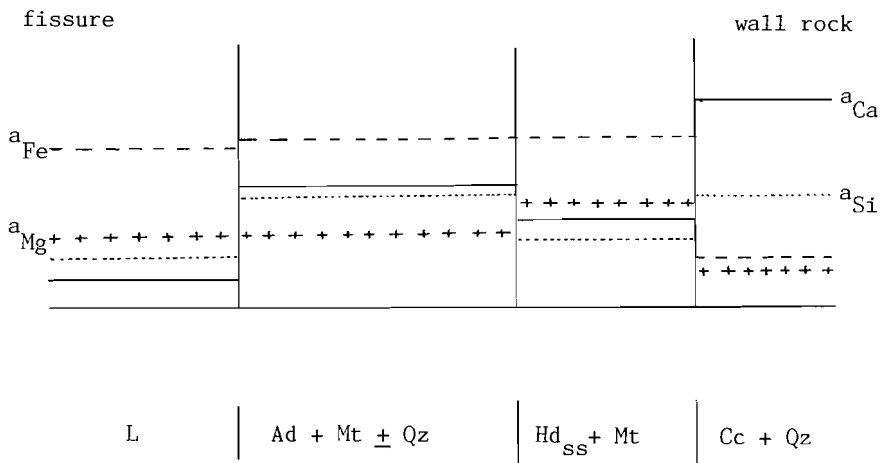
Such a metasomatic zonation with apparent activity alterations is not possible in isobaric-isothermic diffusion, percolation or pervasion metasomatism.

FLUID FLOW AND PLUTONIC INTRUSIONS

Extensive percolation and pervasion metasomatism require fluid
flow, and fluids only flow if they are forced to do so. In an intrusive
system the driving force of the fluid flow may be a density contrast or
a pressure difference, depending on whether the solid rock system is an
open system with high bulk rock permeabilities in which hydrostatic
equilibrium is maintained, or a low-permeability, largely closed fluid
flow system with large lateral fluid pressure differences, or the fluid
flow may be enforced by the combined actions of density and pressure
variations.

In a high-permeability, typically open fluid flow system there is
a rapid exchange of fluids. As in a given location the temperature of
the solids changes due to heat transfer to or from a nearby location,
fluid pressures will change accordingly. The pressure perturbations
created in this way will induce a fluid flow and, in a perfectly open
system, the fluid flow will be sufficiently large to level down the
pressure disturbances (almost) instantaneously. Everywhere within the
perfectly open fluid flow system fluid pressures will be maintained at
the hydrostatic equilibrium.

In a perfectly open intrusive system hydrostatic equilibrium will
be maintained in the 'hot' plutonic rocks as well as in the 'cold'
country rocks. The lateral temperature differences within the
intrusive system are only reflected in lateral variations in the fluid
density. With time the plutonic rocks will cool and in the surrounding
country rocks temperatures will rise. In the plutonic rocks fluid
densities will increase, and in the country rocks fluid densities will
decrease. There will be a net fluid flux from the external environment
into the pluton. Due to the action of gravity the fluids will
circulate into the pluton in regular, wide, laminar convection cells
(Norton and Knight, 1977; Cathles, 1977).

In an open intrusive system a significant amount of mixing will
occur of the initially present, magmatic fluids with the inflowing,
externally derived solutions. The chemical as well as the isotopic

153.

composition of the magma-derived fluids will change significantly due to the fluid mixing and, in time, the fluid compositions everywhere in the open circulation system will become about equal to the chemical and isotopical composition of the (meteoric) waters in the external environment. There may be a net influx of dissolved materials along with the inflowing solutions, viz. from the external reservoir into the pluton.

In a largely closed, low-permeability system only a limited amount of fluids can percolate along the transport channels in the solid rocks, and the fluid flow will only have a limited effect on the existing temperature distributions in the solids. In the idealized case of a 'perfectly closed' fluid flow system, where the amount of fluids can be neglected relative to the amount of solids, and the heat transfer by the convecting fluids is small relative to the conductive heat transfer in the solids, the temperatures of the percolating fluid particles will change along with the temperature changes in the solids. through which they pass, and the fluid pressures will change accordingly. The temperatures and pressures of the percolating fluids will change (almost) as in a completely closed system without fluid flow. The fluid densities will be (nearly) constant as they are in a completely closed system, and lateral temperatures are mostly reflected in fluid pressure differences only.

In a low-permeability, largely closed intrusive system large differences in temperature and fluid pressure may exist between the 'hot' pluton and its 'cold' environment. As a magma solidifies and degasses the magmatic fluids may have considerably higher initial temperatures and pressures than the fluids in the surrounding country rocks. There will be a net fluid flux from the plutonic heat and fluid source into the external environment, and the fluids may percolate outward from the pluton along the transport channels in the solid rocks. If the P_f- T gradients are sufficiently large with respect to the bulk permeability of the rocks, the pneumatolytic solutions may eddy rapidly along the cracks and fractures in a whirling pattern of irregular fluid circulations.

In a largely closed intrusive system, with a net fluid flux from
the pluton into the country rocks, there will be no significant amount
of mixing of the outflowing, magma-derived solutions with fluids from
the external reservoir. Apart from (minor) changes due to the
incorporation of fluids initially present in the country rocks, the
chemical and isotopic composition of the magma-derived solutions will
only change in response to chemical interactions with the solids. In a
largely closed intrusive system there will be a net transport of
dissolved materials along with the outflowing solutions from the pluton
into the surrounding country rocks.

SKARN FORMATION AND FLUID FLOW REGIME AT SERIPHOS

At the time of the final solidification of the granodioritic magma
fluid pressures must have been high in the Seriphian pluton (P_f= 3-4kb)
much higher than the hydrostatic equilibrium pressure of 300-400 bar or
the lithostatic equilibrium pressure of 1-1.5 kb at the assumed
intrusion depth of 3-4 km (see Chapter VI). The high pressures of the
primary fluids as well as their magmatic origin point to degassing of
the solidifying magma in a magma-chamber that was enclosed by contact
metamorphic country rocks with low bulk rock permeabilities. Initially
large fluid pressure gradients must have existed between the degassing
pluton and the surrounding metasedimentary rocks.

Shortly after the final solidification of the main mass of the
granodiorite, at the time of the (auto-) brecciation and (hydro-)
fracturing of the magmatic rocks and of the adjacent contact
metamorphic rocks, fluid pressures still were high in and around the
pluton. In the early, HT-stages of metasomatism cm-wide, bleached zones
were formed along the cracks and fractures in the main mass of the
granodiorite by the action of magma-derived, aqueous $NaCl-KCl-MgCl_2$-
$CaCl_2$-($FeCl_2$?)-brines with fluid pressures of some 3 - 2 kb, at
temperatures of 750 - 450 ^{0}C. Adjacent to the intrusive contact
massive, often brecciated pyroxene-garnet skarns and magnetite deposits

were formed at temperatures of 600 - 400 ^{0}C from dominantly magmatic, aqueous $NaCl-(KCl)-CaCl_2-MgCl_2-(FeCl_2?)$-brines with fluid pressures of some 2 - 1 kb. The pressure difference between the fluids within the pluton and the skarn fluids confirms the existence of large fluid pressure gradients across the intrusive contact. The common occurrence of coarse-grained, unzoned, bi- tri-mineralic hd-ad-mt mixtures in a singular, pervasion type of metasomatic 'zoning' in the HT-pneumatolytic, massive skarn and ore deposits suggests a turbulent type of fluid flow regime during the early stages of the skarn formation.

Around the pneumatolytic deposits the scapolite-bearing contact metamorphic hornfelses are usually epidotized. The epidotization probably results from the laminar infiltration of Fe-rich metasomatic solutions from the high-permeability, pervasive pyroxene-garnet-magnetite deposits into the low-permeability, aluminous wall rocks.

In the MT-stages of the metasomatic evolution at Seriphos dm-cm wide, vein-type epidote-actinolite-hematite and ilvaite-actinolite-magnetite deposits were formed along cracks and fractures cross-cutting the previously formed HT-skarn deposits as well as the country rocks up to 400 - 500 m perpendicular to the intrusive contact. The MT-deposits were formed at temperatures of 450 - 350 ^{0}C and fluid pressures of 1.5 to 0.5 kb from $NaCl-MgCl_2-(KCl-CaCl_2-FeCl_2?)$-rich, hydrous solutions with a largely magmatic origin. Occasionally the MT-vein deposits may show a percolation type of metasomatic zonation (f.e. the alternating hedenbergite/ilvaite(+actinolite) zones along cracks and fractures in the massive pyroxene skarn zone of SW-Seriphos probably represent a sequence of alternating infiltration metasomatic zones). The decreased fluid pressures, the vein-type occurrence of the MT-MP deposits, and the formation of infiltration metasomatic zones, suggest that, as fluid pressures decreased and fluid pressure gradients diminished during the MT-stages, the fluid flow system in the skarns gradually changed from a pneumatolytic system dominated by turbulent fluid flow into a system with a mainly laminar type of fluid flow regime.

156.

At temperatures of 400 – 300 ^{0}C, in the MT–LT stages of the metasomatic evolution, when fluid pressures had dropped to values close to the hydrostatic equilibrium pressure (P_f= 300 – 400 bar), cm–mm wide, vein-type actinolite-hematite-quartz-calcite deposits were formed in the country rocks up to 700 – 800 m from the intrusive contact, and in the central veins of the bleached zones in the granodiorite. The deposits precipitated from hydrous $NaCl$–$MgCl_2$(KCl–$CaCl_2$–$FeCl_2$?) solutions with a largely magmatic origin. The formation of calcite within the intrusive points to a transport of chemical components (Ca, CO_2) from the carbonatic country rocks into the pluton. Towards the late stages of the MT–metasomatic evolution, when lateral fluid pressure gradients had largely vanished, the hydrothermal convection system probably had changed from a largely closed fluid flow system into a largely open circulation system with wide, laminar convection cells convecting through the carbonatic country rocks as well as into the granodiorite pluton.

During the final stages of the post–magmatic, convective cooling of the Seriphian pluton LT quartz–calcite–limonite deposits were formed in the country rocks up to distances of more than 1000 m perpendicular to the intrusive contact, and in the central veins of the bleached zones in the granodiorite. The LT–deposits precipitated at temperatures below 300^{0}C from CO_2–containing, hydrous $NaCl$–$MgCl_2$ solutions with fluid pressures of P_f = 300 – 400 bar. The hydrostatic pressures and the presence of 'externally derived' CO_2 indicate that the hydrothermal fluid flow system was a largely open circulation system.

The relatively high salt contents of the aqueous solutions (20 – 15 eq.wt% NaCl), as well as the likely presence of $MgCl_2$ (and $FeCl_2$?), and the relatively high $\delta^{18}O$–values of the water phase ($\delta^{18}O_{H_2O}$= 2–4%.) do not point to the introduction of large amounts of dilute, low–$\delta^{18}O$ 'meteoric' waters into the open circulation system, and possibly the LT–hydrothermal solutions were mainly re-cycled, magma–derived solutions that had re-equilibrated completely in the course of the metasomatic evolution.

CONCLUSION

The chronological evolution in the mode of occurrence and spatial
distribution of the skarn formations at Seriphos indicate that during
the post-magmatic evolution of the granodiorite intrusion the
hydrothermal convection system gradually changed from a largely closed
fluid flow system with large, lateral fluid pressure gradients
especially across the intrusive contact, to a largely open
circulation system with overall maintenance of hydrostatic equilibrium.
This is in agreement with the fluid inclusions and isotopic evidence.

The mode of occurrence and the metasomatic zonations in the
multi-stadial skarn formations suggest that, in the course of the
metasomatic evolution, the fluid flow regime gradually changed from a
pneumatolytic, turbulent type of fluid flow regime with small-scale,
pervasive fluid intrusions along cracks and fractures close to the
intrusive contact, to a laminar type of fluid flow regime with wide,
regular convection cells that probably extended up to considerable
distances from the intrusive contact.

Comparison of the temporal and spatial evolution of the fluid flow
behavior with the quantitative estimates of the amounts of skarn
formations in the field emphasizes that, in addition to chemical
controls, the intensity of the fluid percolation also was a major
control of the metasomatic mass redistributions in and around the
granodorite intrusive at Seriphos.

> In our speculations we can postulate any ideal
> conditions we like, but they should at least be
> within the limits of possibility.
>
> Aristotle, The Politics II-vi, ±350 B.C.

CHAPTER IX: A HEAT AND MASS EXCHANGE MODEL

The observed evolution of the magmatic, contact metamorphic and
contact metasomatic-hydrothermal events at Seriphos, and the
reconstructed P,T-developments during the events can be used to define
a simplified model for the heat and mass exchanges associated with the
granodiorite intrusion. The model can be tested by comparing model
results with theoretical and experimental studies, and with field
observations.

GENERAL CONCEPT

At Seriphos the contact metamorphic aureole formed as a
consequence of the temperature rise accompanying the emplacement of the
magma body. The stresses associated with the solidification and
degassing of the magma caused a widespread (hydro-)fracturing of the
solidified plutonic rocks and of the surrounding contact metamorphic
rocks. The resulting increase in the permeabilities of the rocks
permitted intense post-magmatic, hydrothermal activities along the
newly formed transport channels. At Seriphos a clear distinction can be
made between the early, magmatic stages of the intrusion with mainly
'dry' upheating of the country rocks and cooling of a still largely
molten body of granodioritic magma, and the later, post-magmatic stages
with hydrothermal cooling of both the solidified intrusive rocks and
the country rocks.

A model for the granodiorite intrusion at Seriphos should also comprise two stages. In the first stage of the model the magma can be considered as a liquid and the surrounding country rocks can be regarded as non-permeable solids. In the second stage of the model the granodiorite can be considered a solid and both the magmatic and the contact metamorphic rocks can be defined as permeable solid media.

The temperature developments in and around an intrusive not only depend on the nature of the media in the considered system, they are also strongly influenced by the shape and size of the intrusive body (Jaeger, 1961; Marsh, 1977). At Seriphos only the apex of the intrusion is exposed. The circular outline of the pluton and the ductile updoming of the country rocks over the shallow, post-orogenic intrusion, however, suggest a globular, diapiric type of magmatic body (Grout, 1945; Fyfe, 1970). The radius of the magma diapir is in the order of 5 to 10 km (see fig.3).

THE FIRST, MAGMATIC STAGE OF THE MODEL

introduction

The intrusion of a large body of magma into the upper levels of the earth's crust involves the introduction of a large amount of heat into a relatively cold environment. The heat is introduced by the intruding mass of magma and the dominant mechanism of heat transport, therefore, by definition is convection. Since the magma emplacement at Seriphos apparently was not compelled by external forces such as tectonic forces or orogenic movements, the magma movement must have resulted from density differences caused by temperature gradients, and the convection must have been free convection. The heat effects of the magma intrusion can be considered to result from the introduction of a large body of freely convecting magma into an environment consisting of cold, solid country rocks.

At the contact between a convecting melt and a solid wall, a thermal boundary layer can be defined as the layer where 99% of the temperature difference between the wall and the main mass of the
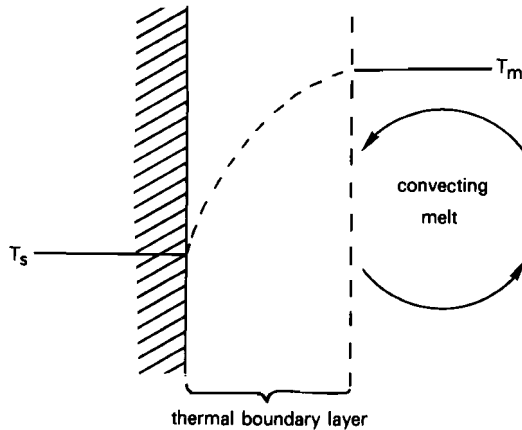
Fig.35: In the 'thermal boundary layer' 99% of the temperature
transition is localized between the main mass of the
convecting magma melt and the permanently solid wall.

convecting melt is localized (fig.35)(see Eckert and Drake, 1959). In
intrusive systems this boundary layer can be regarded as a mixing layer
along the intrusive contact containing an unstable mixture of molten
magma, solidified magma and entrapped fragments of the solid wall
rocks. Because of the continuously interchanging actions of magma
solidification, magma injection and re-melting of solids, the
temperatures in this unstable boundary layer vary continually in time
and place and the temperatures can only be described in terms of an
average temperature distribution. In the central parts of the
convecting melt body, outside the thermal boundary layer, the melt
temperatures can be considered uniform and equal (apart from the small,
vertical variation as a function of the adiabatic gradient).

formulation
     In the first stage of the model for the granodiorite intrusion at
Seriphos it is assumed that a spherical body of magma with an initial,
uniform temperature T_m(t=0) is instantaneously emplaced in an infinite,
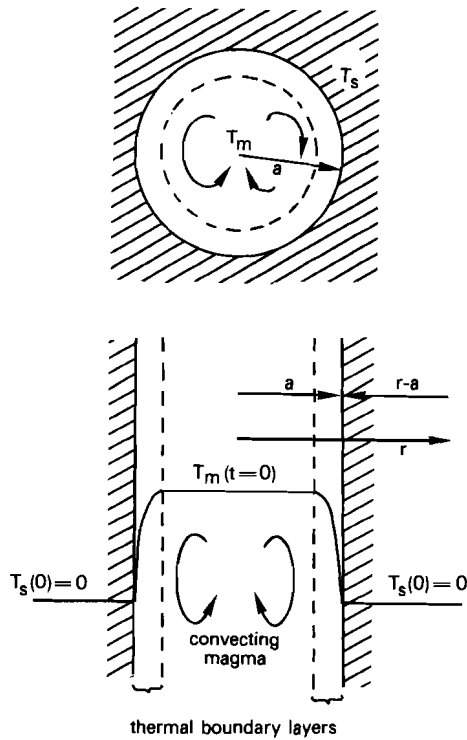non-permeable, solid environment with an initial, uniform temperature

Fig.36: Schematic review
   of the initial conditions
of the first stage,
spherical symmetrical
model for the granodiorite
intrusion at Seriphos.
(see text).

$T_s(t=0) = 0$. In the melt free convection is considered to be the
dominant mechanism of heat transport; in the surrounding solids heat is
only transferred by conduction. Between the two media a thermal
boundary layer exists where the temperature transition is localized
between the main mass of the convecting melt and the permanently solid
environment. If the thickness of this boundary layer is small relative
to the size of the melt body, its heat content can be neglected and the
heat exchange in the model system can simply be expressed in terms of a
well-stirred fluid with a uniform temperature $T_m(t)$ and a solid medium
with a temperature distribution $T(r-a)$ ($r-a=$ radial distance from the
melt/solid boundary situated at r=a; t = time after the emplacement of
the melt body at t=0)(fig.36).

With $T_c(t)$ as the contact temperature in the solid at r=a, the
convective heat flux Q(t) through the boundary layer is given by
Newton's law:

$$Q(t) = 4\pi a^2.h.\Delta T(t) \qquad\qquad , r=a$$

where $\Delta T(t)= T_m(t) - T_c(t)=$ temperature difference across the boundary
layer (ΔT is taken positive in the direction +r of the heat flow), a=
radius of the fluid sphere, and h= convective heat transfer coefficient
For a given set of physical properties h can be considered constant.

The expression for the convective heat flux Q(t) can also be
written as:

$$Q(t) = 4\pi a.Nu.k_m \left\{ T_m(t) - T_c(t) \right\} \qquad , r=a \qquad (9\text{-}1)$$

where $Nu= a.h/k_m=$ Nusselt number of the convection system, and $k_m=$
thermal conductivity of the melt. The Nusselt modulus Nu is a
dimensionless parameter representing the ratio of the convective heat
flux from the melt body to the rate of the conductive heat transfer
($Nu= Q_{cond}/Q_{conv}$). Nu is inversely proportional to the (relative)
thickness of the thermal boundary layer. It is a measure of the vigor
of the convection that is independent of the size of the spherical
convection system.

The convective heat loss from the melt body is equal to the
decrease in internal energy of the body:

$$+ 4\pi a.Nu.k_m(T_m - T_c) = + \frac{4}{3}\pi a^3 \rho_m c_m \frac{\partial T_m}{\partial t} \qquad , r=a \qquad (9\text{-}2)$$

where $\rho_m=$ density of the melt, and $c_m=$ specific heat of the melt.

The convective heat loss from the melt body must also be equal to
the heat conducted from the contact into the surrounding solid:

$$+ 4\pi a.Nu.k_m(T_m - T_c) = + 4\pi a^2.k_s \frac{\partial T}{\partial r} \qquad , r=a \qquad (9\text{-}3)$$

where $k_s=$ thermal conductivity of the solid, and $\partial T/\partial r=$ temperature
gradient in the solid at the melt/solid boundary (like ΔT in eq.(9-1),
$\partial T/\partial r$ is taken positive in the direction +r).

163.

The temperature distribution in the solid, as a function of the distance r from the centre of the melt sphere, has to satisfy the differential equation of heat conduction in a spherical system:

$$\frac{\partial T}{\partial t} = \kappa_s \left(\frac{\partial^2 T}{\partial r^2} + \frac{2}{r} \frac{\partial T}{\partial r} \right) \qquad , \quad r \geq a \qquad (9\text{-}4)$$

where $\kappa_s = k_s/\rho_s c_s$ = thermal diffusivity of the solid; ρ_s = density of the solid, and c_s = specific heat of the solid.

By substituting $\Theta = r.T$ the differential equation (9-4) simplifies to:

$$\frac{\partial \Theta}{\partial t} = \kappa_s \cdot \left(\frac{\partial^2 \Theta}{\partial r} \right) \qquad , \quad r \geq a \qquad (9\text{-}5)$$

The boundary conditions (9-2) and (9-3) at r=a give:

$$4\pi a . Nu . k_m (T_m - \frac{\Theta}{a}) = \frac{4}{3} \pi a^3 \rho_m c_m \frac{\partial T_m}{\partial t} = 4\pi a . k_s . (\frac{\partial \Theta}{\partial r} - \frac{\Theta}{a})$$

or:

$$\frac{\partial \Theta}{\partial r} = \frac{a^2 \rho_m c_m}{3 k_s} \frac{\partial T_m}{\partial t} + \frac{\Theta}{a} \qquad , \quad 0 < t \leq T, \ r=a \qquad (9\text{-}6)$$

$$\frac{\partial \Theta}{\partial r} = Nu . \frac{k_m}{k_s} . T_m - (Nu . \frac{k_m}{k_s} - 1)\frac{\Theta}{a} \quad , \quad 0 < t \leq T, \ r=a \qquad (9\text{-}7)$$

The initial conditions are:

$$T_m = T_i \qquad , \quad t=0 , \ 0 \leq r < a \qquad (9\text{-}8)$$

$$\Theta_0 = 0 \qquad , \quad t=0 , \ r > a \qquad (9\text{-}9)$$

A solution that satisfies the differential equation (9-5), the boundary conditions (9-6) and (9-7), and the initial conditions (9-8) and (9-9), and that results in $\Theta \to 0$ for t>0, $r \to \infty$ can be found by applying the Laplace transform to the temperature $\Theta(r,t)$, that is multiplying $\Theta(r,t)$ by e^{-pt} and integrating it with respect to t from 0 to ∞:

$$L|\Theta(r,t)| = \bar{\Theta} = \int_0^\infty e^{-pt}\Theta(r,t)dt \qquad (9\text{-}10)$$

where p is a number whose real part is positive and large enough to make the integral (9-10) convergent. With the theorems:

$$L|\Theta_1 \pm \Theta_2| = L|\Theta_1| \pm L|\Theta_2|$$

$$L|\partial^n \Theta / \partial r^n| = \partial^n \bar{\Theta} / \partial r^n$$

$$L|\partial \Theta/\partial t| = p.L|\Theta| - |\Theta_0|$$

the subsidiary differential equation becomes:

$$\frac{\partial^2 \bar{\Theta}}{\partial r^2} - \frac{p}{\kappa_s}\bar{\Theta} = -\frac{\Theta_0}{\kappa_s}$$

Substitution of $\Theta_0 = 0$ and $p = \kappa_s . q^2$ results in:

$$\frac{\partial^2 \bar{\Theta}}{\partial r^2} - q^2 \bar{\Theta} = 0 \qquad\qquad , \ r \geqq a \qquad (9\text{--}11)$$

The subsidiary boundary conditions become:

$$\frac{\partial \bar{\Theta}}{\partial r} = \frac{a^2}{\kappa_s v} \left| p.\bar{T}_m - T_i \right| + \frac{\bar{\Theta}}{a} \qquad\qquad , \ t=0, \ r=a \quad (9\text{--}12)$$

where $v = 3\rho_m c_m / \rho_m c_m$

and

$$\frac{\partial \bar{\Theta}}{\partial r} = s.\bar{T}_m - (s-1)\frac{\bar{\Theta}}{a} \qquad\qquad , \ t=0, \ r=a \quad (9\text{--}13)$$

where $s = Nu.k_m / k_s$

The general solution for (9–11), (9–12) and (9–13) that is finite for $r \to \infty$ is:

$$\bar{\Theta} = \Phi(p).e^{-q(r-a)} \qquad\qquad\qquad (9\text{--}14)$$

where $\Phi(p)$ has to be found from the fact that $\bar{\Theta}$ and $\partial\bar{\Theta}/\partial r$ are continuous at $r - a = 0$.

From (9–12) and (9–13) it follows:

$$\left(\frac{a^2}{v}q^2 - s\right)\bar{T}_m + s.\bar{\Theta} = \frac{a^2}{\kappa_s v}T_i \qquad\qquad (9\text{--}15)$$

From (9–13) it follows:

$$\frac{\partial\bar{\Theta}}{\partial r} = q.\bar{\Theta} = s.\bar{T}_m - (s-1)\frac{\bar{\Theta}}{a}$$

$$\bar{\Theta} = \frac{s.\bar{T}_m}{q + (s-1)/a} \qquad\qquad (9\text{--}16)$$

Substitution of (9–16) into (9–15) results in:

$$\bar{T}_m = \frac{aq + (s-1)}{\kappa_s . \left| a^3q^3 + a^2q^2(s-1) - aqsv + sv \right|} . a^2 T_i \qquad (9\text{--}17)$$

$$\bar{\Theta} = \frac{as}{\kappa_s . \left| a^3q^3 + a^2q^2(s-1) - aqsv + sv \right|} . a^2 T_i \qquad (9\text{--}18)$$

(compare Carslaw and Jaeger, 1959, p.349).

165.

In the $\Phi(p)$-expressions for T and Θ the quantities a, v and s are real numbers, and eq.(9-18) can be rewritten as:

$$\bar{\Theta} = \frac{a^3 \cdot s \cdot T_i}{\kappa_s} \cdot \frac{1}{(aq+\alpha)(aq+\beta)(aq+\gamma)} \cdot e^{-q(r-a)} \qquad (9\text{-}19)$$

$$\bar{\Theta} = \frac{a^3 s T_i}{\kappa_s}\left[\frac{1}{(\alpha-\beta)(\alpha-\gamma)} \cdot \frac{e^{-q(r-a)}}{(q+\alpha/a)} - \frac{1}{(\alpha-\beta)(\beta-\gamma)} \cdot \frac{e^{-q(r-a)}}{(q+\beta/a)} - \frac{1}{(\beta-\gamma)(\alpha-\gamma)} \cdot \frac{e^{-q(r-a)}}{(q+\gamma/a)}\right]$$

where α, β and γ are the roots of the equations:

$$\left.\begin{array}{c} \alpha + \beta + \gamma = 1 - s \\ \alpha\beta + \alpha\gamma + \beta\gamma = -sv \\ \alpha\beta\gamma = sv \end{array}\right\} \qquad (9\text{-}20)$$

For each of the Laplace transforms $w(p)=\frac{1}{(q+1)} \cdot e^{-q(r-a)}$ in eq.(9-19) the corresponding expression for $w(r,t)$ is:

$$w(r,t)=\left(\frac{\kappa_s}{\pi t}\right)^{\frac{1}{2}} \cdot e^{-(r-a)^2/4\kappa_s t} - 1\kappa_s e^{1(r-a)+\kappa_s t 1^2} erfc\left[\frac{r-a}{2\sqrt{\kappa_s t}} + 1\sqrt{\kappa_s t}\right] \qquad (9\text{-}21)$$

where $erfc(x)$ is the tabulated function:

$$erfc(x) = 1 - erf(x) = \frac{2}{\sqrt{\pi}} \int_x^\infty e^{-\xi^2} d\xi$$

(see Carslaw and Jaeger, 1959).

In the solid medium, with an intial, uniform temperature $T_s=$ (t=0), surrounding a sphere with a well-stirred melt with an intial, uniform temperature $T_i(t=0)$ the distribution of the temperature $T_s(r-a,t)$ at any location r-a from the melt/solid boundary at r=a, and at any time t after the initiation of the model at t=0, is given by:

$$\frac{T_s(r-a,t)}{T_i} = \frac{a}{r} \frac{Nu(k_m/k_s)}{(\alpha-\beta)(\alpha-\gamma)(\beta-\gamma)}\left[-\alpha(\beta-\gamma)J(\alpha) + \beta(\alpha-\gamma)J(\beta) - \gamma(\alpha-\beta)J(\gamma)\right] \qquad (9\text{-}22)$$

where

$$J(\alpha) = e^{(\alpha/a)(r-a) + \kappa_s t(\alpha/a)^2} erfc\left[\frac{r-a}{\sqrt{\kappa_s t}} + \frac{\alpha}{a}\sqrt{\kappa_s t}\right]$$

and α, β and γ are given by:

$$\alpha + \beta + \gamma = 1 - Nu(k_m/k_s)$$
$$\alpha\beta + \alpha\gamma + \beta\gamma = -3Nu \cdot \kappa_m/\kappa_s$$
$$\alpha\beta\gamma = 3Nu \cdot \kappa_m/\kappa_s$$

166.

The corresponding change in the uniform temperature $T_m(t)$ of the well-stirred melt inside the convecting, spherical melt body ($r < a$) as a function of the time t after the initiation of the model is given by the formulation:

$$\frac{T_m(t)}{T_i} = \frac{1}{(\alpha-\beta)(\alpha-\gamma)(\beta-\gamma)} \left| -\alpha(\beta^2-\gamma^2)I(\alpha) + \beta(\alpha^2-\gamma^2)I(\beta) - \gamma(\alpha^2-\beta^2)I(\gamma) \right|$$

where $\qquad I(\alpha) = J(\alpha)_{r-a=0} = e^{\kappa_s t(\alpha/a)^2} \ \mathrm{erfc}(\frac{\alpha}{a} \sqrt{\kappa_s t})$ $\qquad\qquad$ (9-23)

and α, β and γ are as in eq.(9-22).

results

Figures 37a-d show temperature distributions in and around the spherical melt body as calculated with eqs.(9-22) and (9-23).

In fig.37a the temperature development is given as a function of the time t after the initiation of the model as expressed by the dimensionless parameter $\sqrt{\kappa_s t}/a$; Nu, κ_m and κ_s are considered constants. In the initial stages of the model melt temperatures drop rapidly and in the adjacent solid temperature rises are fast. As time progresses and cooling continues melt temperatures continue to drop, and in the adjacent solid temperatures first pass through a maximum before they decrease. As $t \to \infty$ all temperatures approach zero, thermodynamic equilibrium is re-established and the heat anomaly disappears.

As long as convection continues and a temperature difference $\Delta T(t)= T_m(t) - T_c(t)$ is maintained across the convective boundary layer at $r=a$, the drop in $\Delta T(t)$ will always be larger than the change in the contact temperature $T_c(t)$. The drop in the convective heat flux $Q_c(t)$ from the melt into the solid, therefore, will always be faster than the conductive propagation of the change into the solid. In the solid medium surrounding the convectively cooling melt body the temperature distributions are 'convex' or 'S-shaped'.

Fig.37b confirms that, with higher Nusselt number or increasing vigor of the thermal convection in the melt, the convective heat flux across the boundary layer increases. For a given time and given values of the thermal diffusivities κ_m and κ_s, temperatures in the solid are
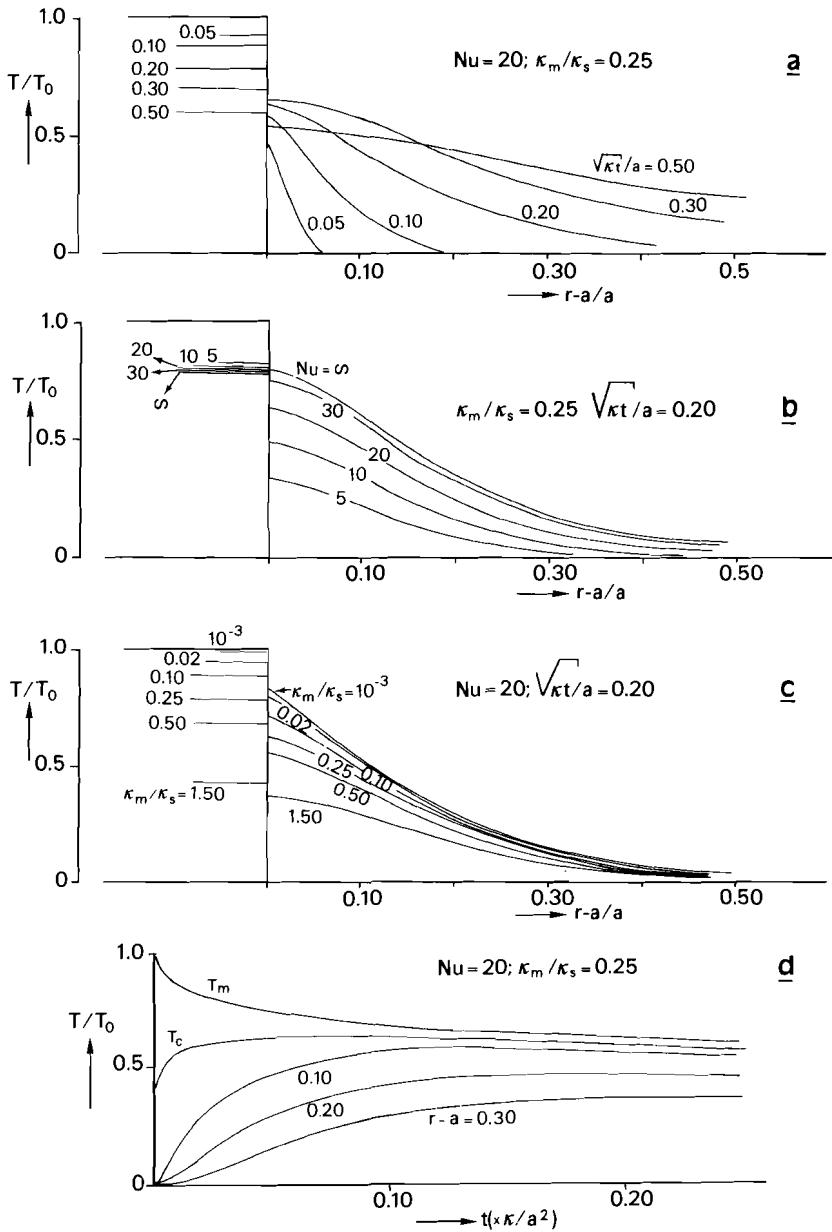
Fig.37: Temperature distributions in and around a well-stirred,
spherical melt body as calculated with the first stage,
magmatic model as functions of the model parameters
a: $\sqrt{\kappa_s t}/a$; b: Nu; c: κ_m/κ_s ; d: r-a,t (see text).

higher for higher Nusselt number and temperatures in the melt are lower
for higher Nusselt number. Since, in the early stages of the evolution,
the total melt mass is much larger than the total mass of heated
solids, the indicated temperature drops in the melt in fig.37b are much
smaller than the corresponding temperature rises in the adjacent solid.

Fig.37c illustrates that small κ_m/κ_s-ratios, corresponding with
small thermal diffusivities $\kappa_m = k_m/\rho_m c_m$ of the melt relative to the
thermal diffusivity κ_s of the solid, result in higher melt temperatures
and higher temperatures in the solid for given values of Nu and $\sqrt{\kappa_s t}/a$.

In fig.37d the evolution of T_m, T_c, $T_{(r-a=0.1)}$, $T_{(r-a=0.2)}$, $T_{(r-a=0.3)}$
is given as a function of the time $t(.\kappa_s/a^2$ sec) as computed with Nu=20
and κ_m/κ_s=0.25. The results confirm that the major changes,
particularly in T_m and T_c, occur in the early stages of the model,
immediately after its initiation. In the advanced stages of the model
the continued heat transfer mainly results in a further widening of the
thermal aureole in the solid.

In the model Nu and κ_m/κ_s determine the temperature distribution
in the melt and in the solid for any given value of $\sqrt{\kappa_s t}/a$. Both
parameters are considered constants. Nu, κ_m and κ_s, however, depend on a
large number of temperature dependent properties such as thermal
conductivity, density, specific heat, and melt viscosity. The results
of fig.37d illustrate that temperature dependent changes in Nu and κ_m/κ_s
mainly affect the temperatures computed for the initial stages of the
model. As time progresses and temperature changes slow down, the model
more and more approaches a constant property system.

application

The model calculations can· be compared with the temperature
reconstuction for the final stages of the magmatic-contact metamorphic
event at Seriphos as deduced from the mineralogical and petrological
evidence (Chapter IV, figs.9 and 12). For any given set of parameters
Nu, κ_m/κ_s, t and a ($\sqrt{\kappa_s t}/a$) the model gives a unique solution for the
temperature drop in the convecting, spherical melt body and the
corresponding temperature distribution in the surrounding solid medium.
For any specific value of the radius a of the melt body there will be

only one set of parameters Nu, κ_m/κ_s and $\sqrt{\kappa_s t}/a$ which produces a model temperature curve comparable with the temperature distribution reconstructed for Seriphos.

At the time of the intrusion the initial temperature in the wall rocks at Seriphos probably was about $100\,^0C$, this being the temperature at an intrusion depth of 3–4 km under a geothermal gradient of 25 – 30 ^0C/km. This temperature can be regarded as the zero level in the model. For an initial temperature of the intruding magma of $T = 900\,^0C$ and an eutectic solidification temperature of $T = 750\,^0C$ for the granodiorite, the following rounded–off parameter combinations give model temperature curves which coincide well with the temperature reconstruction for Seriphos:

$$a = \ \ 2.5 \ km \ : \ \ Nu = 10 \ \ , \ \kappa_m/\kappa_s = 0.08 \ \ , \ \ \sqrt{\kappa_s t}/a = 0.35$$
$$a = \ \ 5.0 \ km \ : \ \ Nu = 15 \ \ , \ \kappa_m/\kappa_s = 0.13 \ \ , \ \ \sqrt{\kappa_s t}/a = 0.25$$
$$a = \ \ 7.5 \ km \ : \ \ Nu = 20 \ \ , \ \kappa_m/\kappa_s = 0.25 \ \ , \ \ \sqrt{\kappa_s t}/a = 0.20$$
$$a = 10.0 \ km \ : \ \ Nu = 30 \ \ , \ \kappa_m/\kappa_s = 0.66 \ \ , \ \ \sqrt{\kappa_s t}/a = 0.10$$

Magmas crystallize over a melting range. In the model gradual crystallization of the melt upon cooling can be accounted for by assuming a linear release of the heat of fusion (L_f) over the melting range $T_1 - T_e$. This results in an increase in the specific heat of the melt according to the expression:

$$c_m = c_o + L_f/(T_1 - T_e) \tag{9-24}$$

where c_m= specific heat of the crystallizing melt; c_o= specific heat of the melt without melting or congealing; L_f= latent heat of fusion; T_1= liquidus temperature, and T_e= eutectic temperature. With eq.(9–24) and the physical and thermal constants given in table X a value κ_m/κ_s= 0.2 is found for a melt in which all fusion heat (L_f) is lineary released over the melting range $T_1 - T_e = T_i - T_e = 900 - 750 = 150\,^0C$. A value κ_m/κ_s= 0.3 is found for a partial melt with 40% solids and a linear release of only 60% of the latent heat of fusion over the melting range $T_i - T_e$. According to the petrological evidence the intruding granodiorite magma at Seriphos initially probably contained some 20 – 40 % crystals. With a value κ_m/κ_s= 0.2 – 0.3 the model gives a temperature distribution comparable with the temperature reconstruction

for Seriphos if the radius of the spherical melt body is between 6 and
9 km. The geological map of Seriphos shows that a melt body with a
radius of about 7.5 km agrees well with the actual dimensions of the
granodiorite pluton at Seriphos (fig.3).

In a melt body with free, natural convection the vigor of the
convection depends upon the buoyant forces created by the temperature
and density differences in the melt due to its cooling along the walls.
Experimental and theoretical studies have established the relation:
$$Nu = y(Gr.Pr)^Z = y(Ra)^Z \qquad (9-25)$$
where the Grashof number Gr represents the ratio of buoyant to viscous
forces in the melt, the Prandtl number $Pr = \mu_m/\rho_m\kappa_m$ is a ratio of melt
properties (μ_m= viscosity), and y and z are constants depending on the
specific geometry, the flow regime, and the boundary conditions of the
considered system. The dimensionless group Gr.Pr is also called the
Rayleigh number Ra= Gr.Pr of the convection system and, as Nu, it is a
measure of the vigor of the convection. For a spherical cavity
containing a high Prandtl number ($\mu_m \gg \rho_m\kappa_m$), Newtonian melt in laminar
convection Nu is given by:
$$Nu = 0.50 \left[\frac{g \cdot \varepsilon \cdot \rho_m (T_m - T_c) \cdot a^3}{\mu_m \kappa_m} \right]^{1/4} \qquad (9-26)$$
where g= gravitational acceleration, ε= isobaric expansivity, μ_m=
viscosity, and $T_m - T_c$= temperature difference within the melt body
(Kreith, 1976; Hardee and Larson, 1977). For a 'Seriphian' value Nu= 20
the corresponding value for the Rayleigh number in eq.(9-26) is 2.6×10^6
For Newtonian melts this value for Ra corresponds to a flow regime in
the melt body dominated by laminar convection (see f.e. Hofmann, 1976).
With the 'Seriphian' values Nu = 20, κ_m/κ_s= 0.25, a = 7.5 km and
$T_m - T_c$= 750 - 600 = 150^0C for the very final stages of the magmatic
model, near the final solidification of the melt body at T_m= 750^0C, and
with the thermal and physical constants listed in table X the
calculated viscosity from eq.(9-26) is μ_m= 1.4×10^{15} poises (gr/cm.sec).
Experimental viscosity measurements by Shaw (1965) and Murase and
McBirney (1973) indicate that (apparent) viscosities in the order of
10^{15} poises may occur in granitic melts during the very final stages of

TABLE X

Physical constants used in the model computations

for the first stage, magmatic model

K_m =	0.021	J/cm.sec.$^{\circ}$C	K_s =	0.025	J/cm.sec.$^{\circ}$C
ρ_m =	2.3	gr/cm^3	ρ_s =	2.6	gr/cm^3
c_m =	4.2	J/gr.$^{\circ}$C	c_s =	0.9	J/gr.$^{\circ}$C
κ_m =	0.002	cm^2/sec	κ_s =	0.011	cm^2/sec
L_f =	500	J/gr	g =	981	cm/sec^2
c_o =	0.84	J/gr.$^{\circ}$C	ε =	5x10$^-$	$^{\circ}$C^{-1}

the crystallization and dehydration of the magmas, when they have become semi-solid or Bingham plastic crystal mushes (see Shaw et al., 1968).

The thickness δ_t of the thermal boundary layer for a laminar convecting, high Prandtl number, Newtonian melt is approximately given by:

$$\frac{\delta_t}{x} \simeq 4(Ra)^{-1/4} \simeq 2(Nu)^{-1} \qquad (9\text{-}27)$$

(Eckert and Drake, 1972; Hardee and Larson, 1977). For the Seriphos model system, with $Nu \simeq 20$ and $x \simeq a = 7.5$ km the calculated thickness of the thermal boundary layer is $\delta_t = 750$ meter. The average temperatures in the thermal transition zone between the permanently solid wall rocks and the main mass of the convecting magma have reached 99% of the uniform magma temperature T_m at a distance of about 750 meters from the intrusive contact. The average temperature distribution in the thermal boundary layer can be approximated by:

$$\frac{T_y - T_c}{T_m - T_c} \simeq \frac{3}{2}\frac{y}{\delta_t} - \frac{1}{2}\left[\frac{y}{\delta_t}\right]^3 \qquad (9\text{-}28)$$

where y= distance from the wall towards the main mass of the melt, and T_y = average temperature in the boundary layer at the distance y from the solid wall (Eckert and Drake, 1972).
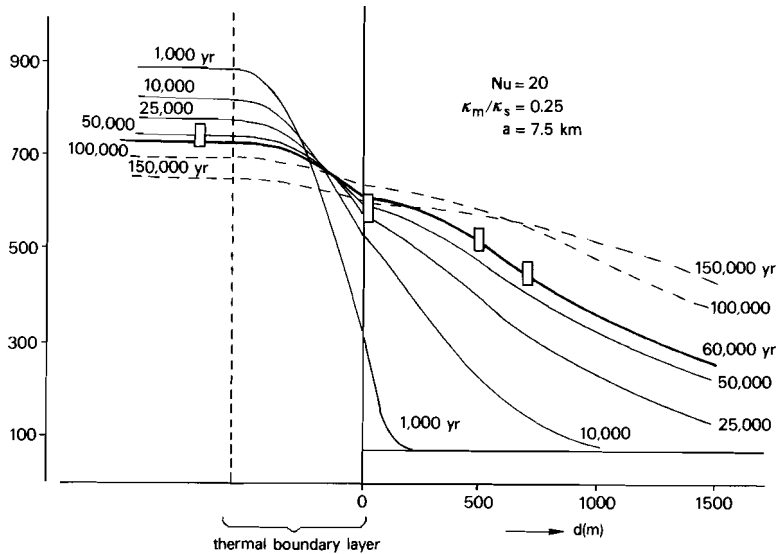
Fig.38: Modelled temperature evolution for the contact metamorphic
aureole at Seriphos (see text).

In fig.38 temperature distributions are given as calculated with
the model parameters Nu = 20, κ_m/κ_s= 0.25, a = 7.5 km, $T_i \simeq T_m$(t=0)= 900^0
and T_s(t=0)= 100^{0}C. The temperatures in the wall rocks and in the main
mass of the magma body were computed with eqs. (9-22) and (9-23), and
the temperature distributions in the thermal boundary layer were
calculated with eqs.(9-27) and (9-28). According to the model
computations the temperature at the intrusive contact increases with
time and the contact metamorphic aureole gradually expands outward; the
contact metamorphic zones and isograds gradually move away from the
intrusive contact. For t = 60,000 yrs the computed temperature
distribution coincides with the temperature distribution indicated by
the positions of the contact metamorphic isograds in the contact
aureole at Seriphos.

discussion
     In the first, magmatic stage of the model for the granodiorite
intrusion at Seriphos it is assumed that a body with a freely

173.

convecting, homogeneous magma melt is instantaneously emplaced in a
uniform, non-permeable solid environment of infinite extension. The
heat effects of chemical reactions and mass diffusions are neglected
relative to the heat exchanges resulting from conduction and (magma)
convection, and the model is considered a constant-property system in
which all heat effects can be described in terms of the (constant)
model parameters κ_m/κ_s and Nu. The vertical geobaric and geothermal
gradients are ignored relative to the P,T-gradients perpendicular to
the intrusive contact.

In the model it is assumed that the temperature of the main mass
of the convecting magma body is uniform and that the temperature
development in the surrounding solid is radial symmetrical. Comparison
of the model calculations with the temperature reconstruction for the
contact aureole at Seriphos, therefore, implies the neglect of vertical
variations in magma density (adiabatic expansion) and initial wall rock
temperature (geothermal gradient). Magma compressibilities are very
small and adiabatic temperature variations within the uniform, main
mass of the convecting magma due to the geobaric gradient can be
neglected (the adiabatic gradient of a magma is $\beta_0 \simeq 0.4^0 C/km$; Murase
and McBirney, 1973). Due to the geothermal gradient the convective heat
loss from the (uniform) melt body decreases with depth as $T_m - T_c$
decreases, and the total heat loss from the melt body will be smaller
than the heat loss evidenced in the apical parts of the system. The
total volume of the magma body probably is smaller than the melt volume
predicted from the model.

The crystallization of natural magmas is a complicated kinetic
process involving a large number of temperature and pressure dependent
actions (nucleation and crystal growth, mass diffusion, phase
transitions ;see f.e. Hargraves, 1980). The model assumption of a
linear release of the latent heat of fusion of the magma, L_f, over the
temperature range $T_{liquidus} - T_{eutectic}$, therefore, seems an inaccurate
conception. Magma crystallization may also involve the release of
volatiles. Their migration into the adjacent country rocks is coupled
with a subtraction of heat from the magma and an addition of heat to
the wall rocks. In the country rocks endothermic contact metamorphic

174.

reactions absorb heat. Adequate data to account for all these effects
are lacking. Non-linear release of the latent heat of fusion, L_f, of
the magma over the temperature range $T_1 - T_e$ affects the specific heat,
c , of the crystallizing magma and changes the value of the thermal
diffusivity $k_m/\rho_m c_m$ in the model. Additional heat transport from the
magma into the surrounding solids by migrating fluids increases the
effective conductivity k_s of the solids and it increases the value of
the thermal diffusivity $\kappa_s = k_s/\rho_s c_s$ in the model. Heat absorption by
endothermic chemical reactions increases the specific heat, c_s, of the
solids and it decreases the value of the thermal diffusivity κ_s in the
model. The results of fig.37c, however, show that the model is not very
sensitive to minor changes in the ratio κ_m/κ_s , and within the scope of
the present study the assumption that κ_m/κ_s is constant seems a fair
assumption.

In the model it is assumed that the Nusselt number Nu is constant
during the convective cooling of the magma body. According to eq.(9-26)
Nu is controlled by a large number of parameters $(g, \varepsilon, \rho_{\bar{m}}, T_m - T_c, a, \mu_m, \kappa_m)$
In magmatic systems the viscosity μ_m is by far the most important of
these parameters, and μ_m exponentially decreases with increasing
temperature. In Newtonian melts the temperature dependence of μ_m is
given by $\mu_m(T) = A.\exp|E(\mu)/RT|$, where $E(\mu) =$ activation energy of
viscous flow, R= gas constant, and A is a constant. As a consequence of
the exponential increase of μ_m with decreasing temperature, Nu will
exponentially decrease with prolonged cooling of the convection system,
and the convective heat transfer will exponentially decrease with time
(see Spera, 1980). In the initial stages of the intrusion melt
temperatures will drop faster and contact temperatures will rise more
rapidly than calculated with the fixed-Nu model. The total cooling time
will be less than predicted from the model.

In the model it is assumed that the granodioritic magma is a
Newtonian melt. In a Newtonian melt the shearing stress (τ) is directly
proportional to the strain rate ($\dot{\varepsilon}$):

$$\tau = \mu_m \cdot \dot{\varepsilon}$$

Experimental studies indicate that above the liquidus natural magmas
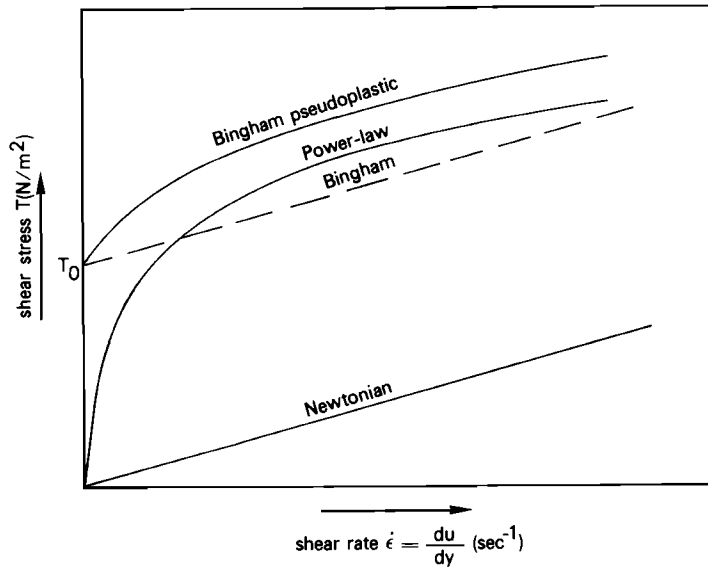behave as Newtonian melts (Shaw et al., 1966). At temperatures below

Fig.39: Examples of various rheology models for magma and lava
        (from Hardee and Dunn, 1981).

the liquidus the magma shear stress is a non-linear function of the
shear rate of the magma, and the partial melt seems to behave as a
power-law fluid, or perhaps as a Bingham plastic or Bingham pseudo-
plastic material (Bird et al., 1966; Shaw et al., 1968; Pinkerton and
Sparks, 1978; Hardee and Dunn, 1981)(see fig.39). In a power-law fluid
the shear stress (τ) is related to the strain rate ($\dot{\epsilon}$) as $\tau = m\dot{\epsilon}^n$, where
m and n are constants, and $m\dot{\epsilon}^{n-1}$ is an effective viscosity. In a
Bingham plastic a yield stress τ_o must be exceeded before the fluid
behaves as a Newtonian fluid, and $\tau = \tau_o + \mu_m\dot{\epsilon}$ or $\mu_m^* = \mu_m + \tau_o/\dot{\epsilon}$, where $\mu_m^* =$
apparent (Newtonian) viscosity, and $\mu_m =$ effective viscosity. In a
Bingham pseudoplastic material, once the yield stress τ_o is exceeded,
the fluid behaves as a power-law fluid. In non-Newtonian fluids the
effective viscosity, in general, is significantly less than the
apparent (Newtonian) viscosity. In combination with the exponential
increase in viscosity at decreasing temperature non-Newtonian behavior
of the magma enhances the tendency to slow down convection as

176.

temperatures drop and the magma crystallizes. Convection may cease
before the magma is entirely solidified.

In the model it is implicitly assumed that the granodiorite magma
is a Newtonian melt in free convection. For a constant-property,
Newtonian melt in a spherical cavity the criteria for free convection
are:

$$Ra \simeq 10^4 - 10^9 \text{ for laminar convection}$$

$$(9-29)$$

$$Ra > 10^9 \text{ for turbulent convection}$$

and

$$\delta_v = \delta_t (Pr)^{1/3} \leq a \qquad (9-30)$$

where $Pr = \mu_m / \rho_m \kappa_m$ = Prandtl number of the melt, $\delta_t (= 2.Nu^{-1})$ = thickness
of the thermal boundary layer; δ_v = thickness of the hydrodynamical
boundary layer (defined as the layer in which 99% of the velocity
change between the freely convecting, main mass of the liquid and the
(stationary) wall is localized), and a= radius of the spherical melt
body (Batchelor, 1954; Hardee and Larson, 1977). With the thermal
parameters given in table X, and with $T_m - T_c$= 750 - 600 = 150 °C,
a= 7.5 km the critical viscosity for the onset of laminar convection is
$\mu_m \approx 4.10^{17}$ poises (Ra= 10^4), and for the onset of turbulent convection
the magma viscosity must be less than 4.10^{12}p. (Ra= 10^9). (Apparent)
viscosities in the order of $\mu^* = 10^{15}$p. may occur in granitic melts
during the very final stages of the magma solidification and
convection, therefore, should be possible throughout the entire cooling
history of the partial magma melt. In silicate melts, however, the
(apparent) Prandtl number $Pr^* = \mu_m^* / \rho_m \kappa_m$ is extremely large and the
(apparent) thickness of the hydrodynamic boundary layer, $\delta_v^* \approx \delta_t (Pr^*)^{1/3}$,
approaches infinity. According to the second critical condition for
free convection, $\delta_v \ll a$, magma convection should be impossible. Magmas,
however, are not constant-property, Newtonian melts, and in
non-Newtonian melts the effective viscosity, generally, is
significantly less than the apparent (Newtonian) viscosity. The
effective thickness of the hydrodynamical boundary layer could be
significantly less than the thickness of the apparent velocity field
(see Marsh, 1982). Magmas do intrude, after all.

The assumption of instantaneous emplacement in the model for the granodiorite intrusion at Seriphos presupposes that the magma emplacement is rapid relative to the rate of the heat loss from the body. Marsh (1977) and Marsh and Kantha (1978) worked out a Stokesian model for the viscous ascent of convecting, spherical magma blobs melting their way up through a solid lithosphere ($\mu_{wall} \gg \mu_{magma}$). According to their model the ascent velocity U of the magma sphere is given by:

$$U = \frac{1}{(0.46)^2} \cdot \frac{\kappa_m}{a} \cdot (Nu)^2 \qquad (9-31)$$

Substitution of the 'Seriphian' values Nu= 20, a= 7.5km and κ_m= 2.10 cm/s gives a velocity U= 5.10^{-6} cm/s or 160 cm/yr. The time required for the granodiorite sphere to ascent with this speed from an assumed depth of origin of 15 - 20 km to an intrusion depth of 2 - 3 km is 10,000 - 15,000 years. This ascent time is small relative to the life time of about 60,000 years found for the magmatic stage of the intrusion model (see fig.38).

In Marsh' model, as in the present model for the granodiorite intrusion at Seriphos, all thermal and physical properties are considered constant. Non-Newtonian magma behavior and temperature dependent viscosity changes, however, not only affect the cooling history of the magma, they also affect the ascent of the magma: upon cooling the ascent velocities will decrease exponentially. The presence of a geothermal gradient still enhances the exponential tendency of the velocity decrease. At depth the initial temperature of the surrounding wall rocks is higher, the magma is hotter, the magma viscosity is smaller, and Nu is larger than near the earth's surface. The convecting magma blob will be able to melt its way up through the lithosphere by (partial) melting the adjacent wall rocks. As the magma body approaches the earth's surface convection will slow down exponentially, and Nu rapidly decreases. The country rocks are not heated up to their melting point and magma ascent can only continue by stoping, or by marginal shattering (as assumed in the model). Magma ascent comes to a halt.

An accurate model for the intrusion and convective-conductive cooling of a magma diapir in the upper levels of the earth's crust

should comprise the combined actions of non-Newtonian magma behavior,
increasing magma viscosity and decreasing ascent velocity. At present
such a model is not available. The presented evidence, however,
suggests that these non-linear effects mainly affect the temperature
distributions during the initial stages of the intrusion. The shape and
magnitude of the temperature distributions modelled for the final
stages of the intrusion probably are not essentially altered by the
non-linear magma behavior.

THE SECOND, HYDROTHERMAL STAGE OF THE MODEL

introduction

In the final stages of a magmatic intrusion the convective forces
in the magma melt will drop below the yield stress of the (pseudo-)
plastic, nearly eutectic crystal mush. Magma convection may halt almost
instantaneously, probably before the magma has solidified completely.
A sudden change in the behavior of the magmatics not only affects
their thermal bearing (convection → conduction), it may also cause
a sudden and intense fracturing of the intrusive rocks and of the
surrounding contact metamorphic rocks. Due to the fracturing bulk rock
permeabilities may increase sufficiently to allow hydrothermal fluid
migrations and the convective transfer of heat and dissolved chemicals
along the newly formed transport channels.

formulation

In the second stage of the model for the granodiorite intrusion at
Seriphos it is assumed that the magma has solidified instantaneously,
that is sudden relative to the rate of the heat and mass transfer. Due
to magma degassing and the volumetric changes associated with the
solidification of the magma, the magmatic rocks and the surrounding
wall rocks have become fractured and bulk rock permeabilities have
become sufficiently large to allow the convective transfer of heat and
mass by metasomatic solutions. As in the first, magmatic stage of the
model, the intrusive system is considered a radial symmetrical sphere.

179.

The lithostatic pressure is considered uniform and constant. The
vertical geothermal and (fluid) pressure gradients are neglected
relative to the variations in temperature and (fluid) pressure created
by the intrusion perpendicular to the intrusive contact. In the model T
and P_f are referred to a state of equilibrium in which the reference
temperature T_o is given by the regional geothermal gradient and the
depth of the intrusion, and the reference fluid pressure P_o is assumed
to be equal to the hydrostatic pressure at the given intrusion depth.

In the largely closed fluid flow system the fluid flow will be
largely controlled by the lateral fluid pressure differences within the
radial symmetrical intrusion system, and the fluid pressures P_f will
change with T. Let, at any time and place within the fluid flow system,
there be a singular, continuous $P_f-(V_f)-T$ relationship between the
(local) value of the fluid pressure $P_f^* = P_f - P_o$ and the (local)
temperature $T^* = T - T_o$ that can be described by the expression:

$$P_f - P_o = \beta . P_o (T - T_o)^\gamma$$

(9-32)

or
$$P_f^* = \beta . P_o (T^*)^\gamma$$

where T_o and P_o respectively are the reference temperature and fluid
pressure, $\beta(^oC^{-\gamma})$ is a (temperature dependent) coefficient of
volumetric expansion, and γ is a dimensionless parameter describing the
temperature dependency of β ; γ is assumed to be independent of T, and
β and γ are considered constants.

The fluid pressure gradient, ∇P, at any time and place, similarly
is expressed by:

$$\nabla P = \beta . P_o . \nabla T^\gamma$$

(9-33)

where ∇T^γ is the gradient of $(T - T_o)^\gamma$ $(= \partial T^\gamma / \partial r$ in the radial
direction of the spherical symmetrical model system).

In a permeable solid medium fluid pressure variations will lead to
fluid flow. The magnitude of the fluid flow is given by Darcy's law:

$$\bar{u} = -\frac{k}{\nu} . \nabla P$$

(9-34)

where $\bar{u}(= dm_f/dAdt)=$ average mass flux of the fluid, defined as the average or net mass of fluid dm_f passing a representative area dA of the porous medium per unit time dt; $k=$ (average) permeability of the rock; $\nu =$ kinematic viscosity of the fluid ($\nu = \mu/\rho$), and $\nabla P=$ fluid pressure gradient.

Combination of the equations (9–33) and (9–34) leads to the momentum equation:

$$\bar{u} = - \frac{k}{\nu} \beta\, P_o . \nabla T^\gamma \qquad\qquad (9\text{–}35)$$

In the equations (9–34) and (9–35) the fluid flux $\bar{u}$ represents the average or net mass of fluid passing a representative area of the porous solid in a unit time. The permeability k is the overall permeability of that area. The equations (9–34) and (9–35) do not describe the flow of individual fluid particles along specific transport channels. Small scale variations in fluid flow and local-scale fluid circulations are not defined. The fluid percolations along the cracks and fractures in the rock are only measured according to their net contribution to the overall fluid flux $\bar{u}$ across the representative area of the fractured solid.

The mass of fluid going into a representative volume element of the porous solid medium per unit time must be equal to the mass flow going out of the elementary volume minus the gain in fluid mass during the unit time. The change in mass flux per volume segment and unit time is given by the divergence $\nabla\cdot\bar{u}$ of the mass flux $\bar{u}$:

$$\nabla\cdot\bar{u} = \nabla\cdot(- \frac{k}{\nu} \beta\, P_o\ \nabla T^\gamma)$$

where $\nabla\cdot\bar{u}$ ($= -dm_f/dVdt)=$ change dm_f in the fluid mass m_f in the elementary volume dV over the time dt. A decrease in the mass flux $\bar{u}$ of the fluids during the passage of the migrating solutions through a representative volume of the porous solid, a negative divergence $\nabla\cdot\bar{u}$, corresponds to a net addition of fluid to the elementary segment, and an increase in $\bar{u}$, or a positive divergence $\nabla\cdot\bar{u}$, depicts a net removal of fluid from the volume dV.

In the model system it is assumed that, at any time and place, the

fluid pressure P_f and the (fluid) temperature T are completely defined
by the singular, continuous relationship (9-22):

$$P_f - P_o = \beta \, P_o (T - T_o)^{\gamma}$$

All changes in fluid mass due to density changes, porosity changes,
variations in the compressibility of the fluid, and also sources or
sinks of fluid by (magma) degassing and/or chemical reactions involving
volatiles, therefore, are implicitly included in the expression:

$$\nabla \cdot \bar{u} = -\beta \, P_o \nabla \cdot (\frac{k}{\nu} \, \nabla T^{\gamma})$$

If, in addition, it is assumed that, at the initiation of the
model, the permeability increase accompanying the solidification and
degassing of the magma is instantaneous and complete, and that k does
not change with time:

$$\nabla \cdot k = 0$$

and that ν_{H_2O} = constant, the conservation of mass condition simplifies
to:

$$\nabla \cdot u = - \frac{k}{\nu} \beta \, P_o (\nabla \cdot \nabla T^{\gamma}) \qquad (9-36)$$

The migrating fluids transport heat proportional to their mass
flux and heat content. This convective heat flux adds up to the
conductive heat transfer, and per unit time the total heat flux q_{tot}
across a representative surface of the porous solid is:

$$q_{tot} = q_{conv} + q_{cond} = \bar{u} c_f T^* - K_s \, \nabla T^*$$

where c_f = specific heat of the fluid; K_s = thermal conductivity of the
fluid saturated, porous solid without fluid flow, and T^* = temperature
$T - T_o$.

An addition of heat to an elementary volume of the porous solid
changes its internal energy. The rate of the energy change is given by
the divergence of the heat flux q_{tot} :

$$\frac{\partial E}{\partial t} = - \nabla \cdot q_{tot} = - \nabla \cdot (\bar{u} c_f T^*) + \nabla \cdot (K_s \, \nabla T^*) \qquad (9-37)$$

If the heat effects of chemical reactions, phase transitions and thermal strains are neglected, the only changes in internal energy are temperature changes in the solids, and temperature and pressure changes in the fluids. If the heat capacity of the fluids in a given rock volume is neglected relative to the heat capacity of the solids (porosity Π <<1), the change in internal energy corresponds to:

$$\frac{\partial E}{\partial t} = c_s \rho_s \frac{\partial T}{\partial t} \tag{9-38}$$

where c_s= specific heat of the solids, and ρ_s= solid density.

A fluid packet, migrating through a given elementary volume of the porous solids, exchanges heat with the surrounding solids. If the heat exchange is rapid relative to the velocity of the fluid flow, both the fluid temperature and the temperature in the coexisting solids will be equal at any time and place. As this (local) equilibrium temperature T^* of both the fluids and the solids changes with time due to the heat transfer, the fluid pressure P_f^* will change accordingly, and a change in fluid flux will occur across the volume element. Thus, for $c_f \simeq$ constant, the change in the convective heat flux is given by:

$$\nabla \cdot q_{conv} = \nabla \cdot (c_f \bar{u} T^*) = c_f (T^* \nabla \cdot \bar{u}) + c_f (\bar{u}, \nabla T^*) \tag{9-39}$$

where $(\bar{u}, \nabla T^*)$= scalar product of the vectors $\bar{u}$ and ∇T^*.

Substitution of the equations (9-35),(9-36),(9-38), and (9-39) into (9-37) leads to the energy equation:

$$c_s \rho_s \frac{\partial T}{\partial t} = + c_f \frac{k}{v} \beta P_o T^* \nabla \cdot \nabla T^\gamma + c_f \frac{k}{v} \beta P_o (\nabla T^\gamma, \nabla T) + K_s \nabla \cdot \nabla T \tag{9-40}$$

Expansion of (9-40) with respect to the radius r of the spherical model system results in: (9-41)

$$c_s \rho_s \frac{\partial T}{\partial t} = c_f \frac{k}{v} \beta P_o T^* \left[\frac{\partial^2 T^\gamma}{\partial r^2} + \frac{2}{r} \frac{\partial T^\gamma}{\partial r} \right] + c_f \frac{k}{v} \beta P_o \left\{ \frac{\partial T^\gamma}{\partial r} \cdot \frac{\partial T}{\partial r} \right\} + K_s \left[\frac{\partial^2 T}{\partial r^2} + \frac{2}{r} \frac{\partial T}{\partial r} \right]$$

The differential equation (9-41) describes the transient temperature developments in the radial symmetrical intrusion model as a result of the combined actions of heat conduction and the convective transfer of heat by migrating fluids. Obviously fluid convection increases the heat exchanges. The increase is proportional to the permeability k of the

porous solid medium. The intensity of the heat exchanges also depends on the local equilibrium temperature $T^* = T - T_0$, and on the local value of the fluid pressure gradient $\partial P^*/\partial r = \beta \, P_0 \partial T^\gamma/\partial r$.

For a given set of model parameters and given boundary conditions the equation (9-41) can be solved numerically for any given initial distribution of T^*. The temperature distribution T_n^m ($= T - T_0$) at any time $t = m.\Delta t$ can be computed from the initial temperature distribution T_n^0 by step-wise calculation of the temperatures T_n^1 in the n node points $r = n.\Delta r$ in which the space coordinate r is subdivided, and repeating this procedure for m subsequent time increments Δt (see f.e. Kreith, 1973; Schuh, 1965). From a given temperature distribution $T_{n-1}^m, T_n^m, T_{n+1}^m$ in the node points n-1,n,n+1 at the time $t = m.\Delta t$, the temperature $T_n^{m=1}$ in the node n at the time $t = (m+1)\, \Delta t$ is given by the finite difference expression of eq.(9-41):

$$T_n^{m+1} = p_{r,n+1}^m (T_{n+1}^{\gamma m} - T_n^{\gamma m}) + p_{r,n-1}^m (T_{n-1}^{\gamma m} - T_n^{\gamma m}) + q(T_{n+1}^{\gamma m} - T_{n-1}^{\gamma m})(T_{n+1}^m - T_{n-1}^m) +$$

$$+ \, s_{r,n+1}(T_{n+1}^m - T_n^m) + s_{r,n-1}(T_{n-1}^m + T_n^m) + T_n^m$$

where

$$p_{r,n+1}^m = \left(\frac{n}{n-\frac{1}{2}}\right)^2 \cdot \frac{c_f}{c_s \rho_s} \, \frac{k}{\nu} \, \beta P_0 \cdot \frac{1}{2}(T_{n+1}^m + T^m) \cdot \frac{\Delta t}{(\Delta r)^2}$$

$$p_{r,n-1} = \left(\frac{n-1}{n-\frac{1}{2}}\right)^2 \cdot \frac{c_f}{c_s \rho_s} \, \frac{k}{\nu} \, \beta P_0 \cdot \frac{1}{2}(T_{n-1}^m + T_n^m) \, \frac{\Delta t}{(\Delta r)^2}$$

$$q = \frac{c_f}{c_s \rho_s} \, \frac{k}{\nu} \, \beta P_0 \frac{\Delta t}{4(\Delta r)^2}$$

$$s_{r,n+1} = \left(\frac{n}{n-\frac{1}{2}}\right)^2 \frac{K_s}{c_s \rho_s} \, \frac{\Delta t}{(\Delta r)^2}$$

$$s_{r,n-1} = \left(\frac{n-1}{n-\frac{1}{2}}\right)^2 \frac{K_s}{c_s \rho_s} \, \frac{\Delta t}{(\Delta r)^2} \tag{9-42}$$

The stability condition is:

$$\left[\frac{c_f}{c_s \rho_s} \, \frac{k}{\nu} \, \beta P_0 \cdot \frac{1}{2}(T_{n+1}^{\gamma m} - T_n^{\gamma m})_{max} + \frac{K_s}{c_s \rho_s}\right] \frac{\Delta t}{(\Delta r)^2} \leq \frac{1}{4}$$

The finite difference expression for the corresponding fluid flux u_n^m at the time $t = m.\Delta t$ in the node $r = n.\Delta r$ is given by the numerical expansion of the momentum equation (9-35) with respect to the radius r:

$$\bar{u} = -\frac{k}{\nu}\,\beta P_o\,\partial T^\gamma/\partial r$$

$$\bar{u}_n^m = +\frac{k}{\nu}\,\beta P_o\,\frac{1}{2}\left[\frac{T_{n-1}^{\gamma m} - T_{n+1}^{\gamma m}}{\Delta r}\right] \tag{9-43}$$

The rate of addition or removal of fluid at the node r= n. r at the time t= m.Δt is given by the numerical expansion of the mass balance (9-36) with respect to the radius r of the spherical model system:

$$\nabla\cdot\bar{u} = -\frac{dm_f}{dt} = -\frac{k}{\nu}\,\beta P_o\left[\frac{\partial^2 T^\gamma}{\partial r^2} + \frac{2}{r}\frac{\partial T^\gamma}{\partial r}\right] \tag{9-44}$$

$$\left[\frac{dm_f}{dt}\right]_n^m = \frac{(m_f)_n^{m+1} - (m_f)_n^m}{\Delta t} = +\frac{k}{\nu}\beta P_o\left[\left(\frac{n}{n-\frac{1}{2}}\right)^2(T_{n+1}^{\gamma m} - T_n^{\gamma m}) + \left(\frac{n-1}{n-\frac{1}{2}}\right)^2(T_{n-1}^{\gamma m} - T_n^{\gamma m})\right]\frac{1}{(\Delta r)^2}$$

The total amount (ΔM_f) of fluid, added or subtracted at the location r= n.Δr over the time t= m.Δt elapsed since the initiation of the model at t=0, is given by the time integral of eq.(9-4) over the time t= m.Δt:

$$(\Delta M_f)_n^m = \sum_{i=o}^m \left(\frac{dm_f}{dt}\right)_n^m \cdot\Delta t = \Delta t\left[\left(\frac{dm_f}{dt}\right)_n^{m=1} + \left(\frac{dm_f}{dt}\right)_n^{m=2} + \cdots + \left(\frac{dm_f}{dt}\right)_n^m\right] \tag{9-45}$$

The migrating fluids may also carry dissolved chemicals. Diffusion of the chemicals through (stationary considered) solutions leads to diffusion metasomatism. Transport of the dissolved components along with the migrating solutions results in infiltration metasomatism, that is in percolation or pervasion metasomatism.

The diffusive transport of a component i through a representative area of a fluid saturated, porous solid is given by Fick's first law:

$$\bar{J}_{D,i} = -D_i\,\nabla m_i \tag{9-46}$$

where $\bar{J}_{D,i}$= mass flux of i, defined as the average, net molar amount of i passing the elementary area per unit time; ∇m_i= molality gradient of i across the area element, and D_i= diffusivity of i in the porous solid saturated with a static fluid.

The mass flux $\bar{J}_{I,i}$ of a component i along with the migrating solution is given by:

$$\bar{J}_{I,i} = \bar{u}\cdot m_i \tag{9-47}$$

where $\bar{u}$= average mass flux of the fluid, or the average, net fluid mass

185.

dm_f passing a representative area of the porous solid in a unit time, and m_i= molality of i in the fluid, defined as the molar amount n_i of i per fluid mass m_f.

The total mass flux $\bar{J}_i$ due to the combined actions of fluid flow and diffusion is:

$$\bar{J}_i = \bar{J}_{I,i} + \bar{J}_{D,i} = \bar{u}m_i - D_i\nabla m_i \qquad (9-48)$$

A decrease in the mass flux of i during the passage of the migrating solutions through an elementary volume segment of the porous solid corresponds to a net addition of i to the volume element, and vice versa. The rate of addition or removal of i in the elementary volume is given by the divergence of the mass flux of i:

$$\frac{\partial n_i}{\partial t} = -\bar{\nabla}\cdot\bar{J}_i = -\nabla\cdot(\bar{u}m_i) + \nabla\cdot(D_i\nabla m_i) \qquad (9-49)$$

where $n_i (= m_i \cdot m_f)$ denotes the total molar amount of i dissolved in the total fluid mass m_f in the volume element.

If local chemical equilibrium is maintained between a solid phase I_S and the percolating metasomatic solution, a fluid packet migrating through the porous solid at any location x_i and time t will adapt the local equilibrium molality $m_i^*(T^*,x_i,t)$ determined by the equilibrium constant $K_i^*(T)$ of the local dissolution equilibrium of I_S at $T^*(x_i,t)$. I_S will dissolve or precipitate in order to maintain m_i^*, and the change in the mass flux of i during the passage of the migrating solutions through a representative volume element of the porous solid becomes:

$$\frac{\partial n_i^*}{\partial t} = -\nabla\cdot\bar{J}_i = -\nabla\cdot(\bar{u}m_i^*) + \nabla\cdot(D_i\nabla m_i^*) =$$
$$= -(m_i^*\nabla\cdot\bar{u}) - (\bar{u}, \nabla m_i^*) + \nabla\cdot(D_i\nabla m_i^*) \qquad (9-50)$$

where m_i^*= equilibrium molality of the locally buffered component i at the (local) temperature T^* of the infinitesimal volume element, and $\partial n_i^*/\partial t$= rate of addition or removal of i to or from the i-saturated solution in the elementary volume because of the combined actions of infiltration and diffusion metasomatism. $(m_i^* \nabla\cdot\bar{u})$ denotes the amount dn_i of i added to the volume element due to a net addition of a solution mass dm_f (containing m_i^*), the scalar vector product $(u, \nabla m_i^*)$ represents the amount dn_i' added to the solution in the volume element because of a

186.

change in m_i^* (at constant u), and $\nabla\cdot(D_i\nabla m_i^*)=$ diffusive contribution.

Substitution of the eqs.(9-35),(9-36) into (9-50) results in:

$$\frac{\partial n_i^*}{\partial t} = + \frac{k}{\nu}\beta P_o(m_i^*\nabla\cdot\nabla T) + \frac{k}{\nu}\beta P_o(\nabla T^\gamma,\nabla m_i^*) + \nabla\cdot(D_i\nabla m_i^*) \qquad (9-51)$$

The differential equation (9-51) describes the rate of addition or removal of a locally buffered component i to or from a metasomatic solution due to combined infiltration-diffusion metasomatism in a fluid saturated, porous solid medium subjected to transient temperature changes. In a given system with constant physical properties and a uniform composition, the direction of the mass exchanges (addition or removal) is determined by the direction of the temperature changes (the direction of the fluid flow), and by the gradient of the (local) equilibrium molality m_i^* as determined by the (temperature dependent) equilibrium constant K_i^* of the (local) dissolution equilibrium of the solid phase I_s. The intensity of the metasomatic mass exchanges is mainly determined by the permeability k of the porous solid and the fluid pressure gradient $\nabla P = \beta\, P_o.\nabla T^\gamma$.

In low-permeability, nearly closed rock systems diffusion may be a significant mechanism of mass transport. In systems with sufficient transport channels infiltration metasomatism will be the dominant mechanism of mass transport. Near the contacts of cooling intrusives temperature gradients are high and temperature changes are fast. Infiltration metasomatism will be by far the dominant process in the formation of contact metasomatic skarn and ore deposits. In the model for the post-magmatic heat and mass exchanges in and around the radial symmetrical intrusion, therefore, diffusion can be neglected and the metasomatic mass exchanges are accurately described by the expansion of the infiltration terms in eq.(9-51) with respect to the radius r of the sphere:

$$\frac{\partial n_i^*}{\partial t} = + \frac{k}{\nu}\beta P_o m_i^* \left|\frac{\partial^2 T^\gamma}{\partial r^2} + \frac{2}{r}\frac{\partial T^\gamma}{\partial r}\right| + \frac{k}{\nu}\beta P_o\left|\frac{\partial m_i^*}{\partial r}\frac{\partial T^\gamma}{\partial r}\right| \qquad (9-52)$$

The first term in eq.(9-52) ($= m_i^*.dm_f/dVdt$) denotes the addition of i as a result of the addition of a m_i^*-containing fluid mass dm_f to an elementary volume dV of the porous solid in the time dt, and the second term ($= m_f.dm_i^*/dVdt$) represents the addition of i to the fluid

mass m_f in the representative volume element dV over the time dt due to a change in the local equilibrium molality m_i^*. If local equilibrium is instantaneously maintained everywhere along the fluid flow path, every change in $m_i^*(= n_i^*/m_f^*)$ will immediately be reflected in a corresponding change in the amount of coexisting I_s, that is in a corresponding amount of dissolution or precipitation of I_s. At every instance, therefore, the (local) rate of dissolution or precipitation of solid I_s is given by:

$$\frac{\partial I_s^*}{\partial t} = + \frac{k}{\nu} \beta P_0 \left| \frac{\partial m_i^*}{\partial r} \frac{\partial T^\gamma}{\partial r} \right| \tag{9-53}$$

The finite difference expression of eq.(9-53) is: $\qquad$ (9-54)

$$\left(\frac{\partial I_s^*}{\partial t}\right)_n^m = \frac{(I_s^*)_n^{m+1} - (I_s^*)_n^m}{\Delta t} = + \frac{k}{\nu} \beta P_0 (m_{i_{n+1}}^{*m} - m_{i_{n-1}}^{*m})(T^{\gamma m}_{n+1} - T^{\gamma m}_{n-1})\frac{1}{4(\Delta r)^2}$$

For any given set of model parameters, and a given temperature dependence of m_i^*, that is for given values of $(m_i^*)_{n+1}^m$ at T^{*m}_{n+1} and $(m_i^*)_{n-1}^m$ at T^{*m}_{n-1}, the equation (9-54) can be solved at any location $r= n.\Delta r$ at any time $t= m.\Delta t$ using the temperature distribution T^{*m}_{n+1}, T^{*m}_{n-1}, calculated with eq.(9-42).

The total amount $(\Delta I_s)_n^m$ of the solid phase I_s that is precipitated or dissolved at a given location $r= n.\Delta r$ over the time $t= m.\Delta t$ elapsed since the initiation of the fluid flow model at $t=0$, is given by the time integral of eq.(9-54) over the time $t= m.\Delta t$:

$$(\Delta I_s)_n^m = \sum_{i=0}^{m} \left|\frac{\partial I_s}{\partial t}\right| . \Delta t = \Delta t \left[\left|\frac{\partial I_s^*}{\partial t}\right|_n^{m=1} + \left|\frac{\partial I_s^*}{\partial t}\right|_n^{m=2} + \dots + \left|\frac{\partial I_s^*}{\partial t}\right|_n^{m} \right] \tag{9-55}$$

application

Thermodynamic analysis of the metasomatic phase assemblages at Seriphos, and $^{18}O/^{16}O$-determinations on coexisting mineral pairs, show that metasomatism proceeded at steadily diminishing temperatures (Chapter V). Fluid inclusion studies point to gradually decreasing fluid pressures during the post-magmatic, hydrothermal cooling stages of the intrusive system (Chapter VI). According to these investigations fluid pressures dropped from some 4-3 kb at $T= 750\,^0C$ in the unaltered granodiorite, through 3-2 kb at 700-500 ^0C in the bleached intrusive rock, and 2-1 kb at 550-450 ^0C in the HT garnet-quartz skarns, to $1\frac{1}{2}-\frac{1}{2}$

TABLE XI
Physical constants used in the model computations

for the second stage, hydrothermal model

ν_f =	2×10^{-3}	cm^2/sec	($= \nu_{H_2O}(20^oC)$
c_f =	4.2	$J/gr.^oC$	
c_s =	0.9	$J/gr.^oC$	
ρ_s =	2.6	gr/cm^3	
K_s =	0.025	$J/cm.sec.^oC$	

kb in the epidote/ilvaite deposits at 450–350 ^oC, while during the late, LT-stages of the hydrothermal evolution fluid pressures dropped to the hydrostatic equilibrium pressure P_f= 400–300 bar at T= 200–100 ^oC (see fig.29).

In the simplified, radial symmetrical model for the post–magmatic hydrothermal heat and mass exchanges in and around the granodiorite intrusion at Seriphos a satisfactory approximation for the modelled, singular relationship (9–32):

$$P_f^* = P_f - P_o = \beta\,P_o(T - T_o)^\gamma = \beta P_o(T^*)^\gamma$$

is given by the expression:

$$\boxed{P_f^* = 3.10^{-4}.(T^*)^{3.5}} \qquad\qquad (9-56)$$

where $\qquad P_f^* = P_f - 300$ bars $\quad ; \quad T^* = T - 100$ ^oC

The relationship (9–56) is a best–fit approximation of the actually observed P_f–T changes in the metasomatic system near the apical parts of the Seriphian intrusion as deduced from the thermodynamic, isotopic and fluid inclusions evidence.

Figures 40 – 41 illustrate the major characteristics of the behavior of the hydrothermal fluid in the second stage of the model for the granodiorite intrusion at Seriphos, as calculated with the P_f–T relationship (9–56), and all other physical properties considered constants (their values are listed in table XI). The initial temperature distribution at the time $\tau = t_e$ of the 'sudden' solidification of the magma and the 'instantaneous' fracturing of the
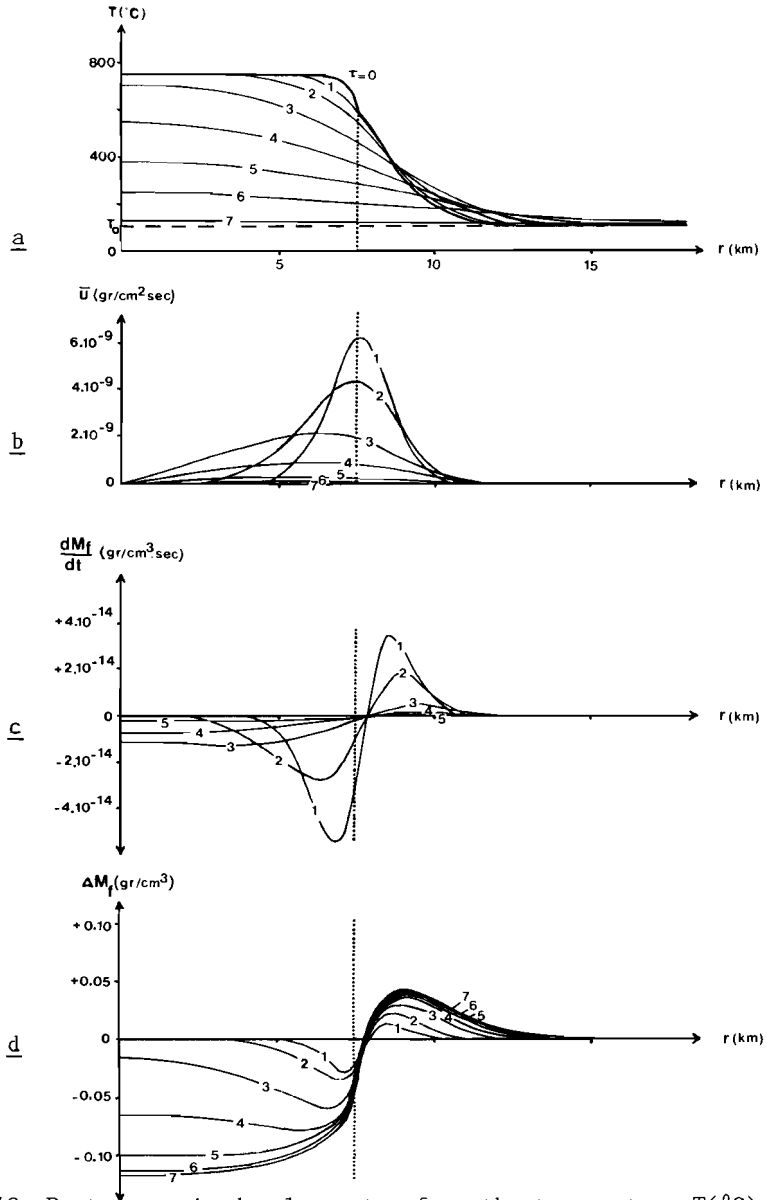
Fig.40: Post-magmatic developments of a: the temperature T(^{0}C);
b: the fluid flux $\bar{u}$ (gr/cm^{2}.sec); c: the rate of addition
or removal of fluid dM_f/dt (gr/cm^{3}.sec), and d: the total
amount of fluid added or subtracted ΔM_f(gr/cm^{3}) in and around
the spherical intrusion model for a constant permeability
k= 10^{-15}cm^{2}. 1: 10,000 yr; 2: 25,000 yr; 3: 100,000 yr;
4: 250,000 yr; 5: 500,000 yr; 6: 1,000,000 yr; 7: 3,000,000 yr

190.

uniform solid medium, was taken from the first stage magmatic model for the parameter values Nu= 20, κ_m/κ_s= 0.25, and a= 7.5 km, and $\sqrt{\kappa_s t}/a$= 0.20 or t_e = 60,000 years (eqs.(9-22),(9-23)).

In fig.40a post-magmatic temperature developments are shown for the (uniform) bulk rock permeability k= 10^{-15} cm^2 as calculated with eq.(9-42)(for n= 40; Δr= 750 m). In fig.41a temperature distributions are given for different values of the (uniform) permeability k and the time τ = 25,000 yrs after the initiation of the second stage model. Obviously an increase in permeability increases the rate of the heat exchanges.

Figs.40b and 41b give the net or average mass flux $\bar{u}$ (gr/cm^2.sec) as calculated with eq.(9-43) for, repectively, various values of the time τ at k= 10^{-15}cm^2, and various values of the bulk rock permeability k at τ= 25,000 yrs. With increasing permeability the magnitude of the mass flux increases, and with time the intensity of the fluid flow decreases.

The figures 40c and 41c give the addition and subtraction rates $\partial m_f/\partial t$ (gr/cm^3.sec) of the metasomatic solution as calculated with eq.(9-44) for various values of τ at k= 10^{-15}cm^2(fig.40c), and for different values of k at τ= 25,000 yrs. With increasing time and decreasing permeability the intensity of the fluid exchanges decreases, while the metasomatic aureole gradually expands. Since k is taken constant in the uniform solid medium, the sphere of influence of the hydrothermal activities may expand up to considerable distances from the intrusive contact.

In figs.40d and 41d the integrated, total fluid amounts ΔM_f (gr/cm (eq.9-45) are presented that have been added or have been removed in the spherical symmetrical model system since its initiation at τ= 0. For k $\geq$ 10^{-14}cm^{2}the total fluid amounts, computed to have been removed from the intrusive, become very high, much higher than the 0.05 - 0.10 gr/cm^3 (3-5 wt% H$_2$O) that could have been released as 'primary magmatic fluid' from a solidifying granodiorite magma.

In fig.42 the total, integrated fluid amounts ΔM_f are shown, calculated to have been added or subtracted in the model system for
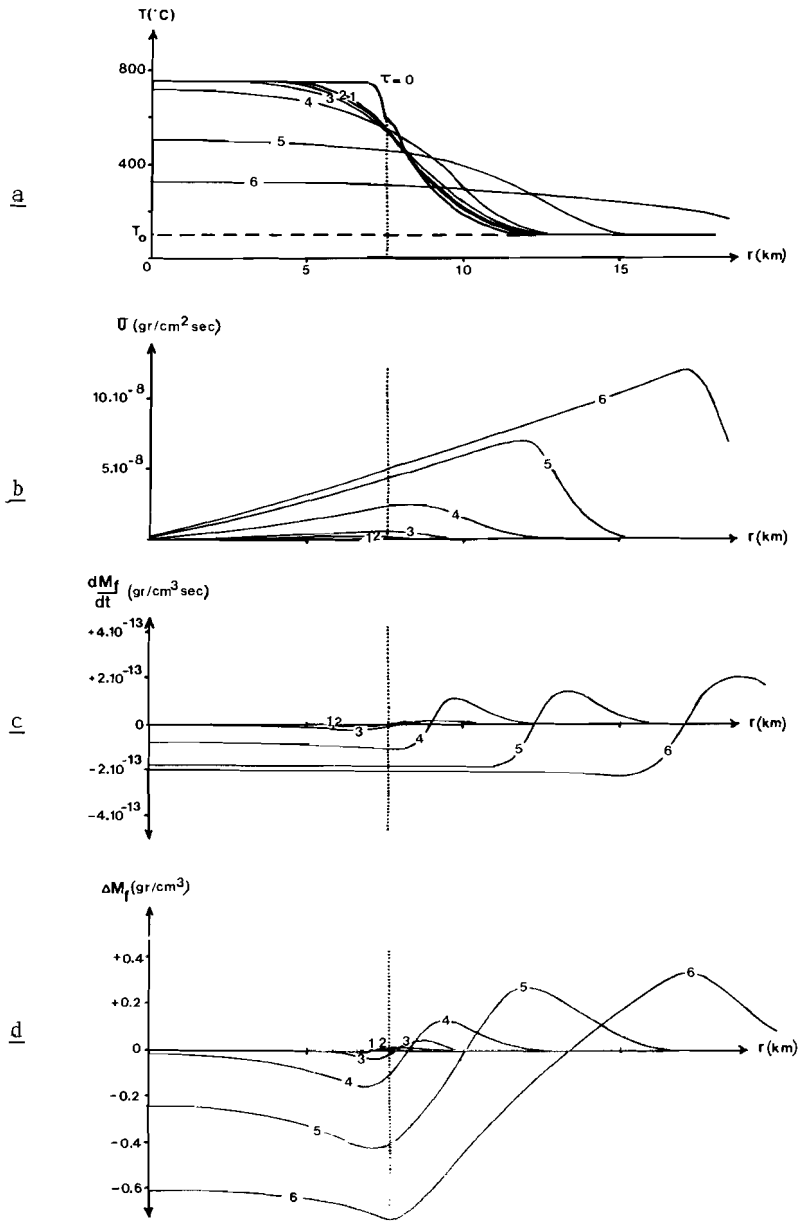
191.

Fig.41: Post-magmatic developments of $\underline{a}$: $T(^{0}C)$; $\underline{b}$: $\bar{u}(gr/cm^2sec)$;
$\underline{c}$: dM_f/dt (gr/cm^3sec); $\underline{d}$: ΔM_f (gr/cm^3) at the time
τ = 25,000 yr after the initiation of the model for different
(uniform bulk rock permeabilities k. 1: $k= 10^{-17}cm^2$;
2: $k= 10^{-16}$ cm^2; 3: $k= 10^{-15}$ cm^2; 4: $k= 10^{-14}$ cm^2; 5: $k= 10^{-13}$ cm^2;
6: $k= 10^{-12}$ cm^2.

192.

different values of the permeability k. The results indicate that
only for a bulk rock permeability $k \simeq 10^{-15}$ cm^2 the total amount of
fluid, released from the pluton upon cooling down to the reference
situation at T_0, P_0 is about 0.11 gr/cm^3, or 5 wt% H$_2$O. For a uniform
and constant value $k \simeq 10^{-15}$ cm^2, and the 'Seriphian' P_f-T relationship
$P_f^* = 3.10^{-4} \cdot (T^*)^{2.5}$, the model calculations indicate a realistic amount
of fluid release from the granodiorite intrusive. A permeability $k \simeq 10^{-15}$
cm^2 is a value, typical for unfractured or only slightly fractured
crystalline rocks (Norton and Knapp, 1977). It is the minimum
permeability that controls the rate of the fluid flow in the permeable
rock system. Such a low (minimum) value for the bulk rock permeability
k in the intrusive system at Seriphos confirms that, as a whole, the
post-magmatic, hydrothermal convection system at Seriphos indeed must
have been a largely closed fluid flow system (see Chapter VIII, and
'discussion').

To illustrate the application of the second stage, hydrothermal
model of the granodiorite intrusion at Seriphos for quantitative
indications of the post-magmatic, metasomatic redistributions of
mineral components in and around the cooling pluton, consider the
dissolution of quartz according to the equilibrium:

$$SiO_2 + 2H_2O = H_4SiO_4^0 \qquad\qquad (9-57)$$

$$K_{qz} = \frac{a_{H_4SiO_4^0}}{f_{H_2O}^2}$$

With the enthalpy and entropy data given by Robie et al.(1978), and
assuming a $a_{H_4SiO_4} \simeq m_{H_4SiO_4^0}$ ($\gamma \simeq 1$), and $\Delta c_p \simeq 0$, the temperature
dependence of the equilibrium constant, K_{qz}, is given by:

$$\ln K_{qz} = -\Delta G_r^0/RT \simeq -\Delta H_r^0/RT + \Delta S_r^0/R = +\frac{7818}{T(K)} - 28.44$$

and

$$\log m_{H_4SiO_4^0} = +\frac{3395}{T(K)} - 12.35 + 2 \log f_{H_2O} \qquad (9-58)$$

where $m_{H_4SiO_4^0}$ = molality of the solute species $H_4SiO_4^0$ in the hydrous
solution (gmol $H_4SiO_4^0$/kg H$_2$O); f_{H_2O}= fugacity of H$_2$O (bar), and T(K)=
absolute temperature (^{0}K).

193.
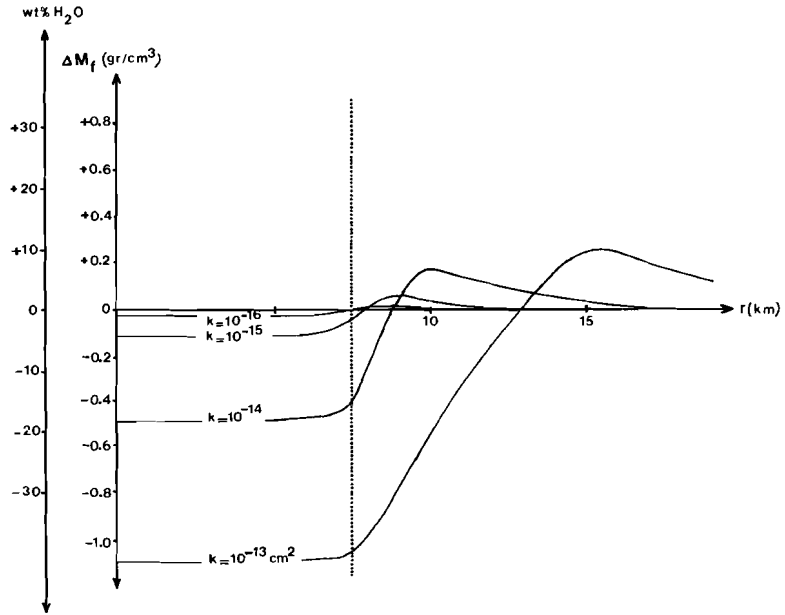
Fig.42: Total, integrated fluid amounts ΔM_f (gr/cm^3), added or subtracted in the model system for $\tau \to \infty$, and assuming different values for the (uniform) bulk rock permeability k (see text).

In the simplified model system the fluid pressure $P_f^* = P_f - 300$(bar) is singularly related to the local equilibrium temperature $T^* = T - 100^\circ C$ according to eq.(9-56):

$$P_f^* = 3.10^{-4} \cdot (T^*)^{2.5}$$

For a pure H_2O-fluid and the H_2O-fugacity data given by Helgeson and Kirkham (1974), the value of f_{H_2O} at every P_f^*, T^* in the model system can be satisfactory approximated by the expression:

$$\log f_{H_2O}^* \simeq -\frac{555}{T(K)} + 1.82 + 0.0021 \cdot T(K) \qquad (9-59)$$

Substitution of (9-59) into (9-58) results in the expression:

$$\log m_{H_4SiO_4^0}^* \simeq +\frac{2285}{T(K)} - 8.71 + 0.0042 \cdot T(K) \qquad (9-60)$$

for the local equilibrium molality $m_{H_4SiO_4^0}^*$ of the (only) 'inert' component SiO_2 in the transient mass exchange model for the

194.

granodiorite intrusion at Seriphos (provided $m^*_{H_4SiO_4^0}$ indeed is solely controlled by the dissolution equilibrium (9-57)).

In fig.43 the modelled, metasomatic redistributions of (solid) quartz are presented as quantified by the SiO_2-dissolution expression (9-60), and the mass exchange equations (9-54) and (9-55) for $k = 10^{-15}$ cm^2 and different times τ(years) elapsed since the initiation of the second stage model at $\tau = 0$. In fig.43c the precipitation rates $d(Qz)/dt$ (mgmol $qz/cm^3 \cdot sec$) are plotted against the radius r of the spherical symmetrical intrusion model. In fig.43d the integrated, total amounts of dissolved or precipitated quartz (mgmol quartz/cm^3 rock) are shown as functions of τ and r. Fig.43b gives the corresponding temperature distributions, and in fig.43a the modelled local equilibrium molality $m^*_{H_4SiO_4^0}$ is plotted as a function of $T(^0C)$.

The results of fig.43 illustrate that, in the model system, quartz is but slightly mobilized by the hydrothermal activities. Only near the intrusive contact the model computations indicate a (very moderate) net precipitation of quartz during the early, HT-stages of the metasomatic evolution (0.01 - 0.02 mgr quartz per cm^3 rock, or 10 - 20 gr/m^3). At large distances from the intrusive contact, and at low temperatures, quartz dissolves because of the strong increase in the SiO_2-solubility at T <400^0C. For $\tau \to \infty$, $T^* \to 0$ quartz dissolution will prevail everywhere, but this dissolution will be largely 'in situ', that is largely without a net transport of $H_4SiO_4^0$.

The model results for quartz are not in conflict with the field observations in and around the granodiorite intrusive at Seriphos.

A somewhat more complicated illustration of the application of the second stage, hydrothermal model for the granodiorite intrusion at Seriphos concerns the metasomatic transport of Fe along with a HCl-bearing, hydrous solution in continuous local equilibrium with magnetite and/or hematite, and the model simulation of the corresponding dissolution and precipiation rates of the two Fe-minerals

According to the experiments of Frantz et al.,(1978), and of Eugster and Chou (1979), the solubility of magnetite in supercritical, Cl-bearing H_2O-solutions (T $\geq 400^0C$) is dominantly controlled by the

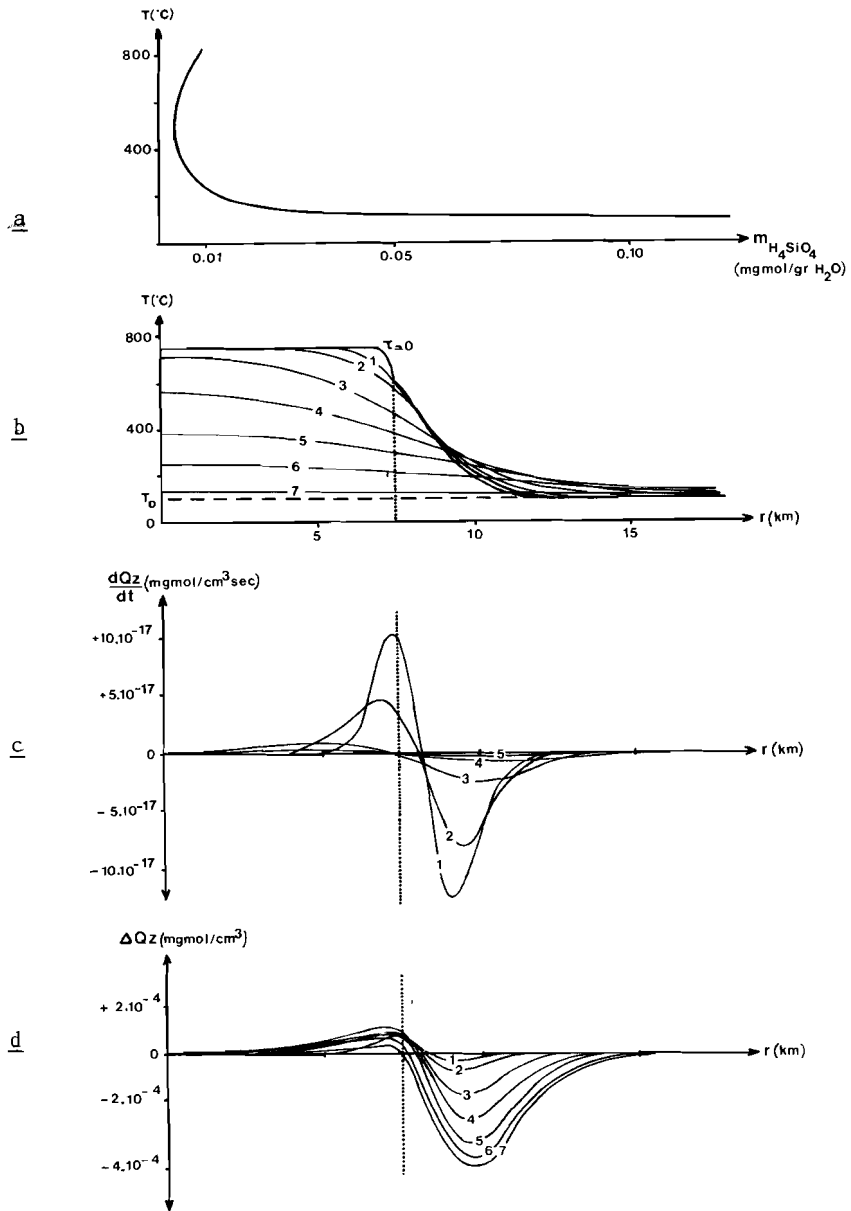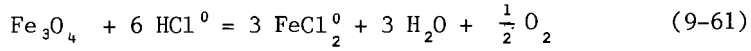Fig.43: Modelled metasomatic redistributions of (solid) quartz
a: SiO_2-solubility as function of $T(^\circ C)$; b: $T(^\circ C)$;
c: rate of precipitation or dissolution; d: total amounts
of redistributed SiO_2.
$k = 10^{-15} cm^2$; 1: 10,000 yr; 2: 25,000 yr; 3: 100,000 yr;
4: 250,000 yr; 5: 500,000 yr; 6: 1,000,000 yr; 7: 3,000,000 yr

equilibrium:

$$Fe_3O_4 + 6\ HCl^0 = 3\ FeCl_2^0 + 3\ H_2O + \tfrac{1}{2}\ O_2 \qquad (9\text{-}61)$$

$$K_I(Mt) = (a_{FeCl_2^0})^3 \cdot f_{H_2O}^3 \cdot f_{O_2}^{1/2} \Big/ (a_{HCl^0})^6$$

With the free energy data for $G_f^0(FeCl_2^0) - G_f^0(HCl^0)$ given by Frantz et
al.(1978), and for $G_f^0(H_2O)$, $G_f^0(O_2)$, $G_f^0(Fe_3O_4)$ given by Robie et al.
(1978) (for $\Delta c_p = 0$), the equilibrium constant $K_I(Mt)$ is also given by:

$$-RT\ \ln K_I(Mt) = 26T - 68440$$
$$\qquad (9\text{-}62)$$

so that:

$$\log K_I(Mt) = 3\log(a_{FeCl_2^0}) + 3\log f_{H_2O} + \tfrac{1}{2}\log f_{O_2} - 6\log(a_{HCl^0}) = +\frac{14860}{T(K)} - 5.65$$

where the fugacities of H_2O and O_2 are referred to the standard state
of the perfect gas at $298^0 K$, 1 bar, and the activities of the aqueous
solutes $FeCl_2^0$ and HCl^0 are referred to a hypothetical one-molal
solution at the standard state $298^0 K$, 1 bar.

At increasing pH, decreasing T and/or decreasing ρ_{H_2O}, associated
HCl^0 decomposes:

$$HCl \cdot pH_2O + (m+n-p)H_2O = H^+ \cdot mH_2O + Cl^- \cdot nH_2O \qquad (9\text{-}63)$$
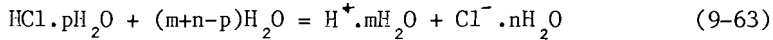
According to the experimental results of Frantz et al.(1983), the
temperature dependence of the dissociation constant $K(HCl)$ of HCl^0
(at the temperatures of interest) can be accurately approximated by the
expression:

$$\log K(HCl) \simeq \log\left[a_{H^+} \cdot a_{Cl^-}\Big/a_{HCl}\right] = +\frac{3875}{T(K)} - 5.405 + 14.93\log\rho_{H_2O} \qquad (9\text{-}64)$$

so that:

$$\log\left|a_{HCl^0}\big/a_{Cl^-}\right| = -\frac{3875}{T(K)} + 5.405 - pH - 14.93\log\rho_{H_2O} \qquad (9\text{-}65)$$

where ρ_{H_2O}= density of the H_2O-fluid in gr/cm^3.

Combination of the equilibrium constants (9-62) and (9-64) results
in the expression: $\qquad (9\text{-}66)$

$$\log\left|a_{FeCl_2^0}\big/(a_{Cl^-})\right| = -\frac{2797}{T(K)} + 8.93 - \log f_{H_2O} - \tfrac{1}{6}\log f_{O_2} - 2pH - 29.86\log\rho_{H_2O}$$

At decreasing temperature and decreasing pH, associated FeCl
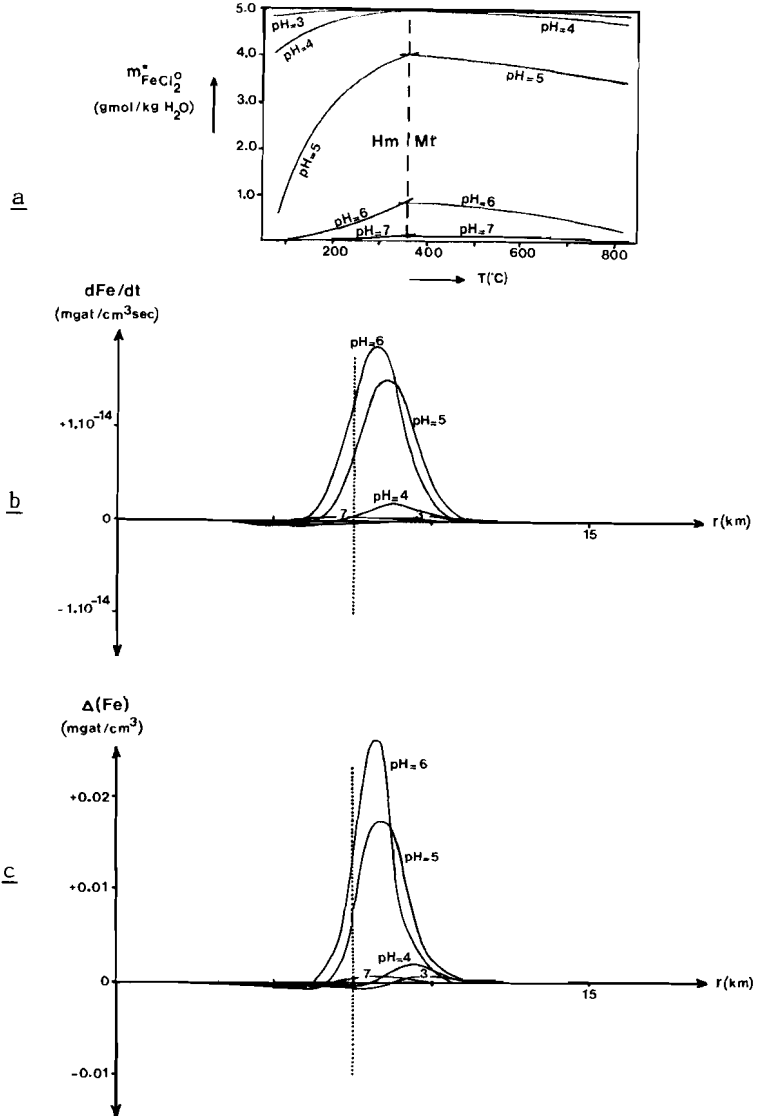decomposes to $FeCl^+$ and Fe^{++}, but at the T-pH conditions of interest in

197.

Fig.44: Metasomatic behavior of magnetite/hematite in the Seriphos
model system. a: solubity of mt/hm as a function of T(°C)
and pH; b: precipitation rates dFe/dt for various pH-values
and k= 10^{15} cm^2, τ = 25,000 yr; c: total amounts ΔFe.

198.

the model system (T >100°C, pH >3) it can be shown that the $FeCl_2^0$ dissociation does not significantly affect the Fe-solubility in the Cl-bearing, metasomatic solution.

At decreasing temperature and increasing f_{O_2}, magnetite is replaced by hematite:

$$Fe_2O_3 + 4H^+ + 4Cl^- = 2FeCl_2^0 + 2H_2O + \frac{1}{2}O_2 \qquad (9-67)$$
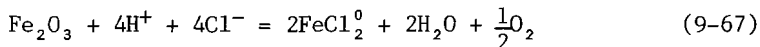
With $G_f^0(Fe_2O_3)$ given by Robie et al.(1978), the expression describing the dissolution of hematite in the Cl-bearing solution becomes: (9-68)

$$\log|a_{FeCl_2^0}/(a_{Cl^-})| = -\frac{2123}{T(K)} +11.02 - \log f_{H_2O} - \frac{1}{4}\log f_{O_2} - 2pH - 29.86\log \rho_{H_2O}$$

Thermodynamic analysis of the mineral assemblages in the skarn and ore deposits at Seriphos indicates that, in a given rock unit, the oxygen fugacity $f_{O_2}^*$ can be described as a singular function of T^* (see Chapter V). For instance, in the gneiss-unit and the higher stratigraphic levels of the schist-unit (arrow A in fig.22), $f_{O_2}^*$ changes with T^* according to the approximation:

$$\log f_{O_2}^* \simeq -\frac{8520}{T(K)} - 10.95 \qquad (9-69)$$

In the model system for the granodiorite intrusion at Seriphos P_f^* is singularly related to T^* (eq. 9-56), and the water fugacity $f_{H_2O}^*$ can be approximated by the expression (9-59):

$$\log f_{H_2O}^* \simeq -\frac{555}{T(K)} + 1.82 + 0.0021xT(K) \qquad (9-70)$$

The fluid inclusions investigations of the metasomatic formations at Seriphos (Chapter VI) indicate $\rho_{H_2O} \simeq 0.75$ gr/cm³, and high Cl-contents in the hydrous solution (30-50 eq.wt% NaCl or m_{Cl_t} 5-10).

In fig.44a the total molalities $m_{Fe}^*(= m_{FeCl_2^0}^*)$ are presented as functions of T(°C) and pH, as calculated by simultaneous solution of the equations (9-65),(9-66) and (9-68) with the parameter values $\rho_{H_2O} \simeq$ 0.75 gr/cm³, $m_{Cl(tot)} = 2m_{FeCl_2^0} + m_{HCl^0} + m_{Cl^-} = 10$, $f_{H_2O}^*$ given by eq.(9-59), $f_{O_2}^*$ given by eq.(9-69), and assuming ideal behavior of the metasomatic solution ($a_i^* \simeq m_i^*$). The results show that m_{Fe}^* changes with T only for pH= 4 - 7, and that a drastic change in the solubilities of magnetite and hematite occurs from pH= 4 to pH= 7.

In fig.44b the dissolution/precipitation rates dFe/dt(mgat/cm³ sec)

T(°C)

800

600

400

200

T_0

0

$T_r 0$

1
2
3
4
5
6
_1_

5   10   15

r (km)

_a_

dFe/dt
(mgat/cm^{3}sec)

$+3.10^{-14}$

$+2.10^{-14}$

$+1.10^{-14}$

0

-1.10^{-14}

-2.10^{-14}

1
2
3
4
5

r (km)

_b_

$\triangle$(Fe)
(mgat/cm^3)

$+0.04$

$+0.02$

0

-0.02

7
6
5
4
3
2
1

r (km)

_c_
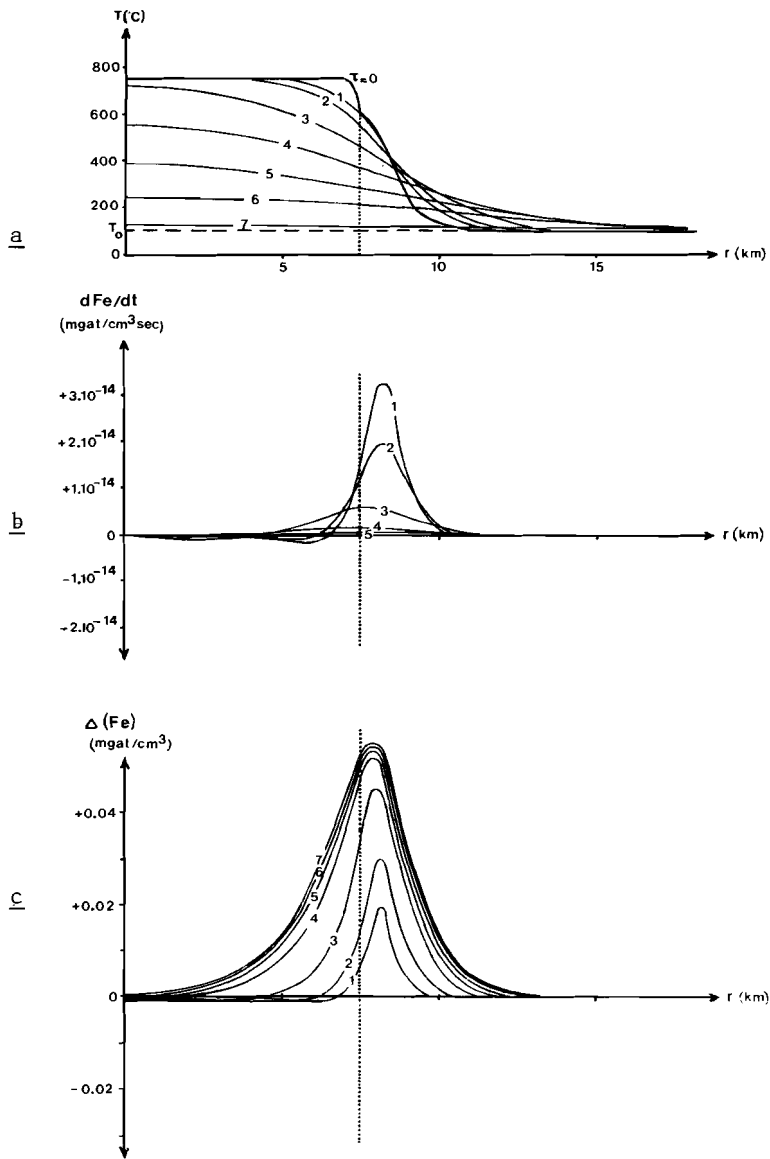
Fig.45: Temporal evolution of the quantitative redistribution of
magnetite + hematite for k= 10^{-15} cm^2, pH= 6. a: T(°C);
b: dFe/dt; c: ΔFe.
1: 10,000 yr; 2: 25,000 yr; 3: 100,000 yr; 4: 250,000 yr;
5: 500,000 yr; 6: 1,000,000 yr; 7: 3,000,000 yr.

200.

of magnetite + hematite are given in the transient heat and mass
exchange model for the granodiorite intrusion at Seriphos as computed
for, respectively, the (constant) pH-values 3, 4, 5, 6, 7, and
k= $10^{15}cm^2$, τ= 25,000 years. In fig.44c the total, integrated amounts
of redistributed. Fe-oxide are plotted for different (constant)
pH-values of the metasomatic solution, and k= $10^{-15}cm^2$, τ = 25,000 yr.
There is a clear maximum in the intensity of the Fe-redistributions at
pH= 5 - 6, that is at those (constant) pH-values at which the
solubilities of the Fe-oxides most strongly vary with T.

In figs.45a,b,c the temporal evolution of the quantitative
redistribution of magnetite + hematite is presented as computed for the
(uniform and constant) permeability k= 10^{-15} cm^2 and the (constant)
value pH= 6. According to the model simulation, magnetite precipitation
is most intense in the early, HT-stages of the metasomatic evolution in
country rocks near the intrusive contact, while at the same time there
is (some) leaching of Fe_3O_4 from the plutonic rocks near the intrusive
contact. With time, the computed intensities of the leaching and
precipitation rates decrease, while the domain of Fe-oxide
precipitation gradually spreads out, outward into the country rocks as
well as inward into the pluton. These general characteristics of the
simulated temporal evolution of the Fe-redistributions are in good
good agreement with the field observations at Seriphos. Since both k
and pH were taken constant in the model simulation, however, the
metasomatic aureole expands up to considerable distances outward from
the intrusive contact, and the spatial distribution of the
Fe-precipitations is much less pronounced than in the field (compare
fig.33, Chapter VII).

In fig.46 the total amounts of metasomatically redistributed Fe
are shown as calculated for $\tau \rightarrow \infty$, k= $10^{-15}cm^2$, and various pH-values.
The results indicate that, for an overall, average bulk rock
permeability k= $10^{-15}cm^2$, only at pH= 5 - 6 (constant) the total
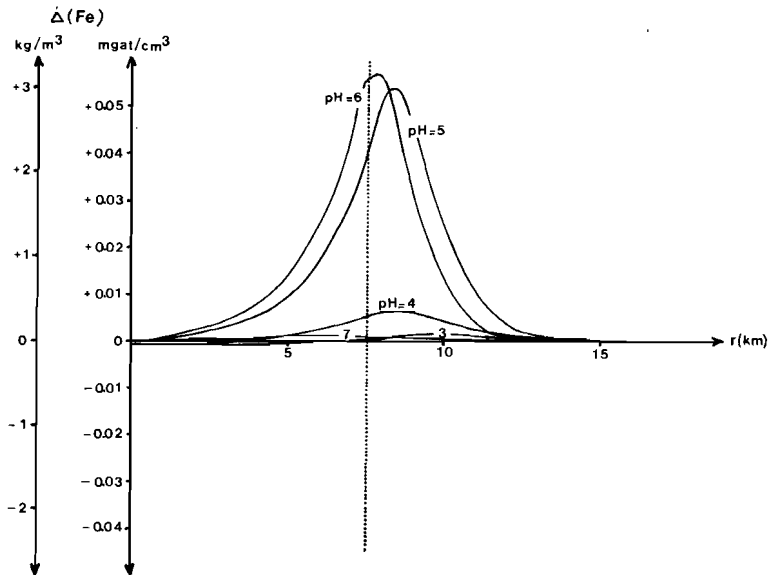amounts of leached and precipitated Fe are comparable with the field
estimates at Seriphos.

Fig.46: Total amounts of redistributed Fe (mgat/cm^3; kg Fe/m^3)
as computed for $\tau \to \infty$, k= 10^{-15}cm^2, and various pH-values
in the spherical symmetrical model system for the post-
magmatic stages of the granodiorite intrusion at Seriphos.

discussion

In the second, hydrothermal stage of the model for the
granodiorite intrusion at Seriphos it is assumed that a uniform,
spherical body of magma melt instantaneously solidifies and degasses so
that, at the time of the initiation of the model, a limited amount of
'primary magmatic fluid' is confined, at high temperature and
pressure, in a limited volume of magmatic rock. The total volume of the
magmatic rock body is indicated by the first stage, magmatic model and
field observations. The initial temperature and pressure of the
magmatic fluid are deduced from petrological evidence in combination
with fluid inclusions data.

With time the limited amount of magma-derived, primary metasomatic
solutions may flow out of the plutonic reservoir, transporting both

heat and dissolved chemicals into the surrounding wall rocks. The model describes the transient heat and mass transfer from the plutonic heat and fluid source into the wall rocks under the assumption of an instantaneous and uniform (hydro-) fracturing of the entire solid rock system at the time of the initiation of the model, and by assuming continuous maintenance of thermal as well as chemical local equilibrium. The permeability k of the uniformly fractured, solid rock system is considered uniform and constant. The P_f-ρ_f-T path of the fluids in the metasomatic exchange system is assumed to be described by a singular, continuous relationship $P_f^* = \beta P_o (T^*)^\gamma$, with numerical values deduced from the observed P_f-T evolution in the metasomatic deposits formed in the apical parts of the intrusive system at Seriphos. The vertical geobaric and geothermic gradients are ignored relative to the P_f-T gradients perpendicular to the intrusive contact.

In the model it is assumed that the magma has solidified instantaneously, that is sudden relative to the rate of the heat and mass exchanges. Natural magmas, however, crystallize over a temperature range and, in natural situations, the solidification of the magma body will take some time. In the inner parts of the pluton liquid magma may persist, while in the outer and apical parts magmatic rock has already crystallized. At Seriphos, for instance, the presence of aplitic dykes cross-cutting previously formed granodiorite rocks and HT-skarn deposits points to the existence of a still substantially liquid granodioritic magma in the inner parts of the intrusive while, at the same time, in the outer, apical parts of the pluton the already solidified magmatic rocks were subjected to intense hydrothermal activities and metasomatic mass exchanges.

The results of the simplified model simulation, however, indicate that for the moderate-low bulk rock permeabilities under consideration, the propagation of the modelled, post-magmatic heat and mass exchanges into the central parts of the spherical pluton also takes time. In the model a considerable fraction of the early, HT-metasomatic alterations is computed to take place before a noticeable cooling affects the central parts of the intrusive (see fig.45a,b,c). Although factually

203.

incorrect, the model assumption of instantaneous magma solidification probably does not, in essence, affect the applicability of the model with respect to the natural situation.

Theoretical prediction of the fluid migrations in a given hydrothermal fluid flow system requires accurate knowledge of the P_f-V_f-T changes of the fluid in the transient heat and mass exchange system. In general, such knowledge is not a priori available.

In the second, hydrothermal stage of the model for the granodiorite intrusion at Seriphos an approximated P_f-V_f-T relationship is used, based on the P_f-T changes observed in the metasomatic deposits developed in the now-exposed, apical parts of the intrusive system. Temperature and fluid pressure are assumed to be singularly related according to the continuous relationship (9-56):

$$P_f - P_o = \beta \ (T - T_o)^\gamma = 3.10^{-4}(T - T_o)^{2.5}$$

This relationship is considered to comprise all the effects of magma degassing, density changes in the fluid phase, porosity changes in the solids, sources or sinks of fluid due to chemical reactions involving volatiles, and variations in the compressibility of the hydrothermal solution.

Magma degassing must have introduced considerable amounts of fluid into the hydrothermal fluid flow system. The model only indirectly accounts for this 'primary magmatic' fluid production. After computation of the total amount of fluid that may have been released from the intrusive body upon cooling down from the initial situation at $T^*, P^*, \tau = 0$ to the hydrostatic reference situation at $T_o, P_o, \tau \rightarrow \infty$, an estimation is made of what is likely to be a realistic amount of magmatic fluid production on the basis of petrological evidence (3-5 wt% H_2O). In the natural situation degassing of the granodioritic magma takes place near the time of its final (not entirely sudden) solidification, and the amount of fluid production may have been inhomogeneous due to magmatic differentiations.

The neglect of the vertical geothermic and geobaric gradients implies that the spherical symmetrical model cannot account for the preferentially upward migration of the metasomatic solutions towards

the cooler, lower-pressure apical parts of the intrusive system. Also, in the late, LT-LP stages of the evolution, the 1-dimensional model cannot encounter the inflow of fluids due to open circulation convection. The total amount of fluids escaping through the apical parts of the intrusive, therefore, may have been larger than assumed in the model computations. The modelled total volume of the plutonic fluid source as deduced from the first stage, magmatic model on the basis of the contact metamorphic temperature distribution in the (apical) contact aureole at Seriphos, on the other hand, probably also is too large because of the neglect of the effects of the geothermic and geobaric gradients on the magma convection. The increased fluid output in the apical parts of the intrusive system due to the vertical P_f- T grdients, therefore, will be at least partially compensated by the increased total fluid volume implicitely encompassed by the model simulation. And both the isotopic and chemical evidence in the upper parts of the Seriphian intrusive system also point to the action of only a limited amount of fluid in the now exposed parts of the metasomatic exchange system (~ 6.5 wt% H_2O), and a limited amount of fluid re-cycling (2-3x)(see Chapter VII).

The model assumption that the P_f- T relationship, as deduced from the apical parts of the Seriphian metasomatic system, is valid everywhere throughout the spherical symmetrical model system, and also the assumption that the fluid viscosity ν_{H_2O} is a constant, certainly introduces inaccuracies. These simplifications, however, will not affect the basic outcome of the model simulation.

As a consequence of the model assumption of a singular, continuous P_f-T relationship everywhere throughout the model system, for instance, the heated, contact metamorphic rocks adjacent to the intrusive contact are modelled to have initial fluid pressures, and fluid contents, that are probably too high for an unfractured contact metamorphic rock. The total amount of fluid involved, however, is negligeably small relative to the total amount of fluid in the system, and only in the very early stages of the model simulation, the use of one, singular, continuous P_f-T relationship may lead to some (minor) inaccuracies in the description of the metasomatic evolution in the contact metamorphic

rocks adjacent to the intrusive contact.

As is evidenced by the fluid inclusions observations, noticeable variations in fluid density occur in the Seriphian fluid flow system (f.e. in the HT-skarns). Metasomatically induced dissolutions and precipitations of minerals, and (hydro-)fracturing, must have produced noticeable porosity changes. In addition, chemical reactions involving volatiles may have acted as sources or sinks of fluid. The use of an empirically established P_f-T relationship based on observed changes in temperature and fluid pressure, therefore, seems an attractive method to avoid the very complicated reasoning that otherwise would be necessary for an accurate description of the P_f-V_f-T changes in natural situations.

At the time of the final solidification of the granodioritic magma at Seriphos, the stresses associated with the degassing of the magma and the volumetric changes accompanying its phase transition caused an intense fracturing both of the magmatic rocks and of the adjacent wall rocks. Due to this fracturing bulk rock permeabilities increased sufficiently to permit the convective exchange of heat and mass by migrating solutions.

In the second stage of the model for the granodiorite intrusion at Seriphos it is assumed that the permeability increase accompanying the 'sudden' solidification of the magma body, is sudden, uniform and constant. In natural situations, however, large-scale fracturing takes time, the permeability increase will not be uniform, and the permeabilities will change with time (see f.e. Knapp and Knight, 1977; Knapp and Norton, 1981).

Some indication of the spatial distribution of the permeability increase in and around the Seriphian pluton can be obtained by a simplified steady-state analysis of the thermal stresses associated with the spherical symmetrical model intrusion.

In a radial symmetrical model system only the radial displacements w have to be considered. For lineary elastic materials the radial symmetrical strain components associated with a radial displacement w of an infinitesimal segment of the sphere are given by:

$$e_{rr} = \frac{\partial w}{\partial r} \quad ; \quad e_{\Theta\Theta} = e_{\phi\phi} = \frac{w}{r} \tag{9-70}$$

where e_{rr}= radial strain component in the direction of the radius r of the spherical system, and $e_{\Theta\Theta}$, $e_{\phi\phi}$= tangential strain components perpendicular to the radius r. The volumetric increase Δ of an elementary segment of the sphere due to a displacement w is given by:

$$\Delta = e_{rr} + e_{\Theta\Theta} + e_{\phi\phi} \tag{9-71}$$

The corresponding stress components σ_{rr} and $\sigma_{\Theta\Theta} = \sigma_{\phi\phi}$ are:

$$\sigma_{rr} = (\lambda + 2\mu)\frac{\partial w}{\partial r} + 2\lambda\frac{w}{r} \quad ; \quad \sigma_{\Theta\Theta} = \sigma_{\phi\phi} = \lambda\frac{\partial w}{\partial r} + 2(\lambda + \mu)\frac{w}{r} \tag{9-72}$$

where λ and μ are Lame's parameters. The general equation of equilibrium for an elementary segment of the radial symmetrical sphere, at rest and without internal body forces, is (f.e. Love,1944):

$$\frac{\partial \sigma_{rr}}{\partial r} + \frac{2}{r}(\sigma_{rr} - \sigma_{\Theta\Theta}) = 0 \tag{9-73}$$

Temperature changes induce volume changes. In an elastic solid material the spherical expansions e_{rr} and $e_{\Theta\Theta} = e_{\phi\phi}$, produced by a temperature increase T^*, are given by:

$$e_{rr} = \frac{\sigma_{rr}}{E} - 2\frac{\upsilon}{E}\sigma_{\Theta\Theta} + \xi T^* \tag{9-74}$$

$$e_{\Theta\Theta} = \frac{\sigma_{\Theta\Theta}}{E} - \frac{\upsilon}{E}(\sigma_{\Theta\Theta} + \sigma_{rr}) + \xi T^* \tag{9-75}$$

where E= Young's modulus, υ = Poisson's ratio, ξ = thermal expansivity of the solid, and $T^*= T - T_o$= temperature increase (see Timoshenko, 1944). The unit increase in volume is given by:

$$\Delta = e_{rr} + 2e_{\Theta\Theta} = \frac{1 - 2\upsilon}{E}\left[\sigma_{rr} + 2\sigma_{\Theta\Theta}\right] + 3\xi T^* \tag{9-76}$$

The corresponding thermal stresses are:

$$\sigma_{rr} = \frac{E}{1 + \upsilon}\left[e_{rr} + \frac{\upsilon}{1 - 2\upsilon}\Delta\right] - \frac{E\xi T^*}{1 - 2\upsilon} \tag{9-77}$$

$$\sigma_{\Theta\Theta} = \frac{E}{1 + \upsilon}\left[e_{\Theta\Theta} + \frac{\upsilon}{1 - 2\upsilon}\Delta\right] - \frac{E\xi T^*}{1 - 2\upsilon} \tag{9-78}$$

Substitution of the equations (9-64),(9-65) and (9-57) into the equilibrium equation (9-60) leads to the differential equation:

$$\left|\frac{\partial^2 w}{\partial r^2} + \frac{2}{r}\frac{\partial w}{\partial r} - \frac{2}{r^2}w\right| = \frac{1 + \upsilon}{1 - \upsilon}\xi\frac{\partial T}{\partial r}$$

or:

$$\frac{\partial}{\partial r}\left|\frac{\partial w}{\partial r} + 2\frac{w}{r}\right| = \frac{1 + \upsilon}{1 - \upsilon}\xi\frac{\partial T}{\partial r} \qquad (9\text{-}79)$$

Integration over r gives:

$$\frac{\partial}{\partial r}(r^2 w) = \frac{1 + \upsilon}{1 - \upsilon}\xi T^* r^2 + C_1 r^2$$

and a second integration leads to:

$$w = \frac{1 + \upsilon}{1 - \upsilon}\frac{\xi}{r^2}\int_{r_1}^{r_2} T^* r^2 dr + \frac{1}{3}C_1 r + \frac{C_2}{r^2} \qquad (9\text{-}80)$$

Substitution of $e_{rr} = \partial w/\partial r$, $e_{\Theta\Theta} = w/r$ and $\Delta = e_{rr} + 2e_{\Theta\Theta}$ into (9-66) gives:

$$\Delta = \frac{1 + \upsilon}{1 - \upsilon}\xi T^* + C_1 \qquad (9\text{-}81)$$

and substitution of (9-68) and (9-67) into respectively (9-64) and (9-65) results in the expressions:

$$\sigma_{rr} = -\frac{2E}{(1 - \upsilon)r^3}\xi\int_{r_1}^{r_2} T^* r^2 dr + \frac{E}{3(1 - 2\upsilon)}C_1 + \frac{2E}{(1 + \upsilon)r^3}C_2 \qquad (9\text{-}82)$$

$$\qquad (9\text{-}83)$$

$$\sigma_{\Theta\Theta} = \frac{E}{(1 - \upsilon)r^3}\xi\int_{r_1}^{r_2} T^* r^2 dr + \frac{E}{3(1 - 2\upsilon)}C_1 + \frac{E}{(1 + \upsilon)r^3}C_2 - \frac{E\xi T^*}{(1 - \upsilon)}$$

where the integration constants C_1 and C_2 have to be determined from the initial and boundary conditions.

For a homogeneous spherical shell with an initial, uniform temperature T_o and an initial, uniform lithostatic pressure P_s the boundary conditions are:

$$(\sigma_{rr})_{T_o} = (\sigma_{\Theta\Theta})_{T_o} = -P_s \qquad , \quad r_1 < r < r_2 \qquad (9\text{-}84)$$

and the integration constants are:

$$C_1 = \frac{-3(1 - 2\upsilon)}{E}P_s \qquad ; \qquad C_2 = 0$$

The thermal stresses are given by:

$$\sigma_{rr} = -\frac{2E}{(1 - \upsilon)r^3}\xi\int_{r_2}^{r_1} T^* r^2 dr - P_s \qquad , \quad r_1 < r < r_2 \quad (9\text{-}85)$$

$$\sigma_{\Theta\Theta} = \frac{E}{(1 - \upsilon)r^3}\xi\int_{r_2}^{r_1} T^* r^2 dr - \frac{E\xi T^*}{(1 - \upsilon)} - P_s \qquad , \quad r_1 < r < r_2 \quad (9\text{-}86)$$
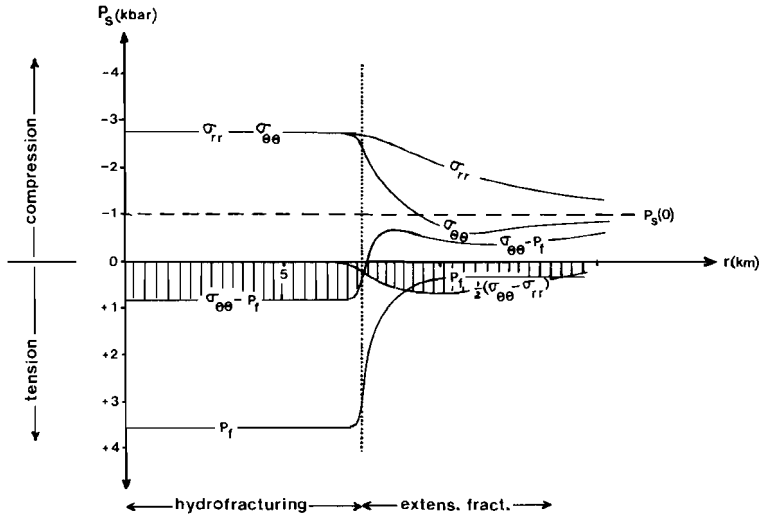
208.

Fig.47: Simplified stress analyses in and around the spherical
symmetrical intrusion model at the time of the (assumed)
sudden solidification and (auto-)brecciation (see text).

The equations (9-85) and (9-86) give the thermal stresses σ_{rr} and $\sigma_{\theta\theta}$
that are induced in a uniform, lineary elastic, solid spherical shell
due to a radial symmetrical temperature increase $T^*(r)$ relative to a
uniform, initial reference temperature T_0. The confining pressure is P_s
the thermal expansivity ξ is considered to be independent of $T^*(r)$.

In the spherical model system for the granodiorite intrusion at
Seriphos the initial (reference) temperature is $T = 100^0C$; the
(reference) lithostatic pressure is taken as $P_s = 1$ kbar. In the
spherical shell representing the contact metamorphic aureole, the
temperature rises accompanying the magma intrusion will produce thermal
stresses as given by the eqs.(9-85) and (9-86), and the temperature
rises $T^*(r)$ given by the final stages of the first, magmatic stage
model. Within the intrusive body the thermal stresses associated with
the final solidification of the magma can be assumed to result
similarly from a temperature increase $T^*(r) = T_m$ relative to the
reference temperature T_0. Fig.47 shows the stresses σ_{rr} and $\sigma_{\theta\theta}$
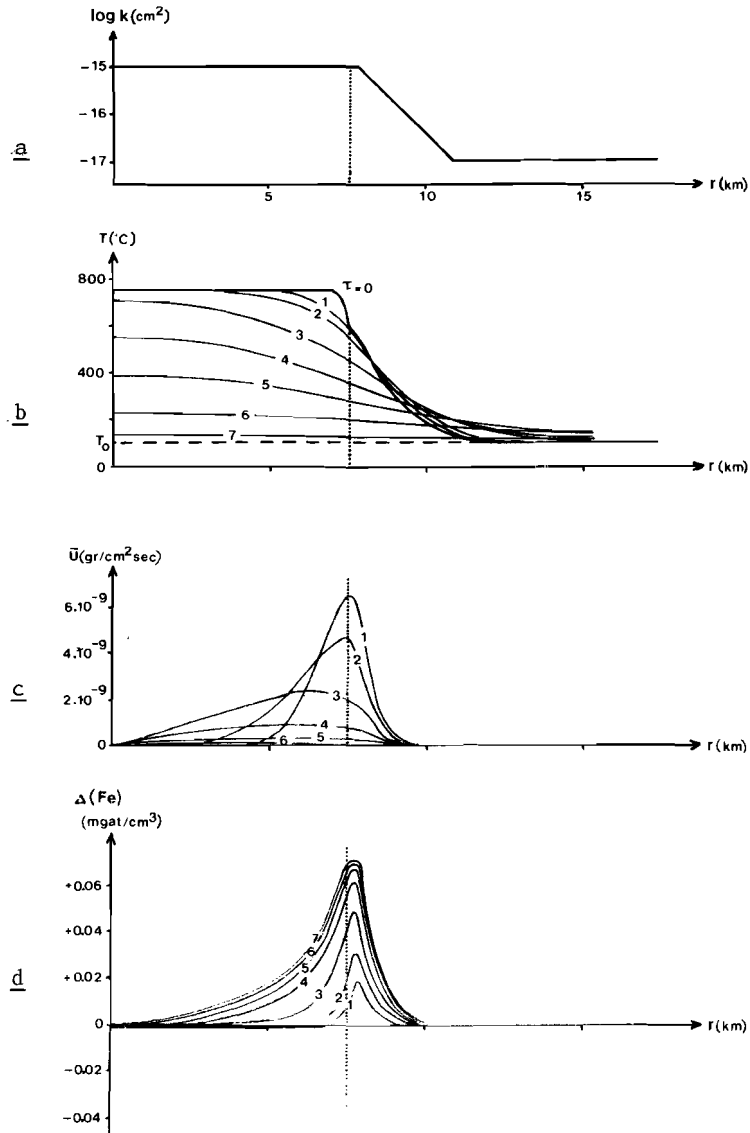calculated with the equations (9-85) and (9-86) for $r_1 \to 0$ and $r_2 \to \infty$,

209.

Fig.48: Temporal evolution of b: $T(^0C)$; c: $\bar{u}(gr/cm^2sec)$; d: ΔFe (mgat/cm^3) for the non-uniform permeability distribution given in the upper fig.48a.

1: 10,000 yr; 2: 25,000 yr; 3: 100,000 yr; 4: 250,000; 5: 500,000 yr; 6: 1,000,000 yr; 7: 3,000,000 yr.

and the media properties $E= 8.10^5$ bar, $\upsilon = 0.20$, $\xi = 4.10^{-6}\,°C^{-1}$ (Clark, 1966). Fig.47 also gives the fluid pressures P_f as calculated with eq.(9-56) and the (same) temperature distribution $T^*(r)$

In the intrusive body the calculated fluid pressures P_f exceed the modelled stresses $\sigma_{rr}= \sigma_{\theta\theta}$ by some 800 bar. Such effective tensile stresses $\sigma'_{\theta\theta} = \sigma_{\theta\theta}- P_f$ are sufficiently large to produce hydraulic fracturing (Jaeger and Cook, 1979). It is in agreement with the field observations at Seriphos, where the intrusive rocks, and the country rocks immediately adjacent to the intrusive contact, are cross-cut by a tight network of small fractures without predominant structural orientations.

In the contact aureole the radial stresses σ_{rr} remain negative (compressive), but the tangential stresses $\sigma_{\theta\theta}$ may become smaller than the confining, reference lithostatic pressure $P_s= 1$ kb (tensional) (fig.47). The deviatoric stress, $(\sigma_{\theta\theta}-\sigma_{rr})/2$, has its maximum about half way across the thermal aureole (compare Timoshenko and Goodier, 1970; Marsh, 1982). In the contact aureole the deviatoric stresses may produce extensional fractures that radiate outward from the intrusive. This is in agreement with the field observations in the contact aureole at Seriphos, where late-magmatic, aplitic dykes and fracture zones with hydrothermal Pb-Zn mineralizations, for instance, point radially outward from the granodiorite pluton.

The simplified steady state analysis of the thermal stresses associated with the granodiorite intrusion at Seriphos indicates that in the intrusive system the bulk rock permeability k will vary with the position relative to the intrusive contact. In the hydro-fractured intrusive rocks bulk rock permeabilities may have values about $k= 10^{-13}$ cm^2 . In the tensionally fractured contact metamorphic aureole the permeabilities may be between 10^{-13} and 10^{-15} cm^2, and at large distances from the intrusive contact the unfractured, regional metamorphic greenschists may have $k= 10^{-15}$ cm^2.

In fig.48 results are given of the second stage, hydrothermal model for the Seriphian granodiorite intrusion, assuming a non-uniform distribution of the (constant) permeability $k(cm^2)$ (fig.48a). Because of the higher permeabilities in the central parts of the spherical
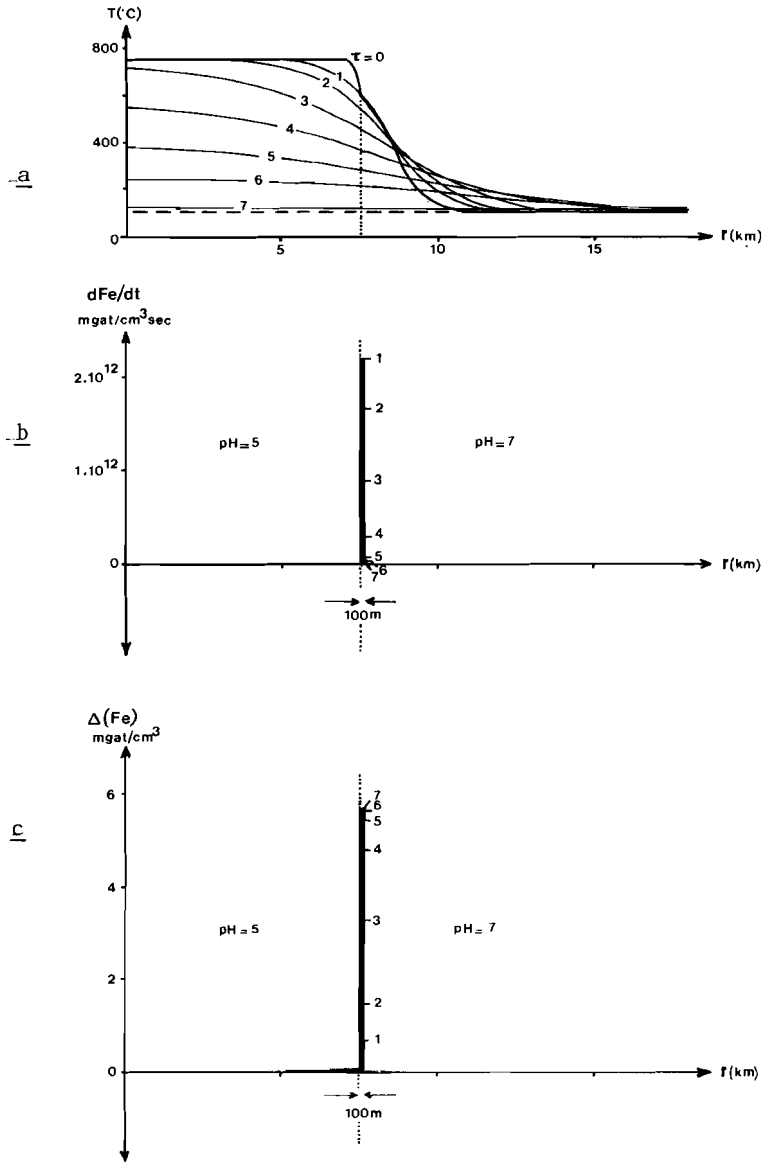
Fig.49: Modelled temperatures (a), Fe precipitation rates (b), and
total amounts of precipitated Fe (c) assuming a 100m wide
metasomatic boundary at the intrusive contact with a pH
contrast from pH=5 to pH=7 across the boundary; k= 10^{-15} cm^2 .
1: 10,000 yr; 2: 25,000 yr; 3: 100,000 yr; 4: 250,000 yr;
5: 500,000 yr; 6: 1,000,000 yr; 7: 3,000,000 yr.

symmetrical model system, the spatial evolutions of, for instance, the temperature $T(^0C)$ (fig.48b), the fluid flux u (gr/cm^2.sec) (fig.48c), and the total amount of precipitated magnetite + hematite, ΔFe (mgat/cm^3) (fig.48d) change relative to a uniform permeability system (compare figs. 37,40 with 48). The time-scale of the hydrothermal cooling, and the scale of the metasomatic mass redistributions, however, remain largely the same. Due to the permeability variations the modelled Fe-precipitation is concentrated closer to the intrusive contact, but the computed total amounts of precipitated Fe are virtually the same as in a system with a uniform permeability k= 10 cm (compare figs.42d and 47d). At Seriphos the Fe-deposits are predominantly concentrated along the intrusive contact.

In natural mass exchange systems lithological contacts or mineral stability boundaries may lead to sudden changes in the solubilities of dissolved chemicals (see also Chapter VIII). For instance, on one side of a metasomatic contact (environment I) the solubility of an 'inert' component i may be given by the local equilibrium molality $m_i^*(I)$, and on the other side of the metasomatic boundary (environment II) the solubility of i may be locally buffered at the equilibrium molality $m_i^*(II)$. At the metasomatic boundary an abrupt change in m_i^* may exist and, as long as local equilibrium is maintained at both sides of the boundary, the abrupt change in m_i^* will persist.

The net amount of i, transported with the fluids from environment I into a representative area of the metasomatic boundary in a unit time, is given by:

$$\bar{J}_c(I) = \bar{u}_c \cdot m_i^*(I) \qquad\qquad (9\text{-}87)$$

The net mass flux of i introduced into environmment II adjacent to the boundary is given by:

$$\bar{J}_c(II) = \bar{u}_c \cdot m_i^*(II) \qquad\qquad (9\text{-}88)$$

The difference in mass flux $\bar{J}_c$ across the metasomatic contact is precipitated as I_s, at a rate given by:

$$\left(\frac{\partial I_s}{\partial t}\right)_c = \bar{u}_c \left| m_i^*(I) - m_i^*(II) \right| \qquad\qquad (9\text{-}89)$$

In the radial symmetrical model system for the granodiorite intrusion at Seriphos substitution of the momentum equation (9-35) into (9-89) results in the expression:

$$\left|\frac{\partial I_s}{\partial t}\right|_c = -\frac{k}{\nu}\,\beta P_o \left|\frac{\partial T^\gamma}{\partial r}\right|_c \;\left| m_i^*(I) - m_i^*(II) \right| \qquad (9\text{-}90)$$

In fig.49 results are given of the metasomatic re-distribution of magnetite/hematite in the Seriphos model system as calculated for a Cl-bearing hydrothermal solution with total m_{Cl}= 10, and a pH-controlling metasomatic boundary at the intrusive contact. At the left, intrusive side of the boundary the pH is externally fixed at the value pH= 5; at the right, country rock side pH= 7 constant. For reasons of representation and comparison the Fe-amounts calculated to have been precipitated at the metasomatic boundary (mgat/cm³sec, resp. mgat/cm³) are assumed to be deposited in a 100m wide zone adjacent to the intrusive contact.

The model computations show that, especially in the early, HT-stages of the metasomatic evolution Fe-precipitation rates are very high at the intrusive contact (fig.49b). With time the precipitation rates decrease at the boundary but, even if precipitation of Fe takes place at both sides of the intrusive contact, the boundary itself remains the main side of Fe deposition. The concentration of Fe persists as long as the metasomatic front is active and metasomatism continues. The total amounts of precipitated magnetite/hematite may become very high at the metasomatic contact (fig.49c). This is in agreement with the field observations at Seriphos, where almost pure magnetite bodies of several hundreds of thousands of tonnes are found in the vicinity of the intrusive contact.

In fig.50 a comparison is made between the spatial distribution of the total Fe-precipitations (in kg Fe/m³) in the contact-nearby reaches of the granodiorite intrusion at Seriphos, as indicated by field estimates (I in fig. 50), and as calculated by the second stage, hydrothermal model for the granodiorite intrusion for $\tau \to \infty$ and a: a uniform permeability k= 10^{-15}cm² and a uniform and constant pH= 6 of the m_{Cl}= 10 metasomatic solution (II in fig.50); b: a uniform
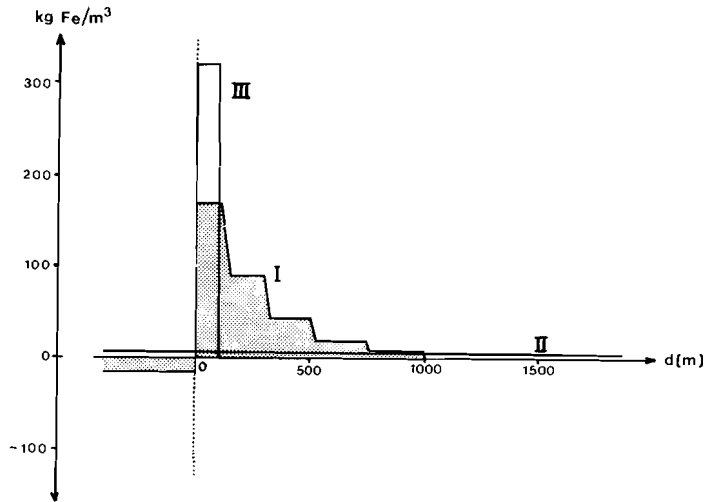
Fig.50: Comparison of the spatial distributions and total amounts of
Fe-precipitations (in kg/m³) near the intrusive contact at
Seriphos I: as indicated by field estimates; II: as modelled
for a (uniform) permeability k= 10^{-15} cm² and pH=6 constant;
III: as computed assuming a 100 m wide metasomatic boundary
across the intrusive contact with pH=5 at the intrusive side
and pH= 7 at the metasedimentary side of the contact (see text)

permeability k= 10^{-15} cm² and a pH contrast across a 100 m wide
metasomatic boundary across the intrusive contact, from pH= 5 in the
intrusive rocks to pH=7 in the country rocks (III in fig.50). In all
instances the total amounts of Fe are comparable, but the spatial
distributions differ considerably.

The spatial distribution of the Fe-precipitations at Seriphos,
with highly concentrated, pneumatolytic magnetite deposits immediately
adjacent to the intrusive contact grading into dominantly vein-type
deposits at a distance from the intrusive contact, suggests that in the
early, HT-stages of the metasomatic evolution Fe-precipitation was
mainly chemically controlled (pervasion metasomatic), while in the more
MT-LT stages the chemical exchanges between the migrating solutions and
the unaltered wall rocks largely ceased (percolation metasomatism),
local chemical buffering became less effective, and the spatial
distribution of the Fe-precipitations was more thermally and
structurally controlled.

215.

CONCLUSION

    The results of the simplified, two stage model simulation of the
transient heat and mass exchanges associated with the magmatic and
post-magmatic phases of the granodiorite intrusion at Seriphos, in
general, are very well in agreement with the field observations, in
spite of the many (over-) simplifications necessary in a theoretical
analysis. The results indicate that, due to magma convection, S-shaped
temperature distributions can be produced in the contact metamorphic
aureole, and that the temperatures indicated by the contact metamorphic
isograds probably are maximum temperatures reached more or less
simultaneously as a result of the conductive heating of the country
rocks. After the solidification of the magma, and the (hydro-)
fracturing of the porous solids, the convective transfer of heat and
dissolved chemicals along with the outflowing primary magmatic fluids
in a, as a whole, largely closed fluid flow system, led to the
formation of extensive multi-stadial metasomatic skarn and ore
deposits, especially in the contact metamorphic rocks adjacent to the
intrusive contact (see the review fig.51).
    The results indicate that the application of simplified models is
a useful tool in investigating the many complicated and interrelated
processes that control the transient heat and mass exchanges between a
given pluton and its environment. A more detailed treatment must await
further advances in our knowledge of multi-component dissolution
equilibria. These may be provided by a better theoretical model of
concentrated solutions at high temperatures and pressures, in
conjunction with experimental investigations, and supported by chemical
analyses of natural solutions in fluid inclusions. Even so, the
combination of specific, directed field and laboratory investigations
into a simple, yet accurate model provides already useful information
on the effective heat and fluid output of a pluton, and its potential
as a source of economically important ore deposits.

I:(CONVECTIVE) INTRUSION OF THE MAGMA
   FORMATION OF A CONTACT METAMORPHIC AUREOLE

T ~ 800°C
P_f ~ 4-3 kb

≤ 600°C   ≥ 100°C
2-1 kb   0.5 kb
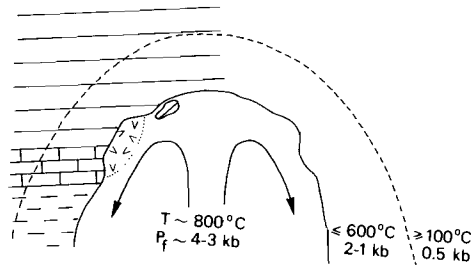
II:DEGASSING OF THE MAGMA AMD (HYDRO-) FRACTURING
   FORMATION OF HT-HP PNEUMATOLYTIC SKARN AND ORE DEPOSITS

Fe,Mg,Mn,etc.

Fe, Mg, Mn,etc.

T ~700°C
P_f~ 4-3 kb

≤ 600°C   ≥ 100°C
2-1 kb   0.5 kb
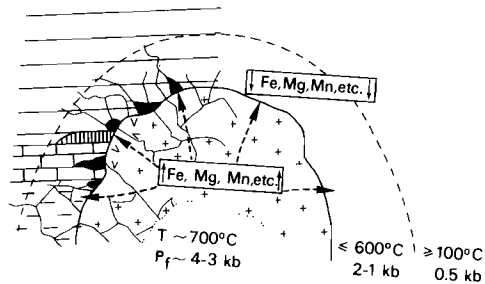
III:CONTINUED PRESSURE-INDUCED, HYDROTHERMAL COOLING OF THE PLUTON
    FORMATION OF MT-MP VEIN-TYPE SKARN AND ORE DEPOSITS

IV:HYDROSTATIC, CONVECTIVE COOLING OF THE PLUTON
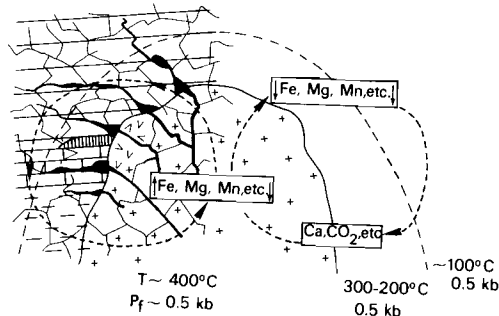   FORMATION OF LT-LP VEIN-TYPE AND GEODIC MINERALIZATIONS

Fe, Mg, Mn,etc.

Fe, Mg, Mn,etc.

Ca,CO_2,etc

T~ 400°C
P_f ~ 0.5 kb

300-200°C   ~100°C
0.5 kb   0.5 kb

Fig.51: Schematic review of the evolution of the granodiorite intrusion
        at Seriphos.

217.

REFERENCES

Althaus,E.,Karotke,E.,Nitsch,K.,Winkler,H.G.F.,(1970): An experimental
    re-examination of the upper stability limit of muscovite plus
    quartz.
    N.Jb.Min.Mh.,325-336.
Altherr,R.,Schliestedt,M.,Okrusch,M.,Seidel,E.,Kreuzer,H.,Harre,W.,
    Lenz,H.,Wendt,I.,Wagner,G.A.,(1979): Geochronology of
    high-pressure rocks in Sifnos (Cyclades,Greece).
    Contr.Min.Petr.,v.70,245-255.
Altherr,R.,Kreuzer,H.,Wendt,I.,Lenz,H.,Wagner,G.A.,Keller,J.,Harre,W.,
    Hohndorf,A.,(1982): A Late Oligocene/Early Miocene high
    temperature belt in the Attic-Cycladic crystalline complex (SE
    Pelagonian,Greece).
    Geol.Jb.,E23,97-164.
Andriessen,P.A.M.,Boelrijk,N.A.I.M.,Hebeda,E.H.,Priem,H.N.A.,
    Verdurmen,E.A.T.,Verschure,R.H.,(1979): Dating the events of
    metamorphism and granitic magmatism in the Alpine orogeny of
    Naxos (Cyclades,Greece).
    Contr.Min.Petr.,v.69,215-222.
Aubouin,J.,(1965): Geosynclines.
    Elsevier,Amsterdam.
Ballindas,I.,(1906): The island Seriphos. Its geological construction
    and metal occurrences.
    Bull.Phys.Soc.,Athens,v.1,58-74 (in greek).
Barsukov,V.L.and Kurilchikova,G.E.,(1957): Conditions of formation of
    endogene szaibellyite.
    Geochem.Int.,v.4,368.
Batchelor,G.K.,(1954): Heat transfer by free convection across a closed
    cavity between vertical boundaries at different temperatures.
    Q.Appl.Math.,v.12,209-233.
Beane,R.E.,(1974): Biotite stability in porphyry copper environment.
    Econ.Geol.,v.69,241-256.

Bird,R.B.,Ste t,W.E.and Lightfoot,E.N.,(1966): Transport phenomena.
Wiley aɪu ∪ons,New York.

Boctor,N.Z.,Popp,R.K.and Frantz,J.D.,(1980): Mineral-solution
equilibria-IV: Solubilities and the thermodynamic properties of
$FeCl_2^0$ in the system $Fe_2O_3-H_2-H_2O-HCl$.
Geochim.Cosmochim.Acta,v.44,1509-1518.

Brady,J.B.,(1975):: Chemical components and diffusion.
Am.J.Sci.,v.275,1073-1088.

Burt,D.M.,(1971): Some phase equilibria in the system Ca-Fe-Si-C-O-H.
Carnegie Inst.Wash.Yb.,v.70,178-197.

Burt,D.M.,(1972): Mineralogy and geochemistry of Ca-Fe-Si skarn
deposits.
Ph.D.thesis Harvard Univ.

Carslaw,H.S.and Jaeger,J.C.,(1959): Conduction of heat in solids.
Clarendon Press,Oxford.

Cathles,L.M.,(1977): An analysis of the cooling of intrusives by
ground-water convection which includes boiling.
Econ.Geol.,v.72,804-826.

Chapell,B.W.,(1978): Granitoids from the Moonbi District, New England,
E-Australia.
J.Geol.Soc.Austr.,v.25,267-283.

Clark,S.P.,(1966),(ed.): Handbook of physical constants.
Geol.Soc.Am.Inc.,Memoir 97.

Clayton,R.N.and Epstein,S.,(1958): The relationship between $^{18}O/^{16}O$-
ratios in coexisting quartz, carbonate and iron oxides from
various geological deposits.
J.Geol.,v.66,352-373.

Clayton,R.N.and Mayeda,T.K.,(1963): The use of bromine pentafluoride in
the extraction of oxygen from oxides and silicates for isotopic
analysis.
Geochim.Cosmochim.Acta.,v.27,43-52.

Crawford,M.L.,(1981): Phase equilibria in aqueous fluid inclusions. In:
Hollister,L.S.and Crawford,M.L.,(eds.): Fluid inclusions:
applications to petrology.
Short Course Handb.Min.Ass.Canada,Galgary.

219.

Davis,E.N.,(1966): Der geologisch Bau der Insel Siphnos.

    Geol.Geophys.Res.Athens,X-3,161-220 (in greek with german summary)

Davis,E.N.,(1972): Der geologische Bau der Insel Kea.

    Geol.Soc.Greece Bull.,v.9,252-265 (in greek with german summary).

Didier,J.,(1973): Granites and their enclaves: developments in

    petrology,3.

    Elsevier,Amsterdam.

Dixon,J.E.,(1968): The metamorphic rocks of Syros, Greece.

    Ph.D.Thesis (unpubl.),University of Cambridge.

Durr,St.,Altherr,R.,Keller,J.,Okrusch,M.,Seidel,Z.,(1978): The median

    Aegean belt; stratigraphy, structure, metamorphism, magmatism.

    In: Closs,H.,Roeder,D.,Schmidt,K.,(eds): Alps, Apennines,

    Hellenides.

    E.Schweitzerbart,Stuttgart.

Eckert,E.R.G.and Drake,R.M.,(1972): Analysis of heat and mass transfer.

    McGraw-Hill,New York.

Einaudi,M.T.,Meinert,L.D.and Newberry,R.J.,(1981): Skarn deposits.

    Econ.Geol.75th Anniv.Vol.,317-391.

Einaudi,M.T.and Burt,D.M.,(1982): Terminology, classification and

    composition of skarn deposits.

    Econ.geol.,v.77,745-755.

Epstein,S.and Taylor,H.P.,(1967): Variation of $^{18}O/^{16}O$ in minerals and

    rocks. In: Abelson,P.H.(ed.): Researches in geochemistry.

    Wiley,New York,2,29-62.

Ernst,W.G.,(1966): Synthesis and stability relations in ferrotremolite.

    Am.J.Sci.,v.264,37-65.

Eugster,H.P.and Chou,I.M.,(1979): A model for the deposition of

    Cornwall-type magnetite deposits.

    Econ.Geol.,v.74,763-774.

Fletcher,R.C.and Hofmann,A.W.,(1974): Simple models of diffusion and

    combined diffusion-infiltration metasomatism. In: Hofmann,A.W.,

    Giletti,B.T.,Yoder,H.S.and Yund,R.A.(eds.): Geochemical transport

    and kinetics.

    Carnegie Inst.Wash.Publ.634,231-241.

Fonteilles,M.,(1978): Les mecanismes de la metasomatose.
    Bull.Min.,v.101,166-194.

Frantz,J.D.and Marshall,W.L.,(1983): Electrical conductances and
    ionization constants of acids and bases in supercritical aqueous
    fluids: hydrochloric acid from 100 to 700 C and at pressures to
    4000 bars.
    Carnegie Inst.Wash.Yb.,v.82,372-377.

Friedman,I.and O'Neil,J.R.,(1977): Compilation of stable isotope
    fractionation factors of geochemical interest. In: Data Geochem.,
    6th ed.Geol.Surv.Prof.Paper 440 KK.

Fyfe,W.S.,(1970): Some thoughts on granitic magmas. In: Newall,G.and
    Rast,N.(eds.): Mechanisms of igneous intrusion.
    Spec.Iss.Geol.J.,v.2,201-216.

Fytikas,M.,Giuliani,O.,Innocenti,F.,Marinelli,G.,Mazzuoli,R.,(1976):
    Geochronological data on recent magmatism of the Aegean Sea.
    Tectonophys.,v.31,T29-T34.

Gorzhevskii,D.I.and Kozerenko,V.N.,(1970): On the depth problem of
    post-magmatic deposits. In: Pouba,Z.,Stemprok,M.,(eds.): Problems
    of hydrothermal ore deposits.
    E.Schweizerbart,Stuttgart,161-165.

Graig,H.,(1961): Standard for reporting concentrations of deuterium and
    oxygen-18 in natural waters.
    Science,v.133,1833.

Groot,C.de,(1975): Etude des mineralisations ferriferes et associees
    dans les skarns de Seriphos.
    These doct.,Univ.de Nancy,203p.

Grout,F.F.,(1945): Scale models of structures related to batholiths.
    Am.J.Sci.,v.243-A,260-284.

Gustafson,W.I.,(1974): The stability of andradite, hedenbergite and
    related minerals in the system Ca-Fe-Si-O-H.
    J.Petrol.,v.15,455-496.

Guy,B.,(1979): Petrology and isotope geochemistry of the scheelite-
    bearing skarns at Costabonne,Eastern Pyrenees,France.
    Ph.D.thesis (unpubl.),Ecole Nat.Sup.Mines,Paris.238p.

Guy,B.,(1984): Contribution to the theory of infiltration metasomatic
    zoning; the formation of sharp fronts: a geometric model.
    Bull.Min.,v.107,93-105.

Hardee,H.C.and Larson,D.W.,(1977): The extraction of heat from magmas
    based on heat transfer mechanisms.
    J.Volc.Geotherm.Res.,v.2,113-144.

Hardee,H.C.and Dunn,J.C.,(1981): Convective heat transfer in magmas
    near the liquidus.
    J.Volc.Geotherm.Res.,v.10,195-207.

Hargraves,R.B.,(1980)(ed.): Physics of magmatic processes.
    Princeton Univ.Press,Princeton.

Helgeson,H.C.and Kirkham,D.H.,(1974): Theoretical prediction of the
    thermodynamic behavior of aqueous electrolytes at high pressures
    and temperatures,I: summary of the thermodynamic/electrostatic
    properties of the solvent.
    Am.J.Sci.,v.274,1089-1198.

Hofmann,A.,(1972): Chromatographic theory of infiltration metasomatism
    and its application to feldspars.
    Am.J.Sci.,v.272,69-90.

Holdaway,M.J.,(1972): Thermal stability of Al-Fe-epidote as a function
    of f_{O_2} and Fe-content.
    Contr.Min.Petr.,v.37,307-340.

Holman,J.P.,(1976): Heat transfer,4th ed.
    McGraw-Hill,New York.

Jaeger,J.C.,(1961): The cooling of irregularly shaped igneous bodies.
    Am.J.Sci.,v.259,721-734.

Jaeger,J.C.and Cook,N.G.W.,(1979): Fundamentals of rock mechanisms,3rd
    Chapman & Hall,London.   ed.

Jansen,J.B.H.and Schuiling,R.D.,(1976): Metamorphism on Naxos:
    petrology and geothermal gradients.
    Am.J.Sci.,v.276,1225-1253.

Jansen,J.B.H.,(1977): The geology of Naxos.
    Geol.Geophys.Res.Athens,XIX-1,1-100.

Jong,A.F.M.de and Salemink,J.,(1984): O-18/O-16 and fluid inclusion
    data from skarn and ore deposits at Seriphos, Greece.
    Terra Cognita, Special Issue ECOG VIII, Braunlage, 34-35.
Knapp,R.B.and Knight,J.E.,(1977): Differential thermal expansion of
    pore fluids: Fracture propagation and microearthquake production
    in hot pluton environments.
    J.Geophys.Res.,v.82,2515-2522.
Knapp,R.B.and Norton,D.,(1981): Preliminary numerical analysis of
    processes related to magma crystallization and stress evolution in
    cooling pluton environments.
    Am.J.Sci.,v.281,35-68.
Kornprobst,J.,Lienast,J-R.,Vilminiot,J.C.,(1979): The high-pressure
    assemblage at Milos, Greece: a contribution to the petrological
    study of the basement of the Cycladic Archipelage.
    Contr.Min.Petr.,v.96,49-63.
Kotelnikov,A.R.,(1978): Hydrothermal stability of scapolite.
    Geochem.Int.,v.15,83-85.
Korzhinskii,D.S.,(1952): The distinction between infiltration and
    diffusion metasomatic columns with respect to minerals of variable
    composition (in russian).
    Akad.Nauk.SSSR,Dodklady,v.86,597-600.
Korzhinskii,D.S.,(1959): Physicochemical basis of the analysis of the
    paragenesis of minerals.
    Consultants Bur.,New York.
Korzhinskii,D.S.,(1965): The theory of systems with perfectly mobile
    components and processes of mineral formation.
    Am.J.Sci.,v.263,193-205.
Korzhinskii,D.S.,(1970): Theory of metasomatic zoning (transl.J.Agrell)
    Clarendon,Oxford.
Kreith,F.,(1976): Principles of heat transfer,3rd ed.
    Harper & Row,New York.
Ktenas,C.,(1917): Sur les relations petrographiques existant entre
    l'ile de Serifos et les formations environnantes.
    Compt.Rend.de l'Ac.d.Sci.,v.158,878.

Kurshakova,L.D.,(1971): Stability field of hedenbergite on the
     log p_{O_2} - T -diagram.
     Geochem.Int.,v.8,340-349.

Lindgren,W.,(1933): Mineral deposits, 4th ed.
     McGraw-Hill,New York.

Liou,J.G.,(1973): Synthesis and stability relations of epidote,
     $Ca_2Al_2FeSi_3O_{12}(OH)$.
     J.Petrol.,v.14,381-413.

Liou,J.G.,(1974): Stability relations of andradite + quartz in the
     system Ca-Fe-Si-O-H.
     Am.Min.,v.59,1016-1025.

Liou,J.G.,Kuniyoshi,S.and Ito,K.K.,(1974): Experimental studies of the
     phase relations between greenschist and amphibolite in a bazaltic
     system.
     Am.J.Sci.,v.274,613-632.

Love,A.E.H.,(1927): Mathematical theory of elasticity,4th ed.
     Dover,New York.

Luth,W.C.,(1969): The systems $NaAlSi_3O_8-SiO_2$ and $KAlSi_3O_8-SiO_2$ to 20kb
     and the relationship between H_2O-content,P_{H_2O} and P_{total} in
     granitic magmas.
     Am.J.Sci.,v.267-A,325-341.

Maar,P.A.van der,(1978): Fasenanalyse.
     Intern report,Dept.Geochem.,Univ.Utrecht,90p.

Maar,P.A.van der,(1981): The geology and petrology of Ios, Cyclades,
     Greece.
     Ann.Geol.Pays Hell.,XXX,206-224.

Maar,P.A.van der,and Jansen,J.B.H.,(1983): The geology of the
     polymetamorphic complex of Ios, Cyclades, Greece, and its
     significance for the Cycladic Massif.
     Geol.Rundschau,v.72,283-299.

Marinos,G.,(1951): Geology and metallogenesis of Seriphos island.
     (in greek with english summary).
     Geol.Geoph.Res.,Athens,I-4,95-127.

Marsh,B.D.,(1978): On the cooling of ascending andesitic magma.
     Royal Soc.London Philos.Trans.A,v.288,611-635.

Marsh,B.D.and Kantha,L.H.,(1978): On the heat and mass transfer from
    an ascending magma.
    Earth Planet.Sci.Lett.,v.39,435-443.
Marsh,B.D.,(1982): On the mechanics of igneous diapirism, stoping and
    zone melting.
    Am.J.Sci.,v.282,808-855.
Matthews,A.,Goldsmith,J.R.and Clayton,R.N.,(1983a): Oxygen isotope
    fractionations involving pyroxenes: the calibration of mineral-
    pair geothermometers.
    Geochim.Cosmochim.Acta,v.47,631-644.
Matthews,A.,Goldsmith,J.R.and Clayton,R.N.,(1983b): Oxygen isotope
    fractionation between zoisite and water.
    Geochim.Cosmochim.Acta,v.47,645-654.
Mel'nik,Y.P.,(1972): Thermodynamic parameters of compressed gases and
    metamorphic reactions involving water and carbon dioxide.
    Geochem.Int.,v.9,419-426.
Metz,P.W.,(1970): Experimentelle Untersuchungen des Metamorphose von
    kieseligen dolomitischen Sedimente II: Die bildungsbedingungen
    des Diopsids.
    Contr.Min.Petr.,v.28,221-250.
Murase,T.and McBirney,A.R.,(1973): Properties of some common igneous
    rocks and their melts at high temperatures.
    Geol.Soc.Am.Bull.,v.84,3563-3592.
Myashiro,A.,(1973): Metamorphism and metamorphic belts.
    Allen & Unwin,London.
Newton,R.C.,(1966): Some calc-silicate equilibrium relations.
    Am.J.Sci.,v.264,204-222.
Norton,D.L.and Cathles,L.M.,(1973): Breccia pipes - products of
    exsolved vapor from magmas.
    Econ.Geol.,v.68,540-546.
Norton,D.L.and Knapp,R.B.,(1977): Transport phenomena in hydrothermal
    systems: The nature of rock porosity.
    Am.J.Sci.,v.277,913-936.

Norton,D.L.and Knight,J.,(1977): Transport phenomena in hydrothermal
    systems: Cooling plutons.
    Am.J.Sci.,v.277,937-981.
Orville,P.M.,(1975): Stability of scapolite in the system Ab-An-NaCl-
    CaCO at 4 kb and 750 C.
    Geochim.Cosmochim.Acta,v.39,1091-1105.
Papanikolaou,D.J.,(1980): Contribution to the geology of the Aegean
    Sea: the island of Paros.
    Ann.Geol.Pays Hell.,XXX,65-96.
Pilipenko,P.P.,(1945): Skarns and mineralization (in russian).
    Trudy MGRI,v.13.
Pinkerton,H.and Sparks,R.S.,(1978): Field measurements on the rheology
    of lava.
    Nature,v.276,383-385.
Pitcher,W.S.,(1979): The nature, ascent and emplacement of granitic
    magmas.
    J.Geol.Soc.London,v.136,627-662.
Piwinskii,A.J.,(1968): Studies of batholitic feldspar: Sierra Nevada,
    Calif.
    Contr.Min.Petr.,v.17,204-223.
Piwinskii,A.J.,(1973): Experimental studies of igneous rock series,
    central Sierra Nevada batholith,California,part II.
    N.Jb.Min.Mh.,v.5,193-215.
Popov,V.E.,(1970): On the depth of formation and relationships of
    hydrothermal-sedimentary, hydrothermal and skarn iron ores. In:
    Pouba,Z.and Stemprok,M.,(eds.): Problems of hydrothermal ore
    deposits.
    E.Schweizerbart,Stuttart,213-216.
Potter,R.W.,(1977): Pressure corrections for fluid-inclusions
    homogenization temperatures based on the volumetric properties of
    the system $NaCl-H_2O$.
    J.Res.U.S.Geol.Surv.,v.5,603-607.

Potter,R.W.and Brown,D.L.,(1977): The volumetric properties of aqueous
    sodium chloride solutions from 0 to 500°C and pressures up to 2000
    bars on a regression of available data in the literature.
    U.S.Geol.Surv.Bull.,v.1421-C.

Poty,B.,Leroy,J.and Jachimowicz,L.,(1976): Un nouvel appareil pour la
    mesure des temperatures sous le microscope: l'installation de
    microthermometrie CHAIX-MECA.
    Bull.Soc.Fr.Min.Crist.,v.99,182-186.

Reverdatto,V.V.,Sharapov,V.N.and Melamed,V.G.,(1970): The controls and
    selected pecularities of the origin of contact metamorphic
    zonation.
    Contr.Min.Petr.,v.29, 310-337.

Robie,R.A.,Hemingway,B.S.and Fisher,J.R.,(1978): Thermodynamic
    properties of minerals and related substances at 298.15°K and
    1 bar (10^5 Pascals) pressure and at higher temperatures.
    Bull.U.S.Geol.Soc.,v.1452.

Rose,A.W.and Burt,D.M.,(1979): Hydrothermal alteration. In: Barnes,H.L.
    (ed.): Geochemistry of hydrothermal ore deposits,2nd ed.
    Wiley and Sons,New York,173-235.

Salemink,J.,(1977): De geologie van Seriphos.
    Intern report,Dept.Geochem.Univ.Utrecht,239p.

Salemink,J.,(1980): On the geology and petrology of Seriphos island
    (Cyclades,Greece).
    Ann.Geol.Pays Hell.,XXX,342-365.

Salemink,J.,Schuiling,R.D.,Jong,A.F.M.de and Anten,P.,(1984):
    Quantification of the skarn and ore formations at Seriphos,Greece.
    Final report EEC contract no. MPP142NL,93p.

Schafer,K.and Lax,E.,(1962): Landolt-Bornstein Zahlenwerte und
    Funktionen aus Physik, Chemie, Astronomie, Geophysik und Technik,
    6th ed.,v.II-2b.
    Springer,Berlin.

Schuh,H.,(1965): Heat transfer in structures.
    Pergamon,Oxford.

Schurmann,K.and Hellner,E.,(1966): Stability of metamorphic amphiboles:
    the tremolite-ferroactinolite series.
    J.Geol.,v.74,322-331.

Schurmann,K.,(1967): Hydrothermale experimentelle Untersuchungen an
    metamorphen monoklines Hornblende.
    N.Jb.Min.Mh.,v.11,346-353.

Shaw,D.M.,(1960a): The geochemistry of scapolite. part I: Previous work
    and general mineralogy.
    J.Petrol.,v.1,218-260.

Shaw,D.M.,(1960b): The geochemistry of scapolite. part II: Trace
    elements, petrology and general geochemistry.
    J.Petrol.,v.1,261-285.

Shaw,H.R.,(1963): Obsidian-H O viscosities at 1000 and 2000 bars in
    temperature range 700 to 900 C.
    J.Geophys.Res.,v.68,6337-6343.

Shaw,H.R.,(1965): Comments on viscosity, crystal settling and
    convection in granitic magmas.
    Am.J.Sci.,v.263,120-152.

Shaw,H.R.,Wright,T.L.,Peck,D.L.and Okamura,R.,(1968): The viscosity of
    basaltic magma: an analysis of field measurements in Makaopuhi
    lava lake,Hawaii.
    Am.J.Sci.,v.266,225-263.

Shaw,H.R.,(1974): Diffusion of H_2O in granitic liquids: Part I:
    Experimental data; Part II: Mass transfer in magma chambers. In:
    Hofmann,A.W.,Giletti,B.J.,Yoder,H.S.and Yund,R.A.(eds.):
    Geochemical transport and kinetics.
    Carnegie Inst.Wash.Publ.634,139-170.

Smeth,J.B.de,(1975): Geological map of Greece: Kythnos island.
    Nat.Inst.Geol.Min.Res.,Athens.

Smirnov,V.I.,(1976): Geology of mineral deposits.
    Mir Publishers,Moscow.

Taylor,H.P.,(1968): The oxygen isotope geochemistry of igneous rocks.
    Contr.Min.Petr.,v.19,1-71.

Taylor,H.P.,(1977): Water/rock interactions and the origin of H_2O in
      granitic batholiths.
      J.Geol.Soc.,v.133,509-588.
Taylor,B.E.and Liou,J.G.,(1978): The low-temperature stability of
      andradite in C-O-H fluids.
      Am.Min.,v.63,378-393.
Thompson,J.B.,(1959): Local equilibrium in metasomatic processes. In:
      Abelson,P.H.(ed.): Researches in geochemistry.
      Wiley and Sons,New York,427-457.
Thompson,J.B.,(1970): Geochemical reaction and open systems.
      Geochim.Cosmochim.Acta.,v.34,529-551.
Timoshenko,S.P.,(1944): Strength of materials.
      D.van Nostrand,New York.
Timoshenko,S.P.and Goodier,J.N.,(1970): Theory of elasticity,3rd ed.
      McGraw-Hill,New York.
Uchida,E.,(1979): The physico-chemical study of the skarnization in the
      Shinyama ore deposit of the Kamaishi mine,NE-Japan.
      Ph.D.thesis (unpubbl.),Univ.Tokyo,224p.
Varekamp,J.C.,(1975): De barieten en fluorieten van Serifos.
      Intern report,Dept.geochem.,Univ.Utrecht.,49p.
Vergouwen,L.,(1976): Skarnmineralisaties op Serifos.
      Intern report,Dept.geochem.,Univ.Utrecht,90p.
Verkaeren,J.,(1971): Les grenats birefringents des skarns a magnetite
      de San Leone (Sardaigne SW).
      Bull.Soc.Fr.Min.Crist.,v.94,492-499.
Weisbrod,A.,Poty,B.,Touret,J.,(1976): Les inclusions fluides en
      geochimie-petrologie: tendences actuelles.
      Bull.Soc.Min.Crist.,v.99,140-152.
Whitney,J.A.,(1975): The effect of pressure, temperature and X_{H_2O} on
      phase assemblages in four synthetic rock compositions.
      J.Geol.,,v.83,1-31.
Winkler,H.G.F.,(1979): Petrogenesis of metamorphic rocks,5th ed.
      Springer,Berlin.

Wood,B.J.and Fraser,D.G.,(1977): Elementary thermodynamics for
geologists.
Oxford Univ.Press,Oxford.

Wyllie,P.J.,(1977): Crustal anatexis: an experimental review.
Tectonophys.,v.43,T41-T71.

Zen,E-An,(1966): Some topological relationships in multisystems of n+3
phases,I: General theory, unary and binary systems.
Am.J.Sci.,v.264,401-427.

Zen,E-An,(1967): Some topological relationships in multisystems of n+3
phases,II: Unary and binary metastable sequences.
Am.J.Sci,v.265,871-897.

Zen,E-An and Rooseboom,E.H.,(1972): Some topological relationships in
multisystems of n+3 phases,III: Ternary systems.
Am.J.Sci.,v.272,677-710.

Zharikov,V.A.,(1970): Skarns.
Int.Geol.Rev.,v.12,541-559,619-647,760-769.

sample locations
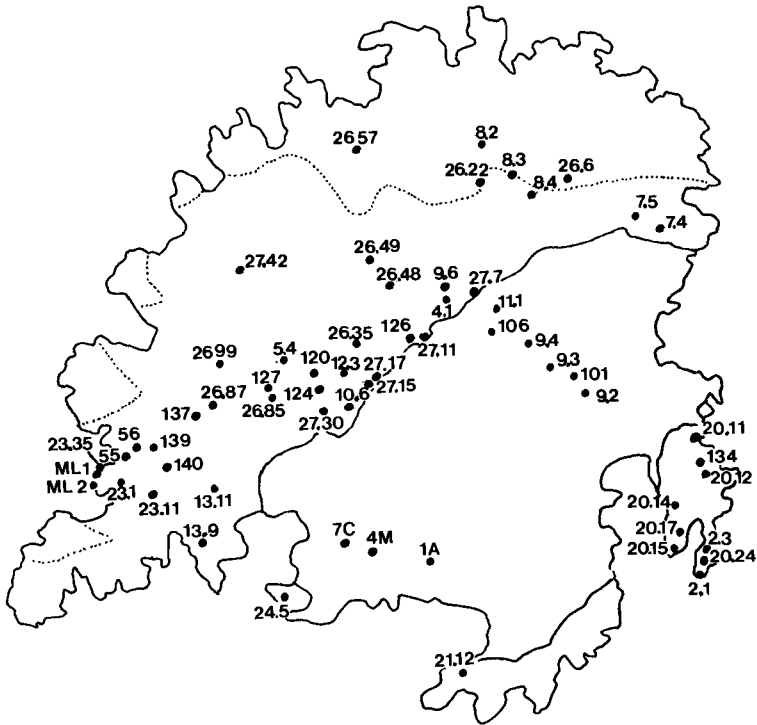
CURRICULUM VITAE

(Toegevoegd op verzoek van het College van Dekanen van de
Rijksuniversiteit Utrecht).

De schrijver van dit proefschrift werd geboren op 25 juli 1948 te
Rheden. In 1966 werd het diploma HBS-B behaald aan de Rijks HBS te Den
Helder, en werd begonnen met de studie Geologie aan de
Rijksuniversiteit te Utrecht. In mei 1971 werd het kandidaatsexamen G2
afgelegd, en in juni 1978 het doktoraal examen met hoofdvak Geochemie
en bijvakken Petrologie en Strukturele en Toegepaste Geologie. Tijdens
de studie, in de jaren 1968 tot 1976, werden student-assistentschappen
vervuld bij het Vening Meinesz Laboratorium, afdeling Geochemie. Van
1980 tot 1985 was de schrijver, met onderbrekingen, werkzaam bij de
Rijksuniversiteit Utrecht, o.a. als wetenschappelijk assistent en
adjunct wetenschappelijk ambtenaar bij de afdeling Geochemie in het
kader van een tweetal EEG-projecten.